Terms and Conditions of Use of Digitised Theses from Trinity College Library Dublin

Copyright statement

All material supplied by Trinity College Library is protected by copyright (under the Copyright and Related Rights Act, 2000 as amended) and other relevant Intellectual Property Rights. By accessing and using a Digitised Thesis from Trinity College Library you acknowledge that all Intellectual Property Rights in any Works supplied are the sole and exclusive property of the copyright and/or other IPR holder. Specific copyright holders may not be explicitly identified. Use of materials from other sources within a thesis should not be construed as a claim over them.

A non-exclusive, non-transferable licence is hereby granted to those using or reproducing, in whole or in part, the material for valid purposes, providing the copyright owners are acknowledged using the normal conventions. Where specific permission to use material is required, this is identified and such permission must be sought from the copyright holder or agency cited.

Liability statement

By using a Digitised Thesis, I accept that Trinity College Dublin bears no legal responsibility for the accuracy, legality or comprehensiveness of materials contained within the thesis, and that Trinity College Dublin accepts no liability for indirect, consequential, or incidental, damages or losses arising from use of the thesis for whatever reason. Information located in a thesis may be subject to specific use constraints, details of which may not be explicitly described. It is the responsibility of potential and actual users to be aware of such constraints and to abide by them. By making use of material from a digitised thesis, you accept these copyright and disclaimer provisions. Where it is brought to the attention of Trinity College Library that there may be a breach of copyright or other restraint, it is the policy to withdraw or take down access to a thesis while the issue is being resolved.

Access Agreement

By using a Digitised Thesis from Trinity College Library you are bound by the following Terms & Conditions. Please read them carefully.

I have read and I understand the following statement: All material supplied via a Digitised Thesis from Trinity College Library is protected by copyright and other intellectual property rights, and duplication or sale of all or part of any of a thesis is not permitted, except that material may be duplicated by you for your research use or for educational purposes in electronic or print form providing the copyright owners are acknowledged using the normal conventions. You must obtain permission for any other use. Electronic or print copies may not be offered, whether for sale or otherwise to anyone. This copy has been supplied on the understanding that it is copyright material and that no quotation from the thesis may be published without proper acknowledgement.

Perturbative study of the Chirally Rotated Schrödinger Functional in Lattice QCD

by
Pol Vilaseca Mainar
supervised by
Stefan Sint

A Project submitted to
The University of Dublin
for the degree of
Doctor in Philosophy

School of Mathematics
University of Dublin
Trinity College

September 2013

Declaration

This project has not been submitted as an exercise for a degree at any other University. Except where otherwise stated, the work described herein has been carried out by the author and by Dr. Stefan Sint. This project may be borrowed or copied upon request with the permission of the Librarian, University of Dublin, Trinity College. The copyright belongs jointly to the University of Dublin and Pol Vilaseca Mainar.

Signature of Author: 

Perturbative study of the Chirally Rotated Schrödinger Functional in Lattice QCD

Abstract

In this thesis we study the renormalization and $O(a)$ improvement of the Chirally Rotated Schrödinger Functional (χSF) in perturbation theory. The χSF was originally proposed in [1] as a way of rehabiliting the mechanism of automatic $O(a)$ improvement in the Schrödinger Functional formulation. In order to achieve this in the interacting theory, the finite coefficient of a dimension 3 boundary counterterm has to be tuned. After this, $O(a)$ effects originating from the bulk action or from insertions of composite operators in the bulk will be absent in physical quantities. As in any lattice regularization with SF boundary conditions, extra $O(a)$ effects arise from the boundaries and are cancelled by tuning two dimension 4 boundary coefficients.

One of the main objectives of this thesis is to determine to one loop in perturbation theory the boundary coefficient z_f and the critical mass m_c necessary to restore the symmetries broken by the lattice regulator and to recover the situation of automatic $O(a)$ improvement. We obtain these coefficients for several renormalization conditions and show that different definitions yield differences which vanish at a rate of $O(a)$.

We then calculate the contribution to the SF running coupling due to fermions regulated with the χSF. From there, we are able to extract the fermionic part of the boundary improvement coefficient for the gauge action. Having subtracted the boundary $O(a)$ effects, we study the remaining lattice artefacts in the step scaling functions. We then define a one parameter family of renormalized couplings and relate the resulting renormalization schemes to the $\overline{\text{MS}}$ scheme.

Finally, we study the coupling for strongly interacting theories others than QCD. We find that the cutoff effects in the step scaling function for these theories can be very large even after $O(a)$ improvement. We then devise some strategies with which we reduce the residual cutoff effects.

Acknowledgments

I WANT TO MAKE SURE that those who have been around me in the last years know how important their company has been! So I'd like to thank everyone without whom, in one way or another, none of this would have been possible

First of all, I want to thank Stefan Sint, my supervisor, for opening the gates to a world of magic and for giving me all the opportunities he has given me. I will be eternally grateful for all the things I have learned in those long visits to his office. I also appreciate his close supervision and the critical reading of my work.

A mis padres, por educarme y quererme, por la paciencia y por el apoyo incondicional en cualquier situación. A Papá, proque te he llevado en mi corazón a cada rincón del planeta. A Mamá, porque siempre me acordé de lo que un día tu escribiste, pensando en mí, como ahora piensas.

Als amics!! A en Ramon, Gabriel, Tomás, i a en Saül, perque junts vam donar les primeres passes en aquest món fenomenal. A en David, per la confiança que he rebut al llarg de tots aquests anys, i per les mil històries que vindran.

To my buddies around the world! Without whom the last years wouldn't have been such a surreal adventure. To Ashley Cooke, for riding with me all around the planet. Ah, and for letting me drive without having a license. To Mario Schröck and Eric Endress, because you don't cover 3370 km every week of your life. To Pan Kessel, for an invaluable friendship and for offering me his hand during dark times. To Oliver Schlotterer, for his humour, wisdom and comprehension. To Dmitry 'Mitch'

Shcherbakov, with who I hope to explore his frozen motherland. To the Quantum Warriors, for sharing a passion in front of a blackboard during the rainy cold evenings in Inis Fáil.

And then, specially, I'd like to thank my bros. Yeah, yo bros! For sharing everything in the last three years. Joy, worries, laughs and bad moments. Tim Harris, for making me feel welcomed and for helping me with my terrible spelling. Graham Moir, because we have walked a long long way together, and because thanks to him the headquarters were a fun place even if from the window you could only see a grey wall of concrete. Mattia Dalla Brida, for sharing roof and evenings, for those morning walks across Rathmines in which I enjoyed and learned a lot, and for carrying with me the weight of a very heavy rock. And, finally, my very sincere thanks to Darran MacMaghnusa, who has given me much more than he will ever imagine.

Contents

Listing of figures

To those who dream.

"-How many wishes do I get?
-As many as you want. And the more wishes you make, the more magnificent Fantasia will become.
-Really?
-Try it.
-My first wish is..."

Bastian and The Childlike Empress

1

Introduction: The world so far...

... SEEMS TO BE very well described by the Standard Model (SM) of particle physics, a quantum field theory which describes three of the four fundamental interactions known in nature, i.e. electromagnetism and the weak and strong nuclear forces. Almost half a century after its original proposal [2–4], it has been extremely successful in explaining a wide range of phenomena with extraordinary levels of precision. Its validity has been further confirmed with the recent discovery of a Higgs-like particle by both the Atlas [5] and CMS [6] experiments at CERN, which was the last milestone of the theory still to be observed. Although tensions do indeed exist between the values of some observables predicted by the theory and their value measured experimentally,[1] these deviations are generally attributed to the difficulty in their calculation and

[1]For instance, the anomalous magnetic moment of the muon or the edges of the unitary triangle of the CKM matrix elements.

measurement and do not change the general perspective that the SM is experimentally unchallenged. Any confirmed deviation from SM predictions would be a smoking gun for new physics yet to be discovered, and would represent a boost for new theoretical effort.

Quantum Field Theory (QFT) is the mathematical structure upon which the SM is built. It unifies the principles of special relativity and quantum mechanics leading to a framework suitable for describing phenomena in particle physics. In a field theory, the basic degrees of freedom are represented as fields, i.e. functions of space-time which transform under a specific representation of the Poincarè group. These are upgraded during the quantization procedure to operators acting on a Hilbert space. The resulting quantum fields obey commutation or anti-commutation relations according to the spin-statistics theorem. Particle states are constructed as excitations produced by acting on the vacuum-state with operators built as products of quantum fields.

The field content in the SM is divided in two categories, matter fields and force carriers. Matter fields are represented as spin 1/2 fermions divided into two subcategories as quarks (which are the constituents of hadrons) and leptons (like the electron and the neutrinos). Force carriers are the mediators of interactions and are represented as massless spin 1 vector bosons. These are the photon mediating electromagnetism (EM), the $W^{\pm}$ and Z bosons responsible for the weak interactions, and the eight gluons associated to the strong force. All interactions in the SM are encoded in a gauge symmetry based on the group $SU(3)_{\mathrm{c}} \times SU(2)_{\mathrm{L}} \times U(1)_{\mathrm{Y}}$. The $SU(2)_{\mathrm{L}} \times U(1)_{\mathrm{Y}}$ part describes the combined electroweak interactions. The last ingredient of the SM is the spin-0 Higgs field responsible for breaking the $SU(2)_{\mathrm{L}} \times U(1)_{\mathrm{Y}}$ electroweak symmetry down to the $U(1)_{\mathrm{EM}}$ of electromagnetism, generating masses for the weak bosons.[2] It is also responsible for producing fermion masses via Yukawa interactions.

The $SU(3)_{\mathrm{c}}$ sector describes the strong interactions in terms of quarks and gluons. The theory for the strong interactions was built by Fritzsch, Gell-Mann and Leutwyler as a non-Abelian gauge theory based on the symmetry group $SU(3)$, with an associated charge called color [12]. The theory was named Quantum ChromoDynamics (QCD), and so far it is widely accepted as the correct theory of strong interactions. It explains accurately phenomena from the scale of hadronic physics at low energies

[2] Although this symmetry breaking mechanism receives its name after Peter Higgs, it was simultaneously developed by Englert, Brout, Guralnik, Kibble and Higgs [7–11].

to the production of jets in high energy collisions and the properties of quark gluon plasmas.

The non-Abelian nature of QCD implies that gluons, apart from mediating the strong force between quarks, also interact among themselves. The strength of the interactions is described by the QCD coupling α_s. It's value depends on the energy scale at which an interaction occurs. It is therefore referred as a running coupling $\alpha_s(\mu)$ which "runs" or evolves with energy, adopting large values at low energies and small values at large energies.[3] This behaviour of strong interactions leads to the phenomena of *asymptotic freedom* and *confinement.*

Asymptotic freedom is a feature of some gauge theories in which their coupling becomes asymptotically weaker at short distances. It was discovered in 1973 by Frank Wilczek and David Gross [13, 14], and by David Politzer [15] independently.[4]. Before the discovery that strong interactions become weaker at very high energies, many theorists believed QFT to be inconsistent because of the presence of *Landau poles*, i.e. a divergent coupling at finite energy. Asymptotically free theories do not develop Landau poles, and hence they meant a rehabilitation of QFT as fundamental theories up to arbitrarily large energy scales.

Confinement refers to the fact that quarks do not exist as physycal states in nature. Only states obtained as a colorless combination of quark fields occur. Although the property of confinement has not yet been proven analytically from QCD, numerical calculations have provided large amount of evidence indicating that QCD does in fact confine.

As a consequence of asymptotic freedom, at sufficiently large energies for which the running coupling becomes small, QCD can be studied in perturbation theory. Theoretical predictions calculated this way show a very good agreement with experimental observations.

At low energies perturbation theory cannot be applied. Kenneth Wilson proposed a non-perturbative construction of field theories [17] based on the path integral approach. In this construction the continuum space-time is discretized into a four dimensional Euclidean lattice. The discretization introduces a cutoff in momenta

[3]The low energy behaviour of the strong coupling is not universal and deppends on the details of its definition.

[4]In 1969 Iosif Khriplovich already discovered asymptotic freedom for the $SU(2)$ Yang-Mills theory, but understood it only as a mathematical curiosity. Gerardus t'Hooft also noticed the phenomena in 1972 [16], but did not publish his observations.

proportional to the inverse lattice spacing a^{-1}. The lattice formulation, apart from providing a fully non-perturbative definition of a field theory, permits to evaluate the path integral numerically via Monte Carlo methods [18]. When this construction is applied to QCD, the discretised theory is denoted by *Lattice QCD* (LQCD).

Any QFT must be properly renormalized before any meaningful prediction can be made. The lattice formulation provides a regularization, which is a necessary step in the renormalization of the theory. In presence of the regulator, all quantities of QCD are finite. However, they will depend on the cutoff a^{-1}. To obtain a physical prediction the regulator ultimately has to be removed by taking the limit $a \to 0$. The renormalization procedure consists in rewriting the parameters of the theory in terms of some physical quantities which are kept fixed as the cutoff is removed. The remaining renormalized theory is then finite and fully predictive.

The observables used in the renormalization process have to be computable within the framework being used. Hence, in a perturbative calculation, for the renormalization of the theory one would a priori use high energy quantities[5] computed in perturbation theory. For a non-perturbative calculation, the renormalization has to be done non-perturbatively. For this, suitable physical observables are low energy quantities like hadron masses or decay constants.

The lattice version of a theory should not be understood as an approximation of a continuum one. Instead, it should be seen as a direct definition of a theory which is otherwise undefined in the continuum. Once the lattice theory is defined and after it is properly renormalised, the continuum theory is recovered by sending the lattice spacing to zero.

The Monte Carlo evaluation of a path integral requires the number of degrees of freedom to be finite. This means that a numerical calculation will always have to be performed at finite lattice spacing. Continuum results will be obtained only after an extrapolation procedure. In practice, computational limitations can restrict simulations to rather coarse lattices. Special care has to be taken to perform the extrapolation procedure correctly. For this reason, discretization effects should be as small as possible.

The pure Yang-Mills sector of LQCD has leading cutoff effects directly of $O(a^2)$. Concerning fermions, several formulations are available by now, each coming with its own advantages and drawbacks. In this thesis we will consider the original formulation

[5] Like, for instance, jet cross sections.

by Wilson [17] for which chiral symmetry is explicitely broken. Formulations of fermions which do not respect chiral symmetry are affected by $O(a)$ cutoff effects.

Symanzik introduced a way to improve systematically the rate at which quantities computed in the lattice theory converge to their continuum values [19, 20]. This process is called the *Symanzik improvement programme*. The $O(a)$ improvement of a theory is achieved by adding a set of counterterms to the lattice theory and to the interpolating fields. These counterterms respect all the symmetries of the lattice theory. They come with coefficients which can be appropriately tuned to remove $O(a)$ effects from physical quantities. This process has been successfully applied mainly to reduce cutoff effects from $O(a)$ to $O(a^2)$ in several theories. However, the non-perturbative tuning of improvement coefficients can be a very demanding task.

There are formulations which enjoy the property of automatic $O(a)$ improvement [21].[6] This does not mean that $O(a)$ discretization effects are absent. Rather, as a consequence of the symmetries of the theory, all quantities with a physical continuum limit are affected only by lattice artefacts with even powers of the lattice spacing, while quantities which vanish in the continuum limit are affected by odd powers of the lattice spacing. Hence, in this situation, leading discretization effects in physical quantities are of $O(a^2)$.

The lattice construction can be used as well in perturbation theory at high energies. Hence, lattice field theory permits to build a bridge between the low energy sector of the theory and the high energy regime. When this connection is established, the renormalization of the theory at a perturbative scale can be done using low energy observables computed non-perturbatively. This way, the renormalization is done without any error associated to the truncation of a perturbative series or the absence of any possible non-perturbative effect. Moreover, low energy quantities as, for instance, the proton mass, are known to a very high level of accuracy. It is desirable then to use them in renormalization conditions instead of other high energy quantities which might be affected by much larger experimental uncertainties.

A strategy for carrying out this connection is based on using finite volume renormalization schemes [22]. In these, the theory is formulated in a volume $V = L^4$ and the renormalization scale is identified with the physical size via $\mu = 1/L$. Different energy scales can then be explored simply by increasing or decreasing the volume of the system. The scale dependence of observables is studied by computing them at

[6] For instance, twisted mass Wilson fermions at maximal twist.

different volumes. In this way the running of physical quantities can be probed from low energies all the way up to very high energies.

Particularly useful finite volume renormalization schemes are those based on the Schrödinger Functional [23]. These are the ones we will consider in this thesis and will be discussed in extensive detail further on. Essentially, they account for the formulation of the theory on a hyper-cylindrical manifold with fixed boundaries in the temporal direction and periodic in the spatial directions. Schrödinger functional schemes are gauge invariant, mass independent (by renormalising in the chiral limit) and suitable for evaluation with both Monte Carlo and perturbative methods. The Schrödinger functional is by now a widely used tool to address non-perturbative problems in QCD [24–30], and in other strongly interacting theories [31–34].[7]

A problem in Schrödinger Functional schemes is the presence of extra sources of $O(a)$ cutoff effects in physical quantities. These are caused by the mere presence of the temporal boundaries together with the boundary conditions for the fields. These lattice artefacts do not arise from the breaking of any continuum symmetry. They will hence be present in any lattice regularization, even in those which display leading cutoff effects of $O(a^2)$ in the absence of boundaries. Following Symanzik's programme, discretization effects arising from the boundaries can be removed by adding boundary counterterms to the action and adjusting their coefficients accordingly.

For Wilson quarks in the SF there is another class of $O(a)$ effects coming from the bulk. This might be surprising a priori since massless Wilson quarks in finite volume are expected to be automatically $O(a)$ improved [21]. The argument for automatic $O(a)$ improvement relies on chiral symmetry being a symmetry of the continuum action. However chiral symmetry is explicitly broken by the SF boundary conditions and hence the argument for automatic $O(a)$ improvement fails [1]. The remaining $O(a)$ effects thus have to be cancelled through the usual $O(a)$ counterterms to the Wilson fermion action and composite fields.

The recently proposed chirally rotated version of the Schrödinger Functional (χSF) [1] implements the mechanism of automatic $O(a)$ improvement on the SF formulation. In the continuum (and chiral) limit it is directly related to the standard SF formulation via a chiral rotation of the fermion fields. The chirally rotated fields satisfy modified boundary conditions which respect a version of chiral symmetry aug-

[7] See [35] for a nice and recent review on the study of strongly interacting theories beyond QCD regulated on the lattice.

mented with a flavour structure. In this situation, the argument for automatic $O(a)$ improvement can be resurrected in terms of the upgraded chiral symmetry. Physical observables are then only affected by $O(a^2)$ discretization effects (provided that the effects from the boundaries have been removed) without the need of introducing new operators in the bulk.

The objective of this thesis is to study the renormalization properties of the χSF in perturbation theory. The coefficients for the renormalization of the action and for the improvement of the boundaries will be calculated to 1-loop in perturabtion theory, These are needed to remove $O(a)$ effect from the boundaries and to ensure that automatic $O(a)$ improvement of the bulk is at work. Since the SF and χSF formulations are equivalent in the continuum limit, we will compare several quantities in both formulations and study their convergence as the continuum limit is approached. After that, we will compute perturbatively the renormalized coupling for the χSF and the cutoff effects on the step scaling function. Finally, we will consider the application of the χSF in the study of strongly interacting theories beyond QCD.

This thesis is organised as follows. In chapter 2 we discuss some ideas of the lattice regularization of QCD and give some definitions which will be needed in the rest of the thesis. In chapter 3 we discuss the problem of non-perturbative renormalization. We review the key ideas of finite volume renormalization schemes and their application to compute the non-perturbative evolution of observables in QCD and other strongly interacting theories. Chapter 4 is entirely devoted to review the basic notions of Schrödinger Functional schemes, both in the continuum and the lattice. Following closely [23] we discuss some conceptual aspects of the SF in the pure Yang-Mills theory, after which we include fermions as in [36]. Then we present the version of the SF regularised on the lattice with the Wilson gauge action and Wilson fermions, and the application of Symanzik's improvement programme to remove $O(a)$ cutoff effects from it. The discussion in these 3 chapters does not introduce anything new. They are aimed as a review to provide with the necessary definitions and set up the framework for the following chapters. In chapter 5 we define a set of correlation functions in both the standard and chirally rotated Schrödinger functional setups, and evaluate them at 1-loop in perturbation theory. We use these perturbative results to study several renormalization and improvement conditions for the counterterms in the χSF, and to show that the mechanism of $O(a)$ improvement is at work. Moreover, since both SF formulations are equivalent in the chiral and continuum limit, we study some

universality relations between the correlation functions in both setups. Chapter 6 is divided in two main parts. First, we compute the running coupling in perturbation theory. In particular, we compute the contribution due to fermions regularised in the χSF setup at 1-loop. By studying its asymptotic behaviour in a/L, we are able to extract the fermionic contribution to the boundary improvement coefficient of the gauge action. Then we compare the size of the cutoff effects in the SF and the χSF at different stages of the improvement programme. The second part of chapter 6 is focused on the definition of a new family of renormalized couplings with which we construct a new pair of renormalization schemes which we denote as SF_ν and χSF_ν respectively. Just as the SF and the χSF, the schemes SF_ν and χSF_ν are equivalent in the continuum and chiral limits. Using data available in the literature, we compute the cutoff effects in the step scaling functions for this family of couplings up to 2-loop order in perturbation theory. Finally, we compute the 3-loop β-function in the SF_ν together with the coefficients needed to relate this family of couplings to the more common $\overline{\text{MS}}$ scheme. The ideas discussed in chapter 6 are used in chapter 7 to study the coupling for other strongly interacting theories. We compute the contribution to the coupling due to fermions in non-fundamental representations for both the SF and χSF setups. After this, we show the cutoff effects for the step scaling function for these theories and propose strategies to reduce the size of the residual cutoff effects. Finally, in chapter 8 we summarise all the results presented in this thesis and give some concluding remarks.

"Roads? Where we're going, we don't need roads."

Dr. Emmett L. Brown

2

QCD regularized on a lattice

THE QUANTIZATION OF FIELD THEORIES is a delicate issue which can lead to meaningless divergent results when conducted in a naïve way. It is not enough to start with a classical action and quantize the theory by writing the path integral[1] as in non-relativistic quantum mechanics. In order to define a quantum field theory properly one has to regularize it by introducing an ultra-violet cutoff and specify the integration measure of the fields in the path integral.

A possible approach for doing this is to expand the path integral in powers of the coupling constant, and regularize the resulting series order by order. This perturbative approach works extremely well when dealing with weakly coupled theories like QED or high energy QCD. However, when theories are strongly coupled like in the low energy regime of QCD, perturbation theory is of no use at all.[2]

Low energy hadronic physics and other strongly coupled phenomena require a non-

[1] The path integral or any other quantization procedure.

[2] There are other unsatisfactory issues with perturbation theory. For instance, it is only an asymptotic expansion. The sum of the series to all orders does not converge, and hence does not define the thory beyond the perturbative level.

perturbative formulation of QCD. This can be achieved by regulating the theory on a space-time lattice. The lattice regulator provides a fully non-perturbative definition of QCD which is, moreover, suitable for a numerical approach. The present chapter is entirely devoted to explaining the very basics of lattice field theory and introducing the main concepts and notation which will appear through the rest of this thesis.

In section 2.1 we will briefly review some basics of continuum QCD. Some emphasis will be given on the continuum symmetries of the theory. In section 2.2 we first introduce the generalities of the lattice formulation of field theories and then we proceed to translate QCD into lattice language. Finally, in section 2.3, we will discuss Symanzik's effective theory as a description of the cutoff effects in the regulated theory, and Symanzik's improvement program for improving the scaling of physical observables with the cutoff.

2.1 QCD IN THE CONTINUUM

Quantum ChromoDynamics (QCD) is the sector of the SM describing the strong nuclear force. It is a local quantum field theory of Yang-Mills fields coupled to N_f flavors of quarks, based on the local symmetry group $SU(3)$.

The gluon fields are described by massless anti-Hermitean algebra-valued vector fields which read

$$A_\mu(x) = ig_0 A^a_\mu(x) T^a, \qquad a = 1, .., 8; \tag{2.1}$$

where g_0 is the QCD coupling, $A^a_\mu(x)$ are real valued vector potentials, and T^a are the generators of the color group[3] (see appendix A.3 for our conventions on the group generators). The algebra-valued field strength tensor is denoted by

$$F_{\mu\nu}(x) = \partial_\mu A_\nu(x) - \partial_\nu A_\mu(x) + [A_\mu(x), A_\nu(x)]\,. \tag{2.2}$$

The term with the commutator in $F_{\mu\nu}$ is non-zero due to the non-Abelian nature of Yang-Mills theories, and encodes the gluonic self interactions.

Quarks are described by anticommuting Dirac spinors $\psi_{\alpha fc}(x)$ and $\overline{\psi}_{\alpha fc}(x)$ transforming under the fundamental representation of the color group. Here α denotes

[3]Since in this thesis we mainly focus on the lattice version of QCD, our notation conventions are chosen to match the usual notation of LQCD, where the gauge coupling g_0 is absorbed within the gauge potential $A_\mu(x)$. Other conventions in which the fields are hermitean are also possible.

the Dirac index, f labels the flavour component ($f = u, d, s, c, t, b$ for the up, down, strange, charm, truth and beauty quarks flavours), and c is the color index. Other theories can be constructed by considering another gauge group or by using fermion fields transforming under other representations of the color group (these options will be discussed in section 3.4.1).

The euclidean action of QCD is given by 2 terms

$$S_{\mathrm{QCD}} = S_{\mathrm{G}}[A] + S_{\mathrm{F}}[\psi, \overline{\psi}, A]. \tag{2.3}$$

The gluonic part of the QCD action describes the dynamics and propagation of gluons, and reads

$$S_{\mathrm{G}}[A] = -\frac{1}{2g_0^2} \int d^4x \ \mathrm{tr}\left[F_{\mu\nu}(x) F_{\mu\nu}(x)\right], \tag{2.4}$$

where the trace is taken over the components of the colour group. The fermion action S_{F} describes the dynamics of quark fields and their interaction with gluon fields, and is given by

$$S_{\mathrm{F}}[\psi, \overline{\psi}, A] = \sum_f \int d^4x \ \overline{\psi}_f(x) \left(\gamma_\mu D_\mu + m_f\right) \psi_f(x), \tag{2.5}$$

where only the flavour index f is written explicitly and m_f is the mass of quark f. The conventions for the Dirac matrices γ_μ can be found in appendix A.2. The QCD actions for every single flavour are identical except for the value of the mass m_f. The operator D_μ is the covariant derivative

$$D_\mu = \partial_\mu + A_\mu. \tag{2.6}$$

The fermion and gauge fields transform under non-Abelian local gauge transformations generated by $\Omega(x) \in SU(3)$ according to

$$\begin{aligned} \psi(x) &\longrightarrow \psi'(x) = \Omega(x)\psi(x), \\ \overline{\psi}(x) &\longrightarrow \overline{\psi}'(x) = \overline{\psi}(x)\Omega(x)^\dagger, \\ A_\mu(x) &\longrightarrow A'_\mu(x) = \Omega(x)A_\mu(x)\Omega(x)^\dagger + \Omega(x)\partial_\mu\Omega(x)^\dagger. \end{aligned} \tag{2.7}$$

These transformations leave invariant the QCD action

$$S_{\mathrm{QCD}}[\psi', \overline{\psi}', A'] = S_{\mathrm{QCD}}[\psi, \overline{\psi}, A]. \tag{2.8}$$

The path integral for QCD is given by

$$\mathcal{Z} = \int \mathcal{D}[\psi, \overline{\psi}]\mathcal{D}[A]e^{-S_{\text{QCD}}[\psi,\overline{\psi},A]}. \tag{2.9}$$

The functional integral eq.(2.9) is just a formal mathematical expression lacking a precise meaning until properly regularized. In section 2.2 we will proceed to introduce a lattice regularization. In the continuum, only perturbative regularizations are possible.

The action S_{QCD} is invariant under Poincaré transformations, i.e. under Lorentz transformations and under space-time translations. It is also invariant under the discrete symmetries given by charge conjugation $\mathcal{C}$, parity $\mathcal{P}$ and time reversal $\mathcal{T}$.[4]

For massless quarks, S_{QCD} is scale invariant. This invariance is lost during the quantization procedure leading to the appearance of a dimensionful scale Λ_{QCD} through the process of *dimensional transmutation*. In the modified minimal subtraction renormalization scheme $\overline{\text{MS}}$, which is the most common in perturbative frameworks, this scale is denoted by $\Lambda_{\overline{\text{MS}}}$.[5]

In the massless theory, left and right handed components of the fermion fields are decoupled and the action S_{QCD} can be separated into two independent contributions from the left and right handed quarks. As a result, the full chiral symmetry group of classical QCD with N_f massless quarks is

$$U(N_f)_L \otimes U(N_f)_R = SU(N_f)_L \otimes SU(N_f)_R \otimes U(1)_V \otimes U(1)_A. \tag{2.10}$$

The $U(1)_V$ symmetry corresponds to baryon number conservation. The axial $U(1)_A$ group is a symmetry only of the classical theory but not of the quantized theory. The absence of $U(1)_A$ at the quantum level is called the *axial anomaly*.

Therefore, the symmetry group of quantized QCD is simply

$$SU(N_f)_L \otimes SU(N_f)_R \otimes U(1)_V. \tag{2.11}$$

In the presence of fermion masses, left and right components of the fermion field mix and the action S_{QCD} is not invariant any more under axial transformations. If the quark masses are degenerate $m_i = m_j \ \forall i, j$, the mass term will be invariant only

[4] In the quantum level the axial anomaly leads to a source of $\mathcal{CP}$ violation

[5] The scale Λ_{QCD} will depend on the renormalization scheme (see section 3.2).

under simultaneous transformations $L = R$ (where $L \in SU(N_f)_L$ and $R \in SU(N_f)_R$), such that the symmetry group eq.(2.11) is reduced to

$$SU(N_f) \otimes U(1)_V. \tag{2.12}$$

Finally, for massive quarks with non-degenerate masses, the chiral group is explicitly broken down to

$$\prod_{f=1}^{N_f} U(1)_f = U(1)_u \otimes U(1)_d \otimes ... \otimes U(1)_{N_f}, \tag{2.13}$$

with every $U(1)_f$ corresponding to individual flavor conservation.

Since the physical values of the up quark and down quark massess are much smaller than the QCD scale $\Lambda_{\overline{\text{MS}}}$, the group $SU(2)_L \otimes SU(2)_R$ is a very good approximate symmetry. The mass of the strange quark is however of the same order of $\Lambda_{\overline{\text{MS}}}$, and hence $SU(3)_L \otimes SU(3)_R$ is more strongly broken.

As a consequence of the approximate chiral symmetries one would expect that the spectrum of QCD displays degeneracies in the mass of parity doublets of hadrons. However, these are not observed experimentally at all. In fact, even if the fermions are massless, chiral symmetry turns out to be spontaneously broken by the dynamics of QCD, and the chiral group is reduced to eq.(2.12). This is the cause for which the degeneracy in parity doublets is not observed. Also, following Goldstone's theorem, when a global symmetry is spontaneously broken one expects massless Goldsone bosons to occur. For $N_f = 2$ these correspond to the pions π^+, π^- and π^0.[6] However, in nature, since chiral symmetry is explicitly broken by the quark mass terms, the Goldstone bosons are not exactly massless.

Chiral symmetry is responsible for some important phenomena of QCD. Hence, special care has to be taken to ensure that these phenomena are correctly realized in the regularized theory.

When regularizing a theory, some continuum symmetries might be broken by the regulator. As a consequence of this, predictions of the regularized theory will differ from those of the final renormalized theory. These deviations are of course unphysical effects that must disappear when the regulator is removed. The breakdown of contin-

[6]For $N_f = 3$ the Goldstone bosons are the 3 pions, the kaons K^+, K^0, $\overline{K}^0$ and K^-, and the η-meson.

uum symmetries will affect the renormalization patterns of the theory. For instance, as we will see in section 2.2.2, the explicit breaking of chiral symmetry in Wilson's original formulation of fermions in the lattice will imply additive renormalization of the fermion masses, in contrast to the typical multiplicative renormalization expected in presence of chiral symmetry.

Lorenz and gauge invariane of the QCD action still allows an extra term given by

$$S_\theta = -i\frac{\theta g_0^2}{64\pi^2}\int dx^4 \epsilon^{\mu\nu\rho\sigma} F^a_{\mu\nu}(x) F^a_{\rho\sigma}, \tag{2.14}$$

usually denoted as θ term. Its contribution is proportional to the winding number and it is hence responsible for instanton effects. It is a source of P and CP violation, although these effects can be made very small through a very small value of the angle θ. The θ term leaves invariant the equations of motion (since it is proportional to a total divergence) and it is irrelevant in perturbation theory. The complex nature of eq.(2.14) makes it very difficult to deal with in numerical simulations since it introduces a sign problem. However, high precision experiments constrain the value of the angle to $|\theta| < 3 \times 10^{-10}$. It is hence typically ignored in calculations.[7] We will do so all along this thesis.

2.2 The lattice regularization

When a calculation using local interactions is done in a naïve way, the results are often inconsistent due to short-distance divergences. For the present discussion let's consider a generic theory governed by an Euclidean action $S_{\rm E}[\phi]$, where the field content of the theory is left unspecified and is denoted collectively by $\phi(x)$. The formal expression for the path integral is given by the integral over all field configurations

$$\mathcal{Z} = \int \mathcal{D}[\phi] e^{-S_{\rm E}[\phi]}. \tag{2.15}$$

[7]There are several attempts to explain the small value of the $\theta-$term and the presence of P and CP symmetries in strong interations. The most commone involve new particles called axions which, however, have never been observed. Another option postulates the up quark to be massless. In the latter it is possible to see that even if there was a θ term in the action, it would not contribute at all.

To give any meaning to expressions like eq.(2.9) and eq.(2.15) one must first regulate the theory by removing all states with energies larger than a cutoff Λ. In presence of a regulator the theory is finite and calculations of matrix elements or scattering amplitudes can be done. These quantities, however, will depend on the cutoff scale Λ. In the regulated theory, the ultra-violet (UV) divergences have been exchanged by a sensitivity to the cutoff Λ. Moreover, physical quantities will still be divergent if the limit $\Lambda \to \infty$ is taken with the couplings in S_{E} held fixed.

The bare parameters of a theory are, however, functions of the cutoff. The dependence of physical observables on the cutoff is such that a change in Λ can be compensated by a change in the couplings. The overall physical quantities are then left invariant and well-defined results can be obtained when the cutoff is removed. This process is called renormalization.[8] Physical conclusions must be independent of the particular regularization chosen and from the renormalization procedure.

There are many regularizations available (dimensional regularization, Pauli-Villars, higher derivatives, lattice,...). Although they might be very different in nature, they all share some common features. They all introduce a new scale Λ into the theory, such that contributions to physical observables coming from momentum larger than Λ are highly suppressed, while contributions with momentum $p \ll \Lambda$ behave as they do in the unregulated theory. All the regulators introduce unphysical features at momentum scales of order of Λ. These are irrelevant for scales much lower than Λ, and should disappear when the regulator is removed.

Among the possible regulators available, the only non-perturbative one is the lattice regularization, which consists in replacing the continuum space-time $\mathbb{R}^4$ with a discrete set $\mathbb{Z}^4$, which is denoted as *the Lattice*. The original field theory is then reformulated on the lattice: space-time derivatives in the action $S_{\mathrm{E}}[\phi]$ are replaced by finite differences and the original fields $\phi(x)$ become functions ϕ_x defined only at the points

$$x = a\hat{n}, \qquad \hat{n} \in \mathbb{Z}^4, \tag{2.16}$$

where a is the distance between points known as *lattice spacing*. The discretization

[8] This is the main topic of the present thesis. Specific renormalization strategies are presented in chapter 3 and discussed all the way along this work.

of space time provides the cutoff in momentum. The Fourier transformed fields

$$\widetilde{\phi}(p) = a^4 \sum_x e^{ipx} \phi_x, \tag{2.17}$$

can only adopt values of the momenta p lying within the 4-dimensional Brillouin zone given by a hypercube with sides of length $2\pi/a$. Hence any mode of momentum $p > \Lambda = \pi/a$ is removed from the theory.

When the path integral is defined for the lattice theory the integration measure can be specified unambiguously. The integral over all field configurations is reduced to a multiple integral over the values of the field ϕ_x at all lattice points

$$\mathcal{Z} = \prod_x \int_{-\infty}^{\infty} d\phi_x e^{-S_{\mathrm{E}}[\phi]}. \tag{2.18}$$

In fact, if the action $S_{\mathrm{E}}[\phi]$ was describing a free theory, eq.(2.18) would simply be a Gaussian integral which can be carried out analytically.

If, moreover, the regulated theory is restricted to a finite volume $L^3 \times T$, the number of degrees of freedom ϕ_x in eq.(2.18) becomes finite, leaving the functional integral suitable for a numerical evaluation through Monte Carlo methods (see section 2.2.2).

The lattice regulator is removed by taking the limit $a \to 0$, which in the lattice jargon is called the *continuum limit*. It is important that in the continuum limit all the symmetries of continuum QCD are recovered, which might have been broken in presence of the regulator. Among these symmetries, the most essential one is $SU(3)$ local gauge symmetry. Gauge symmetry is manifestly preserved by the lattice regulator, which is another fact for which the lattice is a particularly appealing regularization.

The lattice construction does not damage the quantum-mechanical structure of the theory, but it has severe consequences on the space-time properties. The most direct one is that space-time translations are reduced to discrete translations from point to point. Moreover, the group of spatial rotations $SO(3)$ is reduced down to the cubic group O_h. This is reflected on the spectrum of the theory. Since there is not a one to one correspondence between the irreducible representations of $SO(3)$ and O_h, the quantum numbers of states in the lattice theory do not correspond diretly to the quantum numbers of states in the continuum theory. These are not severe problems for studying the low lying states of the spectrum, but induce complications for example for studying excited states or when attempting to define the energy-

momentum tensor on the lattice.

Finally, when the theory is formulated on finite volume, particle momenta is restricted to discrete values

$$p_k = \frac{2\pi}{L} n_k, \qquad k = 1, 2, 3, \qquad n_k \in \mathbb{Z}, \tag{2.19}$$

which has direct effects on multi-particle states.

After discussing the role of the lattice regulator in a generic way, in the following subsections we describe how to transcribe the different parts of the QCD action eq.(2.3) to a lattice form and then quantize it via the path integral formalism.

2.2.1 The QCD action on the lattice

Gauge fields on the lattice are not directly imported from the continuum formulation. Instead they are obtained (as in the continuum) by demanding that the action remains gauge invariant once written in the lattice form. While in the continuum this is achieved through the fields A_μ, in the lattice one is forced to use instead the parallel transporters $U(x, x + a\hat{\mu}) \in SU(3)$, which connect neighbouring points x and $x + a\hat{\mu}$ through

$$U(x, x + a\hat{\mu}) = \mathcal{P} \exp\left\{ \int_0^a dt \; A_\mu(x + \hat{\mu}t) \right\}, \tag{2.20}$$

where $\mathcal{P}$ denotes path ordering and $\hat{\mu}$ is the unit vector in the μ direction. The field $A_\mu(x)$ can be assumed to be constant along the path from x to $x + a\hat{\mu}$, and thus eq.(2.20) can be approximated by the simpler expression

$$U_\mu(x) = e^{aA_\mu}, \qquad U_\mu \in SU(3), \tag{2.21}$$

where $U_\mu(x)$ are taken to be the gauge fields in the lattice theory. Note that $U_\mu(x) = U(x, x + a\hat{\mu}) + O(a)$.

A gauge field U_μ assigns a $SU(3)$ matrix to every pair of points $(x, x + a\hat{\mu})$. U_μ are therefore referred as link variables. The hermitean conjugate $U_\mu(x)^\dagger$ can be defined as the link variable associated to the pair $(x, x + a\hat{\mu})$ with opposite orientation to $U_\mu(x)$. The fields $U_\mu(x)$ and $U_\mu(x)^\dagger$ take values on the Lie group $SU(3)$, in contrast to the $A_\mu(x)$ fields which take values in the Lie algebra. A set of values for all link

variables on the lattice

$$U = \{U_\mu(x),\ \forall \mu, x\}\,, \tag{2.22}$$

is referred as a *gauge field configuration.*

The lattice gauge fields transform under local gauge transformations $\Omega(x) \in SU(3)$ as

$$\begin{aligned} U_\mu(x) &\longrightarrow U'_\mu(x) = \Omega(x) U_\mu(x) \Omega(x + a\hat{\mu})^\dagger, \\ U_\mu(x)^\dagger &\longrightarrow U'_\mu(x)^\dagger = \Omega(x + a\hat{\mu}) U_\mu(x)^\dagger \Omega(x)^\dagger. \end{aligned} \tag{2.23}$$

The simplest choice of lattice action for the gauge fields preserving local gauge invariance was constructed by Wilson [17] by considering the product of parallel transporters around an elementary square. The so called Wilson gauge action, written in terms of the link variables, is given by

$$S_{\rm G}[U] = \frac{\beta}{N} \sum_x \sum_{\mu<\nu} \mathrm{Re\ tr}\,[\mathbb{I} - P_{\mu\nu}(x)]\,; \qquad \beta = \frac{2N}{g_0^2}, \tag{2.24}$$

where N is the number of colors, the trace is taken over color components, and β is called the *inverse coupling.* The field $P_{\mu\nu}(x)$ is a closed loop around a *plaquette* (i.e, a square with sides of length a), given by

$$P_{\mu\nu}(x) = U_\mu(x) U_\nu(x + a\hat{\mu}) U_\mu(x + a\nu)^\dagger U_\nu(x)^\dagger, \tag{2.25}$$

and called a *plaquette field.*

Inserting the definition eq.(2.21) into the gauge action $S_{\rm G}[U]$ it can be seen that in the (naïve) continuum limit[9]

$$S_{\rm G}[U] \xrightarrow{a\to 0} -\frac{1}{2g_0^2} \sum_{\mu\nu} \sum_x a^4 \mathrm{tr}\,[F_{\mu\nu}(x) F_{\mu\nu}(x)] + O(a^5), \tag{2.26}$$

so that the continuum form of $S_{\rm G}[U]$ reproduces the pure Yang-Mills action eq.(2.4).

The lattice regularization of eq.(2.4) is not unique and we have presented here only the simplest option eq.(2.24). Other regularizations have been formulated aiming towards a better convergence of the quantized theories to the continuum action as

[9]By naïve continuum limit we denote the limit $a \to 0$ of a discrete action at a classical level where no renormalization takes place. By full continuum limit, or *continuum limit*, we refer to the removal of the cutoff in the quantum theory which takes place together with the renormalization of the theory, in which the bare parameters become functions of the cutoff.

$a \to 0$. A guiding principle to build lattice regularized actions is that in the naïve continuum limit they should converge to the classical continuum action eq.(2.4).[10]

Concerning the discretization of the fermion action, many possibilities exist as well. They usually take the generic bilinear form

$$S_{\mathrm{F}}[\psi, \overline{\psi}, U] = a^4 \sum_x \overline{\psi}(x) \left(D + m_0\right) \psi(x), \tag{2.27}$$

where $\psi(x)$ and $\overline{\psi}(x)$ are spinor fields, with color and flavor componentes, defined on the lattice sites x. The dependence of $S_{\mathrm{F}}[\psi, \overline{\psi}, U]$ on the gauge field U comes from within the Dirac operator.

Different fermion regularizations correspond to different discretizations of the continuum Dirac operator. The main force driving the construction of alternative regularizations is the problem of how to realize chiral symmetry on the lattice. In fact, the *Nielsen-Ninomiya theorem* states that any discretization of the Dirac operator which is hermitean and leads to an action local and translationally invariant, either breaks chiral symmetry or generates extra unphysical fermion species called doublers [38, 39].

The expression which encodes chiral symmetry on the lattice is the so called *Ginsparg-Wilson* relation [40]

$$D\gamma_5 + \gamma_5 D = aD\gamma_5 D. \tag{2.28}$$

This relation permits to construct a modified chiral transformation which leaves the lattice action for massless quarks invariant [41]. Dirac operators D which satisfy eq.(2.28) respect exact lattice chiral symmetry. However, due to the Nielsen-Ninomiya theorem, these can not be ultra-local but they will have long range interactions between distant neighbours which decay exponentially.

Keeping chiral symmetry on the lattice is important for several reasons.[11] However, dealing with a Dirac operator which is non-local at finite lattice spacing is a very demanding task. We will not discuss chiral formulations in the rest of this thesis.

[10] The naïve continuum limit is a sufficient but not necessary condition to obtain a valid regularized action. The *topological lattice actions* have been recently proposed[37], which do not have a classical continuum counterpart but lead to the correct quantum continuum limit.

[11] For example, to build non-perturbative formulations of chiral theories like electro-weak interactions. Moreover, leading cutoff effects for formulations satisfying eq.(2.28) are of order $O(a^2)$.

Here we will focus only on Wilson's original formulation of lattice fermions, called the *Wilson fermion action* $S_{\mathrm{WF}}[\psi, \overline{\psi}, U]$. It is explicitely given by introducing in eq.(2.27) the Wilson-Dirac operator D_{W} defined as

$$D_{\mathrm{W}} = \sum_{\mu} \frac{1}{2} \left\{ \gamma_\mu \left[\nabla^*_\mu + \nabla_\mu \right] - a \nabla^*_\mu \nabla_\mu \right\}. \tag{2.29}$$

The covariant derivatives on the lattice act on fermion fields as[12]

$$\begin{aligned} \nabla_\mu \psi(x) &= \frac{1}{a} \left[U_\mu(x) \psi(x + a\hat{\mu}) - \psi(x) \right], \\ \nabla^*_\mu \psi(x) &= \frac{1}{a} \left[\psi(x) - U_\mu(x - a\hat{\mu})^\dagger \psi(x - a\hat{\mu}) \right]. \end{aligned} \tag{2.30}$$

The last term in eq.(2.29) is the Wilson term. It effectively projects the doublers out of the theory. This term, however, breaks explicitly chiral symmetry.

The discrete symmetries respected by the Wilson fermion action $S_{\mathrm{WF}}[\psi, \overline{\psi}, U]$ are the same as for the continuum action, namely $\mathcal{C}$, $\mathcal{P}$ and $\mathcal{T}$,.

The Wilson Dirac operator D_{W} satisfies also γ_5-hermiticity, that is

$$D^\dagger_{\mathrm{W}} = \gamma_5 D_{\mathrm{W}} \gamma_5. \tag{2.31}$$

As a consequence, the eigenvalues of D_{W} are real or come in complex conjugate pairs. This implies that the determinant of D_{W} is real. For an even number of quarks the determinant is not only real but positive, which is crucial in order to perform a Monte Carlo evaluation of the path integral (see subsection 2.2.2).

The full lattice QCD action S_{LQCD} is the sum of the gauge part and the fermionic part

$$S_{\mathrm{LQCD}}[U, \psi, \overline{\psi}] = S_{\mathrm{G}}[U] + S_{\mathrm{WF}}[U, \psi, \overline{\psi}]. \tag{2.32}$$

2.2.2 The QCD path integral with a lattice regulator

Once the lattice form of the QCD action has been specified, we are ready to define the integration measures and to write the path integral regulated on the lattice. In the path integral formulation of QFT operators $\widehat{\mathcal{O}}$ in a Hilbert space translate into functionals $\mathcal{O}[\psi, \overline{\psi}, U]$ in the space of fields. Expectation values of the operator $\widehat{\mathcal{O}}$ are

[12] A list with the action of some lattice derivative operators is included in appendix A.5

represented as functional integrals over the space of all field configurations

$$\langle \mathcal{O} \rangle = \frac{1}{\mathcal{Z}} \int \mathcal{D}[\psi, \overline{\psi}] \mathcal{D}[U] \mathcal{O}[\psi, \overline{\psi}, U] e^{-S_{\text{LQCD}}[\psi, \overline{\psi}, U]}, \tag{2.33}$$

where $\mathcal{Z}$ is the lattice path integral given by

$$\mathcal{Z} = \int \mathcal{D}[\psi, \overline{\psi}] \mathcal{D}[U] e^{-S_{\text{LQCD}}[\psi, \overline{\psi}, U]}. \tag{2.34}$$

The fermionic measure is characterized as

$$\mathcal{D}[\psi, \overline{\psi}] = \prod_x \prod_{\alpha,c,f} d\psi_{\alpha,c,f}(x) d\overline{\psi}_{\alpha,c,f}(x), \tag{2.35}$$

where $d\psi$ and $d\overline{\psi}$ are Grassmann measures and α, c and f denote Dirac, color and flavour indices, and x is the discrete space-time coordinate. The fermion measure eq.(2.35) is completely regularized. The integration properties of Grassman variables are collected in Appendix A.6.

The measure for the gauge fields is defined by

$$\mathcal{D}[U] = \prod_x \prod_\mu dU_\mu(x), \tag{2.36}$$

where μ is a Lorentz index and dU is the Haar measure on $SU(N)$. Since the link variables take values on the compact space of $SU(N)$ (in contrast to the continuum, where the fields A_μ take values on the non-compact Lie algebra $su(N)$), the Haar measure dU is finite. It is conveniently normalized such that

$$\int_{SU(N_c)} dU = 1. \tag{2.37}$$

Moreover, there is no need to gauge fix on the lattice[13]. See appendix A.6 for the properties of the Haar measure.

Both Grassmann and Haar measures are gauge invariant. This ensures that only expectation values of gauge-invariant observables are non-zero.

Assuming degenerate quark masses, the path integral eq.(2.34) depends on only two parameters, i.e. the bare coupling g_0 and the bare quark mass m_0. Due to asymptotic

[13]In the lattice world there are no ghosts... unless you perturbate it!

freedom (see chapter 3), the continuum limit is reached by setting $g_0 \to 0$. The Wilson fermion action has been shown to be renormalizable to all orders in perturbation theory. As a consequence of the explicit breaking of chiral symmetry by the Wilson term in eq.(2.29), in the quantum theory the fermion mass acquires an additive renormalization besides the usual multiplicative renormalization. Assuming a mass independent renormalization scheme, the renormalization of the bare parameters follows the pattern

$$\begin{aligned} m_R(\mu) &= Z_m(g_0^2, a\mu) m_q(g_0^2, a), \qquad m_q = m_0 - m_c, \\ g_R^2(\mu) &= Z_g(g_0^2, a\mu) g_0^2(a), \end{aligned} \tag{2.38}$$

where μ is the renormalization scale and the Z_X factors are the usual multiplicative renormalization of the quantities X. The parameter m_c is called the *critical mass*. It comes into play multiplying a counterterm

$$\delta S = \sum_x m_c \overline{\psi}(x)\psi(x), \tag{2.39}$$

and it is linearly divergent with the inverse lattice spacing as $a \to 0$. Another consequence of the explicit breaking of chiral symmetry is that the leading cutoff effects are of order $O(a)$, in contrast to $O(a^2)$ behaviour expected for an action with chiral symmetry.

The non-perturbative formulation of lattice field theory provides a way to evaluate the functional integral eq.(2.33) without performing any perturbative expansion. In fact, in the Euclidean version of the theory the exponential of the action[14] $e^{-S_{\text{LQCD}}}$ plays the same role as the Boltzmann weight factor $e^{-\beta H}$ in statistical mechanics. After re-expressing the fermions as pseudofermions in the functional integral (see below), if the resulting action is real and bounded from below the path integral can be interpreted as a statistical system weigthed by the exponential factor $e^{-S_{\text{LQCD}}}$.

Due to the bilinear form of the fermion part of the action, the fermionic functional integral can be carried out analytically, and the path integral eq.(2.33) can be brought to a form more suitable to deal with in numerical calculations.[15] For that, we can

[14] In Minkowski space, the exponential factor is a highly oscillating phase e^{iS} unsuitable for a numerical approach.

[15] This way one avoids the problems of dealing with Grassmann variables numerically.

separate the expectation value into a gauge and a fermionic part as

$$\langle \mathcal{O} \rangle = \langle [\mathcal{O}]_{\mathrm{F}} \rangle_{\mathrm{G}} = \frac{1}{\mathcal{Z}} \int \mathcal{D}[U] \left[\mathcal{O}[\psi, \overline{\psi}, U] \right]_{\mathrm{F}} \mathcal{Z}_{\mathrm{F}}[U] e^{-S_{\mathrm{G}}[U]}, \tag{2.40}$$

where $\langle \cdot \rangle_{\mathrm{G}}$ denotes the expectation value over the gauge fields and $[\cdot]_{\mathrm{F}}$ is the expectation value over the fermion fields given by

$$[\mathcal{O}]_{\mathrm{F}} = \frac{1}{\mathcal{Z}_{\mathrm{F}}[U]} \int \mathcal{D}[\psi, \overline{\psi}] \mathcal{O}[\psi, \overline{\psi}, U] e^{-S_{\mathrm{F}}[\psi, \overline{\psi}, U]}. \tag{2.41}$$

The factor $\mathcal{Z}_{\mathrm{F}}[U]$ is the fermionic partition function

$$\mathcal{Z}_{\mathrm{F}}[U] = \int \mathcal{D}[\psi, \overline{\psi}] e^{-S_{\mathrm{F}}[\psi, \overline{\psi}, U]}. \tag{2.42}$$

Within eq.(2.41) and eq.(2.42), U is understood as an external field which is not an integration variable. At this point, eq.(2.42) can be calculated as a Grassman gaussian integral, leading to

$$\mathcal{Z}_{\mathrm{F}}[U] = (\det(D_m))\,[U], \tag{2.43}$$

with $D_m = D_{\mathrm{W}} + m_0$. The determinant of the massive Dirac opertor D_m is simply referred to as the *fermion determinant*. The original path integral eq.(2.33) can now be rewritten as

$$\langle \mathcal{O} \rangle = \frac{1}{\mathcal{Z}} \int \mathcal{D}[U] \widetilde{\mathcal{O}}[U] (\det(D_m))[U] e^{-S_{\mathrm{G}}[U]}, \tag{2.44}$$

with $\widetilde{\mathcal{O}}[U] = \left[\mathcal{O}[\psi, \overline{\psi}, U] \right]_{\mathrm{F}}$ and where the partition function is given by

$$\mathcal{Z} = \int \mathcal{D}[U] (\det(D_m))[U] e^{-S_{\mathrm{G}}[U]}. \tag{2.45}$$

The numerical Monte Carlo evaluation of expectation values $\langle \mathcal{O} \rangle$ consists in approximating the full integral eq.(2.44) by the average over an ensemble $\mathcal{U}$ of field configurations U_i

$$\frac{1}{\mathcal{Z}} \int \mathcal{D}[U] \widetilde{\mathcal{O}}[U] (\det(D_m))[U] e^{-S_{\mathcal{G}}[U]} \approx \frac{1}{N} \sum_{U_i \in \mathcal{U}} \widetilde{\mathcal{O}}[U_i] + O\left(\frac{1}{\sqrt{N}} \right). \tag{2.46}$$

The field configurations U_i are generated following a probability distribution density

$$dP(U_i) \sim \mathcal{D}[U_i](\det(D_m))[U_i]e^{-S_G[U_i]}. \tag{2.47}$$

This way of generating configurations ensures that the resulting ensemble $\mathcal{U}$ is composed of the configurations dominating the path integral. This technique is called *importance sampling*, and is widely used in statistical mechanics. The expectation value $\langle\mathcal{O}\rangle$ calculated this way would be exact in the limit $N \to \infty$. For a finite ensemble, the statistical errors on the average are of order $1/\sqrt{N}$.

Until here we have briefly discussed how to evaluate numerically the path integral via Monte Carlo techniques. We stress that it is possible to keep track of all the errors along the calculation. By evaluating $\langle\mathcal{O}\rangle$ a la Monte Carlo one is exchanging errors due to the truncation of a series in a perturbative approach with errors associated with a finite ensemble, which are purely statistical and can always be reduced by enlarging the size of the ensemble. Systematic errors due to the details of the regulator can also be estimated. Understanding the cutoff dependence of different discretizations is going to be the central goal of this thesis. In the following section we begin the description of a Symanzik's programme to understand and remove the cutoff effects of a lattice regulated theory.

2.3 Symanzik's effective theory and $O(a)$ improvement

One of the central ideas underlying renormalization is that the effects that the higher-energy modes have on the low-energy behaviour of a theory can be described by means of a new set of local interactions. This means that in presence of a cutoff Λ, the absence of modes of energies larger than Λ can be compensated by a modification of the original Lagrangian, such that the effects of the modes discarded by the regularization are retained. When the operator structure of the new set of interactions has the same form as the original Lagrangian, the new operators account for a modification of the bare parameters of the theory. If the operator structure is different, then the original Lagrangian is modified to include further terms, each with a new coefficient associated to it.

When the typical energy scales characteristic of a process are much smaller than

the cutoff $p \ll \Lambda$, the physical prediction for an observable $\mathcal{O}(p)$ is given by a series where the expansion parameter is the ratio p/Λ,

$$\mathcal{O}(p) = \mathcal{O}_\Lambda(p,\Lambda) + \sum_{i=1}^{\infty} \left(\frac{p}{\Lambda}\right)^i \mathcal{O}^{(i)}(p,\Lambda), \tag{2.48}$$

$\mathcal{O}_\Lambda(p,\Lambda)$ is the prediction for $\mathcal{O}(p)$ in the cutoff theory, and all the contributions $\mathcal{O}^{(i)}(p,\Lambda)$ within the sum correspond to the effects due to the eliminated modes. They can be reincorporated to the theory order by order in p/Λ, by including in the Lagrangian of the theory with cutoff a new set of local operators. Operators of dimension $4+n$ in the Lagrangian only affect observables to order $(p/\Lambda)^n$ and higher. Hence, in order to obtain a prediction with an accuracy of order $O\left((p/\Lambda)^n\right)$, one must include all interactions involving operators of dimension $n+4$ or less.

The form of the new interactions are fully specified by the symmetries of the regularized theory and the requirement of locality. The details of the dynamics of the high energy modes discarded by the regularization determine the values of the coefficients multiplying the new operators, but do not affect the structure of the operators themselves.

This kind of expansion is in some sense analogous to a multipolar expansion in classical electrodynamics. For example, the specific details of the charge distribution of an atomic nuclei are not relevant for the electrons in the atomic orbitals. The long-range effects of the short-distance structure of the nucleus can be characterised by a finite number of multipole moments (the number of moments depending only on the desired accuracy). The specifics of the nucleus will affect the coefficients of the moments, but not their form.

Symanzik's improvement programme basically accounts for the application of these ideas to the case of a theory with a lattice regulator. The absence of modes of momentum larger than $\Lambda = \pi/a$ is compensated by a new set of local interactions which respect the symmetries of the lattice theory.

In a lattice theory, the values of the lattice spacing a for which numerical calculations can in practice be performed are limited by the available computational capabilities. The way observables depend on a is inherent to the specific observable and to the particular lattice formulation chosen. For this reason, it is important to find formulations for which the leading discretization effects are of $O(a^2)$ rather than $O(a)$.

For the pure gauge theory governed by the Wilson gauge action, leading cutoff effects are already of $O(a^2)$. However, in a theory with fermions, the way observables scale with a depends on how chiral symmetry is realized on the discretized theory. Fermion actions obeying the Ginsparg-Wilson relation are affected by leading $O(a^2)$ effects, while for actions violating chiral symmetry the leading cutoff effects are of $O(a)$ [42].

Unfortunately, using formulations which respect the Ginsparg-Wilson relation is usually too computationally demanding. The remaining alternative is hence to choose formulations which do not respect the Ginsparg-Wilson relation, and eliminate the $O(a)$ discretization effects by means of Symanzik's improvement programme. These are called *improved formulations.*

In Symanzik's improvement programme the lattice theory is described in terms of a continuum local effective theory which respects all the symmetries of the underlying lattice theory. This serves as a parametrization of the cutoff effects of the lattice theory as the continuum limit is approached.[16] The knowledge of the operator structure describing lattice artefacts can be used to anticipate the form of lattice counterterms which can cancel such lattice artefacts. For this, a discretized version of the operators in the effective theory is written and added to the lattice theory.

The action of the effective theory has the general form

$$S_{\text{eff}} = S_0 + a\mathcal{S}_1 + a^2\mathcal{S}_2 + ..., \tag{2.49}$$

where S_0 represents the action of the "would be" continuum theory without cutoff effects, and the terms $\mathcal{S}_i$ account for the description of the lattice artefacts order by order in a. S_{eff} is called the *Symanzik effective action.* Written in terms of lagrangian densities reads,

$$S_{\text{eff}} = \int dx^4 \mathcal{L}_{\text{eff}}(x), \tag{2.50}$$

with the effective Lagrangian given by

$$\mathcal{L}_{\text{eff}}(x) = L_0(x) + a\mathcal{L}_1(x) + a^2\mathcal{L}_2(x) + ..., \tag{2.51}$$

[16]Note that this description only makes sense close to the continuum limit, where the length scales associated to the phenomena of interest are much larger than a. If a is not small enough, the situation would correspond to a cutoff theory where the expansion parameter p/Λ is not small, and hence the effective description would not be valid.

Here $L_0(x)$ is again the "would be" continuum Lagrangian and the $\mathcal{L}_k(x)$ terms are linear combinations of local composite fields of dimension $4+k$, with the same symmetries of the lattice action, and with coefficients c_i,

$$\mathcal{L}_k(x) = \sum_i c_i \mathcal{L}_k^{(i)}(x). \tag{2.52}$$

It is expected from perturbation theory that the coefficients c_i depend at most logarithmically on a [19].

In order to eliminate cutoff effects up to a certain order a^k in the lattice theory one first has to consider all possible operators of dimension $4+k$ in the effective theory. Once all the terms contributing to a specific order k are known, they are translated to a lattice discrete form

$$\mathcal{L}_k \longrightarrow L_k(x) = \sum_i \bar{c}_i L_k^{(i)}(x), \tag{2.53}$$

where $L_k^{(i)}$ denote the discrete versions of $\mathcal{L}_k^{(i)}$. Note that the coefficients c_i of the effective theory are not the same as the coefficients $\bar{c}_i$ multiplying the lattice operators. The Lagrangian terms L_k can then be added to the lattice action, and the coefficients $\bar{c}_i$ of the lattice theory can be tuned to cancel the lattice artefacts proportional to c_i in the effective theory.

The number of terms $\mathcal{L}_k^{(i)}(x)$ at a specific order in k can usually be reduced by restricting the improvement only to on-shell quantities. In this way, relations between different terms $\mathcal{L}_k^{(i)}$ can be found through the classical field equations, and some operators might be eliminated in favour of others.[17]

The $O(a^k)$-improved lattice action S_{I} is obtained by adding to the original lattice action all the terms of dimension $\leq k$ together with explicit powers of the lattice spacing

$$S_{\mathrm{I}} = S + \sum_x \sum_{i=1}^{k} a^i L_i(x). \tag{2.54}$$

The coefficients c_i within eq.(2.53) are fixed in practice by demanding the cancellation of the cutoff effects of $O(a^i)$ in some particular quantities. The specific choice of improvement conditions to impose will depend on every particular case.

[17] Although the field equations are purely classical, the elimination of $O(a)$-effects holds beyond tree level [43].

With the action $S_{\rm I}$ one obtains iprovement of the spectral quantities of the theory. However, in order to obtain improved correlation functions of local composite operators not only the action has to be improved but also the local interpolating fields entering the correlation functions. This can be done, in a similar way as for the action, by parametrizing the lattice artefacts of the composite operator through the effective theory.

Consider a local, gauge invariant, multiplicatively renormalized composite field operator

$$O_R(x) = Z_O O(x), \tag{2.55}$$

where Z_O is the renormalization factor of $O(x)$. The operator $O_R(x)$ in a lattice theory can be described by the continuum effective theory through an effective operator $O_{\rm eff}$ as

$$O_{\rm eff}(x) = O_0(x) + a\mathcal{O}_1(x) + a^2\mathcal{O}_2(x) + ... \tag{2.56}$$

$O_0(x)$ is the operator in the continuum theory and the terms $\mathcal{O}_k(x)$ are built as combinations of local composite operators which respect the same symmetries as the corresponding lattice interpolating field,

$$\mathcal{O}_k = \sum_i b_i \mathcal{O}_k^{(i)}(x). \tag{2.57}$$

The combinations $a^k\mathcal{O}_k(x)$ have the same dimensions as $O_0(x)$.

In this way, an expectation value of a product of the lattice interpolating field eq.(2.55)

$$\langle \mathbf{O}_R \rangle = \langle O_R(x_1)...O_R(x_n) \rangle, \qquad x_i \neq x_j, \tag{2.58}$$

can be described in terms of the effective theory. For that, one takes the expectation value of an operator $\mathbf{O}_{\rm eff}$ constructed with the effective fields eq.(2.56). Expanding the exponential factor of the effective action eq.(2.49) to $O(a)$[18], and using the effective description of the interpolating fields $O_{\rm eff}$, we can write the expectation value

$$\langle \mathbf{O}_{\rm eff} \rangle = \langle \mathbf{O}_0 \rangle_0 - a \int d^4y \langle \mathbf{O}_{\rm eff} \mathcal{L}_1(y) \rangle_0 + a\langle \mathbf{O}_1 \rangle_0 + O(a^2), \tag{2.59}$$

[18]We restrict here to $O(a)$ for clarity on our discussion. This process could be done to any order in a although, as we discuss at the end of this section, in many cases going beyond $O(a)$ improvement turns out to be impractical.

where $\langle\cdot\rangle_0$ denotes the expectation value taken with the action S_0, and

$$\begin{aligned}\mathbf{O}_0 &= O_0(x_1)...O_0(x_n),\\ \mathbf{O}_1 &= \sum_{k=1}^{n} O_0(x_1)...\mathcal{O}_1(x_k)...O_0(x_n).\end{aligned} \tag{2.60}$$

We remark again that the expansion eq.(2.59) makes sense only when the theory is close to the continuum limit, i.e. when a is small enough. The coefficients b_i multiplying the local composite operators within $O_k(x)$ in eq.(2.56) depend logarithmically on the lattice spacing [43]. [19]

Next, similarly to what is done for the improvement of the action, one can use the knowledge of the operators appearing in the effective description $\mathbf{O}_{\text{eff}}$ to anticipate the form of the lattice artefacts, and add to the lattice theory their respective discretized version. For this, one needs to translate the terms in the effective description eq.(2.56) to a lattice language. For $O(a)$-improvement, only the $\mathcal{O}_1$ term is needed,

$$\mathcal{O}_1(x) \longrightarrow O_1(x) = \sum_i \bar{b}_i O_1^{(i)}(x). \tag{2.61}$$

The coefficients $\bar{b}_i$ are tuned to cancel the b_i in the effective theory. The improved interpolating fields O_{I} are obtained by adding eq.(2.61) to the original lattice interpolator

$$O_{\text{I}}(x) = O(x) + a\sum_i \bar{b}_i O_1^{(i)}(x). \tag{2.62}$$

The coefficients $\bar{b}_i$ are determined in the same way as the $\bar{c}_i$, by demanding $O(a)$ effects to vanish from a specific quantity.

Symanzik's improvement program can be understood all together as the extension of the renormalization procedure to the level of irrelevant operators. Improvement conditions for the coefficients $\bar{c}_i$ and $\bar{b}_i$ are obtained by demanding specific quantities to be free from cutoff effects at a specific order. Different choices of improvement conditions at a given order will only induce effects at the following order and higher. Since $\bar{c}_i$ and $\bar{b}_i$ depend on the coupling g_0, one would ideally determine them non-perturbatively. In many situations this task can be too demanding, and a perturbative

[19] Divergences will appear when performing the integral over y in eq.(2.59) due to the occurrence of contact terms $x_k = y$ $(k = 1, ..., n)$. These can be reabsorbed in a redefinition of $O_1(x)$.

estimate of $\overline{c}_i$ and $\overline{b}_i$ is enough.

In principle one could carry out the improvement program to arbitrary order in a. However, this would become impractical due to the large amount of counterterms appearing at higher orders. In fact, for actions with fermions, $O(a^2)$ improvement would involve four fermion operators. Since the resulting action would not be bilinear in the fermion fields could not perform simulations in the way described at the end of section 2.2. Practically, $O(a)$ improvement is enough. The Symanzik improvement programme has been successfully applied to improve the pure Yang-Mills theory to $O(a^2)$, leading to the tree-level Symanzik gauge action [44] and to the Lüscher-Weisz gauge action [45].

Finally, the $O(a)$ improvement program has been applied successfully to remove cutoff effects from the Wilson fermion action eq.(2.27). The on-shell improved action is obtained by adding only one extra dimension 5 counterterm [46] to the action eq.(2.27). This counterterm is usually referred to as the *clover term*, which takes the form

$$\delta S_{\mathrm{SW}} = c_{\mathrm{SW}} \frac{i}{4} a^5 \sum_x \overline{\psi}(x) \sum_{\mu,\nu} \sigma_{\mu\nu} \widehat{F}_{\mu\nu}(x) \psi(x), \tag{2.63}$$

where c_{SW} is the so called Sheikholeslami-Wohlert coefficient, $\sigma_{\mu\nu} = \frac{i}{2}[\gamma_\mu, \gamma_\nu]$, and $\widehat{F}_{\mu\nu}(x)$ is the field strength tensor defined as

$$\widehat{F}_{\mu\nu}(x) = \frac{1}{8a^2} \left\{ Q_{\mu\nu}(x) - Q_{\nu\mu}(x) \right\}, \tag{2.64}$$

with

$$\begin{aligned} Q_{\mu\nu}(x) = {} & U_\mu(x) U_\nu(x + a\hat{\mu}) U_\mu(x + a\hat{\nu})^\dagger U_\nu(x)^\dagger \\ & + U_\nu(x) U_\mu(x - a\hat{\mu} + a\hat{\nu})^\dagger U_\nu(x - a\hat{\mu})^\dagger U_\mu(x - a\hat{\mu}) \\ & + U_\mu(x - a\hat{\mu})^\dagger U_\nu(x - a\hat{\mu} - a\hat{\nu})^\dagger U_\nu(x - a\hat{\mu} - a\hat{\nu})^\dagger U_\mu(x - a\hat{\nu}) \\ & + U_\mu(x - a\hat{\nu})^\dagger U_\mu(x - a\hat{\nu})^\dagger U_\nu(x + a\hat{\mu} - a\hat{\nu}) U_\mu(x)^\dagger. \end{aligned} \tag{2.65}$$

The $O(a)$ improved Wilson fermion action is hence refered to as the *clover action* or *clover regularization*, given by

$$S_{\mathrm{F}}[\psi, \overline{\psi}, U] = a^4 \sum_x \overline{\psi}(x) \left(D_{\mathrm{WI}} + m_0 \right) \psi(x), \tag{2.66}$$

where the improved Dirac operator D_{WI} includes the clover term

$$D_{\mathrm{WI}} = \sum_{\mu} \frac{1}{2} \left\{ \gamma_\mu \left(\nabla_\mu + \nabla^*_\mu \right) - a \nabla^*_\mu \nabla_\mu \right\} + c_{\mathrm{SW}} \frac{i}{4} a \sum_{\mu,\nu} \sigma_{\mu\nu} \widehat{F}_{\mu\nu}. \tag{2.67}$$

The need for $O(a)$ improvement for Wilson fermions arise as a consequence of the explicit breaking of chiral symmetry due to the Wilson term. It is possible to turn this argument around and use chiral Ward identities to impose the restoration of chiral symmetry as tuning condition for the c_{SW} coefficient (and for the coefficients needed to improve the composite fields). In the rest of the thesis we will always use the clover regularization of the fermion action.

"Don't move! He can't see us if we don't move."

Dr. Alan Grant

3

Non-perturbative renormalization

Divergences in quantum field theories appear ultimately due to the fact that the short-distance structure of quantum fields is relevant for the long-distance properties of the theory. In order to render any quantum field theory predictive it first has to go through the process of renormalization. In this chapter we will review the need of renormalizing a theory in a non-perturbative fashion. We will discuss the application of non-perturbative renormalization by means of finite volume schemes in two different contexts. In sections 3.2 and 3.3 we discuss the determination of the fundamental parameters of QCD from hadronic quantities. In section 3.4 we examine the search for infrared fixed points in would be conformal field theories in four dimensions.

3.1 Why go non-perturbative?

The starting point in the renormalization process consists in regulating the theory by eliminating all the modes of momenta larger than a cutoff. Let's consider an

$SU(N)$ gauge theory coupled to N_f mass degenerate quarks, such that the only bare parameters of the theory are the bare coupling g_0 and the bare quark mass m_0. For this discussion, lets consider a lattice regulator as described in section 2.2, such that the cutoff scale is related to the lattice spacing by $\Lambda = \pi/a$. Removing the cutoff corresponds to take the continuum limit $a \to 0$ (see section 2.2). The removal of the high energy modes due to the regularization can be compensated by a readjustment of the bare parameters in the Lagrangian of the cutoff theory. This is done by imposing some renormalization conditions, i.e. by demanding some set of observables of the theory to adopt prescribed values. After the bare parameters are tuned such that the given renormalization conditions are satisfied, all physical quantities remain finite and can be calculated. Observables are hence functions of the bare parameters of the theory and of the lattice spacing, $\mathcal{O}(g_0, m_0, a)$. The regulated theory is then predictive up to effects of $O(a^k)$ which originate due to the removed high momentum modes, where the power k depends on the details of the regularization as discussed in section 2.3.

The cutoff is, however, an artificial notion without physical meaning which will ultimately be removed. As the lattice spacing is sent to zero $a \to 0$, the bare parameters should be modified accordingly such that physical observables remain unchanged. Demanding a physical observable to be independent on the lattice spacing a leads to the *Callan-Symanzik equations*. In a mass independent renormalization scheme, the Callan-Symanzik equation for the obervable $\mathcal{O}$ reads

$$\left\{ a\frac{\partial}{\partial a} + \beta(g_0)\frac{\partial}{\partial g_0} - \gamma_m(g_0)m_0\frac{\partial}{\partial m_0} - \gamma_{\mathcal{O}}(g_0) \right\} \mathcal{O}(g_0, m_0, \Lambda) = 0. \tag{3.1}$$

The functions $\beta(g_0)$, $\gamma_m(g_0)$ and $\gamma_{\mathcal{O}}(g_0)$ are the *β-funtion*, the *mass anomalous dimension* and the *anomalous dimension* of $\mathcal{O}$ respectively. *β-funtion* and *mass anomalous dimension* are defined as

$$\beta(g_0) = a\frac{\partial g_0}{\partial a}; \qquad \gamma_m(g_0) = -\frac{a}{m_0}\frac{\partial m_0}{\partial a}. \tag{3.2}$$

and they determine the dependence of the bare parameters on the cutoff such that physical observables are left unchanged by a modification of a. This is known as the Wilson-Kadanoff (WK) renormalization group, which tells us about how do bare couplings need to be changed as a function of the cutoff scale a such that physical

quantities are left invariant, in contrast to the Gell-Man Low (GL) renormalization group, which tells about how do physical couplings need to be changed as a function of a renormalization scale μ such that physical quantities are left invariant.[1]

The renormalized version of the quantum field theory is obtained by defining the continuum limit. The way the bare parameters g_0 and m_0 have to be modified when taking the continuum limit is determined by eq.(3.2).

The β-function can be expanded in perturbation theory as a power series in the bare coupling g_0. For $SU(N)$ theories with N_f massless fermions, the expansion is given by

$$\beta(g_0) = -b_0 g_0^3 - b_1 g_0^5 + O(g_0^7), \tag{3.3}$$

with the first coefficients, which are independent of the renormalization scheme, given by

$$b_0 = \frac{1}{(4\pi)^2}\left(\frac{11}{3}N - \frac{2}{3}N_f\right), \tag{3.4}$$

$$b_1 = \frac{1}{(4\pi)^4}\left(\frac{34}{3}N^2 - \frac{10}{3}NN_f - \frac{N^2-1}{N}N_f\right). \tag{3.5}$$

For theories with $b_0 > 0$, the bare coupling $g_0 \to 0$ as the cutoff a is sent to 0. These kind of theories are called asymptotically free theories.

The asymptotic form of the β function is the same in both WK and GL renormalization groups. Inserting the expansion eq.(3.3) into eq.(3.2) the latter can be integrated obtaining the relation

$$g(a)^{-2} = b_0 \ln\left(a^{-2}\Lambda_{\rm L}^{-2}\right) + \frac{b_1}{b_0}\ln\left(\ln\left(a^{-2}\Lambda_{\rm L}^{-2}\right)\right) + O\left(1/\ln(a^2\Lambda_{\rm L}^2)\right), \tag{3.6}$$

where $\Lambda_{\rm L}$ is the $\Lambda_{\rm QCD}$ parameter of QCD in the lattice scheme being used. It is important for the present discussion to keep in mind that asymptotic freedom implies that the bare coupling $g_0 \to 0$ as $a \to 0$. As a consequence the continuum limit in an asymptotically free lattice theory is taken by sending the bare coupling g_0 to 0. Another consequence of eq.(3.6) is that a perturbative expansion in terms of g_0 is valid provided that we are close enough to the continuum limit.[2]

[1] In fact, the words "renormalization group" are commonly used for referring both WK and GL, and it is the context which specifies to which of the two one is referring to.

[2] In the Gell-Mann Low renormalization group, asymptotic freedom implies that the renormalized coupling $g_R \to 0$ at high energies $\mu \to 0$.

QCD is an asymptotically free theory. At high energies the physical coupling is small and perturbation theory has been successfully applied to make predictions about cross sections and other processes. However, at energy scales of the order of $\Lambda_{\rm QCD}$ (which are the scales of hadronic physics) a perturbative expansion in terms of the renormalized coupling g_R does not make sense at all. A non-perturbative solution of the theory is required in order to make predictions of the low-energy sector. Unfortunately, there are very few analytic tools available, and very often the only way to determine physics at low-energies is through numerical calculations performed using the lattice formulation of the theory.

Since the bare coupling g_0 becomes weak at small values of a, one might expect to carry the renormalization of the lattice theory perturbatively in terms of g_0.[3] However, calculations of hadronic quantities must be done numerically by evaluating the path integral with Monte Carlo techniques, which require a finite number of degrees of freedom.[4] Hence, computations have to be done with a finite cutoff and, unfortunately, simulations where a is much smaller than the relevant length scales are not possible. In this context, the lattice spacing a is generally not small enough to justify a perturbative expansion in terms of g_0^2. Moreover, the perturbative series in g_0^2 are known to be poorly convergent [47]. Hence, in order to have access to the low-energy sector of the theory, one has to perform the renormalization process non-perturbatively.

Since the formulation of field theories on a lattice is a non-perturbative formulation, it opens the possibility of connecting the high-energy and low-energy sectors of a theory. A theory can be renormalized at low-energies using hadronic experimental inputs and then used to predict high-energy observables. This is particularly relevant, for eample, for the determination of the fundamental parameters of QCD (the QCD scale $\Lambda_{\rm QCD}$ and the invariant quark masses). Once they are determined in terms of low energy constants, which usually have less experimental errors than observables measured at high energies, they can be used as input parameters in the perturbative evaluation of high-energy processes such as jet cross sections.

In the following section we discuss this considering a particular example.

[3] We emphasize again that a perturbative expansion in terms of g_0 is valid close to the continuum limit (i.e. when a is small) independently whether we are at low or high energies.

[4] In fact, with contemporary computational capabilities, a not too large number of degrees of freedom is needed to perform calculations in reasonable times.

3.2 Extracting fundamental parameters of QCD

In order to obtain the running coupling $\alpha = g^2/4\pi$ from experiments one starts by considering an experimental observable $\mathcal{O}(\mu, y)$, which depends on a scale μ and on a set of possible kinematic variables collectively denoted by y.[5] At high energies, $\mathcal{O}(\mu, y)$ can be expanded as a perturbative series of a coupling α_X defined in a specific renormalization scheme X,

$$\mathcal{O}(\mu, y) = A_X(y) + B_X(y)\alpha_X(\mu) + C_X(y)\alpha_X(\mu)^2 + O(\alpha_X^3). \tag{3.7}$$

One can thus use the expansion of the observable $\mathcal{O}(\mu, y)$ as a definition of the running coupling. The running coupling $\alpha_X(\mu)$ is determined first by calculating a few terms A_X, B_X,..., in the expansion eq.(3.7), and then measuring experimentally the observable $\mathcal{O}$. After this, the value of α_X can be extracted directly from eq.(3.7).

The dependence of the QCD parameters on energy is described by the Gell-Mann Low renormalization group. For simplicity, as in section 3.1 we will consider only mass-independent renormalization schemes, such that the β-function (and hence the renormalized coupling) does not depend on the fermion mass.

The RG equation for the coupling $\alpha_X = g_X^2/4\pi$ is given by

$$\mu \frac{\partial g_X}{\partial \mu} = \beta_X(g_X), \tag{3.8}$$

where the β-function in the scheme X has an asymptotic expansion in terms of the renormalized coupling

$$\beta_X(g_X) = -b_0 g_X^3 - b_1 g_X^5 + O(g_X^7), \tag{3.9}$$

and the coefficients b_0 and b_1 are the same as in eq.(3.5). For theories with $b_0 > 0$, eq.(3.9) encodes asymptotic freedom. When inserted into eq.(3.8), the coupling g_X decreases for increasing μ. Since b_0 and b_1 are scheme independent, this general trend will be independent of the particular definition of α_X.

[5] The observable $\mathcal{O}(\mu, y)$ can be any high energy experimental quantity, i.e. jet production ratios, cross-sections for specific scattering processes,...

A special solution to the Callan-Simanzik equation is given by

$$\Lambda_X = \mu \left(b_0 g_X^2\right)^{-\frac{b_1}{(2b_0^2)}} e^{-\frac{1}{(2b_0 g_X^2)}} \exp\left\{-\int_0^{g_X} dx \left[\frac{1}{\beta_X(x)}\frac{1}{b_0 x^3} - \frac{b_1}{b_0^2 x}\right]\right\}, \tag{3.10}$$

called the *Lambda parameter of QCD* in the scheme X. Λ_X is a dimensionful quantity which sets the typical scale for QCD processes. It is a renormalization group invariant (independent on the scale μ) and scheme dependent quantity.

Other couplings α_Y might be defined in another scheme Y. Any renormalized coupling can be related to α_X at high energies through a series of the form[6]

$$\alpha_Y(s\mu) = \alpha_X(\mu) + c_{YX}^{(1)}(s)\alpha_X(\mu)^2 + C_{YX}^{(2)}(s)\alpha_X(\mu)^3 + O(\alpha_X^4), \tag{3.11}$$

where s is simply a scale factor and $c_{YX}^{(i)}$ are coefficients relating the couplings in the two schemes X and Y. The Λ_Y parameter in the Y scheme is related to Λ_X through

$$\frac{\Lambda_X}{\Lambda_Y} = \exp\left\{-\frac{c_{YX}^{(1)}}{(8\pi b_0)}\right\}. \tag{3.12}$$

Although eq.(3.12) depends on the 1-loop coefficient $c_{YX}^{(1)}$ relating the couplings α_Y and α_X it is an exact expression without any errors associated to the truncation of a perturbative expansion. Since Λ_X is a RG invariant quantity, it can be evaluated at any scale μ. The relation eq.(3.12) is hence obtained by comparing eq.(3.10) for the two schemes X and Y, evaluated in the limit $\mu \to \infty$, for which both couplings $g_X(\mu) \to 0$ and $g_Y(\mu) \to 0$ due to asymptotic freedom.

Conventionally, the most widely used scheme for phenomenological computations of processes at high-energies is the $\overline{\text{MS}}$ scheme. For this reason one would ultimately like to relate the coupling α_X and Λ_X parameter obtained in a given scheme X to the more commonly used $\overline{\text{MS}}$ scheme.

The determination of $\alpha_{\overline{\text{MS}}}$ and $\Lambda_{\overline{\text{MS}}}$ from the relation to a scheme X in which quantities can be measured experimentally will have associated errors arising due to two different reasons. Firstly, if α_X is obtained from the expansion eq.(3.7), it will lack any non-perturbative effect like confinement. Even within the perturbative region, the precision reached will be limited by the higher order terms left out of

[6] Any observable $\mathcal{O}$ can be used to define a coupling by means of its perturbative expansion in terms of α_X given by eq.(3.7).

the expansion and also by the absence of possible non-perturbative contributions. Secondly, experimental errors in the determination of the observable $\mathcal{O}(\mu, y)$ will be propagated to α_X and subsequently to $\alpha_{\overline{\rm MS}}$.

The non-perturbative regularization provided by the lattice formulation of field theories permits to circumvent these sources of errors. On one hand, a fully non-perturbative definition of a running coupling can be established, avoiding any errors associated to the truncation of a perturbative expansion like eq.(3.7). On the other hand, a coupling defined in this way can be evaluated in the non-perturbative low energy regime and evolved from low-energies to high energies. Connection to experiments can be done at low energies through observables such as hadron masses or decay constants. The experimental errors associated to such observables are usually much lower than the errors in high energy observables, and hence the induced error in $\alpha_{\overline{\rm MS}}$ when matching between schemes is lower as well.

A very appealing possibility to determine $\alpha_{\overline{\rm MS}}$ is then to establish a non-perturbative definition of a running coupling, connected to experiments at low energies and evolved non-perturbatively to high energies where it can be matched to the $\overline{\rm MS}$ scheme, with a complete control over all error sources. This approach is valid not only for the coupling, but for any scale dependent renormalization parameter like the running quark masses and the renormalization factors of any general composite field operator. Moreover, this kind of strategy constitutes a bridge between the low-energy and the high energy sectors of the theory, thus proving that QCD is indeed a correct description of strong interactions both in the hadronic world and in the scales of high energy collisions.

3.3 Finite size scaling

When trying to establish the connection between high energies and low energies as described in the previous subsection one has to face a clear limitation. Lets assume we have given a non-perturbative definition of the coupling $\alpha(\mu)$. This will be defined in a lattice regulated theory, since the lattice regulator is the only one of non-perturbative nature. In order to make connection with perturbation theory one should be able to evaluate $\alpha(\mu)$ at least at a scale $\mu \sim 10GeV$, which is the typical scale for which PT begins to be reliable in QCD. Then, in order to avoid cutoff effects, the value of the

cutoff should be well above the scale μ

$$\mu \sim 10\text{GeV} \ll 1/a, \tag{3.13}$$

such that extrapolations to the continuum limit can be safely performed. On the other hand, the physical size L of the lattice should be large enough to avoid finite size effects. This means that the volume has to be larger than the largest length scale appearing in the theory, that is, the inverse of the pion mass m_π^{-1},

$$L \gg m_\pi^{-1} \sim 7 \text{ GeV}^{-1} \sim 1.4 \text{ fm}. \tag{3.14}$$

For the pure Yang-Mills theory this same requirement can be expressed in terms of the confinement scale $\sigma^{-1/2} \sim 0.5$ fm.

Bringing together these two considerations one obtains a condition for the range of scales L and a which a single lattice should fulfil, given by

$$L \gg m_\pi^{-1} \sim 7 \text{ GeV}^{-1} \gg \frac{1}{\mu} \sim 0.1 \text{ GeV}^{-1} \gg a. \tag{3.15}$$

This means that numerical calculations should be performed with lattices of size l^4, with $l \equiv L/a \gg 70$ (or $l \equiv L/a \gg 25$ for the pure Yang-Mills theory). Naïve estimates require $l \sim O(10^2)$ and even $O(10^3)$ [48], which is well beyond the computational possibilities at present times and even in the near future. It is too difficult to fit into a single lattice the wide energy range needed to have control over both low-energy hadronic physics and the high energy perturbative regime.

This problem can be bypassed by using finite volume schemes [22] in which one identifies the physical volume of the system with the renormalization scale as

$$\mu = \frac{1}{L}. \tag{3.16}$$

This eliminates the lower end restriction in eq.(3.15).[7] The original problem of considering a wide range of scales is then decomposed into several steps by considering a sequence of physical volumes associated to a sequence of physical scales. A running coupling $\alpha_{\text{FV}}(\mu)$ can be defined in the finite volume scheme. The evolution of renor-

[7] In fact, by doing the identification eq.(3.16) one is taking a finite volue effect as a physical observable

malized coupling $\alpha(\mu)$ with $\mu = 1/L$ can be computed in each step in the sequence. Each step is taken to be small enough such that large scale differences do not occur. The condition eq.(3.15) is hence relaxed simply to $L/a \gg 1$. The energy μ is increased by decreasing L, until the perturbative regime is reached and perturbation theory can be safely applied.

The connection between low and high energies is established as follows. At low energies, the lattice spacing is expressed in physical units [8] using experimental values of hadronic observables. This defines a low energy hadronic scheme (see section 3.3.1). Once the scale is set via hadronic observables, a renormalized coupling $\alpha_{\mathrm{FV}}(\mu)$ is computed sequentially by means of a non-perturbatively defined finite volume scheme, all the way up to the perturbative scales. There, connection is made with perturbative schemes like the $\overline{\mathrm{MS}}$.

The whole process is summarised in the diagram of fig.(3.3.1). The role that the finite volume scheme plays is to be an intermediate scheme to bridge the gap between the hadronic an the perturbative scales.

In order for this strategy to work in practice, the coupling α_{FV} in the finite volume scheme must fulfil, however, some requirements (and so do the other renormalization parameters to be computed using the finite volume scheme). To begin with, it must display small statistical uncertainties when evaluated numerically by means of Monte Carlo techniques, such that it is a computationally accessible observable. Moreover, cutoff effects associated to α_{FV} should be small, such that continuum extrapolations can be performed in a controlled way. Finally, α_{FV} should have a relatively easy to handle perturbative expansion, such that the β-function can be computed at sufficient order and, once the perturbative scales are reached, a good control of the perturbative evolution is achieved.

An example of schemes satisfying these requirements are based on the Schrödinger Functional, which was originally introduced in the context of finite volume schemes in [23] and will be reviewed in detail in chapter 4. By today SF schemes have been successfully applied in computing the running coupling in several occasions by many different groups.[9]

In the following subsections we will discuss the different steps of the strategy sum-

[8] In lattice slang this is called *scale setting*.

[9] E.g. [49, 50] for the pure Yang-Mills theory with $N = 2$ and 3, [27, 29] for QCD with $N_f = 2$ and 4 flavours respectively, and [31–34] for other strongly coupling theories.

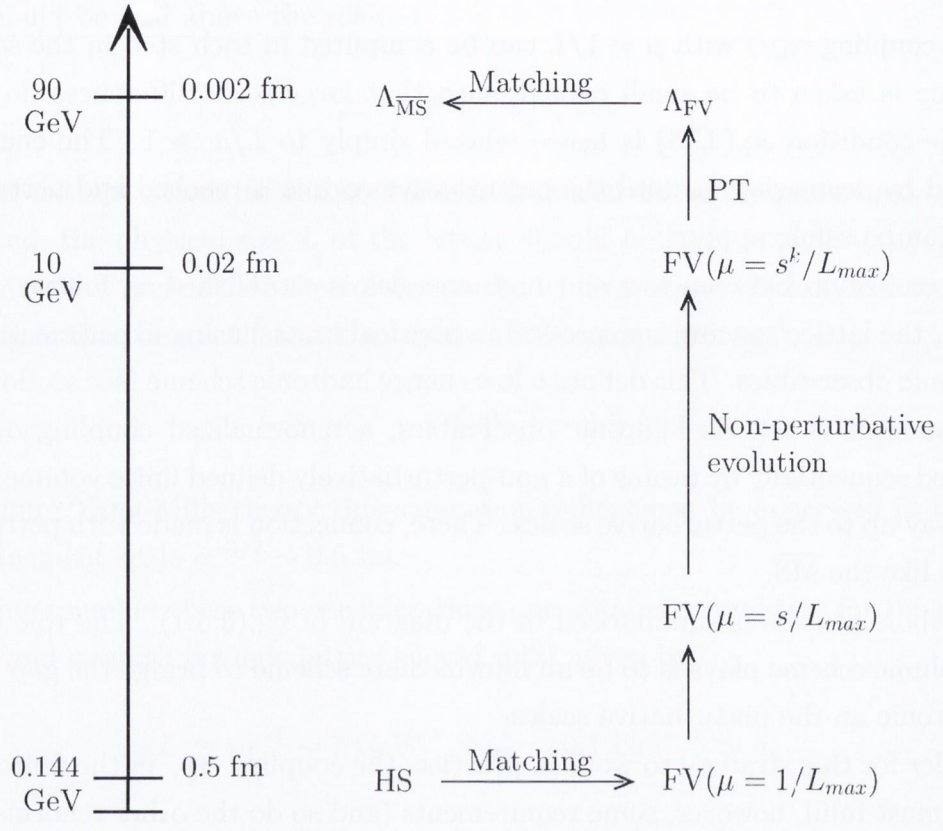

Figure 3.3.1: Sketch of the full strategy of connecting the low energy hadronic regime of QCD with the high energy perturbative regime by means of a finite volume renormalization scheme.

marised in diagram fig.(3.3.1).

3.3.1 Hadronic Schemes and matching at low energies

At low energies it is common to renormalize the theory in terms of a hadronic scheme. In these schemes, one imposes as a renormalization condition that certain hadron masses computed in the lattice theory adopt their real values measured in experiments. This fixes the values of the bare coupling g_0 and the bare quark masses in units of the lattice spacing am_0.

For example, consider a theory with three flavours of quarks with bare masses $m_{0,f}$, $f = u, d, s$. For simplicity, lets assume isospin symmetry is exact $m_{0,u} = m_{0,d} = m_{0,l}$.[10] The masses m_H for a generic hadron H can be extracted from suitable 2-point

[10] We ignore heavier quarks to avoid any complication involving heavy quarks on the lattice.

functions, and will depend on the bare parameters

$$am_H = am_H(g_0, am_{0,l}, am_{0,s}). \tag{3.17}$$

For the renormalization of the theory one has to choose specific hadrons, i.e. $H = p, \pi, K$ for the proton, the pion and the kaon and demand their masses to be equal to their experimental values.[11]

For a specific value of g_0, one fixes the bare masses of the quarks such that the set of conditions

$$\frac{(am_H)}{(am_p)} = \frac{m_H^{\rm exp}}{m_p^{\rm exp}}, \qquad H = \pi, K, \tag{3.18}$$

are satisfied.

A different choice of hadrons leads to another set of renormalization conditions and hence to a different scheme. Then, the lattice spacing can be obtained in physical units by[12]

$$a = \frac{am_p}{m_p^{\rm exp}}. \tag{3.19}$$

Note that eqs.(3.18) and (3.19) are not independent but form a system of coupled equations.

Once the bare parameters have been fixed, the theory has been renormalized[13]. The renormalized theory is predictive and any other quantity can be computed up to cutoff effects. For example, the physical pion decay constant F_π in physical units can be extracted from a lattice calculation through

$$F_\pi = \frac{(aF_\pi)}{a}(1 + O(a)). \tag{3.20}$$

In order to remove the cutoff, this process is repeated at several values of the lattice spacing a such that a controlled continuum extrapolation can be performed.

After the hadronic scheme has been properly set up, the *matching at low energies* between the HS and the FV scheme can be done. This consists in expressing the scale $L_{\rm max}$ of the FV scheme in terms of a hadronic quantity, which in the present example

[11] In practice, using pseudo-scalars is always a good choice since their signal in lattice QCD calculations is usually very clear.

[12] In practice m_p is never used for setting the scale since baryons suffer from signal-to-noise problems. One typically uses the Sommer parameter r_0 [51] or some decay constant F_H, although it is irrelevant for the present discussion.

[13] The bare parameters have been eliminated in favour of some physical quantities.

would be m_p^{-1}. This is done at a matching point where both the coupling $\overline{g}^2_{\mathrm{FV}}(L_{\max})$ in the FV scheme and the hadronic scale in the HS can be properly determined. In this point, the coupling adopts a specific value

$$\overline{g}^2_{\mathrm{FV}}(L_{\max}) = u_0, \tag{3.21}$$

and it is the starting point for the non-perturbative scale evolution towards the high energy regime.

3.3.2 Non-perturbative evolution: Step Scaling

After the connection with the HS has been established, the coupling $\overline{g}^2_{\mathrm{FV}}(L)$ in the FV scheme is ready to be evaluated at several scales. The evolution of the coupling is given by the RG equations eq.(3.8) and dictated by the β-function. If the exact form of the β-function was known then the integration of the RG equations would be possible and, given an initial value of $\overline{g}^2_{\mathrm{FV}}(L)$ at a certain scale, the coupling at any other scale $L' = sL$ could be determined (s being a multiplicative factor). This leads to the definition of the *step scaling function* (SSF), which corresponds to the value of the coupling at the scale $L' = sL$ provided that the coupling at the initial scale L is known,

$$\overline{g}^2_{\mathrm{FV}}(sL) = \sigma(s, \overline{g}^2_{\mathrm{FV}}(L)). \tag{3.22}$$

The SSF can be regarded as an integrated version of the β-function. The two are related via[14]

$$\int_{\bar{g}(L)}^{\sqrt{\sigma(s,\bar{g}^2(L))}} \frac{d\bar{g}}{\beta(\bar{g})} = -\int_L^{sL} \frac{dL'}{L'} = -\ln(s). \tag{3.23}$$

Knowing the SSF permits to reconstruct the running of the coupling $\overline{g}^2_{\mathrm{FV}}(L)$ in a recursive way, starting with an initial value $u_0 = \overline{g}^2_{\mathrm{FV}}(L_{\max})$ and obtaining a sequence of couplings

$$u_k = \overline{g}^2_{\mathrm{FV}}(s^{-k}L), \tag{3.24}$$

evaluated at discrete steps s of the scale. Starting from the hadronic scale, the running coupling can then be evolved to the perturbative scale.

However, the β-function can only be determined analytically to a given order in

[14]Note that since the relation eq.(3.23) is valid for any scheme, we have omitted the subscript referring to the FV scheme here.

perturbation theory and hence a non-perturbative form of $\sigma(s,u)$ must be obtained before the coupling can be evolved. For obtaining the non-perturbative form of the SSF, one thus has to determine $\sigma(s,u)$ from the lattice theory. The lattice form of the SSF is defined as

$$\Sigma(s,u,a/L) = \overline{g}^2_{\rm FV}(sL)\big|_{u=\overline{g}^2_{\rm FV}(L)}\,, \tag{3.25}$$

where g_0 and L/a are fixed. As any other lattice quantity, Σ is subjected to cutoff effects. Hence, to obtain the continuum SSF σ, one must compute $\Sigma(s,u,a/L)$ at several values of a/L and take the continuum limit

$$\lim_{a/L\to 0} \Sigma(s,u,a/L) = \sigma(s,u). \tag{3.26}$$

The full procedure to obtain σ can be summarised in the following steps[15]

- First, the number of lattice points is chosen by fixing the ratio L/a. This sets the resolution in the computation.

- Then, for that value of L/a, the bare coupling g_0 is tuned such that $\overline{g}^2_{\rm FV}(L)$ adopts a specific value of u (renormalization). At this stage the physical volume has been fixed.

- Next, keeping fixed the bare coupling g_0 (and hence the lattice spacing a), the coupling $\overline{g}^2_{\rm FV}(sL)$ is evaluated at a scale sL by simulating on a lattice of volume sL/a. This determines the lattice step scaling function $\Sigma(s,u,a/L)$.

- Repeating this at several values of L/a, the continuum limit is taken and one obtains the continuum step scaling function $\sigma(s,u)$, describing the evolution of $\overline{g}^2_{\rm FV}$ from a scale L to sL.

- This procedure is repeated k times, starting from a value L in the perturbative regime, and going down in energies to the scale $s^kL = L_{\rm max}$ where the matching is done to the Hadronic Scheme.

[15]Note that in the determination of σ one starts at the value of a coupling at high energies and determines a sequence of couplings at lower energies by scaling up the volume of the lattice. Once σ is reconstructed, then the evolution of the coupling is traced from the hadronic scale up to the perturbative scale.

From the data generated through this procedure the SSF can be parametrized as a function of $\overline{g}^2_{\rm FV}(L)$. Once σ is extracted this way, given the initial value of the renormalized coupling $\overline{g}^2_{\rm FV}(L_{\rm max}) = u_0$ at the matching scale, its evolution can be traced up to high energies recursively.

The step scaling function is the central quantity in a finite volume scheme and its precise determination is the main point of many studies. We will study the lattice SSF in perturbation theory and its convergence towards the continuum limit for QCD in section 6.3.4, and for other strongly interacting theories in section 7.1.4.

3.3.3 Evolution at high energies and connection to a perturbative scheme

Once the non-perturbative evolution has been carried out all the way into the perturbative regime at high energies, from this point on the evolution of the coupling can be determined safely by perturbation theory.

At this stage one can perform perturbative expansions in the FV scheme and compute the usual quantities. For instance, from eq.(3.10) the value of $\Lambda_{\rm FV}L$ can be determined in perturbation theory in the FV scheme. Thus, it can be given in units of $L_{\rm max}$, which is subsequently related to a hadronic quantity m_p^{-1} via the matching with the HS.

Once $\Lambda_{\rm FV}$ is known in units of the hadronic scale, the conversion to the perturbative scheme can be performed. The renormalized coupling $\overline{g}^2_{\rm FV}$ can be related to a coupling defined in the $\overline{\rm MS}$ by means of eq.(3.11). Then the parameter $\Lambda_{\overline{\rm MS}}$ in the $\overline{\rm MS}$ scheme is obtained by relating it with $\Lambda_{\rm FV}$ at infinite energy through eq.(3.12). The relation between the coupling in the Schrödinger Functional (introduced in chapter 4) to the $\overline{\rm MS}$ scheme is known up to 2 loops [27, 52].

The final outcome of all this process is $\Lambda_{\overline{\rm MS}}$ determined from hadronic quantities.[16] Before concluding, we remind that other renormalization parameters can of course be computed this way. This strategy has been successfully applied in several occasions [27, 29, 49, 50].

[16] The FV scheme has been an intermediate scheme to bridge the gap between low and high energies, and ultimately must be abandoned in favour of a perturbative scheme useful in phenomenology.

3.4 Looking for an Infra Red fixed point

QCD is the only strongly interacting gauge theory to manifest itself in nature so far. However, it is not the only confining or asymptotically free theory that can be constructed. In fact, it belongs to a wide family of models consisting in Yang-Mills fields coupled to matter, this last represented by a number of fermion fields transforming under a specific representation of the gauge group. These models can be described by means of the generic Lagrangian

$$\mathcal{L} = -\frac{1}{2g^2}\mathrm{tr}\left[F_{\mu\nu}F_{\mu\nu}\right] + \overline{\psi}(x)\left(\gamma_\mu D_\mu + m\right)\psi(x), \tag{3.27}$$

where the gauge group and the flavour content are left unspecified. This is the same Lagrangian that leads to the QCD action, which we have written explicitly for clarity in the present discussion.

A particular theory within the family described by eq.(3.27) is obtained by specifying the rank N of the gauge group $SU(N)$, the number of fermionic flavours N_f in the theory, and the representation $\mathcal{R}$ of the gauge group under which the fermions transform. In principle one can construct theories in which different fermions transform under different representations, or where other kinds of gauge groups are considered like symplectic groups $Sp(N)$. We will not consider these possibilities in the following. Within the family described by eq.(3.27), QCD is recovered by choosing $N = 3$, $N_f = 6$ flavours, and $\mathcal{R}$ to be the fundamental representation of $SU(3)$.

Other theories might have properties very different to those of QCD, like the absence of confinement or spontaneous chiral symmetry breaking, or the presence of phenomena associated to a situation where conformal symmetry is restored at low energies.

The original interest on these exotic theories beyond QCD was motivated by the possibility of using them as candidates for extending the Standard Model (see chapter 1). Strongly coupled theories play an essential role for models of Dynamical Electroweak Symmetry Breaking (DESB), where the standard realisation of the Higgs mechanism is triggered by the spontaneous chiral symmetry breaking in the new strongly interaction sector.[17] Further motivation came from the interest in under-

[17]Since the recent discovery of a light Higgs-like particle [5, 6], some of these ideas have become obsolete. However, the number of possible models that can be constructed using strongly-coupled theories is enormous, and some of them have been shown to posses a light-scalar on their spectrum

standing conformal symmetry in four dimensional quantum field theories and the AdS/CFT correspondence.

In this thesis we will adopt the rather conservative perspective of considering all these theories simply as mathematical objects which can be studied using the same kind of techniques developed for QCD, without worrying about their application for model building or for other exotic (though exciting) theoretical applications.

Strongly-coupled theories described by eq.(3.27) are in fact well suited for numerical simulations using lattice techniques. In the following, we review some of the observables of interest in these theories and discuss the role that finite volume schemes can play on their calculation.

3.4.1 Confining or Conformal?

For massless fermions the classical lagrangian eq.(3.27) is invariant under scale transformations. [18] These are however broken at the quantum level, resulting on the dependence of the coupling on the renormalization scale. As we discussed in section 3.2, the dependence $g(\mu)$ is dictated by the β-function of the theory eq.(3.8). The coefficients of the β-function depend explicitly on the choices $(N, N_f, \mathcal{R})$, which determine a specific theory within the family eq.(3.27). We rewrite here the first 2 coefficients, given in eq.(3.5), keeping the explicit dependence on $(N, N_f, \mathcal{R})$,

$$\begin{aligned} b_0 &= \frac{1}{4\pi}\left(\frac{11}{3}N - \frac{4}{3}T_{\mathcal{R}}N_f\right), \\ b_1 &= \frac{1}{(4\pi)^2}\left[\frac{34}{3}N^2 - \left(4C_2(\mathcal{R}) + \frac{20}{3}N\right)T_{\mathcal{R}}N_f\right], \end{aligned} \tag{3.28}$$

where $T_{\mathcal{R}}$ is the trace normalization and $C_2(\mathcal{R})$ is the quadratic Casimir invariant in the representation $\mathcal{R}$ respectively[55].

The dependence on $(N, N_f, \mathcal{R})$ of the first 2 coefficients of the β-function already indicate that the scaling properties of $g(\mu)$ can be very diverse between different models.

---

which can be matched with the observed particle [53].

[18] In general, quantum field theories which are scale invariant are also be conformally invariant. For this reason, in the context of quantum field theory it is common to find these terms used interchangeably, even though the full conformal group is larger. It is possible, however, to find some examples of scale invariant QFTs which are not conformally invariant [54].

In theories where b_0 and b_1 are positive numbers, which is the case for QCD, the β-function is always negative and displays a zero at $\beta(0) = 0$, called an *ultra violet (UV) fixed point.* Theories falling in this category are characterised by being asymptotically free at high energies and, at low energies, displaying the phenomena of confinement and spontaneous chiral symmetry breaking.

For a given value of N and for a specific representation $\mathcal{R}$, there is a critical number of flavors N_f^{AF} given by

$$N_f^{\mathrm{AF}} = \frac{11N}{4T_{\mathcal{R}}}, \tag{3.29}$$

for which the first coefficient of the β-function b_0 becomes negative. The fixed point $\beta(0) = 0$ is not an UV fixed point any more, so that theories with a flavor content $N_f > N_f^{\mathrm{AF}}$ are characterised by the loss of asymptotic freedom. They behave like a non-abelian version of QED, and are hence referred to be in a non-abelian Coulomb phase.

The emergence of two different behaviours (QCD-like and QED-like) in theories described by the same lagrangian eq.(3.27) can be understood heuristically in terms of a competition between the charge anti-screening effect due to the gauge fields, and the screening effect due to fermion fields. When the number of fermion degrees of freedom is small, the contribution to b_0 is dominated by gauge loops. On the other hand, when the number of fermionic degrees of freedom gets larger, either due to a larger flavour content in the theory or by considering higher dimensional representations, b_0 is dominated by fermion loops and the theory displays QED-scaling behaviour.

If the number of flavours N_f is taken to be large but it is kept below N_f^{AF}, then the number of fermionic degrees of freedom is similar to the number of bosonic degrees of freedom and both contribute comparably to the β-function. In these cases one can find a range of N_f (for any representation $\mathcal{R}$) for which

$$b_1 < 0 \qquad \text{and} \qquad b_0 > 0, \tag{3.30}$$

such that the β-function has a second zero at non-zero coupling, corresponding to a stable infra-red fixed point (IRFP). As the number of flavours is decreased, there will be another threshold N_f^{c} for which the typical QCD-like behaviour is recovered.

Hence, all the theories within the range

$$N_f^c < N_f < \frac{11N}{4T_{\mathcal{R}}} \tag{3.31}$$

possess IR fixed points. This range is colloquially known as the *Conformal Window*. Inside the conformal window theories lack the phenomena of chiral symmetry breaking or confinement. Although these theories are still asymptotically free in the ultra-violet, conformal symmetry is restored in the infra-red, in which the theories display no particle spectrum. The presence or absence of a fixed point is scheme independent (between mass independent schemes).

Perturbatively, the value of the coupling at which the fixed point occurs is given by,

$$\alpha_*^{\text{2-loop}} = -\frac{b_0}{b_1}. \tag{3.32}$$

If $\alpha_*^{\text{2-loop}}$ is small then perturbation theory is reliable and, moreover, the presence of the IRFP ensures that it will remain reliable at all scales. These are the so-called *Banks-Zaks theories* [56, 57]. Some examples of Banks-Zaks theories would be the cases for which the value of N_f is slightly below the upper threshold N_f^{AF} of the conformal window, such that their b_0 coefficient is small.

As the number of flavours N_f is decreased towards the lower edge of the conformal window N_f^c, the coupling at the fixed point ceases to be small and perturbation theory ceases to be a reliable description. The determination of the lower bounds of the conformal window is then a non-perturbative problem, suitable to be explored with the techniques of lattice field theory.

Some analytic approaches for determining N_f exist as well. For instance, a direct estimation of N_f^c can be obtained studying the Schwinger-Dyson equation for the fermion propagator [58]. However, with this approach, it is necessary to truncate the set of diagrams contributing to the fermion self-energy (Ladder-Approximation), introducing systematic errors due to the truncation which are not under control. A fully non-perturbative exploration of the lower bounds of the conformal window is ultimately required.

A set of theories particularly interesting for model builders are those which lie right below the conformal window. These are confining and asymptotically free. However, due to their proximity to the conformal window, their β-function is expected to be

small and the coupling is hence expected to evolve very slowly over a wide range of scales. This peculiar behaviour has lead to call them *walking theories*, where the coupling walks rather than runs. Walking theories can be constructed either by choosing a theory which is very close to the conformal window from its lower edge, or by choosing a theory within the conformal window and introducing artificially a scale on it by including a fermion mass term. The latter are called *mass deformed walking theories.*

Realistic strongly-coupled theories which simultaneously break EW-symmetry and give masses to the fermions are only accommodated within experimental bounds if their coupling constant displays a walking behaviour and if the mass anomalous dimension γ_m is large. Hence, the main observables of interest to measure in a given strongly-coupled theory are

- The coupling $g(\mu)$, to determine whether the theory lies inside or not of the conformal window and, if outside, to identify the walking behaviour.

- The value of the mass anomalous dimension γ_m.

The slow evolution of the coupling in presence of large numbers of fermion degrees of freedom implies that very large changes in physical scale are needed for exploring a reasonable range of coupling strengths. This is in some sense an analogous problem to the one found in the determination of $\Lambda_{\rm QCD}$ from low energy observables discussed in section 3.3. There, a wide range of energy scales had to be considered in order to bridge two well separated scales, i.e. the hadronic scale and the perturbative scales. Here, in contrast, no matching is needed at low energies[19] and no contact with a perturbative scheme is required in these particular studies. The reason for studying a large range of scales comes exclusively from the slow evolution of $g(\mu)$, either as an IR fixed point is approached or because the theory walks.

One is faced again with the problem of fitting a large scale separation within a single lattice. This can be avoided following the exact same strategy as in section 3.3 and considering a finite volume scheme to reconstruct recursively the evolution of the coupling and other renormalization parameters.

[19]The study of beyond QCD theories with FV schemes is aimed to identify fixed points rather than to obtaining high precision estimations from low energy quantities. However, there is also interest in studying the spectrum of these theories (which will be in the electro-weak scale) for determining possible experimental traces in particle accelerators.

The exact same techniques developed originally for QCD can be imported to study this class of theories. In particular, we will see that finite volume schemes based on the Schrödinger functional, which we introduce in chapter 4, are easily adaptable to the present problem. The details of specific constructions originally obtained for QCD might, however, not be optimal for other theories. In fact, in chapter 7, we will see that the cutoff effects present in the SSF for some theories can be rather large if one uses a scheme directly based on choices which are otherwise successful for QCD.

In practice, the theories which have attracted more attention in recent years and which have been more studied in finite volume schemes (and through other methods) are

- $SU(2)$ with $N_f = 2$ adjoint fermions, also called (misleadingly) *Minimal Walking Technicolor*. This is the candidate theory for displaying an IR fixed point with a minimal number of fermionic degrees of freedom [31, 32, 59–62]. There is some consensus for the theory to be conformal. A walking theory could be constructed starting with this particular model and adding a mass deformation explicitly.

- $SU(2)$ with $N_f = 6$ fundamental fermions [63–65].

- $SU(3)$ with $N_f = 2$ symmetric fermions [60, 66–68].

- $SU(3)$ witn $N_f = 8, 10, 12$ and 16 fundamental flavours [34, 69–74]. QCD with a large number of flavours is actually easy to simulate using staggered fermions. These theories are generically called *many flavor QCD*. By considering an increasing number of flavours it is possible to study the transition towards the conformal window.

The search for IRFP can be carried out in some other ways apart from a direct search via a finite volume scheme. For instance, the presence of a fixed point can be indirectly probed by studying the scaling properties of hadron masses and decay constants as the limit of zero fermion mass is approached (see [35] and references therein). If the massless theory possesses an IRFP, the hadron masses and decay constants are expected to behave as power laws in the fermion mass. Another possibility to extract the mass anomalous dimension is based on on the scaling of the spectral density of the Dirac operator [75]. Ultimately, when exploring theories beyond QCD where there

is no experimental guidance at all, it is important to obtain evidence with as many methods as possible.

"Thunderdome. How do I get in there? "

Mad Max

4

Schrödinger functional schemes

The Schrödinger Functional (SF) was originally introduced in [76], and adapted as a finite volume scheme in [23] to deal with the problem of non-perturbative renormalization. SF schemes have the advantage that both Monte Carlo and perturbative calculations are feasible on them. So far, they have been widely used both in QCD [27, 29, 49, 50] and in exploring BSM theories [31–34]. In the present chapter we will review the presentation of the SF. First we discuss the formal continuum theory. In section 4.1 we closely follow [23] to introduce the SF for the pure Yang-Mills theory and comment on its renormalizability and quantum mechanical interpretation. In section 4.2 we discuss the inclusion of fermions as originally presented in [36]. The lattice regulated form of the SF is introduced in section 4.3, where we discuss a second implementation of Wilson fermions motivated by the mechanism of automatic $O(a)$-improvement. Finally, in section 4.4, we briefly comment on how to set up perturbation theory in SF schemes.

The objective of the chapter is not to present anything new, but to collect a set of definitions to prepare the ground for the rest of this thesis. We refer the reader to

the original literature for a more detailed presentation of these ideas.

4.1 The Schrödinger functional for the Yang-Mills theory

From now on, the space-time manifold is taken to be a hyper-cylinder $\mathcal{M} = L^3 \times T$ in euclidean space-time. The Schrödinger Functional in the path integral representation is defined as the Euclidean partition function with the fields respecting fixed boundary conditions at the temporal boundaries. Gauge fields $A_\mu(x)$ are algebra valued fields defined for $x \in \mathcal{M}$. They are taken to be periodic in the spatial directions

$$A_\mu(x + L\widehat{k}) = A_\mu(x). \tag{4.1}$$

Dirichlet boundary conditions are imposed in the temporal boundaries, given by

$$A_k(x) = \begin{cases} C_k^\Omega(\mathbf{x}), & x_0 = 0, \\ C'_k(\mathbf{x}), & x_0 = T, \end{cases} \tag{4.2}$$

where C and C' are classical gauge potentials and A^Ω is the gauge transformed field A with the gauge transformation

$$A_k^\Omega(x) = \Omega(x) A_k(x) \Omega^{-1}(x) + \Omega(x) \partial_k \Omega^{-1}(x), \qquad \Omega \in SU(N), \tag{4.3}$$

In order to preserve the periodicity of A_μ, only periodic functions Ω are allowed,

$$\Omega(x + L\widehat{k}) = \Omega(x). \tag{4.4}$$

The gauge functions Ω can be understood as a mapping from a three dimensional torus to the gauge group $SU(N)$. These kind of functions are topologically non-trivial and fall into disconnected classes labelled by an integer winding number. However, since we are ultimately interested in lattice formulations of the SF, where this difficulty does not occur, we will ignore topology for the rest of this presentation.

The Schrödinger functional for the Yang-Mills theory is then defined as the functional integral over all gauge field configurations $A_\mu(x)$ with $0 \leq x_0 \leq T$, respecting

the boundary conditions eq.(4.1) and eq.(4.2), and reads

$$\mathcal{Z}[C, C'] = \int \mathcal{D}[\Omega] \int \mathcal{D}[A] e^{-S_G[A]}, \tag{4.5}$$

with the gauge action given by the standard Yang-Mills action eq.(2.4) restricted to $\mathcal{M}$

$$S_G[A] = -\frac{1}{2g_0^2} \int_0^T dx_0 \int_0^L d^3\mathbf{x} \, \mathrm{tr} \left\{ F_{\mu\nu}(x) F_{\mu\nu}(x) \right\}. \tag{4.6}$$

The measures are defined as

$$\mathcal{D}[A] = \prod_{x,\mu,a} dA_\mu^a(x), \qquad \mathcal{D}[\Omega] = \prod_x d\Omega, \tag{4.7}$$

where $A_\mu^a(x)$ are the components of $A_\mu(x)$ in a basis of the lie algebra $su(N)$, and where $d\Omega$ denotes the Haar measure of the gauge group $SU(N)$. The integration over Ω in eq.(4.5) together with the appearane of the gauge transformed boundary fields in eq.(4.2) can be regarded as a gauge average which enforces the SF eq.(4.5) to be a gauge invariant functional of the boundary fields

$$\mathcal{Z}[C'^{\Omega}, C^{\Omega}] = \mathcal{Z}[C', C]. \tag{4.8}$$

In the Schrödinger piture, this corresons to a projection on the physial subspace of gauge invariant wave funtions. Once a lattice regulator is introdued, this projetion corresponds to the integration ove timelike link variables [23].[1]

4.1.1 Quantum Mechanical interpretation

The path integral representation is suitable for formulating the SF with a lattice regulator aiming to perform Monte Carlo calculations. It is this formalism the one we will follow in the rest of this thesis. However, it is worth to consider the Hamiltonian formalism to give a clear quantum mechanical meaning to the SF.[2]

In the Hamiltonian construction, the theory is specified at a time x_0 by assuming

[1] The integration over Ω is required to guarantee gauge invariance of the functional integral in presence of boundaries.

[2] Although we have already given the definition of the SF in terms of the path integral in setion 4.1 (which is what is ultimately neeed for numerical calculations), the SF is formally constructed starting from the Hamiltonian formulation.

the field variables to be operators following canonical commutation relations, and writing down the Hamilton operator. The SF can then be understood as the quantum mechanical transition amplitude from a state $|C\rangle$ to another state $|C'\rangle$ after an Euclidean time T.

To see this one can use the Schrödinger picture of quantum field theory.[3] The quantum mechanical states are the wave-functionals $\Psi[A]$ of the gauge fields, which form a Hilbert s[illegible] $\langle\Psi|\ \Psi'\rangle = \int \mathcal{D}[A]\Psi[A]^*\Psi'[A]$, given by

$$\langle\Psi|\ \Psi'\rangle = \int \mathcal{D}[A]\Psi[A]^*\Psi'[A], \quad \mathcal{D}[A] = \prod_{\mathbf{x},k,a} dA_k^a(\mathbf{x}). \tag{4.9}$$

Any classical gauge field C defines a state $|C\rangle$ of $\mathbb{H}$ through

$$\langle C|\ \Psi\rangle = \Psi[C]. \tag{4.10}$$

The operators $\hat{A}(\mathbf{x})$ act on these wave functionals as

$$\hat{A}_k^a(\mathbf{x})\Psi[C] = C_k^a\Psi[C]. \tag{4.11}$$

Physical states must be gauge invariant, hence they must satisfy

$$\Psi[A^\Omega] = \Psi[A]. \tag{4.12}$$

The space of gauge invariant states forms a subspace of $\mathbb{H}$. Any state in $\mathbb{H}$ can be projected to the physical subspace by means of the projector $\mathbb{P}$, which acts on wave functionals[4] as

$$\mathbb{P}\Psi[A] = \int \mathcal{D}[\Omega]\Psi[A^\Omega]. \tag{4.13}$$

The canonically conjugate fields of the gauge potential is the chromo-electric field represented by the functional derivatives

$$\hat{F}_{0k}^a(\mathbf{x}) = -i\frac{\delta}{\delta A_k^a(\mathbf{x})} = \hat{E}_k^a(\mathbf{x}). \tag{4.14}$$

[3] Analogously to the Schrödinger picture in non-relativistic quantum mechanics, temporal evolution is entirely contained in the states of the theory.

[4] This is ultimately the reason for the presence of the integral over Ω in the definition of the SF eq.(4.5).

The magnetic components of the field strength tensor are

$$\hat{F}^a_{kl}(\mathbf{x}) = \partial_k \hat{A}^a_l(\mathbf{x}) - \partial_l \hat{A}^a_k(\mathbf{x}) + f^{abc}\hat{A}^b_k(\mathbf{x})\hat{A}^c_l(\mathbf{x}), \tag{4.15}$$

where f^{abc} are the structure constants of $SU(N)$. Using these fields, the Hamilton operator is defined as[5]

$$\mathcal{H} = \int_0^L d^3\mathbf{x} \left\{ \frac{g_0^2}{2}\hat{F}^a_{0k}(\mathbf{x})\hat{F}^a_{0k}(\mathbf{x}) + \frac{1}{4g_0^2}\hat{F}^a_{kl}(\mathbf{x})\hat{F}^a_{kl}(\mathbf{x}) \right\}. \tag{4.16}$$

The Euclidean time evolution operator is now given by $e^{-\mathcal{H}x_0}$ and the SF can finally be defined as the matrix elements of $e^{-\mathcal{H}x_0}$ between gauge invariant states, by

$$\mathcal{Z}[C', C] = \langle C' | \, e^{-\mathcal{H}x_0}\mathbb{P} \, | C \rangle \,, \tag{4.17}$$

where the projector $\mathbb{P}$ ensures invariance of the SF under gauge transformations of C and C'.

From this discussion it can be concluded that the SF $\mathcal{Z}[C', C]$ is the Euclidean propagation amplitude to go from a field configuration C to another field configuration C' after an Euclidean time T.

Inserting a complete set of states in eq.(4.17) we obtain the spectral decomposition

$$\mathcal{Z}[C', C] = \sum_{n=0}^{\infty} e^{-E_n T}\Psi_n[C']\Psi_n[C]^*, \tag{4.18}$$

where E_n and $|\Psi_n\rangle$ are the eigenvalues and eigenfunctions of $\mathcal{H}$.

4.1.2 The induced Background Field

An interesting feature of the Schrödinger Functional formulation is that it permits a well defined treatment of field theories in the presence of a *background field* (BF). In the Yang-Mills theory, for given boundary values C and C', the background field B induced by the boundary fields is the solution to the classical field equations satisfying the boundary conditions

$$B_k(x)|_{x_0=0} = C_k(\mathbf{x}), \quad B_k(x)|_{x_0=T} = C'_k(\mathbf{x}). \tag{4.19}$$

[5]The Hamilton operator commutes with the projector $\mathbb{P}$.

The background field obtained this way[6] is a global minimum of the classical action[7]

$$S[A] > S[B], \quad \forall A \neq B^{\Omega}, \tag{4.20}$$

unique up to gauge transformations [23], around which perturbation theory can be unambiguously defined. For weak couplings g_0, the path integral eq.(4.5) is dominated by fields around the absolute minima of the action so it can be computed by a saddle point expansion. The effective action

$$\Gamma[B] \equiv -\ln \mathcal{Z}[C', C] \tag{4.21}$$

has then a regular perturbative expansion around B

$$\Gamma[B] = \frac{1}{g_0^2}\Gamma_0[B] + \Gamma_1[B] + g_0^2\Gamma_2[B] + ..., \tag{4.22}$$

with the leading term given by

$$\Gamma_0[B] = g_0^2 S[B]. \tag{4.23}$$

The higher order terms are sums of vacuum bubble Feynman diagrams.[8] Note that since the background field B and the pair of boundary values C and C' are in one to one correspondence one can leave B as the argument of the effective action Γ.

There is a lot of freedom in choosing the boundary fields C and C', and a specific choice is of no fundamental importance. However, for practical considerations which will be clear later in this chapter, we will restrict ourselves to a specific family of background fields induced by abelian, isotropic and spatially constant boundary gauge fields given by

$$C_k = \frac{i}{L}\mathrm{diag}\left(\phi_1, ..., \phi_N\right), \quad C'_k = \frac{i}{L}\mathrm{diag}\left(\phi'_1, ..., \phi'_N\right), \qquad k = 1, 2, 3. \tag{4.24}$$

[6]Typically, starting from the equations of motion and the boundary conditions it is difficult to find the induced background field B. One can proceed the other way around, giving a starting ansatz for the field B, defining the boundary conditions such that eq.(4.19) holds, and proving that B is a unique solution to the field equations leading to a global minima of the classical action.

[7]B^{Ω} denotes the gauge transformed BF, where Ω is the generalisation of eq.(4.3) to all space-time points and directions.

[8]We will deal with the contribution of Γ_1 later in chapter 6, in presence of a lattice regulator which will render the diagrams well defined.

Here ϕ_i and ϕ'_i are boundary phases which must satisfy[9]

$$\sum_{i=1}^{N} \phi_i = \sum_{i=1}^{N} \phi'_i = 0. \tag{4.25}$$

They are allowed to depend, at most, on a set of dimensionless parameters.[10]

The BF induced by the boundaries eq.(4.24) is given (in the temporal gauge) by[11]

$$B_0 = 0, \quad B_k = C_k + \frac{x_0}{T}\left(C'_k - C_k\right), \qquad k = 1, 2, 3. \tag{4.26}$$

The resulting field strength tensor is a constant chromo-electric field

$$G_{0k} = \partial_0 B_k = \frac{C'_k - C_k}{T} = i\frac{(\phi' - \phi)}{TL}, \quad k = 1, 2, 3, \tag{4.27}$$

with vanishing chromo-magnetic components $G_{kl} = 0$. The classical action associated to these fields is given by

$$S[B] = \frac{3L}{g_0^2 T} \sum_{\alpha=1}^{N} \left(\phi'_\alpha - \phi_\alpha\right)^2. \tag{4.28}$$

This choice of fields is particularly useful for giving a definition of a running coupling as will be seen in chapter 6. Moreover, a stability theorem exists [23] which ensures that, provided that the phases in eq.(4.24) fall within a specific region denoted as *fundamental domain*, then the field B induced by the boundaries will indeed be a minimum of the action.

Another useful reason for choosing the boundaries as in eq.(4.24) is that once we regulate the theory on a lattice (see section 2.2), the number of boundary counterterms needed for the improvement of the theory a la Symanzik turns out to be reduced by one for this choice. Also, the classical lattice action will converge towards the continuum limit at a rate with high powers in a.

All these features make the background fields of this class a very appealing choice.

[9] Obviously, since the gauge fields are algebra valued, they must be traceless.

[10] The number of dimensionless parameters the phases can depend on will by given by the rank of the gauge group under consideration

[11] This form is trivially found by solving the YM field equations imposing C and C' as boundary conditions and using the ansatz of B being abelian and spatially constant.

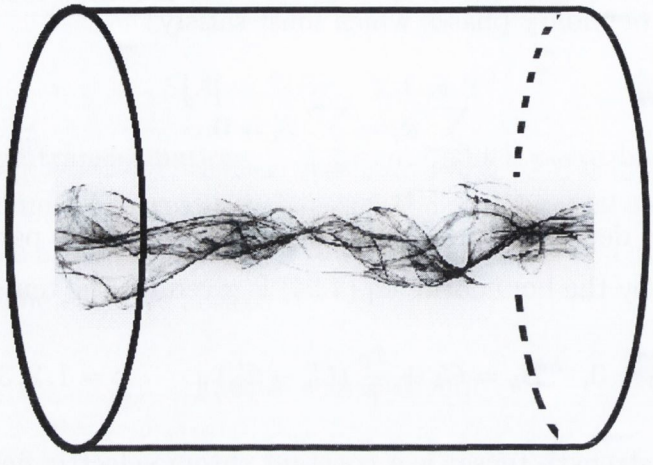

Figure 4.1.1: Dramatic impression of a Schrödinger functional with a background field.

However, there is still a lot of freedom in the choice of values for the boundary phases ϕ_i and ϕ'_i. A common criteria used in the literature [49, 50] for this choice is the following [77]. Each set ϕ_i corresponds to a point inside the fundamental domain, and so does ϕ'_i. It has been empirically observed that the signal-to-noise ratio in Monte Carlo simulations is larger if the points corresponding to the two sets of phases are far from the domain's edge, they are as far as possible from each other, and where the two boundaries are on equal footing. This can be done by choosing points related through a symmetry of the fundamental domain. Hence, given the first set of phases ϕ_i, the second set ϕ'_i is chosen by applying a charge conjugation followed by a central conjugation on C.

A typical choice of boundary phases for $SU(2)$ is given by

$$\begin{aligned} \phi_1 &= -\eta, & \phi'_1 &= (\eta - \pi), \\ \phi_2 &= \eta, & \phi'_2 &= (\pi - \eta), \end{aligned} \tag{4.29}$$

and, for $SU(3)$, by

$$\begin{aligned} \phi_1 &= \eta - \pi/3, & \phi'_1 &= -(\eta - \pi), \\ \phi_2 &= \eta(\nu - 1/2), & \phi'_2 &= \eta(\nu + 1/2) + \pi/3, \\ \phi_3 &= -\eta(\nu + 1/2) + \pi/3, & \phi'_3 &= -\eta(\nu - 1/2) + 2\pi/3, \end{aligned} \tag{4.30}$$

with η and ν being dimensionless parameters, the role of which will become clear

later, and which we will use to define a renormalized coupling in chapter 6.

BF constructed this way have proven to be very useful in QCD. However, the criteria presented here will have to be reviewed when considering theories with fermions transforming under two index representations of the gauge group in chapter 7.

4.1.3 Renormalization of the Schrödinger functional

Once the SF has been defined, the question is whether a renormalizable QFT remains renormalizable once it is formulated on a manifold with boundaries. In general, new divergences do appear, which are not present in the absence of boundaries. The reason is that radiative corrections can generate extra relevant[12] local composite operators at the boundaries respecting all the symmetries of the theory.

Symanzik studied the ϕ^4 theory formulated in the SF [76, 78]. Without giving a full proof, he presented arguments to expect that the SF is finite to all orders of perturbation theory after the usual renormalization of the bare mass m_0 nd coupling λ_0, and by including the boundary counterterms

$$\int_{x_0=T} d^3\mathbf{x} \left\{ Z_1\phi^2 + Z_2\phi\partial_0\phi \right\} + \int_{x_0=0} d^3\mathbf{x} \left\{ Z_1\phi^2 - Z_2\phi\partial_0\phi \right\}, \tag{4.31}$$

to the bare action.

For a pure Yang Mills theory, in [23] it was shown that at 1-loop order, in contrast to the scalar field theory, the SF remains finite after just the normal renormalization of the bare coupling g_0, without any extra boundary counterterm. This is so because no fields of dimension $d \leq 3$ with the same symmetries as the Yang-Mills action occur,[13] and hence the presence of boundaries does not introduce extra divergences.

Symanzik gave the conjecture that for any given QFT renormalizable in the absence of boundaries, the SF formulation of the theory can be made finite by, in addition to the standard renormalization, adding to the bare action boundary counterterms formed by all possible composite fields of dimension $d \leq 3$ integrated over the boundaries.

Although a general proof to all orders in perturbation theory does not exist yet[14],

[12] Any operator with dimension $d \leq 3$ will be relevant at the boundaries.

[13] Assuming that parity $\mathcal{P}$ is conserved

[14] The reason of this mainly being that power counting in momentum space is not possible due to the breaking of translation invariance in the temporal directions.

Symanzik's conjecture is widely believed to be valid. In fact, the conjecture is supported both by several 1 and 2 loop calculations performed in YM and QCD [52, 79, 80], and beyond perturbation theory by Monte Carlo simulations [27, 29, 49, 50].

4.2 The inclusion of fermions

Fermions were formulated in the SF for the first time in [36]. The same way as it is done for the gauge fields, boundary conditions have to be imposed on the fermion fields $\psi(x)$ and $\overline{\psi}(x)$ on the temporal boundaries. It is important to note that since the Dirac operator is a first order differential operator, only half of the components of the fermion fields need to be fixed at the boundaries in order to obtain a unique solution to the Dirac equation. This can be done by fixing[15]

$$\begin{aligned} P_+\psi(x)|_{x_0=0} &= \rho, & P_-\psi(x)|_{x_0=T} &= \rho', \\ \overline{\psi}(x)\, P_-|_{x_0=0} &= \overline{\rho}, & \overline{\psi}(x)\, P_+|_{x_0=T} &= \overline{\rho}, \end{aligned} \tag{4.32}$$

with the projectors given by

$$P_\pm = \frac{1}{2}\left(1 \pm \gamma_0\right). \tag{4.33}$$

The fields $\psi(x)$ and $\overline{\psi}(x)$ are taken to be periodic in the spatial directions. The action for the fermion fields in the hyper-cylinder $\mathcal{M}$ is given by

$$\begin{aligned} S_F[\psi(x),\overline{\psi}(x)] \;=\; & \int_0^T dx_0 \int_0^L d^3\mathbf{x}\overline{\psi}(x)\left(\gamma_\mu D_\mu + m\right)\psi(x) \\ & - \int_0^L d^3\mathbf{x}\,\left[\overline{\psi}(x)P_-\psi(x)\right]\Big|_{x_0=0} - \int_0^L d^3\mathbf{x}\,\left[\overline{\psi}(x)P_+\psi(x)\right]\Big|_{x_0=T}. \end{aligned} \tag{4.34}$$

In the covariant derivative D_μ we allow for a constant $U(1)$ background field,

$$D_\mu = \partial_\mu + A_\mu + \frac{i}{L}\theta_\mu, \qquad \theta_\mu = (1-\delta_{\mu 0})\,\theta. \tag{4.35}$$

The field θ can be reabsorved in the periodic boundary conditions by means of an abelian gauge transformation which renders the fermion fields to be periodic up to a

[15] In the lattice regularized theory it can be shown [36] that these conditions lead to a QM interpretation similar to that in section 4.1.1.

phase

$$\psi(x + L\hat{k}) = e^{i\theta}\psi(x), \qquad \overline{\psi}(x + L\hat{k}) = e^{-i\theta}\overline{\psi}(x). \tag{4.36}$$

The SF formulation of a QFT with gauge fields coupled to fermions can be now formally defined in the continuum as the Euclidean path integral

$$\mathcal{Z}[C', \rho', \overline{\rho}'; C, \rho, \overline{\rho}] = \int \mathcal{D}[\Omega] \int \mathcal{D}[A]\mathcal{D}[\psi, \overline{\psi}] e^{-S[A,\psi,\overline{\psi}]}, \tag{4.37}$$

with the total euclidean action given by

$$S = S_G[A] + S_F[A, \psi, \overline{\psi}], \tag{4.38}$$

where the gauge action is given in eq.(4.6). The measures $\mathcal{D}[\Omega]$ and $\mathcal{D}[A]$ are the same as eq.(4.7). The fermionic measure is given by

$$\mathcal{D}[\psi, \overline{\psi}] = \prod_{\mathbf{x}} \prod_{\alpha,c,f} d\psi(\mathbf{x})_{\alpha,c,f} d\overline{\psi}(\mathbf{x})_{\alpha,c,f}, \tag{4.39}$$

where $d\psi$ and $d\overline{\psi}$ are Grassman measures, and α, c and f are Dirac, colour and flavour indexes.

It is also common to define the boundary fields $\zeta(\mathbf{x})$, $\overline{\zeta}(\mathbf{x})$, $\zeta'(\mathbf{x})$ and $\overline{\zeta}'(\mathbf{x})$ as the functional derivatives

$$\begin{aligned} \zeta(\mathbf{x}) &= \frac{\delta}{\delta\overline{\rho}(\mathbf{x})}, \qquad & \zeta'(\mathbf{x}) &= \frac{\delta}{\delta\overline{\rho}'(\mathbf{x})}, \\ \overline{\zeta}(\mathbf{x}) &= -\frac{\delta}{\delta\rho(\mathbf{x})}, \qquad & \overline{\zeta}'(\mathbf{x}) &= -\frac{\delta}{\delta\overline{\rho}'(\mathbf{x})}. \end{aligned} \tag{4.40}$$

These are meaningful when inserted into the path integral, where they act as functional derivatives on the Boltzmann factor. Within this context, they have the effect of inserting certain combinations of $\psi(x)$ and $\overline{\psi}(x)$ close to the temporal boundaries.

The fields eq.(4.40) can be identified with the non-Dirichlet components of the quark fields at the boundaries,

$$\begin{aligned} P_-\psi(x)|_{x_0=0} &= \zeta(\mathbf{x}), \qquad & P_+\psi(x)|_{x_0=T} &= \zeta'(\mathbf{x}), \\ \overline{\psi}(x)\, P_-|_{x_0=0} &= \overline{\zeta}(\mathbf{x}), \qquad & \overline{\psi}(x)\, P_+|_{x_0=T} &= \overline{\zeta}'(\mathbf{x}). \end{aligned} \tag{4.41}$$

They will play an important role in the construction of correlation functions in chapter

5.

Concerning the renormalizability of the SF eq.(4.37), in contrast to the pure Yang Mills theory, there are indeed gauge invariant composite fields of dimension 3 respecting the same symmetries as the action eq.(4.35), which lead to extra renormalization at the boundaries. These operators are

$$\overline{\psi}P_-\psi\big|_{x_0=0} \qquad \text{and} \qquad \overline{\psi}P_+\psi\big|_{x_0=T}\,, \tag{4.42}$$

so that the corresponding counterterms must be added to the bare action to render the SF finite. These counterterms can be reabsorbed in the form of a multiplicative renormalization of the boundary fields,

$$\begin{aligned} \rho_R &= Z_b^{-1/2}\rho, \qquad \rho'_R = Z_b^{-1/2}\rho', \\ \overline{\rho}_R &= Z_b^{-1/2}\overline{\rho}, \qquad \overline{\rho}'_R = Z_b^{-1/2}\overline{\rho}'. \end{aligned} \tag{4.43}$$

From here, one can see that by choosing homogeneous boundary conditions for the fermion fields

$$\begin{aligned} P_+\psi(x)\big|_{x_0=0} &= 0, \qquad P_-\psi(x)\big|_{x_0=T} = 0, \\ \overline{\psi}(x)\, P_-\big|_{x_0=0} &= 0, \qquad \overline{\psi}(x)\, P_+\big|_{x_0=T} = 0, \end{aligned} \tag{4.44}$$

that is, by setting $\rho = \overline{\rho} = \rho' = \overline{\rho'} = 0$, then the renormalization factor Z_b is not needed and the SF remains finite after the standard renormalization of the bare parameters g_0 and m_0.[16]

To conclude this section it is important to point out that no fermionic zero modes occur in presence of boundary conditions of the kind eq.(4.44). It was shown in [36] that such boundary conditions induce a minimum eigenvalue of the Dirac operator proportional to the inverse of the temporal extent, which will be finite even for vanishing physical quark mass. By setting $m_q = 0$ one thus obtains unambiguously a mass independent renormalization scheme for which the RG equations are simple. Moreover, once implemented with a lattice regulator, the Dirac operators can always be inverted and MC simulations can hence be carried out in the massless limit.

Summarising, the SF is a non-perturbatively defined finite volume and mass independent renormalization scheme. Some particular regularizations in the framework of lattice gauge theory will be discussed in the following sections.

[16] The renormalization factor Z_b will show up again in chapter 5, when using the boundary fields in the construction of correlation functions.

4.3 The SF regularized on the lattice

The lattice regularization leads to a fully non-perturbative definition of the SF which makes it suitable for being used as a finite volume scheme to deal with the problem of non-perturbative renormalization. The space-time manifold is reduced to a hyper-cylindrical grid superimposed to the conitinuum manifold $\mathcal{M}$

$$\Gamma_{\mathrm{E}} = \left\{ x | \frac{x}{a} \in \mathbb{Z}^4; \quad 0 \leq x_0 < T, \quad 0 \leq x_k < L, \quad k = \{1,2,3\} \right\}, \tag{4.45}$$

where T and L are assumed to be integer multiples of the lattice spacing.

We will proceed here as in chapter 2, writing first a discrete form of the action and then building up the regulated path integral. Continuum actions are not regularized on a lattice in a unique way, although the details of the specific regularization chosen should not matter in the continuum limit. For the gauge action we will use Wilson's original proposal (see section 2.2.1) adapted to the SF setup [23]. For fermions we will consider two different regularizations. These will be the standard Wilsonian formulation, originally written in the SF in [36], and a modification with a chiral twist leading to the recently proposed chirally rotated χSF [1].

4.3.1 The Yang-Mills SF on the lattice

Lattice gauge fields U are constructed as in infinite volume. A gauge field U assigns a link variable $U_\mu(x) \in SU(N)$ to every pair of points $(x, x+a\hat{\mu})$, defined in Γ_{E}. Gauge transformations $\Omega(x) \in SU(N)$ are defined on the lattice sites x and act on the link variables as

$$U_\mu(x) \longrightarrow U_\mu^\Omega(x) = \Omega(x) U_\mu(x) \Omega(x + a\hat{\mu})^{-1}. \tag{4.46}$$

The periodicity in the spatial directions of both gauge fields and gauge transformations is the same as in the continuum

$$U_\mu(x + L\hat{k}) = U_\mu(x), \qquad \Omega(x + L\hat{k}) = \Omega(x). \tag{4.47}$$

In the temporal boundaries one has to prescribe fixed values for the spatial link variables

$$W_k(\mathbf{x}) = U_k(x)|_{x_0=0}\,, \qquad W_k'(\mathbf{x}) = U_k(x)|_{x_0=T}\,. \tag{4.48}$$

These must be related to the continuum fields C and C' in order to establish a connection with the continuum SF. We identify $W_k(\mathbf{x})$ with the parallel transporter from $x + a\hat{k}$ to x determined by the boundary field C, namely

$$W_k(\mathbf{x}) = \mathcal{P} \exp \left\{ a \int_0^1 dt C_k(x + a\hat{k} - at\hat{k}) \right\}, \tag{4.49}$$

and similarly for $W'_k(\mathbf{x})$. Note that for the abelian and spatially constant fields of eq.(4.24) their lattice version simply reads

$$W_k = e^{aC_k}, \qquad W'_k = e^{aC'_k}. \tag{4.50}$$

The construction eq.(4.49) is gauge covariant. By performing a gauge transformation $C \to C^\Omega$ (see eq.(4.3)) the fields W_k transform as eq.(4.46).

The gauge action $S_G[U]$ of a lattice gauge field is taken to be the Wilson gauge action [17] eq.(2.24) restricted to Γ_{E}

$$S_{\mathrm{G}}[U] = \frac{1}{g_0^2} \sum_{x \in \Gamma_{\mathrm{E}}} \sum_{\mu,\nu} \omega_{\mu\nu}(x) \mathrm{Re\ tr} \left[\mathbb{I} - P_{\mu\nu}(x) \right], \tag{4.51}$$

where $P_{\mu\nu}(x)$ is the plaquette field defined as in eq.(2.25) and $\omega_{\mu\nu}(x)$ is a weight factor which takes the values

$$\omega_{\mu\nu}(x) = \begin{cases} 1/2, & \text{for spatial plaquettes at } x_0 = 0 \text{ and } x_0 = T, \\ 1, & \text{otherwise.} \end{cases} \tag{4.52}$$

The lattice regularized SF for the pure Yang-Mills theory can now be defined as the path integral over all gauge fields U satisfying the boundaries eq.(4.48),

$$\mathcal{Z}[C', C] = \int \mathcal{D}[U] e^{-S_{\mathrm{G}}[U]}, \qquad \mathcal{D}[U] = \prod_{x,\mu} dU_\mu(x). \tag{4.53}$$

Here dU is again the normalized gauge invariant Haar measure on $SU(N)$, and the product $\prod_{x,\mu}$ runs over all lattice points and directions such that the links associated to the pair $(x, x + a\hat{\mu})$ fall in the interior of the lattice. Note that the SF can be left as a functional on the continuum fields C and C' since they are directly related to W

and W' via eq.(4.49) and eq.(4.50).[17]

The average over the gauge group present in eq.(4.5) is not needed in the lattice since the functional integral eq.(4.53) is already invariant under arbitrary gauge transformations of the boundary fields [23].

As in the continuum, boundary conditions for the gauge fields give rise to a background field. We focus here on the Abelian and spatially constant fields introduced in section 4.1.2. The boundary conditions eq.(4.48) lead to a field configuration V, non-degenerate up to gauge transformations, which minimises the action. It is related to the continuum theory via

$$V_\mu(x) = \exp(aB_\mu(x)), \tag{4.54}$$

satisfying the boundary conditions

$$V_\mu(x)|_{x_0=0} = W_k(\mathbf{x}), \quad V_\mu(\mathbf{x})|_{x_0=T} = W'_k(\mathbf{x}). \tag{4.55}$$

Before accepting the field V as a good choice of BF it has to be shown that it is indeed a solution to the field equations derived from the Wilson action. In order to write them, we introduce the covariant divergence of the plaquette field eq.(2.25)

$$d^*P_\mu(x) = \sum_{\nu=0}^{3} \left\{ P_{\mu\nu}(x) - V_\nu(x-a\hat{\nu})^{-1} P_{\mu\nu}(x-a\hat{\nu}) V_\nu(x-a\hat{\nu}) \right\}, \tag{4.56}$$

where the plaquette here is evaluated on the background field V configuration. The lattice action is stationary if and only if the traceless anti-hermitean part of $d^*P_\mu(x)$ vanishes, that is

$$d^*P_\mu(x) - d^*P_\mu(x)^\dagger - \frac{1}{N}\mathrm{Tr}\left\{ d^*P_\mu(x) - d^*P_\mu(x)^\dagger \right\} = 0. \tag{4.57}$$

It is easy to show that the field eq.(4.54) indeed satisfies eq.(4.57). The action corresponding to V is then given by

$$S_G[V] = \frac{3TL^3}{g_0^2} \sum_{\alpha=1}^{N} \left\{ \frac{2}{a^2} \sin\left[\frac{a^2}{2TL} (\phi'_\alpha - \phi_\alpha) \right] \right\}^2. \tag{4.58}$$

[17] This is useful since in the continuum limit C and C' are kept fixed while a is sent to zero.

Note that the action eq.(4.58) converges to the continuum limit at a rate of $O(a^4)$, in contrast to the expected $O(a^2)$ convergence expected from the Wilson gauge action. This means that constant abelian background fields lead to minimal cutoff effects already at the classical level.[18]

To conclude the discussion on the background field, we recall that in order to accept eq.(4.54) as a correct background field, one still has to show that V is indeed a configuration with least action and that any other field with the same action should be obtained by gauge transforming V. A mathematical proof of this exists [23].

It is worth to observe as well that a quantum mechanical interpretation of the lattice SF analogous to that of the continuum exists, and can be established by means of the transfer matrix construction. In the temporal gauge ($U_0(x) = 0$) the transfer matrix $\mathbb{T}_0$ is given by $\mathbb{T}_0 = e^{-a\mathcal{H}}$, where $\mathcal{H}$ is the Hamiltonian operator of the lattice theory. $\mathbb{T}_0$ is an hermitean operator which acts on Schrödinger wave functionals $\Phi[W]$ as a discrete version of a step evolution operator. Physical wave functionals $\Phi[W]$ form again a subspace of the full Hilbert space. It is possible to introduce a state $|W\rangle$ (in analogy to $|C\rangle$ in the continuum) and define the SF as

$$\mathcal{Z}[C', C] = \langle W' | \, (\mathbb{T}_0)^{T/a} \, \mathbb{P} \, | W \rangle \,, \tag{4.59}$$

where $\mathbb{P}$ is the projector on the physical subspace. This expression is completely analogous to the continuum expression eq.(4.17). This means that the interpretation of the SF as the Euclidean propagation kernel from a state $|W\rangle$ to $|W'\rangle$ in a discrete number of steps separated by intervals a is entirely valid in the regularized theory. A spectral decomposition analogous to eq.(4.18) can be obtained for all values of the lattice spacing.

4.3.2 Improvement of the pure Yang-Mills theory

When a theory formulated in a manifold with boundaries is regulated on a lattice[19] additional cutoff effects might be generated by the presence of the boundaries. The reason is analogous to the need of extra renormalization described in section 4.1.3, since new local operators of dimension $d \geq 4$ might occur in the dimension 3 boundaries, which were not present in the original theory. Symanzik's improvement pro-

[18] This was in fact one of the motivations for the introduction of this class of background fields.

[19] In fact, this statement will be true in presence of any regulator, not only on the lattice

gram, described in section 2.3, can be applied in the case at hand to remove both the standard bulk cutoff effects and the extra lattice artefacts generated at the boundaries. For obtaining an improvement to $O(a)$ one thus has to consider all possible dimension 5 bulk counterterms and dimension 4 boundary counterterms with the same symmetries of the lattice action.

For the pure Yang-Mills theory, as has been explained in section 2.3, there are no dimension 5 gauge invariant operators and hence no bulk counterterms are necessary at this order. There are, however, two possible dimension 4 operators at the boundaries, given by

$$\mathrm{tr}\,\{F_{0k}F_{0k}\}\,, \qquad \mathrm{tr}\,\{F_{kl}F_{kl}\}\,. \tag{4.60}$$

The two possible boundary counterterms are then obtained by summing any local lattice expression for the operators eq.(4.60). The counterterms can be arranged resembling the operator structure already present in the Wilson action. By writing separately the spatial plaquettes and the temporal boundary plaquettes, one obtains the counterterm action

$$\begin{aligned}\delta S_{\mathrm{G,b}}[U] &= \frac{1}{2g_0^2}(c_s-1)\sum_{\mathbf{x}}\sum_{k,l=1}^{3}\mathrm{ReTr}\,\{\mathbb{I}-P_{kl}(\mathbf{x})\}|_{x_0=0,T} \\ &+ \frac{1}{g_0^2}(c_t-1)\sum_{\mathbf{x}}\sum_{k=1}^{3}\mathrm{ReTr}\,\{\mathbb{I}-P_{0k}(\mathbf{x})\}|_{x_0=0,T}\,.\end{aligned} \tag{4.61}$$

where c_s and c_t are the improvement coefficients. The improved gauge action is now given by

$$S_{\mathrm{G,I}}[U] = S_{\mathrm{G}}[U] + \delta S_{\mathrm{G,b}}[U]. \tag{4.62}$$

Since the operator structure of $\delta S_{\mathrm{G,b}}$ is the same as for the Wilson action, the improved gauge action $S_{\mathrm{G,I}}$ can be written directly as eq.(4.51) by redefining the weight factors to be

$$\omega_{\mu\nu}(x) = \begin{cases} c_s/2, & \text{for spatial plaquettes at } x_0 = 0 \text{ and } x_0 = T, \\ c_t, & \text{for temporal plaquettes attached to} \\ & \text{the planes } x_0 = 0 \text{ and } x_0 = T, \\ 1, & \text{otherwise.} \end{cases} \tag{4.63}$$

The coefficients c_s and c_t are functions of the bare coupling that can be adjusted to

eliminate the $O(a)$ lattice artefacts coming from the boundaries. An ideal situation would be to obtain a full non-perturbative determination of these coefficients, such that all boundary $O(a)$ effects would be removed. In practice, however, this would be very expensive in terms of computational time. One thus simply determine c_s and c_t to a few orders in perturbation theory. This is enough in practice since boundary effects are expected to be less relevant as lattices get larger. These coefficients can be expanded as a series in g_0^2

$$c_t(g_0) = c_t^{(0)} + c_t^{(1)} g_0^2 + c_t^{(2)} g_0^4 + O(g_0^4), \tag{4.64}$$

$$c_s(g_0) = c_s^{(0)} + c_s^{(1)} g_0^2 + c_s^{(2)} g_0^4 + O(g_0^4), \tag{4.65}$$

with terms

$$c_{s,t}^{(k)} = \sum_{l=0}^{k} c_{s,t}^{(k,l)} N_f^l, \tag{4.66}$$

receiving contributions from both bosonic and fermionic loops.

For the abelian BF we are considering, the terms proportional to c_s do not contribute to any observable. This is so because, since the fields are constant in space, their spatial derivatives vanishes in eq.(4.61).[20]

The coefficients $c_t^{(k,l)}$ involving fermion loops depend on the specific regularization used for the fermions. Their values are known to two loops for the pure Yang-Mills theory and in the standard setup with Wilson fermions (see table 4.4.1). One of the goals of this thesis is the determination to 1-loop in PT of the fermionic contribution $c_t^{(1,1)}$ in the chirally rotated setup described in the following sections (this will be done in chapter 6). Provided that c_t is fixed to one loop, cutoff effects coming from the gauge part of the action due to the boundaries will be reduced to $O(ag_0^4)$.

4.3.3 The standard formulation of Fermions

We will consider two different fermion regularizations in this thesis. In this subsection we present the SF with standard regularization with Wilson fermions, originally given in [36]. Classical fermion fields on the lattice are an assignment of a Dirac spinor with components $\psi(x)_{\alpha,c,f}$ to each lattice site $x \in \Gamma_{\mathrm{E}}$, where α is the Dirac index and the indexes c and f are the color and flavour degrees of freedom. They satisfy the same

[20] This is also true, of course, for a vanishing background field obtained by setting $C_k = C'_k = 0$.

boundary conditions as their continuum counterparts, that is, they are periodic in the spatial directions up to a phase eq.(4.36), and half of their components have prescribed values in the temporal boundaries as in eq.(4.32).

The lattice fermion action for the SF is given by

$$S_{\mathrm{F}}[U,\psi,\overline{\psi}] = a^4 \sum_{x_0=a}^{T-a} \sum_{\mathbf{x}} \overline{\psi}(\mathbf{x}) \left(\mathcal{D}_W + m_0\right) \psi(x), \tag{4.67}$$

where $\mathcal{D}_W$ is the massless Dirac operator with boundaries given by

$$a\mathcal{D}_{\mathrm{W}}\psi(x) = \begin{cases} -U_0(x)P_-\psi(x+a\hat{0}) + K\psi(x), & x_0 = a, \\ aD_W\psi(x), & a < x_0 < T-a, \\ K\psi(x) - U_0(x-a\hat{0})^\dagger P_+\psi(x-a\hat{0}), & x_0 = T-a \end{cases} \tag{4.68}$$

with the infinite volume Wilson Dirac operator D_{W} defined as in eq.(2.29).

The action with SF boundary conditions can be expressed as a sum over all space-time points without any reference to the finite volume. For that, the fields are defined at all space-time points provided that outside the SF volume fermion fields are set to zero and gauge links are set to the identity. The fermion action in the SF is then given by

$$S_{\mathrm{F}}[U,\psi,\overline{\psi}] = a^4 \sum_{x} \overline{\psi}(\mathbf{x}) \left(D_W + m_0\right) \psi(x). \tag{4.69}$$

In SF setups, due to the special role of the time direction, it is useful to write the Dirac operator as a time difference operator given by

$$aD_{\mathrm{W}}\psi(x) = -U_0(x)P_-\psi(x_0+a\hat{k}) + K\psi(x) - U_0(x_0-a,\mathbf{x})^\dagger P_+\psi(x_0-a,\mathbf{x}), \tag{4.70}$$

where K is the time diagonal kernel which reads

$$K\psi(x) = \left(1 + \frac{1}{2}\sum_{k=1}^{3}\left\{a\left(\nabla_k + \nabla_k^*\right)\gamma_k - a^2\nabla_k^*\nabla_k\right\}\right)\psi(x). \tag{4.71}$$

The lattice version of the SF eq.(4.37), with fermions regulated using Wilson's original proposal, is given by

$$\mathcal{Z}[\rho',\overline{\rho}',C';\rho,\overline{\rho},C] = \int \mathcal{D}[\psi,\overline{\psi}]\mathcal{D}[U]e^{-S_{\mathrm{SF}}[\psi,\overline{\psi},U]}, \tag{4.72}$$

with the full SF action obtained by adding eq.(4.51) and eq.(4.69),

$$S_{\rm SF}[\psi,\overline{\psi},U] = S_{\rm G}[U] + S_{\rm F}[\overline{\psi},\psi,U], \tag{4.73}$$

The fermionic measure is defined as

$$\mathcal{D}[\psi,\overline{\psi}] = \prod_{x_0=a}^{T-a}\prod_{\mathbf{x}}\prod_{\alpha,c,f} d\overline{\psi}(x_0,\mathbf{x})_{\alpha,c,f} d\psi(x_0,\mathbf{x})_{\alpha,c,f}, \tag{4.74}$$

where $d\psi$ and $d\overline{\psi}$ are Grassman measures.[21]

The boundary fields eq.(4.40) also have a lattice counterpart. When inserted within correlation functions, they will act as functional derivatives on the Boltzman factor, bringing down products of link variables and fermion fields evaluated next to the boundaries. By choosing only flavour combinations such that contact terms are avoided in correlation functions, they will act as insertions of the fields

$$\begin{aligned}
\zeta(\mathbf{x}) &\longrightarrow U_0(0,\mathbf{x})\psi(a,\mathbf{x}),\\
\overline{\zeta}(\mathbf{x}) &\longrightarrow \overline{\psi}(a,\mathbf{x})U_0(0,\mathbf{x})^\dagger,\\
\zeta'(\mathbf{x}') &\longrightarrow U_0(T-a,\mathbf{x}')^\dagger\psi(T-a,\mathbf{x}'),\\
\overline{\zeta}'(\mathbf{x}') &\longrightarrow \overline{\psi}(T-a,\mathbf{x}')U_0(T-a,\mathbf{x}).
\end{aligned} \tag{4.75}$$

In the literature it is common to find the projectors $P_\pm$ within the definition of the boundary fields. We prefer not to do so and follow the convention in [81], such that the same notation can be used without ambiguities in both the standard and chirally rotated SF setups, the latter introduced in the following section. Consequently, we will have to write the projectors explicitly when building composite operators involving the boundary fields for their insertion in correlation functions in chapter 5.

4.3.4 Improvement of the fermionic theory

Since Wilson fermions break explicitly chiral symmetry, leading cutoff effects are of $O(a)$ (see chapter 2). Again, one can apply Symanzik's improvement programme to achieve an $O(a)$ improvement of the fermionic theory. For that, one needs to consider improvement terms in the bulk volume $\delta S_{\rm V}$ and in the boundaries $\delta S_{\rm F,b}$.

[21] Note that the fields at the boundaries are not integation variables in the path integral.

For on-shell improvement of the bulk one only needs to add a single counterterm to the action. This is the clover term defined in section 2.3 for infinite volume, which will now be restricted to the hyper-cylinder,

$$\delta S_{\mathrm{SW}} = a^5 \frac{c_{\mathrm{SW}}}{4} i \sum_{x_0=a}^{T-a} \sum_{\mathbf{x}} \overline{\psi}(x) \sum_{\mu,\nu} \sigma_{\mu\nu} \widehat{F}_{\mu\nu}(x) \psi(x), \tag{4.76}$$

The Scheikoleslami-Wohlert coefficient can be expanded in terms of g_0^2,

$$c_{\mathrm{SW}} = c_{\mathrm{SW}}^{(0)} + g_0^2 c_{\mathrm{SW}}^{(1)} + O(g_0^4). \tag{4.77}$$

The leading term is $c_{\mathrm{SW}}^{(0)} = 1$. The standard unimproved action is recovered by setting $c_{\mathrm{SW}} = 0$. Note that when including the term eq.(4.76), the time diagonal kernel eq.(4.71) has to be modified accordingly.

Concerning the boundaries, the operators of dimension 4 that can be built are

$$\overline{\psi} P_{\pm} D_0 \psi, \qquad \overline{\psi} P_{\pm} \gamma_k D_k \psi. \tag{4.78}$$

They can be rearranged in two contributions proportional to the parameters $\widetilde{c}_t$ and $\widetilde{c}_s$, in close analogy to the gauge counterterms. The boundary term will be

$$\begin{aligned} \delta S_{\mathrm{F,b}}[U, \overline{\psi}, \psi] = a^4 \sum_{x \in \Gamma_{\mathrm{E}}} \Big\{ & (\widetilde{c}_s - 1) \left[\widehat{\mathcal{O}}_s(\mathbf{x}) + \widehat{\mathcal{O}}'_s(\mathbf{x}) \right] \\ & + (\widetilde{c}_t - 1) \left[\widehat{\mathcal{O}}_t(\mathbf{x}) + \widehat{\mathcal{O}}'_t(\mathbf{x}) \right] \Big\}, \end{aligned} \tag{4.79}$$

with the operators

$$\begin{aligned} \mathcal{O}_s(\mathbf{x}) =& \frac{1}{2} \overline{\rho}(\mathbf{x}) \gamma_k \left(\nabla_k^* + \nabla_k \right) \rho(\mathbf{x}), \\ \mathcal{O}'_s(\mathbf{x}) =& \frac{1}{2} \overline{\rho}'(\mathbf{x}) \gamma_k \left(\nabla_k^* + \nabla_k \right) \rho'(\mathbf{x}), \\ \mathcal{O}_t(\mathbf{x}) =& \left\{ \overline{\psi}(y) P_+ \nabla_0^* \psi(y) + \overline{\psi}(y) \overleftarrow{\nabla}_0^* P_- \psi(y) \right\}_{y=(0,\mathbf{x})}, \\ \mathcal{O}'_t(\mathbf{x}) =& \left\{ \overline{\psi}(y) P_- \nabla_0 \psi(y) + \overline{\psi}(y) \overleftarrow{\nabla}_0 P_+ \psi(y) \right\}_{y=(T-a,\mathbf{x})}. \end{aligned} \tag{4.80}$$

When setting the boundary quark fields to zero, only the part proportional to $\widetilde{c}_t$ contributes to the action. The part proportional to $\widetilde{c}_s$ still appears in contact terms.

However, correlation functions with these terms can be avoided in practice. The fermionic boundary improvement counterterm then reads,

$$\delta S_{\mathrm{F,b}} = a^4 \sum_{x \in \Gamma_{\mathrm{E}}} (\widetilde{c}_t - 1) \frac{1}{a} \overline{\psi}(x) \psi(x) \left(\delta_{x_0,a} + \delta_{x_0,T-a} \right), \tag{4.81}$$

This contribution can be understood as a correction to the bare quark mass next to the boundaries

$$m_0 \to m_0 + a(\widetilde{c}_t - 1)(\delta_{x_0,a} + \delta_{x_0,T-a}). \tag{4.82}$$

The coefficient $\widetilde{c}_t$ is expanded in terms of g_0 by

$$\widetilde{c}_t = \widetilde{c}_t^{(0)} + g_0^2 \widetilde{c}_t^{(1)} + O(g_0^4). \tag{4.83}$$

The perturbative coefficients $\widetilde{c}_t^{(k)}$ are collected in table 4.4.1 at the end of this chapter. The improved fermion action is then given by

$$S_{\mathrm{F,I}} = S_{\mathrm{F}}[U, \psi, \overline{\psi}] + \delta S_{\mathrm{SW}}[U, \psi, \overline{\psi}] + \delta S_{\mathrm{F,b}}[U, \psi, \overline{\psi}]. \tag{4.84}$$

4.3.5 Automatic O(a) improvement?

Massless Wilson fermions[22] in a finite volume are expected to enjoy the property of automatic $O(a)$ improvement [21]. The argument for this to be true, which we collect in the appendix D, relies on chiral symmetry

$$\begin{aligned} \mathcal{R}_5 : \quad & \psi(x) \longrightarrow \psi(x)' = i\gamma_5 \psi(x), \\ & \overline{\psi}(x) \longrightarrow \overline{\psi}(x)' = \overline{\psi}(x) i\gamma_5, \end{aligned} \tag{4.85}$$

being an exact symmetry of the continuum theory. In this situation, observables can be classified as even or odd under the $\mathcal{R}_5$ transformation. Only even observables are physical, and they are only affected by even powers of the lattice spacing a. Odd observables receive contributions from odd powers of a and vanish in the continuum limit.

However, the projector structure of the SF boundary conditions eq.(4.44) breaks chiral symmetry explicitly. The SF projectors $P_{\pm}$ do not commute with the chiral

[22] Understanding by massless that the bare quark mass has been tuned to the critical mass m_c.

transformation $\mathcal{R}_5$ but, instead, they behave as

$$P_{\pm}\gamma_5 = \gamma_5 P_{\mp}, \tag{4.86}$$

which implies that the transformed fields satisfy boundary conditions with complementary projectors

$$\begin{aligned} &P_-\psi'(x)|_{x_0=0} = 0, \qquad && P_+\psi'(x)|_{x_0=T} = 0, \\ &\overline{\psi}'(x)\, P_+|_{x_0=0} = 0, \qquad && \overline{\psi}'(x)\, P_-|_{x_0=T} = 0. \end{aligned} \tag{4.87}$$

Hence, the transformantion $\mathcal{R}_5$ is not a symmetry of the theory any more. Note that the breaking of chiral symmetry by the boundaries happens already at the continuum level and not as a consequence of the lattice regulator[23]. As a consequence, no automatic $O(a)$ improvement happens for massless Wilson fermions with standard SF boundary conditions and, hence, improvement counterterms must be added to the action in the bulk and to composite fields, which would otherwise be absent if automatic $O(a)$ improvement held.

The important question is then whether there is a way to recover automatic $O(a)$ improvement in SF schemes. If there were an alternative symmetry $\widetilde{\mathcal{R}}_5$ and projectors $\widetilde{P}_{\pm}$, such that $\widetilde{\mathcal{R}}_5$ was a symmetry of the continuum theory without boundaries[24], and such that

$$\left\{\widetilde{P}_{\pm}, \widetilde{\mathcal{R}}_5\right\} = 0, \tag{4.88}$$

then the argument for automatic $O(a)$ improvement could be resurrected based on the $\widetilde{\mathcal{R}}_5$ symmetry.

In [1] a modified transformation was proposed by augmenting the $\mathcal{R}_5$ transformation with a flavour permutation obtaining then a new transformation $\mathcal{R}_5^1$ (assuming $\psi(x)$ to be a flavour doublet) given by,

$$\begin{aligned} \mathcal{R}_5^1 : \quad &\psi(x) \longrightarrow \psi(x)' = i\gamma_5\tau^1\psi(x), \\ &\overline{\psi}(x) \longrightarrow \overline{\psi}(x)' = \overline{\psi}(x)i\gamma_5\tau^1, \end{aligned} \tag{4.89}$$

where τ^1 is a Pauli matrix[25] (see appendix A.3 for conventions). The flavour permu-

[23] We remark, once again, that the key ingredient for automatic $O(a)$ improvement to hold is the invariance of the massless continuum theory under $\mathcal{R}_5$ symmetry.

[24] Nevertheless broken by the Wilson term.

[25] An alternative transformation R_5^2 could also be taken, using the Pauli matrix τ^2 instead.

tation does not affect the action in the bulk.

Several boundary conditions can be considered such that eq.(4.88) holds with the transformation $\mathcal{R}_5^1$. Following [1], we will only consider here the boundary conditions obtained using the projectors [26]

$$\widetilde{Q}_{\pm} = \frac{1}{2}\left(1 \pm i\gamma_0\gamma_5\tau^3\right), \tag{4.90}$$

and given by

$$\begin{aligned} &\widetilde{Q}_{+}\psi(x)\Big|_{x_0=0} = 0, \qquad &&\widetilde{Q}_{-}\psi(x)\Big|_{x_0=T} = 0, \\ &\overline{\psi}(x)\,\widetilde{Q}_{+}\Big|_{x_0=0} = 0, \qquad &&\overline{\psi}(x)\,\widetilde{Q}_{-}\Big|_{x_0=T} = 0. \end{aligned} \tag{4.91}$$

These can be obtained from the standard SF boundary conditions eq.(4.44) by applying a non-anomalous axial transformation $R(\alpha)$ to the flavour doublets

$$\psi \longrightarrow R(\alpha)\psi, \qquad \overline{\psi} \longrightarrow \overline{\psi}R(\alpha), \qquad \text{with } R(\alpha) = e^{i\gamma_5\tau^3\alpha/2}. \tag{4.92}$$

The rotated fields satisfy a rotated version of the boundary conditions

$$\begin{aligned} &P_{+}(\alpha)\psi(x)|_{x_0=0} = 0, \qquad &&P_{-}(\alpha)\psi(x)|_{x_0=T} = 0, \\ &\overline{\psi}(x)\gamma_0\, P_{-}(\alpha)|_{x_0=0} = 0, \qquad &&\overline{\psi}(x)\gamma_0\, P_{-}(\alpha)|_{x_0=T} = 0, \end{aligned} \tag{4.93}$$

with the rotated projectors given by

$$P_{\pm}(\alpha) = \frac{1}{2}\left[1 \pm \gamma_0 \exp(i\alpha\gamma_5\tau^3)\right]. \tag{4.94}$$

When taken at $\alpha = \pi/2$, the transformation eq.(4.92) leads to the boundary conditions in eq.(4.91), which give rise to the so called chirally rotated version of the SF (χSF). A lattice regulation of the χSF will hence be automatically $O(a)$ improved by construction.[27]

Since the standard SF and χSF setups are obtained by a rotation $R(\pi/2)$ of the fields, which is a symmetry of the massless continuum theory, both setups are completely equivalent in the continuum (and chiral) limit.

[26] Even if it might be possible to find alternative transformations and boundary conditions such that eq.(4.88) holds, the difficult part is to implement the boundary conditions on the lattice and to show that they lead to a sensible definition of the SF in the continuum and chiral limits.

[27] After tuning the parameter of an extra boundary operator, as will be seen in the following section.

Correlation functions calculated in the two setups are related by the chiral twist eq.(4.92), establishing universality relations of the form

$$\langle O[\psi, \overline{\psi}] \rangle_{\chi\mathrm{SF}} = \langle O[R(-\pi/2)\psi, \overline{\psi} R(-\pi/2)] \rangle_{\mathrm{SF}} \,. \tag{4.95}$$

This situation is analogous to the relation between standard QCD and twisted mass QCD at maximal twist. In fact, a dictionary relating correlation functions in the SF and the χSF can be taken directly from QCD and tmQCD.

The next step in this presentation is to discuss the lattice implementation of the χSF setup.

4.3.6 The χSF on the lattice

On the lattice, boundary conditions can not really be imposed, but rather arise dynamically from the structure of the lattice action near the boundaries [82]. In some cases, the lattice action has to be modified near the boundaries such that in the continuum limit the correct boundary conditions are recovered. This is the situation for the χSF, where in [1] a lattice version is obtained by means of orbifold techniques, in which the theory is formulated on an orbifold and the correct boundary conditions are obtained through an orbifold reflection.

Three different constructions where originally proposed in [1], leading to lattice actions which differ only by cutoff effects at finite lattice spacing. These are based on different ways of establishing the orbifold reflections. One construction is based on a reflection about the time slice at $x_0 = 0$, referred to as a site reflection. the other two constructions are reflections about the would be points $x_0 = \pm a/2$, called link reflections since the point x_0 falls on the middle of a link. In this work we will only focus on the construction with reflection about $x_0 = -a/2$, referred in [1] as "orbifold reflection with an $O(a)$ offset". In this construction, dynamical fermion fields are defined in the interval $0 \leq x_0 \leq T$. [28]

Starting with a theory of Wilson quarks in infinite volume, the orbifold construction gives rise to a fermion action describing a flavour doublet satisfying χSF boundary conditions eq.(4.91). In fact, by following these lines it is only possible to obtain homogeneous boundary conditions for the lattice theory. The action is then given by

[28] In contrast to the standard SF construction, where dynamical fermions are only defined for the interval $0 < x_0 < T$.

$$S_{\mathrm{F}}^{\chi\mathrm{SF}}[U,\overline{\psi},\psi] = a^4 \sum_{x_0=0}^{T} \sum_{\mathbf{x}} \overline{\psi}(x)\,(\mathcal{D}_{\mathrm{W}} + m_0)\,\psi(x), \tag{4.96}$$

where $\mathcal{D}_{\mathrm{W}}$ is the massless Wilson-Dirac operator with boundaries, given by

$$a\mathcal{D}_{\mathrm{W}}\psi(x) = \begin{cases} -U_0(x)P_-\psi(x+a\hat{0}) + (K + i\gamma_5\tau^3 P_-)\psi(x), & x_0 = 0 \\ aD_W\psi(x), & 0 < x_0 < T \\ (K + i\gamma_5\tau^3 P_+)\psi(x) - U_0(x-a\hat{0})^\dagger P_+\psi(x-a\hat{0}), & x_0 = T \end{cases} \tag{4.97}$$

The infinite volume operator aD_{W} in the bulk is the same as eq.(4.70) for the SF and K is, again, the time diagonal kernel given in eq.(4.71). The Dirac operator for the χSF is hence the same as for the SF (for a flavour doublet) with a modification at the boundaries.

The Dirac operator $\mathcal{D}_{\mathrm{W}}$ can be written alternatively as the infinite volume operator D_{W} actiong on $\psi(x)$ for the whole interval $0 \le x_0 \le T$, supplementing the fields with the syntactic extension

$$\psi(-a,\mathbf{x}) = -i\gamma_0\gamma_5\tau^3\psi(0,\mathbf{x}); \qquad \psi(T+a,\mathbf{x}) = i\gamma_0\gamma_5\tau^3\psi(T,\mathbf{x}), \tag{4.98}$$

The χSF boundary conditions in this construction are satisfied up to cutoff effects of $O(a)$

$$\begin{aligned} \widetilde{Q}_+\left(1 - \frac{1}{2}a\partial_0^*\right)\psi(x)\Big|_{x_0=0} &= 0, \qquad \widetilde{Q}_-\left(1 + \frac{1}{2}a\partial_0\right)\psi(x)\Big|_{x_0=T} = 0, \\ \overline{\psi}(x)\gamma_0\,\widetilde{Q}_+\left(1 - \frac{1}{2}a\overleftarrow{\partial}_0^*\right)\Big|_{x_0=0} &= 0, \qquad \overline{\psi}(x)\gamma_0\,\widetilde{Q}_-\left(1 + \frac{1}{2}a\overleftarrow{\partial}_0\right)\Big|_{x_0=T} = 0. \end{aligned} \tag{4.99}$$

We refer again to appendix A.5 for unexplained notation concerning lattice derivatives.

Link reflections give rise to boundary conditions displaced by effects of order a with respect to the continuum ones. This happens essentially since the reflection points $x_0 = \pm a/2$ can not be reached in the lattice theory. Exact boundary conditions for the construction we are considering would be satisfied at the points $x_0 = -a/2, T + a/2$, instead of $x_0 = 0, T$, thus generating the $O(a)$ terms in eq.(4.99).

The massless Dirac operator $\mathcal{D}_{\mathrm{W}}$ satisfies the hermiticity property [1]

$$\tau^1\gamma_5\mathcal{D}_{\mathrm{W}}\gamma_5\tau^1 = \mathcal{D}_{\mathrm{W}}^\dagger. \tag{4.100}$$

The spectrum of $\tau^1\gamma_5\mathcal{D}_{\mathrm{W}}$ is hence bounded from below, with a non vanishing minimum eigenvalue given by

$$|\lambda_0| = \frac{2}{a}\left|\sin\left(\frac{a\pi}{4(T+a)}\right)\right| \xrightarrow{a\to 0} \frac{\pi}{2T}, \tag{4.101}$$

which coincides with the continuum one in the limit $a \to 0$ [36].

As already explained for the standard SF, this guarantees that one can go to zero quark mass without the problems deriving from fermionic zero modes, and hence define a mass independent renormalization scheme.

4.3.7 Renormalization and improvement of the χSF

Once the classical theory is defined on the lattice, the next step is to study the renormalizability of the theory and to go through Symanzik's improvement program to $O(a)$. For understanding the renormalization properties one needs all bulk and boundary operators, of dimension $d \leq 4$ and $d \leq 3$ respectively, which satisfy the symmetries of the lattice theory. For performing the $O(a)$ improvement, the operators needed are of dimension $d = 5$ in the bulk and $d = 4$ at the boundaries.

The bulk counterterms which are allowed by the symmetries are the same as for infinite volume, already discussed in section 2.3. The renormalization of the bulk is hence identical as for the standard SF such that one only needs to consider the renormalization of the bare coupling and the bare mass, this last with the additive renormalization originated due to the presence of the Wilson term. Moreover, the only allowed counterterm of dimension $d = 5$ is the clover term (see eq.(4.76)), which is a pure cutoff effect. In a situation where $O(a)$ improvement holds, the clover term contributes to physical observables only to $O(a^2)$, so it is not needed for improvement to $O(a)$. However, we choose to keep it in our formulation for being able to compare results calculated in both χSF and SF setups.[29] Moreover, its presence will reduce $O(a)$ ambiguities in renormalization conditions which require odd correlation

[29]For both schemes to be equivalent in the continuum limit we must use the same regularization in the bulk.

functions (which are pure cutoff effects as well) to vanish (see below).

Concerning the boundary counterterms, one finds a total of 3 $O(1)$ and 3 $O(a)$ terms respecting the lattice symmetries, which must be added to the χSF lattice action eq.(4.96) with appropriately chosen parameters. In practice, however, many of these counterterms can be ignored. This is so either because they contribute only to $O(a^2)$ in physical correlation functions, because they appear in correlation functions which can be avoided, or because they can be absorbed in the renormalization of the fields at the boundaries as has been discussed in section 4.3.3.

For the renormalization of the theory one is thus left with only an $O(1)$ counterterm, proportional to a parameter z_f and, for the improvement, with an $O(a)$ counterterm proportional to a coefficient d_s (we refer to the original literature for details on the full counterterm structure [36]). These are added to the action as

$$\delta S_{\mathrm{F,b}} = a^4 \sum_x \overline{\psi}(x) \left(\delta_{x_0,0} + \delta_{x_0,T}\right) \left[(z_f - 1) + (d_s - 1) a\mathbf{D}_s\right] \psi(x), \tag{4.102}$$

with

$$a\mathbf{D}_s = \frac{a}{2} \left(\nabla_k + \nabla_k^*\right) \gamma_k. \tag{4.103}$$

The full action for the χSF will then be given by

$$S_{\mathrm{F,I}}^{\chi\mathrm{SF}}[U, \psi, \overline{\psi}] = S_{\mathrm{F}}^{\chi\mathrm{SF}}[U, \psi, \overline{\psi}] + \delta S_{\mathrm{V}}^{\chi\mathrm{SF}}[U, \psi, \overline{\psi}] + \delta S_{\mathrm{F,b}}^{\chi\mathrm{SF}}[U, \psi, \overline{\psi}]. \tag{4.104}$$

The coefficient d_s can be tuned to cancel the $O(a)$ effects coming from the boundaries, and it is analogous to the $\widetilde{c}_t$ coefficient in the standard SF formulation.

The coefficient z_f, however, has no counterpart in the standard SF. It is the coefficient of a relevant operator at the boundaries, which accounts for the restoration of the parity and flavour symmetries $\gamma_5\tau^1$ broken by the regulator. z_f is hence a finite renormalization constant, i.e. scale independent function of the bare coupling. It can be shown [1] that it plays the same role as the finite renormalization of the twisting angle in tmQCD. Tuning z_f appropriately ensures that the correct boundary conditions are realised on the lattice theory, leading to the correct continuum limit.

The 2 counterterms in eq.(4.102) contribute to all correlation functions in the theory, since they enter directly the expression of the Dirac operator. The two coefficients

are functions of the bare coupling with an expansion of the form

$$\begin{aligned} z_f(g_0) &= z_f^{(0)} + z_f^{(1)} g_0^2 + O(g_0^4), \\ d_s(g_0) &= d_s^{(0)} + d_s^{(1)} g_0^2 + O(g_0^4). \end{aligned} \tag{4.105}$$

The leading term $z_f^{(0)} = 1$ is obtained by comparing the free quark propagator in the continuum with the continuum limit of the analytical expression for the lattice quark propagator and requiring them to coincide.

In presence of an offset in the orbifold construction, the coefficient d_s is already needed at the classical level in order to cancel boundary $O(a)$ effects arising due to the displacement of the boundary conditions. For the case at hand, the correct value for the leading term is $d_s^{(0)} = 1/2$, obtained by demanding the absence of $O(a)$ effects in the propagator.[30] A drawback of this is that no analytic expression for the fermion propagator is known if the counterterms eq.(4.102) are included with $d_s^{(0)} \neq 1$, and thus one is forced to invert the Dirac operator numerically when performing a perturbative calculation.

Moreover, one can include a Wilson term in the definition eq.(4.103) obtaining an alternative counterterm

$$a\mathbf{D}_s = \frac{a}{2}\left(\nabla_k + \nabla_k^*\right)\gamma_k - \frac{a^2}{2}\nabla_k^*\nabla_k. \tag{4.106}$$

Adding the extra term is completely harmless since it respects all the symmetries of the lattice action and contributes to physical quantities only to $O(a^2)$. The advantage of this modification is that eq.(4.106) has the same structure as the original Dirac operator eq.(4.70), and hence the counterterm can be easily included in the action by adding a factor d_s in front of the spatial derivatives at the boundaries.[31] It is this alternative we consider for the rest of this work.

Concluding, in the χSF there is only one additional boundary coefficient z_f with respect to the SF. Concerning the improvement coefficient d_s, it might be enough to determine it to a few orders in PT, as has been argued in section 4.3.4 for $\widetilde{c}_t$. On the contrary, z_f has to be determined non-perturbatively.

The tuning of z_f and of the bare mass m_0 to their critical values account for the

[30] In a construction without offset, since the boundary conditions would be exactly realised at the boundaries, d_s would not be needed at tree-level and hence $d_s^{(0)} = 1$.

[31] This is very comfortable when implementing the Dirac operator for a computer simulation.

restoration of the $\gamma_5\tau^1$ symmetry and chiral symmetry respectively. For a numerical simulation z_f and m_0 must be tuned simultaneously and non-perturbatively. Without a full non-perturbative determination of z_f, the $\gamma_5\tau^1$ symmetry might not be properly restored, which would compromise the continuum limit.

As we will see in section 5.4.1 of the following chapter, the tuning of z_f can be done by imposing a $\gamma_5\tau^1$ odd correlation function to vanish. The tuning of m_0 to m_c can be done as usual, by imposing a chiral symmetry violating observable to vanish (for example, $m_{\mathrm{PCAC}} = 0$). One of the main goals of this thesis is to show that the simultaneous tuning of z_f and m_0 is feasible at least to one loop in perturbation theory, and to obtain the one loop coefficients $z_f^{(1)}$, $m_c^{(1)}$ and $d_s^{(1)}$ of the χSF scheme.

4.4 Perturbation theory in Schrödinger functional schemes

Once a fully working non-perturbative formulation of the Schrödinger functional has been given, perturbation theory has to be defined within that setup. A priori, one might wonder why perturbation theory is needed at all provided that we have a fully non-perturbative construction. The reasons are the following.

The first, already explained when discussing non-perturbative renormalization and finite volume schemes in chapter 3, is for matching quantities calculated in a non-perturbative scheme with quantities in perturbative onse like the $\overline{\mathrm{MS}}$ scheme.

Secondly, in the present chapter we have presented the $O(a)$ improved versions of SF formulations following Symanzik's improvement program. Every boundary or volume operator introduced for the improvement comes with a coefficient which is a function of the bare coupling g_0. Ideally, these coefficients should be determined non-perturbatively. But in practice this turns out to be an extremely expensive task, since it requires the tuning of all the improvement parameters to simultaneously satisfy all the needed improvement and renormalization conditions. Perturbation theory can be used here in different ways. On the one hand, it is enough to perform the tuning of boundary improvement coefficients in perturbation theory. These cancel cutoff effects due to insertions of operators at the boundaries, the contribution of which becomes less relevant as lattices get larger. On the other hand, for the coefficients which must be tuned fully non-perturbatively, their perturbative knowledge can be very helpful

as a guide for the computationally expensive tuning.

Moreover, perturbation theory is the only way of having analytic control on the theory as the continuum limit is approached. Close to the continuum limit perturbative calculations and data from simulations should match each other, hence perturbation theory can be used to control that the non-perturbative codes are indeed working correctly.

Finally, perturbation theory can be used to monitor cutoff effects in several observables (see chapters 5, 6 and 7). It can then be used as a laboratory arena to test several improvement strategies before embarking into expensive numerical calculations.

In this section we will briefly sketch the main aspects of a perturbative calculation in the Schrödinger Functional. We assume homogeneous boundary conditions for the fermion fields for the rest of this thesis.

4.4.1 Setting up perturbation theory

When setting up perturbation theory one has to go through a gauge fixing procedure. In a non-perturbative calculation on a lattice setup it is not necessary to fix the gauge since the dynamical gauge fields $U_\mu(x)$ are elements of a compact gauge group. In perturbation theory, the link variables $U_\mu(x)$ have to be expanded as a series in the bare coupling g_0,

$$\begin{aligned} U_\mu(x) &= \exp\{g_0 a q_\mu(x)\} V_\mu(x) = \\ &= \left\{1 + g_0 a q_\mu(x) + \frac{1}{2} g_0^2 a^2 q_\mu(x)^2 + O(g_0^3)\right\} V_\mu(x), \end{aligned} \tag{4.107}$$

where the fields $q_\mu(x)$ are identified with the gluon fields of continuum QCD. For generality, we write the expansion eq.(4.107) around the classical BF $V_\mu(x)$ which is the global minimum of the action eq(4.51).[32] After the expansion, the integration variables $U_\mu(x)$ are replaced in favour of the gluons $q_\mu(x)$. The fields $q_\mu(x)$ live in the non-compact space of the Lie algebra $su(3)$, and hence, the gauge must be fixed.

For details on the gauge fixing procedure in SF schemes we refer to [83] for a case with zero background field, and to [23] for a case with the Abelian background fields given by eq.(4.54). Since the gauge part of the action for both SF and χSF setups is identical, we will be able to reuse the procedures on [83] and [23] for the calculations

[32] In absence of background field one simply would replace $V_\mu(x) \longrightarrow \mathbb{I}$ in eq.(4.107).

in chapters 5, 6 and 7.

As a result of gauge fixing, one has to add to the action a gauge fixing term $S_{\rm gf}[V,q]$ and a term induced by the Fadeev-Poppov determinant $S_{\rm FP}[V,q,c,\overline{c}]$ which governs the ghost fields c and $\overline{c}$. We refer to the literature for explicit expressions of these terms [23, 83].

An additional contribution, which is not present in continuum calculations, has to be considered due to the change from the variables $U_\mu(x)$ to $q_\mu(x)$. The measure in the path integral for the new $q_\mu(x)$ fields is given by

$$\mathcal{D}[q] = \prod_{x,\mu,a} dq^a_\mu(x) \tag{4.108}$$

and it is related to the Haar measure for the link variables via

$$\mathcal{D}[U] = \mathcal{D}[q] e^{-S_{\rm m}[q]}, \tag{4.109}$$

with the term

$$S_{\rm m}[q] = \frac{g_0^2}{8} \sum_{x,\mu,a} q^a_\mu(x) q^a_\mu(x) + O(g_0^4). \tag{4.110}$$

The measure contributes directly to order g_0^2. In this thesis, however, we will only need to expand the action up to $O(g_0)$, so $S_{\rm m}[q]$ will not contribute at this order. We keep it here only for completeness of the present discussion. The total action to consider will hence be the sum of all the terms

$$\begin{aligned} S_{\rm tot}[V,q,c,\overline{c},\psi,\overline{\psi}] =& S_{\rm G}[V,q] + S_{\rm gf}[V,q] + S_{\rm FP}[V,q,c,\overline{c}] \\ &+ S_{\rm F}[V,q,\psi,\overline{\psi}] + S_{\rm m}[q], \end{aligned} \tag{4.111}$$

and the Schrödinger Functional in the path integral representation will be given by

$$\mathcal{Z}[C,C'] = \int \mathcal{D}[q]\mathcal{D}[c]\mathcal{D}[\overline{c}]\mathcal{D}[\psi]\mathcal{D}[\overline{\psi}] e^{-S_{\rm tot}}. \tag{4.112}$$

Lets assume an observable $\mathcal{O}[U]$ to be a product of link variables only. This can be done without loss of generality since, even if we consider an observable $\widetilde{\mathcal{O}}[U,\psi,\overline{\psi}]$ which does depend on the fermion fields, these can always be integrated analytically, as explained in section 2.2.2, by considering separately the fermionic and gauge

expectation values, such that

$$\left[\widetilde{\mathcal{O}}[U,\psi,\overline{\psi}]\right]_{\mathrm{F}} \equiv \mathcal{O}[U]. \tag{4.113}$$

The gauge expectation value $\langle\mathcal{O}\rangle_{\mathrm{G}}$ can be written (re-introducing the quark determinant as an integral over Grassmann variables) as

$$\langle\mathcal{O}\rangle_{\mathrm{G}} = \frac{1}{\mathcal{Z}}\int \mathcal{D}[q]\mathcal{D}[c]\mathcal{D}[\overline{c}]\mathcal{D}[\psi]\mathcal{D}[\overline{\psi}]e^{-S_{\mathrm{tot}}}. \tag{4.114}$$

The observable $\mathcal{O}$ is expanded as a series in powers of g_0,

$$\mathcal{O} = \mathcal{O}^{(0)} + g_0\mathcal{O}^{(1)} + g_0^2\mathcal{O}^{(2)} + O(g_0^3). \tag{4.115}$$

The terms $\mathcal{O}^{(n)}$ contain products of n gluon fields q_μ. Since $\mathcal{O}^{(0)}$ contains no gluon fields, the expectation value becomes trivial

$$\langle\mathcal{O}^{(0)}\rangle_{\mathrm{G}} = \mathcal{O}^{(0)}. \tag{4.116}$$

The expansion of the expectation value eq.(4.114) thus reads

$$\langle\mathcal{O}\rangle_{\mathrm{G}} = \mathcal{O}^{(0)} + g_0\langle\mathcal{O}^{(1)}\rangle_{\mathrm{G}} + g_0^2\langle\mathcal{O}^{(2)}\rangle_{\mathrm{G}} + O(g_0^3). \tag{4.117}$$

Finally, one needs to consider the expansion of the exponential of the total action S_{tot}

$$S_{\mathrm{tot}} = \frac{1}{g_0^2}S_{\mathrm{tot}}^{(-2)} + S_{\mathrm{tot}}^{(0)} + g_0 S_{\mathrm{tot}}^{(1)} + g_0^2 S_{\mathrm{tot}}^{(2)} + O(g_0^3). \tag{4.118}$$

The term $S_{\mathrm{tot}}^{(-2)}$ is the classical action for the background field $V_\mu(x)$. It will only be present for non-zero BF. Moreover, since it does not depend on the gluon variables q_μ, it will cancel out from all expectation values. The Boltzmann factor in the path integral can be separated as

$$e^{-S_{\mathrm{tot}}} = \left[1 - g_0 S_{\mathrm{tot}}^{(1)} + g_0^2\left(\frac{1}{2}S_{\mathrm{tot}}^{(1)2} - S_{\mathrm{tot}}^{(2)}\right) + O(g_0^4)\right] e^{-S_{\mathrm{tot}}^{(0)}}. \tag{4.119}$$

Denoting the gauge field average taken with the free action $S_{\mathrm{tot}}^{(0)}$ as $\langle\cdot\rangle_0$, and inserting

the expansion eq.(4.119) into eq.(4.117), one obtains the contribution

$$\langle \mathcal{O} \rangle_{\mathrm{G}} = \mathcal{O}^{(0)} + g_0^2 \left[\langle \mathcal{O}^{(2)} \rangle_0 - \langle \mathcal{O}^{(1)} \langle [S_{\mathrm{tot}}^{(1)}\rangle]_{\mathrm{F}} \rangle_0 \right] + O(g_0^4). \tag{4.120}$$

No odd terms in g_0 can occur since they involve an odd number of gluon fields, and hence their expectation value yields zero. The term with $S_{\mathrm{tot}}^{(1)}$ is present only for non-zero background fields.

From Symanzik's analysis [84, 85] on the cutoff dependence of Feynman diagrams on the lattice, we expect that a specific l-loop Feynman diagram $f^{(l)}(x)$ can be expressed as an asymptotic series of the form

$$f^{(l)}(a/L) \xrightarrow{a\to 0} \sum_{m=0}^{\infty} \sum_{n=0}^{l} f_{mn}^{(l)} a^m (\ln a)^n \,, \tag{4.121}$$

where $f_{mn}^{(l)}$ are the expansion coefficients to order a^m and with the n-th power of the logarithm. This asymptotic form can be understood from the fact that loops contribute logarithmically to the overall value of the diagram and that, within Symanzik's effective theory, lattice artefacts correspond to irrelevant operators which carry explicit factors of the lattice spacing.

Logarithmically divergent terms can be cancelled by the renormalization of the bare coupling [23]

$$g_0^2 = g_{\mathrm{lat}}^2 + z_1(a\mu) g_{\mathrm{lat}}^4 + \ldots; \qquad z_1(a\mu) = 2b_0 \ln(a\mu). \tag{4.122}$$

The lattice artefacts, which correspond to the coefficients $a\ln(a)^n$, $a^2\ln(a)^n$ can be eliminated order by order through Symanzik's improvement programme.

4.4.2 The inclusion of counterterms

The improved fermion action $S_{\mathrm{F,I}}$ given in eq.(4.84) is a sum of terms corresponding to the unimproved action and the boundary and bulk counterterms. All the parameters which contain an explicit dependence on g_0 can be collectively denoted by the vector $c(g_0) = (m_0, c_{\mathrm{SW}}, \widetilde{c}_t)$ for the standard SF, or $c(g_0) = (m_0, c_{\mathrm{SW}}, z_f, d_s)$ for the χSF.

When computing the expansion of an operator $\mathcal{O}$, it is useful to separate the g_0 contributions due to the expansion of the link variables (either in the action or in

the definition of the observable $\mathcal{O}$ itself) from the contributions coming from the coefficients $c(g_0)$. In this way it is clear how the individiual contributions of each counterterm enter into an expectation value. The coefficients are expanded as

$$c(g_0) = c^{(0)} + g_0^2 c^{(1)} + O(g_0^4). \tag{4.123}$$

Introducing them to the improved action we obtain

$$S_{\mathrm{F,I}}(c) = S_{\mathrm{F,I}}(c^{(0)}) + g_0^2 \sum_i c_i^{(1)} \partial_{c_i} S_{\mathrm{F,I}}(c^{(0)}) + O(g_0^4). \tag{4.124}$$

By defining the correction operators Δ,

$$\partial_{c_i} S_{\mathrm{F,I}}(c^{(0)}) = -a^4 \sum_x \Delta_{c_i}(x)_i, \tag{4.125}$$

we can write the fermion average of an operator $\mathcal{O}$:

$$\langle \mathcal{O} \rangle_{\mathrm{F}} = \langle \mathcal{O} \rangle_{\mathrm{F},c^{(0)}} + g_0^2 \sum_i c_i a^4 \sum_x \langle \mathcal{O} \Delta_i(x) \rangle_{\mathrm{F},c^{(0)}} + O(g_0^4), \tag{4.126}$$

where the average $\langle \cdot \rangle_{\mathrm{F},c^{(0)}}$ denotes the fermion average taken using the improved action $S_{\mathrm{F,I}}(c^{(0)})$ in the Boltzmann factor, with its coefficients fixed to the tree-level values. This separation will be particularly useful in the following chapter, when performing the perturbative expansion of correlation functions.

coefficient	value	references
$m_c^{(1)}\|_{c_{\rm SW}=0}$	$-0.4342856(3)$	[86–88], ★
$m_c^{(1)}\|_{c_{\rm SW}=1}$	$-0.2700753495(2)$	[83, 89], ★
$c_{\rm SW}^{(1)}$	$0.26590(7)$	[83, 89]
$c_{\rm t}^{(1,0)}$	$-0.08900(5)$	[23]
$c_{\rm t}^{(1,1)}$	$0.0191410(1)$	[80], ★
$c_{\rm t}^{(1,1)}\|_{\chi{\rm SF},\, c_{\rm SW}=0}$	$-0.00661445(5)$	★
$c_{\rm t}^{(1,1)}\|_{\chi{\rm SF},\, c_{\rm SW}=1}$	$0.006888(3)$	★
$c_{\rm t}^{(2,0)}$	$-0.0294(3)$	[90]
$c_{\rm t}^{(2,1)}$	$-0.002(1)$	[52]
$c_{\rm t}^{(2,2)}$	$-0.0000(1)$	[52]
$\widetilde{c}_{\rm t}^{(1)}$	$-0.01795(2)$	[83, 91], ★
$d_s^{(1)}\|_{c_{\rm SW}=1}$	$-0.0012(4)$	★
$z_f^{(1)}\|_{c_{\rm SW}=0}$	$0.44031(8)$	★
$z_f^{(1)}\|_{c_{\rm SW}=1}$	$0.223429(3)$	★

Table 4.4.1: List of perturbative coefficients for the gauge group $SU(3)$ and the references where they are extracted from. The symbol ★ means that the coefficient has been either calculated for the first time or recalculated in the this thesis.

"Look for the bare necessities
The simple bare necessities
Forget about your worries and your strife.
I mean the bare necessities
Old Mother Nature's recipes
That brings the bare necessities of life."

Baloo the bear

5

Correlation Functions in Schrödinger Functional schemes.

ALL THE PHYSICAL INFORMATION of a quantum field theory is contained in its correlation functions. Typically, the correlation functions we will consider here have the generic form

$$\langle O(x) O_{\text{ext}} \rangle, \tag{5.1}$$

where $O(x)$ is an interpolating field defined over a finite domain $x \in X \subset \mathcal{M}$, and O_{ext} is an external field defined outside the domain X. When constructing correlation functions, different interpolating fields correspond to different physical observables. For a given $O(x)$, several choices of O_{ext} might be used as different probes of the same physical quantity.

Interpolating fields are constructed as gauge invariant products of the dynamical fields of the theory. For the rest of the chapter we will restrict attention to interpolating fields built as fermion bilinears which, for a generic Dirac structure Γ, take the

form

$$O(x) = \overline{\psi}(x)\Gamma\psi(x). \tag{5.2}$$

In SF schemes it is possible to construct interpolating fields which involve products of derivatives of the boundary fermion fields. When used in a correlation function, they have the effect of inserting dynamical fields close to the boundaries into the functional integral. Interpolating fields constructed in this way are referred as boundary operators and, for a given Dirac structure, they are of the form

$$\mathcal{O} = \int d\mathbf{y}d\mathbf{z}\frac{\delta}{\delta\rho(\mathbf{y})}\Gamma\frac{\delta}{\delta\overline{\rho}(\mathbf{z})}, \quad x_0 = 0, \tag{5.3}$$

$$\mathcal{O}' = \int d\mathbf{y}'d\mathbf{z}'\frac{\delta}{\delta\rho'(\mathbf{y}')}\Gamma\frac{\delta}{\delta\overline{\rho}'(\mathbf{z}')}, \quad x_0 = T. \tag{5.4}$$

Using the relation eq.(4.40), the boundary operators can be rewritten in the more usual form

$$\mathcal{O} = \int d\mathbf{y}d\mathbf{z}\overline{\zeta}(\mathbf{y})\Gamma\zeta(\mathbf{z}), \quad x_0 = 0, \tag{5.5}$$

$$\mathcal{O}' = \int d\mathbf{y}'d\mathbf{z}'\overline{\zeta}'(\mathbf{y}')\Gamma\zeta'(\mathbf{z}'), \quad x_0 = T. \tag{5.6}$$

In the following we will focus on two kinds of correlation functions. The first, which are referred to as boundary to bulk correlation functions, involve a fermion bilinear $O(x)$ defined in the bulk of the manifold and an external field O_{ext} taken to be a boundary operator as the ones in eqs.(5.5) and (5.6).[1] They are generically given by the expression

$$\langle O(x)\mathcal{O}\rangle = \frac{1}{\mathcal{Z}}\int \mathcal{D}[\psi,\overline{\psi}]\mathcal{D}[A]O(x)\mathcal{O}e^{-S[\psi,\overline{\psi},A]}\Big|_{\overline{\rho}=\rho=\overline{\rho}'=\rho'=0}. \tag{5.7}$$

Boundary to bulk correlation functions can be understood as the probability amplitude for a quark and anti-quark pair being created at the boundary at $x_0 = 0$, and propagating to the point x in the bulk, where they are annihilated.[2]

[1] This choice ensures that the external field is defined outside the domain of the interpolating field.

[2] Similar correlation functions can be constructed using the opposite boundary operator eq.(5.6), in which the quarks are created at x and annihilated at the boundary at $x_0 = T$. We will not consider them any further.

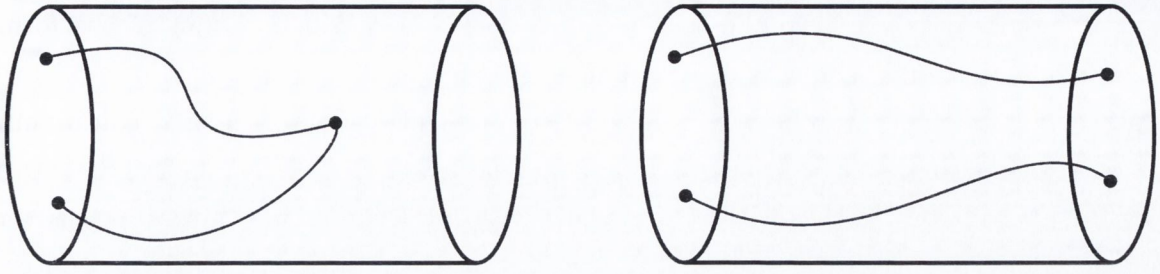

Figure 1: Sketch of a boundary to bulk correlation function (left) and a boundary to boundary correlation function (right).

The second class of correlations are referred as boundary to boundary correlation functions, in which $O(x)$ is chosen to be a boundary operator defined in one of the boundaries and O_{ext} is taken to be another boundary operator defined in the opposite boundary. They are given by

$$\langle \mathcal{O}'\mathcal{O} \rangle = \frac{1}{\mathcal{Z}} \int \mathcal{D}[\psi, \overline{\psi}] \mathcal{D}[A] \mathcal{O}'\mathcal{O} e^{-S[\psi,\overline{\psi},A]} \Big|_{\overline{\rho}=\rho=\overline{\rho}'=\rho'=0} . \tag{5.8}$$

These are proportional to the probability amplitude for the pair quark anti-quark being created at the boundary at $x_0 = 0$, propagating to the other boundary at $x_0 = T$, and being annihilated. A representation of boundary to bulk and boundary to bounary correlation functions is sketched in figure 1.

The renormalized versions of correlation functions eqs.(5.7) and (5.8) have the form

$$\langle O(x)\mathcal{O} \rangle_R = Z_O Z_\zeta^2 \langle O(x)\mathcal{O} \rangle, \qquad \langle \mathcal{O}'\mathcal{O} \rangle_R = Z_\zeta^4 \langle \mathcal{O}'\mathcal{O} \rangle, \tag{5.9}$$

where Z_O is the renormalization factor associated to the interpolating field $O(x)$, and Z_ζ is the wave function renormalization for the boundary fields.

Boundary to bulk correlation functions are generally normalised with boundary to boundary correlation functions in order to cancel the renormalization of the boundary quark fields. This way, one can have access to the renormalization factors Z_O directly. For that, it is useful to consider ratios of

$$\langle O(x)\mathcal{O} \rangle_R / \sqrt{\langle \mathcal{O}'\mathcal{O} \rangle_R}, \tag{5.10}$$

where the Z_ζ renormalization factor cancels out.

In this chapter we will define in detail a set of correlation functions of the form eq.(5.7) and eq.(5.8) and discuss some of their uses in the renormalization and improvement of the χSF scheme. In section 5.1 we will work in a formal continuum framework to define the correlation functions for the standard SF and the χSF setup in the continuum together with a dictionary[3] relating them in the chiral limit. After this is done, we will give a prescription to obtain their lattice regularised counterparts. Section 5.2 is entirely devoted to the expansion to one loop in perturbation theory of all the correlations introduced in section 5.1. A set of Feynman diagrams will be obtained. The numerical evaluation of these diagrams is discussed in section 5.3. Once the diagrams are calculated, we will be ready to use the results of the calculation for the tuning of the parameters z_f and m_0 to their critical values and of the improvement coefficient d_s. This is done in the different subsections of section 5.4. First we will study several renormalization conditions to set the parameters z_f and m_0 to their critical values, and show numerically that different choices of renormalization conditions will only affect physical quantities with $O(a^2)$ effects. Next we will discuss the extraction of the boundary improvement coefficient d_s to one loop. After all the coefficients have been properly determined, we will show that the correct boundary conditions are implemented in the lattice and automatic $O(a)$ improvement is realised. Finally we will check universality relations between correlation functions in the SF and χSF, confirming that both schemes are equivalent in the chiral and continuum limits. All calculations in this chapter are done independently of the gauge group, the number of fermions or the representation under which these transform. As a consequence, all the conclusions we will make here will be valid for all the theories described by the Lagrangian eq.(3.27). We will write all our results as a function of group theoretical factors, such that the values for a particular theory can be obtained by specifying such factors. We will close the chapter in section 5.5 where we will give some concluding remarks on the whole calculation.

5.1 Definitions

We first define the correlation functions in the standard SF followed by the ones in the χSF. It is possible to establish a dictionary between the two bases through eq.(4.95) analogous to that relating QCD with twisted mass QCD. [81].

[3]Borrowed from twisted mass QCD.

The fermion bilinear composite operators we are interested in for using them as interpolating operators in the bulk are the axial and vector flavor currents, given by

$$A_\mu^{f_1 f_2} = \overline{\psi}_{f_1}\gamma_\mu\gamma_5\psi_{f_2}, \quad V_\mu^{f_1 f_2} = \overline{\psi}_{f_1}\gamma_\mu\psi_{f_2}, \tag{5.11}$$

the scalar and axial densities, which read

$$S^{f_1 f_2} = \overline{\psi}_{f_1}\psi_{f_2}, \quad P^{f_1 f_2} = \overline{\psi}_{f_1}\gamma_5\psi_{f_2} \tag{5.12}$$

and the tensor currents

$$T_{\mu\nu}^{f_1 f_2} = \overline{\psi}_{f_1}\mathrm{i}\sigma_{\mu\nu}\psi_{f_2}, \quad \widetilde{T}_{\mu\nu}^{f_1 f_2} = \overline{\psi}_{f_1}\gamma_5\mathrm{i}\sigma_{\mu\nu}\psi_{f_2} \tag{5.13}$$

where $\sigma_{\mu\nu} = \frac{i}{2}[\gamma_\mu, \gamma_\nu]$. Note that the flavour currents are labelled with explicit flavour assignments, while in the literature it is common to index the currents using the generators of the flavour symmetry group. For considering correlation functions with quarks of the same flavour avoiding the complications of disconnected diagrams, it is convenient to consider a setup with four flavours [81], obtained by replacing the quark doublet as

$$\psi = \begin{pmatrix} \psi_u \\ \psi_d \end{pmatrix} \quad \longrightarrow \quad \psi = \begin{pmatrix} \psi_u \\ \psi_d \\ \psi_{u'} \\ \psi_{d'} \end{pmatrix}. \tag{5.14}$$

This way, there will be two up-type quarks and two down-type quarks. Correlation functions between the same flavour types can then be considered by making the flavour assignments $f_1 = u$ and $f_2 = u'$ (or $f_1 = d$ and $f_2 = d'$), such that one always has $f_1 \neq f_2$ an no disconnected diagrams occur.[4]

When this is done, the flavour matrix τ^3 in eq.(4.92) must be replaced by

$$\tau^3 \longrightarrow \mathbb{I}_2 \otimes \tau^3 = \mathrm{diag}(1, -1, 1, -1), \tag{5.15}$$

The chiral rotation eq.(4.92) then leads to the projectors

$$\widetilde{Q}_\pm\Big|_{N_f=2} = \mathrm{diag}(Q_\pm, Q_\mp), \qquad \widetilde{Q}_\pm\Big|_{N_f=4} = \mathrm{diag}(Q_\pm, Q_\mp, Q_\pm, Q_\mp), \tag{5.16}$$

[4]Note that this corresponds to a partially quenhe situation.

where $Q_\pm$ are the projectors reduced in flavour space which read

$$Q_\pm = \frac{1}{2}(1 \pm i\gamma_0\gamma_5). \tag{5.17}$$

[81]. In the standard SF setup the choice of flavours is irrelevant and all flavour combinations in a correlation function are equivalent. Hence, we will ignore flavour indices in the operators when considering correlation functions in the SF basis and only write them explicitly in the χSF setup.

5.1.1 Correlation functions in the SF

The first class of correlation functions we consider are boundary to bulk correlation functions given by

$$f_X(x_0) = -\frac{1}{2}\langle X(x)\mathcal{O}_5\rangle_{\mathrm{SF}}, \qquad X = A_0, V_0, S, P, \tag{5.18}$$

The subscript $\langle\cdot\rangle_{\mathrm{SF}}$ denotes that the correlation function is taken in the standard SF basis. The boundary source fields $\mathcal{O}_5$ are defined as

$$\mathcal{O}_5 = \int d^3\mathbf{y}d^3\mathbf{z}\overline{\zeta}(\mathbf{y})P_+\gamma_5\zeta(\mathbf{z}). \tag{5.19}$$

Conventionally, in the literature, the definition of the boundary fields ζ and $\overline{\zeta}$ include the projectors P_+ and P_-. Since we didn't include them in the definition eq.(4.40) we write them explicitly in the boundary source field. This permits to use the same notation for ζ and $\overline{\zeta}$ in both standard and rotated basis. This notation will also be handy later on when constructing boundary source fields with inverted projectors.

The correlations f_A and f_P are even under the parity symmetry

$$\mathcal{P} : \begin{cases} \psi(x) \longrightarrow \gamma_0\psi(\widetilde{x}), \\ \overline{\psi}(x) \longrightarrow \overline{\psi}(\widetilde{x})\gamma_0, \end{cases} \qquad \widetilde{x} = (x_0, -\mathbf{x}). \tag{5.20}$$

Hence, they do not vanish. On the contrary, f_V and f_S, being parity-odd, will vanish.

After integration of the fermion fields in the functional integral and making use of

Wick's theorem we obtain the expression

$$f_X(x_0) = \frac{1}{2}\int d^3\mathbf{y}d^3\mathbf{z}\langle \mathrm{Tr}\left\{[\psi(x)\overline{\zeta}(\mathbf{y})]_{\mathrm{F}}\Gamma_{\mathcal{O}_5}[\zeta(\mathbf{z})\overline{\psi}(x)]_{\mathrm{F}}\Gamma_X\right\}\rangle \tag{5.21}$$

where the trace acts over spinor and color components, $[\cdot]_{\mathrm{F}}$ denotes the fermion expectation value, $\Gamma_{\mathcal{O}_5}$ is the gamma structure of the boundary operator and Γ_X is the gamma structure of the fermion bilinear. A list with all the possible Γ structures that appear in correlation functions is collected in appendix B. From now on, for notational brevity we will express the two point functions without the explicit sub-index denoting fermion average, i.e. $[\cdot] = [\cdot]_{\mathrm{F}}$.

The next class of correlation functions we consider are boundary to bulk correlation functions defined for interpolating fields with an open spatial index k. These are

$$k_Y(x_0) = -\frac{1}{6}\sum_{k=1}^{3}\langle Y_k(x_0)\mathcal{O}_k\rangle_{\mathrm{SF}}, \qquad Y_k = A_k, V_k, T_{k0}, \widetilde{T}_{k0}. \tag{5.22}$$

The bilinear boundary source fields with an open spatial index are defined as

$$\mathcal{O}_k = \int d^3\mathbf{y}d^3\mathbf{z}\overline{\zeta}(\mathbf{y})P_+\gamma_k\zeta(\mathbf{z}). \tag{5.23}$$

Within this class of correlation functions the non vanishing parity even ones are k_V and k_T, and the vanishing parity odd ones are k_A and $k_{\widetilde{T}}$. Integrating the fermion fields we obtain

$$k_Y(x_0) = \frac{1}{6}\sum_{k=1}^{3}\int d^3\mathbf{y}d^3\mathbf{z}\langle \mathrm{Tr}\left\{[\psi(x)\overline{\zeta}(\mathbf{y})]\Gamma_{\mathcal{O}_k}[\zeta(\mathbf{z})\overline{\psi}(x)]\Gamma_Y\right\}\rangle, \tag{5.24}$$

with the possible Γ structures specified in the appendix.

Finally we consider two types of boundary to boundary correlation functions. The first are given by

$$f_1 = -\frac{1}{2}\langle \mathcal{O}_5\mathcal{O}'_5\rangle_{\mathrm{SF}} \tag{5.25}$$

with the source field at the upper boundary given by

$$\mathcal{O}'_5 = \int d^3\mathbf{y}'d^3\mathbf{z}'\overline{\zeta}'(\mathbf{y}')P_+\gamma_5\zeta'(\mathbf{z}'). \tag{5.26}$$

The second type are the boundary to boundary correlation functions using boundary sources with open spatial indices

$$k_1 = -\frac{1}{6}\sum_{k=1}^{3}\langle \mathcal{O}_k \mathcal{O'}_k \rangle_{\mathrm{SF}} \tag{5.27}$$

with the boundary operator of the top boundary given by

$$\mathcal{O'}_k = \int d^3\mathbf{y}' d^3\mathbf{z}' \overline{\zeta}'(\mathbf{y}') P_+ \gamma_k \zeta'(\mathbf{z}'). \tag{5.28}$$

After fermion integration, they read, respectively,

$$f_1 = \frac{1}{2}\int d^3\mathbf{y} d^3\mathbf{z} d^3\mathbf{y}' d^3\mathbf{z}' \langle \mathrm{Tr}\left\{ [\zeta(\mathbf{z})\overline{\zeta}'(\mathbf{y}')]\Gamma_{\mathcal{O}'_5} [\zeta'(\mathbf{z}')\overline{\zeta}(\mathbf{y})]\Gamma_{\mathcal{O}_5} \right\}\rangle \tag{5.29}$$

and

$$k_1 = \frac{1}{6}\sum_{k=1}^{3}\int d^3\mathbf{y} d^3\mathbf{z} d^3\mathbf{y}' d^3\mathbf{z}' \langle \mathrm{Tr}\left\{ [\zeta(\mathbf{z})\overline{\zeta}'(\mathbf{y}')]\Gamma_{\mathcal{O}'_k} [\zeta'(\mathbf{z}')\overline{\zeta}(\mathbf{y})]\Gamma_{\mathcal{O}_k} \right\}\rangle. \tag{5.30}$$

5.1.2 Correlation functions in the χSF

The correlation functions for the χSF can be constructed by applying the non-singlet chiral transformation eq.(4.92) at maximal twist to the standard correlation functions in the SF [1, 81]. For that, one first has to transform the bilinear fields in eqs.(5.11, 5.12) and (5.13). Since the transformation $R(\alpha)$ distinguishes between flavours, one has to take into account the flavour structure of the bilinear when performing the rotation, obtaining the sets

$$\begin{aligned}
A &\xrightarrow{R(\alpha)} A^{uu'}, A^{dd'}, -iV^{ud}, iV^{du}, \\
V &\longrightarrow V^{uu'}, V^{dd'}, -iA^{ud}, iA^{du}, \\
P &\longrightarrow iS^{uu'}, -iS^{dd'}, P^{ud}, P^{du}, \\
S &\longrightarrow iP^{uu'}, -iP^{dd'}, S^{ud}, S^{du}, \\
T &\longrightarrow i\widetilde{T}^{uu'}, -i\widetilde{T}^{dd'}, T^{ud}, T^{du}, \\
\widetilde{T} &\longrightarrow iT^{uu'}, -iT^{dd'}, \widetilde{T}^{ud}, \widetilde{T}^{du}.
\end{aligned} \tag{5.31}$$

The boundary source fields, which will now contain the projectors $Q_\pm$ instead of $P_\pm$, can be defined such that, when inserted into correlation functions with the fermion bilinears in eq.(5.31), they rotate back to the standard SF boundary source fields as

$$\langle O[R(\pi/2)\psi, \overline{\psi}R(\pi/2)]\mathcal{Q}_5^{f_1 f_2}\rangle_{\chi\mathrm{SF}} = \langle O[\psi,\overline{\psi}]\mathcal{O}_5^{f_1 f_2}\rangle_{\mathrm{SF}} \tag{5.32}$$

Since the chiral rotation $R(\alpha)$ distinguishes between flavours, the structure of the boundary source fields $\mathcal{Q}_5^{f_1 f_2}$ will depend on their flavour content, namely

$$\begin{aligned}
\mathcal{Q}_5^{uu'} &= \int d^3\mathbf{y} d^3\mathbf{z}\overline{\zeta}_u(\mathbf{y})\gamma_0\gamma_5 Q_-\zeta_{u'}(\mathbf{z}),\\
\mathcal{Q}_5^{dd'} &= \int d^3\mathbf{y} d^3\mathbf{z}\overline{\zeta}_d(\mathbf{y})\gamma_0\gamma_5 Q_+\zeta_{d}(\mathbf{z}),\\
\mathcal{Q}_5^{ud} &= \int d^3\mathbf{y} d^3\mathbf{z}\overline{\zeta}_u(\mathbf{y})\gamma_5 Q_+\zeta_{d}(\mathbf{z}),\\
\mathcal{Q}_5^{du} &= \int d^3\mathbf{y} d^3\mathbf{z}\overline{\zeta}_d(\mathbf{y})\gamma_5 Q_-\zeta_{u}(\mathbf{z}).
\end{aligned} \tag{5.33}$$

Similar expressions are found for the boundary operators with open spatial indices $\mathcal{Q}_k^{f_1 f_2}$. In order not to obscure the current discussion we leave the precise definition of the $\mathcal{Q}_k^{f_1 f_2}$ operators to appendix B.

It is convenient to consider here the rotated version of the parity transformation $\mathcal{P}$ given in eq.(5.20)

$$\mathcal{P}_5 : \begin{cases} \psi(x) \longrightarrow i\gamma_0\gamma_5\tau^3\psi(\widetilde{x}), \\ \overline{\psi}(x) \longrightarrow -\overline{\psi}(\widetilde{x})i\gamma_0\gamma_5\tau^3, \end{cases} \qquad \widetilde{x} = (x_0, -\mathbf{x}). \tag{5.34}$$

The boundary to bulk correlation functions eq.(5.18) translate in the rotated basis into

$$\mathrm{g}_X^{f_1 f_2}(x_0) = -\frac{1}{2}\langle X^{f_1 f_2}(x_0)\mathcal{Q}_5^{f_2 f_1}\rangle_{\chi\mathrm{SF}}; \quad X = A_0, V_0, S, P. \tag{5.35}$$

In the chiral limit one obtains a set of relations between correlation functions in the standard and rotated basis. The relations between $\mathcal{P}$-even (SF) and $\mathcal{P}_5$-even (χSF) correlation functions are

$$\begin{aligned}
f_A = &\ \mathrm{g}_A^{uu'} = \mathrm{g}_A^{dd'} = -i\mathrm{g}_V^{ud} = i\mathrm{g}_V^{du},\\
f_P = &\ i\mathrm{g}_S^{uu'} = -i\mathrm{g}_A^{dd'} = \mathrm{g}_P^{ud} = \mathrm{g}_P^{du},
\end{aligned} \tag{5.36}$$

and between odd correlation functions

$$\begin{aligned} f_V = &\ \mathrm{g}_V^{uu'} = \mathrm{g}_V^{dd'} = -i\mathrm{g}_A^{ud} = i\mathrm{g}_A^{du}, \\ f_S = &\ i\mathrm{g}_P^{uu'} = -i\mathrm{g}_P^{dd'} = \mathrm{g}_S^{ud} = \mathrm{g}_S^{du}. \end{aligned} \tag{5.37}$$

The boundary to bulk correlation functions with open spatial indices in the bilinears eq.(5.22), once rotated to the χSF basis, read

$$l_Y^{f_1 f_2}(x_0) = -\frac{1}{6}\sum_{k=1}^{3}\langle Y_k^{f_1 f_2}(x_0)\mathcal{Q}_k^{f_2 f_1}\rangle_{\chi\mathrm{SF}}, \qquad Y_k = A_k, V_k, T_{k0}, \widetilde{T}_{k0}. \tag{5.38}$$

which in the chiral limit are related to the standard basis in a similar way as in eqs.(5.36) and (5.37). The even correlation functions are

$$\begin{aligned} k_V =& l_V^{uu'} = l_V^{dd'} = -il_A^{ud} = il_A^{du}, \\ k_T =& il_{\widetilde{T}}^{uu'} = -il_{\widetilde{T}}^{dd'} = l_T^{ud} = l_T^{du}, \end{aligned} \tag{5.39}$$

and the odd correlation functions

$$\begin{aligned} k_A =& l_A^{uu'} = l_A^{dd'} = -il_V^{ud} = il_V^{du}, \\ k_{\widetilde{T}} =& il_T^{uu'} = -il_T^{dd'} = l_{\widetilde{T}}^{ud} = l_{\widetilde{T}}^{du}. \end{aligned} \tag{5.40}$$

Finally, the boundary to boundary correlation functions eqs.(5.25) and (5.27) are translated into the chiral basis as

$$\mathrm{g}_1^{f_1 f_2} = -\frac{1}{2}\langle \mathcal{Q}_5^{f_1 f_2}\mathcal{Q}'^{f_2 f_1}_5\rangle_{\chi\mathrm{SF}}, \tag{5.41}$$

and

$$l_1^{f_1 f_2} = -\frac{1}{6}\sum_{k=1}^{3}\langle \mathcal{Q}_k^{f_1 f_2}\mathcal{Q}'^{f_2 f_1}_k\rangle_{\chi\mathrm{SF}}. \tag{5.42}$$

Explicit expressions for the boundary source fields $\mathcal{Q}'^{f_1 f_2}_5$ and $\mathcal{Q}'^{f_1 f_2}_k$ can be found in appendix B.

The functions $\mathrm{g}_1^{f_1 f_2}$ and $l_1^{f_1 f_2}$ are related to the standard basis in the chiral limit through

$$\begin{aligned} f_1 =& \mathrm{g}_1^{uu'} = \mathrm{g}_1^{dd'} = \mathrm{g}_1^{ud} = \mathrm{g}_1^{du}, \\ k_1 =& l_1^{uu'} = l_1^{dd'} = l_1^{ud} = l_1^{du}. \end{aligned} \tag{5.43}$$

A remarkable point is that since all the standard SF correlation functions are real valued, the χSF functions will be either purely real or purely imaginary. Moreover, as a consequence of the definition adopted for the boundary source fields in the chiral basis eq.(5.32), the relations between the χSF correlation functions have the same structure as those for the fermion bilinears eq.(5.31). For sake of readibility, in the following sections we will often ignore the flavour indices in the correlation functions unless they are explicitly needed. It is important then to keep in mind that correlation functions in the χSF scheme will always depend on the choice of flavours.

5.1.3 Correlation functions regularized on the lattice

Once a theory is regularized on the lattice all the observables will be replaced by their lattice counterparts. The lattice versions of the correlation functions can be obtained from the continuum ones, defined in the previous sections, in a straight forward way. Firstly, the quark fields appearing in the bulk fermion bilinears are replaced by their lattice counterparts, defined only on the lattice sites. The domain of the interpolating fields will hence be the bulk of the lattice. Secondly, one has to specify the lattice version of the boundary source fields. For that we simply replace the spatial integrals of eq.(5.5) by lattice sums, and identify the boundary fermion fields with the lattice fields near the boundaries via eq.(4.76)

Within this convention, the lattice counterpart of the fermion bilinear boundary sources are given by expressions of the form

$$\mathcal{O} = a^6 \sum_{\mathbf{y},\mathbf{z}} \overline{\zeta}(\mathbf{y}) \Gamma \zeta(\mathbf{z}), \tag{5.44}$$

and similarly for the boundary operators at $x_0 = T$. The lattice version of the boundary to bulk correlation functions in the SF and χSF read, respectively

$$\begin{aligned} f_X(x_0) &= -\frac{1}{2} a^6 \sum_{\mathbf{y},\mathbf{z}} \langle \overline{\psi}(x) \Gamma_X \psi(x) \overline{\zeta}(\mathbf{y}) \Gamma_{\mathcal{O}_5} \zeta(\mathbf{y}) \rangle, \\ g_X^{f_1 f_2}(x_0) &= -\frac{1}{2} a^6 \sum_{\mathbf{y},\mathbf{z}} \langle \overline{\psi}^{f_1}(x) \Gamma_X \psi^{f_2}(x) \overline{\zeta}^{f_2}(\mathbf{y}) \Gamma_{\mathcal{Q}_5}^{f_2 f_1} \zeta^{f_1}(\mathbf{y}) \rangle. \end{aligned} \tag{5.45}$$

For the boundary to boundary correlation functions, their lattice versions are given

by

$$\begin{aligned} f_1 &= -\frac{1}{2}a^{12}\sum_{\mathbf{y},\mathbf{z},\mathbf{u},\mathbf{v}}\langle\overline{\zeta}'(\mathbf{u})\gamma_5 Q_+\zeta'(\mathbf{v})\overline{\zeta}(\mathbf{y})\gamma_5 Q_-\zeta(\mathbf{z})\rangle, \\ \mathrm{g}_1^{f_1f_2} &= -\frac{1}{2}a^{12}\sum_{\mathbf{y},\mathbf{z},\mathbf{u},\mathbf{v}}\langle\overline{\zeta}'^{f_1}(\mathbf{u})\gamma_5 Q_+\zeta'^{f_2}(\mathbf{v})\overline{\zeta}^{f_2}(\mathbf{y})\gamma_5 Q_-\zeta^{f_1}(\mathbf{z})\rangle, \end{aligned} \tag{5.46}$$

Similar expressions hold for the l_Y and l_1 correlations. Explicit expressions for the lattice versions for all the correlation functions f_X, k_Y, g_X, l_Y, f_1, k_1, g_1 and l_1 after performing the fermion functional integration are collected in appendix B. These are the objects we are interested in for the rest of this chapter.

5.2 Perturbative expansion to 1-loop

In this section we will work out in some detail the perturbative expansion of the correlation functions for the χSF eq.(5.35) and (5.38) introduced in the previous section. The ideas for the expansion of correlation functions in the standard SF for zero background field where discussed in [83]. In the present section we will proceed on the same lines as in [92] adapting the calculation to the χSF setup.

5.2.1 Preliminaries

The starting point for the present perturbative calculation is the Wick contracted form of the correlation functions g_X and g_1 found in eqs.(5.45) and (5.46) with the 2 point functions written explicitly using eq.(B.32). In order to be general, we consider for this calculation the possibility of having momentum different from zero in the correlation functions.[5] Momentum $\mathbf{p}$ can be injected by adding a Fourier factor $e^{i\mathbf{p}(\mathbf{y}-\mathbf{z})}$ into the sum within the boundary operator eq.(5.44).[6]

Taking this considerations into account, the observables we are interested in are

$$\begin{aligned} \mathrm{g}_X^{f_1f_2}(x_0,\mathbf{p}) =& \frac{1}{2}\sum_{\mathbf{y},\mathbf{z}} e^{i\mathbf{p}(\mathbf{y}-\mathbf{z})} \\ & \langle \mathrm{Tr}\left\{ S(x;a,\mathbf{y})_{f_2f_2}U_0(0,\mathbf{y})^\dagger\Gamma_{\mathcal{Q}_5}^{f_2f_1}U_0(0,\mathbf{z})S(a,\mathbf{z};x)_{f_1f_1}\Gamma_X\right\}\rangle, \end{aligned} \tag{5.47}$$

[5] Evaluating correlation functions at different $\mathbf{p}$ corresponds to different probes of the same physical observable. In practice, however, we will always evaluate them at $\mathbf{p}=0$ in this work.

[6] This will have the effect of, once we perform a spatial Fourier transformation, projecting the quark propagator to momentum $\mathbf{p}$.

$$\begin{aligned} \mathrm{g}_1^{f_1 f_2} =& \frac{1}{2} \sum_{\mathbf{u},\mathbf{v},\mathbf{y},\mathbf{z}} e^{i\mathbf{p}(\mathbf{u}-\mathbf{v})} e^{i\mathbf{q}(\mathbf{y}-\mathbf{z})} \langle \mathrm{Tr}\, \{ U_0(0,\mathbf{z}) S(a,\mathbf{z};T-a,\mathbf{u})_{f_2 f_2} U_0(T-a,\mathbf{u}) \\ & \Gamma'^{f_2 f_1}_{\mathcal{Q}'_5} U_0^\dagger(T-a,\mathbf{v}) S(T-a,\mathbf{v};a,\mathbf{y})_{f_1 f_1} U_0(0,\mathbf{y}) \Gamma^{f_1 f_2}_{\mathcal{Q}_5} \} \rangle, \end{aligned} \tag{5.48}$$

where $S(x,y)_{ff}$ is the quark propagator for flavor f. Very similar expressions hold for l_Y and l_1. The perturbative expansion of l_Y and l_1 will follow in an almost identical way as for g_X and g_1. We will hence ignore them here and comment on them at the end of subsections 5.2.3 and 5.2.4.

Since in SF schemes the presence of temporal boundaries breaks translation invariance in the temporal direction, we will work in the time-momentum representation in Fourier space. The quark and gluon fields Fourier transformed in the spatial directions are defined through

$$\begin{aligned} \psi(x) &= \frac{1}{L^3} \sum_{\mathbf{p}} e^{i\mathbf{p}\mathbf{x}} \psi(x_0,\mathbf{p}), & \overline{\psi}(x) &= \frac{1}{L^3} \sum_{\mathbf{p}} e^{i\mathbf{p}\mathbf{x}} \overline{\psi}(x_0,\mathbf{p}), \\ q_0(x) &= \frac{1}{L^3} \sum_{\mathbf{p}} e^{i\mathbf{p}\mathbf{x}} q_0(x_0,\mathbf{p}), & q_k(x) &= \frac{1}{L^3} \sum_{\mathbf{p}} e^{i\mathbf{p}\mathbf{x}+ip_k/2} q_k(x_0,\mathbf{p}), \end{aligned} \tag{5.49}$$

with the Lattice momenta $\mathbf{p}$ adopting values $p_k = \frac{2\pi n_k}{L}$, where $n_k \in [0, L-1]$ and $k = 1,2,3$.

The expansions of equations (5.47) and (5.48) to one loop in perturbation theory are of the form

$$\mathrm{g}_X(x_0,\mathbf{p}) = \mathrm{g}_X^{(0)}(x_0,\mathbf{p}) + g_0^2 \mathrm{g}_X^{(1)}(x_0,\mathbf{p}) + O(g_0^4), \tag{5.50}$$

$$\mathrm{g}_1 = \mathrm{g}_1^{(0)} + g_0^2 \mathrm{g}_1^{(1)} + O(g_0^4), \tag{5.51}$$

In order to obtain the tree-level coefficients $\mathrm{g}_X^{(0)}$ and $\mathrm{g}_1^{(0)}$, and the 1-loop coefficients $\mathrm{g}_X^{(1)}$ and $\mathrm{g}_1^{(1)}$, one has to expand the temporal link variables at the boundaries and the quark propagators in eqs.(5.47) and (5.48) to order g_0^2. Moreover, the exponential factor of the action and the measure in the path integral also have to be expanded as explained in section 4.4, together with an appropriate gauge fixing procedure.

The expansion of the link variables reads

$$\begin{aligned} U_\mu(x) &= \mathbb{I} + iag_0 q_\mu^a(x) T^a - \frac{a^2}{2} g_0^2 q_\mu^a(x) T^a q_\mu^b(x) T^b + O(g_0^3), \\ U_\mu(x)^\dagger &= \mathbb{I} - iag_0 q_\mu^a(x) T^a - \frac{a^2}{2} g_0^2 q_\mu^a(x) T^a q_\mu^b(x) T^b + O(g_0^3), \end{aligned} \tag{5.52}$$

The quark propagator has an expansion of the form

$$S(x,y) = \sum_{i=0}^{\infty} g_0^i S^{(i)}(x,y). \tag{5.53}$$

The different terms $S^{(i)}(x,y)$ can be obtained recursively [83] from the defining equations for the quark propagator

$$\left(D_{\mathrm{W}} + m_0\right) S(x,y) = a^{-4} \delta_{x,y} \tag{5.54}$$

By expanding the Dirac operator as a series in g_0

$$D_{\mathrm{W}} = \sum_{k=0}^{\infty} g_0^k D_{\mathrm{W}}^{(k)}, \tag{5.55}$$

and inserting it, together with the expansion eq.(5.53), into eq.(5.54), one obtains the recursive relation

$$\begin{aligned} \left(D_{\mathrm{W}}^{(0)} + m_0\right) S^{(0)}(x,y) &= a^{-4} \delta_{x,y}, \\ \left(D_{\mathrm{W}}^{(0)} + m_0\right) S^{(k)}(x,y) &= -\sum_{j=0}^{k-1} D_{\mathrm{W}}^{(k-j)} S^{(j)}(x,y), \end{aligned} \tag{5.56}$$

where $S^{(0)}(x,y)$ is the free-quark propagator. From eq.(5.56) one can obtain order by order the different terms of the quark propagator. At first order the recursion eq.(5.56) renders

$$S^{(1)}(x,y) = -a^4 \sum_z S^{(0)}(x,z) D_{\mathrm{W}}^{(1)} S^{(0)}(z,y), \tag{5.57}$$

and, at second order,

$$\begin{aligned} S^{(2)}(x,y) = &- a^4 \sum_z S^{(0)}(x,z) D_{\mathrm{W}}^{(2)} S^{(0)}(z,y) \\ &- a^8 \sum_{z,w} S^{(0)}(x,z) D_{\mathrm{W}}^{(1)} S^{(0)}(z,w) D_{\mathrm{W}}^{(1)} S^{(0)}(w,y). \end{aligned} \tag{5.58}$$

The operators $D_{\mathrm{W}}^{(1)}$ and $D_{\mathrm{W}}^{(2)}$ correspond to the quark-gluon vertices at order g_0 and g_0^2 and will be derived explicitly for the action eq.(4.104) in the following subsection.[7]

5.2.2 Feynman Rules

The Feynman rules are obtained to any order in perturbation theory by expanding the action to the desired order. Moreover, as described in subsection 4.4, when performing such expansion one needs to go through a gauge fixing procedure. For the present case we choose to fix the gauge as it is done in [83] and add to the action eq.(4.51) a gauge fixing term [8]

$$S_{\mathrm{gf}} = \lambda_0 (d^* q, d^* q) \tag{5.59}$$

where λ_0 is the gauge fixing parameter and the operator d^* acts over the gluon fields as

$$(d^* q)(x) = \begin{cases} \partial_\mu^* q_\mu(x) & 0 < x_0 < T, \\ a^2/L^3 \sum_{\mathbf{y}} q_0(0,\mathbf{y}) & x_0 = 0, \\ 0 & x_0 = T. \end{cases} \tag{5.60}$$

After gauge fixing and expanding the link variables in eq.(4.51), the quadratic part of the gluon action takes the form

$$S_{\mathrm{G},0} = \frac{1}{2L^3} \sum_{\mathbf{p}} \sum_{x_0,y_0=0}^{T-1} \sum_c q_\mu^c(-\mathbf{p}, x_0) K_{\mu\nu}(\mathbf{p}, x_0, y_0) q_\nu^c(\mathbf{p}, y_0), \tag{5.61}$$

with $q_k(\mathbf{p}, 0) = 0$ for $k = 1, 2, 3$. $K_{\mu\nu}(\mathbf{p}, x_0, y_0)$ is the quadratic gluon operator, the components of which are given in reference [92]. Since the gauge part of the action is the same for the SF and the χSF setups, the quadratic gluon operator, and hence the

[7] Note that the form of these recursive relations are general to any action bilinear on the fermion fields $\overline{\psi}(x)$ and $\psi(x)$.

[8] In the present calculation the gauge part of the action is the same as in [83], so the same gauge fixing procedure can be used.

free gluon propagators, are identical in both cases. The gluon propagator in the SF was calculated in [83] for zero background field, and in [93] in presence of an abelian background field. The free gluon propagator is defined through

$$\langle q_\mu^a(\mathbf{q}, x_0) q_\nu^b(-\mathbf{p}, y_0)\rangle = \delta_{\mathbf{p},\mathbf{q}}\delta_{ab} D_{\mu\nu}(\mathbf{q}, x_0, y_0). \tag{5.62}$$

Pure gluon or gluon-ghost vertices do not occur in the expansion of g_X or g_1 to the present order in perturbation theory, and neither do ghost fields.

The defining expression for the free fermion propagator is the order zero term in eq.(5.56), which we recall here

$$(D_{\mathrm{W}}^{(0)} + m_0) S^{(0)}(x, y) = a^{-4}\delta_{x,y}, \quad x_0, y_0 \in [0, T]. \tag{5.63}$$

When considering the χSF setup with an offset as described in section 4.3.6, since at tree level $d_s^{(0)} = 1/2$, the tree-level operator $D_{\mathrm{W}}^{(0)}$ receives a contribution from the counterterm proportional to d_s, which modifies the free quark propagator with respect to the case without offset [1]. In fact, in this situation, an analytic solution to eq.(5.63) is not known and thus one can only find the free quark propagator $S^{(0)}(x, y)$ numerically. Since the color structure of the operator $D_{\mathrm{W}}^{(0)}$ is trivial, the numerical solution of eq.(5.63) in the time-momentum representation accounts for the inversion of a $4(T+1) \times 4(T+1)$ matrix for a fixed value of the momenta.[9] Details on the algorithm used for the numerical inversion of $D_{\mathrm{W}}^{(0)}$ will be given in section 5.3.

The fermion vertices can be obtained from the order g_0 and g_0^2 terms in the expansion of the fermion action

$$S_{\mathrm{W}} = S_0 + \sum_{n=1}^{\infty} \frac{1}{n!} g_0^n S_W^{(n)}. \tag{5.64}$$

The order g_0 term reads

$$\begin{aligned} S_{\mathrm{W}}^{(1)} = a^4 \sum_x \overline{\psi} D_{\mathrm{W}}^{(1)} \psi = & \frac{a}{L^6} \sum_{\mathbf{p}',\mathbf{p},\mathbf{q}} \delta^{(3)}(\mathbf{p}' + \mathbf{p} + \mathbf{q}) \sum_{x_0,y_0,z_0} \sum_{\mu} \\ & \overline{\psi}(-\mathbf{p}', x_0) q_\mu^a(-\mathbf{q}, z_0) V_\mu^a(\mathbf{p}', \mathbf{p}, \mathbf{q}; x_0, y_0, z_0) \psi(-\mathbf{p}, y_0). \end{aligned} \tag{5.65}$$

Note that here the indices x_0, y_0 and z_0 run from 0 to T, in contrast to the standard

[9] In the time momentum representation $D_{\mathrm{W}}^{(0)}$ is a matrix with 4×4 spinor components and $(T+1) \times (T+1)$ temporal components, at given color and momenta.

SF setup for which they run from 1 to $T-1$. As a consequence of this, the vertices in the χSF have an extra contribution coming from the part of the Dirac operator eq.(4.97) defined at the boundaries. The quark-quark-gluon vertex reads

$$\begin{aligned} V_\mu^a(\mathbf{p}',\mathbf{p},\mathbf{q};x_0,y_0,z_0) =& T^a\left\{V_\mu^{(1)}(\mathbf{r};x_0,y_0,z_0)\right. \\ &\left. + c_{\rm SW}^{(0)} S_\mu^{(1)}(\mathbf{q};x_0,z_0)\delta_{x_0,y_0}\right\}, \end{aligned} \tag{5.66}$$

with $\mathbf{r}=(\mathbf{p}'-\mathbf{p})/2$. The vertex eq.(5.66) gets a contribution from the Wilson part of the fermion action given by

$$V_\mu^{(1)}(\mathbf{r};x_0,y_0,z_0)\begin{cases} = -P_-\delta_{x_0,z_0}\delta_{x_0+a,y_0}(1-\delta_{x_0,T}) & \\ \qquad + P_+\delta_{y_0,x_0-a}\delta_{z_0,y_0}(1-\delta_{x_0,0}), & \mu=0, \\ = \left(\cos(ar_k)\gamma_k - i\sin(ar_k)\right)\delta_{x_0,y_0}\delta_{x_0,z_0}, & \mu=k\neq 0, \end{cases} \tag{5.67}$$

and from the clover term,

$$S_\mu^{(1)}(\mathbf{q};x_0,z_0)\begin{cases} = \frac{1}{4}\left(\delta_{x_0,z_0}+\delta_{x_0-a,z_0}\right)\sum_j \sigma_{j0}\widetilde{q}_j; & \mu=0 \\ = \frac{1}{2}\cos\left(\frac{1}{2}q_k\right)\left\{\frac{i}{2}\left(\delta_{x_0+a,z_0}-\delta_{x_0-a,z_0}\right)\sigma_{0k}\right. & \\ \qquad \left.+\delta_{x_0,z_0}\sum_j \sigma_{jk}\widetilde{q}_j\right\}; & \mu=k\neq 0 \end{cases} \tag{5.68}$$

The order g_0^2 of the fermion action reads

$$\begin{aligned} S_{\rm W}^{(2)} =& \frac{a^2}{2L^9}\sum_{\mathbf{p}',\mathbf{p},\mathbf{q},\mathbf{q}'}\delta^{(3)}(\mathbf{p}'+\mathbf{p}+\mathbf{q}+\mathbf{q}')\sum_{x_0,y_0,z_0,z_0'}\sum_{\mu\nu} \\ & \overline{\psi}(-\mathbf{p}',x_0)V_{\mu\nu}^{ab}(\mathbf{p}',\mathbf{p},\mathbf{q},\mathbf{q}';x_0,y_0,z_0,z_0')q_\mu^a(-\mathbf{q},z_0)q_\nu^b(-\mathbf{q}',z_0')\psi(-\mathbf{p},y_0), \end{aligned} \tag{5.69}$$

with the quark-quark-gluon-gluon vertex given by

$$\begin{aligned} V_{\mu\nu}^{ab}(\mathbf{p}',\mathbf{p},\mathbf{q},\mathbf{q}';x_0,y_0,z_0,z_0') =& \frac{1}{2}\left\{T^a,T^b\right\}V_\mu^{(2)}(\mathbf{r};x_0,y_0,z_0)\,\delta_{\mu\nu}\delta_{z_0,z_0'} \\ & + \frac{1}{2}\left[T^a,T^b\right]c_{\rm SW}^{(0)}S_{\mu\nu}^{(2)}(\mathbf{q},\mathbf{q}';x_0,z_0,z_0')\delta_{x_0,y_0}. \end{aligned} \tag{5.70}$$

The second order vertex also gets a contribution coming from the Wilson action $V_\mu^{(2)}$

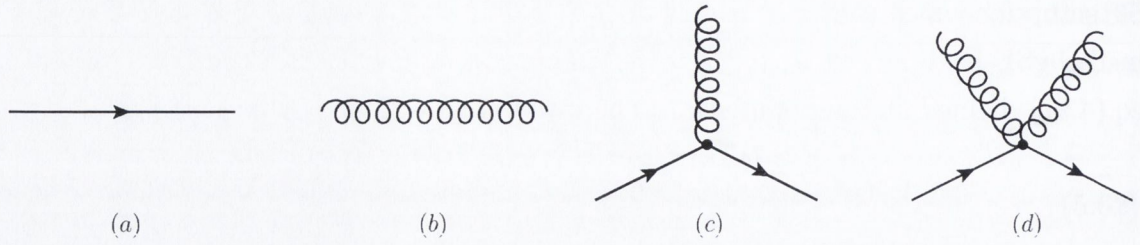

Figure 5.2.1: Diagrammatic representation of the Feynman rules needed in the expansion. (a) Fermion propagator, (b) gluon propagator, (c) quark-quark-gluon vertex and (d) quark quark gluon gluon vertex.

and from the clover term $S^{(2)}_{\mu\nu}$. The contribution from the Wilson action reads

$$V^{(2)}_{\mu}(\mathbf{r}; x_0, y_0, z_0) \begin{cases} = -P_{-}\delta_{x_0,z_0}\delta_{x_0+a,y_0}(1-\delta_{x_0,T}) & \\ \qquad - P_{+}\delta_{y_0,x_0-a}\delta_{z_0,y_0}(1-\delta_{x_0,0}), & \mu = 0, \\ = -\left(\cos(ar_k)\gamma_k - i\sin(ar_k)\right)\delta_{x_0,y_0}\delta_{x_0,z_0}, & \mu = k \neq 0. \end{cases} \tag{5.71}$$

The quark-quark-gluon-gluon vertex will only appear in tadpole diagrams for which the commutator of the generators in eq.(5.70) vanishes. Hence, although in general the clover term contributes to the g_0^2 quark gluon vertex, the explicit expression of $S^{(2)}_{\mu\nu}$ is not needed in the present calculation.

The Feynman rules needed in the expansion of g_X and l_Y at 1-loop are depicted diagrammatically in figure (5.2.1).

5.2.3 Expansion of g_X and l_Y

Once the Feynman rules have been listed we can proceed to the calculation of the terms $\mathrm{g}^{(0)}_X$ and $\mathrm{g}^{(1)}_X$ in the expansion (5.47). From now on, we work in lattice units and set $a = 1$. One also has to take into account the contribution of counterterms as explained in section 4.4.2. For the case at hand, these are the counterterms proportional to d_s and z_f. Moreover, we will also have to consider the contribution due to the mass counterterm eq.(5.101). This is proportional to the critical mass m_c, which has an expansion

$$m_{\mathrm{c}} = m_{\mathrm{c}}^{(0)} + g_0^2 m_{\mathrm{c}}^{(1)} + O(g_0^4). \tag{5.72}$$

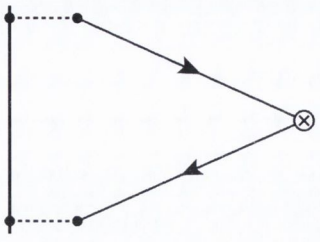

Figure 5.2.2: Diagram for the tree level term $\mathrm{g}_X^{f_1 f_2}(\mathbf{p}, x_0)^{(0)}$.

It is then clear that at order $O(g_0^2)$ there will be an extra contribution proportional to $m_c^{(1)}$ coming from the mass counterterm.[10]

The renormalization factors Z_X and Z_ζ are also expanded as

$$\begin{aligned} Z_X &= 1 + Z_X^{(1)} g_0^2 + O(g_0^4), \\ Z_\zeta &= 1 + Z_\zeta^{(1)} g_0^2 + O(g_0^4). \end{aligned} \tag{5.73}$$

Having said all this, we are ready to do the expansion. The tree level coefficient $\mathrm{g}_X^{f_1 f_2 (0)}$, depicted by the diagram in fig.(5.2.2), is given by

$$\mathrm{g}_X^{f_1 f_2}(\mathbf{p}, x_0)^{(0)} = \frac{1}{2} \mathrm{Tr} \left\{ \Gamma_{\mathcal{Q}_5}^{f_2 f_1} S^{(0)}(\mathbf{p}; 1, x_0)_{f_1 f_1} \Gamma_X S^{(0)}(\mathbf{p}; x_0, 1)_{f_2 f_2} \right\}, \tag{5.74}$$

where the trace is taken over color and spin. Since there are no gluons appearing at this order, the gauge average from eq.(5.47) becomes trivial. Moreover, the color structure of $\mathrm{g}_X^{(0)}$ is also trivial[11] and the color part of the trace yields only a multiplicative factor $\mathrm{d}(\mathcal{R})$. [12] The total contribution to g_X at 1-loop is given by[13]

$$\begin{aligned} \mathrm{g}_X(\mathbf{p}, x_0)^{(1)} = &\sum_n \mathrm{g}_X(\mathbf{p}, x_0)_n^{(1)} + d_s^{(1)} \mathrm{g}_X(\mathbf{p}, x_0)_{d_s}^{(1)} + z_f^{(1)} \mathrm{g}_X(\mathbf{p}, x_0)_{z_f}^{(1)} \\ &+ m_c^{(1)} \frac{\partial}{\partial m_0} \mathrm{g}_X(\mathbf{p}, x_0)^{(0)} + \left(Z_X^{(1)} - 2 Z_\zeta^{(1)} \right) \mathrm{g}_X(\mathbf{p}, x_0)^{(0)}. \end{aligned} \tag{5.75}$$

[10] Since both SF and χSF are equivalent in the continuum, the continuum extrapolation of the coefficient $m_c^{(1)}$ will be the same for the two regularizations. Away from the continuum limit, however, the series $m_c^{(1)}(L/a)$ will differ by cutoff effects.

[11] Since the tree-level propagators are color diagonal.

[12] For QCD (with fundamental fermions) $\mathrm{d}(\mathcal{R}) = N$. Group theoretical factors for the different groups and representations are listed in appendix A.3.

[13] For sake of readability, we have excluded the flavour indices in expression (5.75), keeping in mind that the flavour ordering of the objects in the right hand side is the same as in the left hand side.

Here, the sum over n runs for all the Feynman diagrams listed below, whose individual contribution is referred to as $g_X(\mathbf{p}, x_0)_n^{(1)}$.

Before giving the explicit expressions for the Feynman diagrams it is useful to first compute the functions from which the diagrams are constructed. We first define the quark propagator with the insertion of a fermion bilinear as

$$\mathcal{S}^{f_1 f_2}(\Gamma_X; \mathbf{p}; t_0, x_0, s_0) = S^{(0)}(\mathbf{p}; t_0, x_0)_{f_1 f_1} \Gamma_X S^{(0)}(\mathbf{p}; x_0, s_0)_{f_2 f_2}, \tag{5.76}$$

depicted by diagram (a) in figure (5.2.3). Next we define the 1-loop functions, namely, the contributions to the quark self energy $\Sigma_1^{(1)}$ and $\Sigma_2^{(1)}$, and the 1-loop correction to the bilinear operator $\Gamma_1^{(1)}$ which read, respectively

$$\begin{aligned}\Sigma_1^{(1)}(\mathbf{p}; s_0, t_0)_{ff} =& \frac{1}{L^3} \sum_{\mathbf{q}} \sum_{\mu,\nu} \sum_{u_0, u_0'} \sum_{s_0', t_0'} D_{\nu\mu}(\mathbf{q}; u_0', u_0) V_\mu^a(\mathbf{p}, -\mathbf{p}-\mathbf{q}, \mathbf{q}; s_0, t_0', u_0) \\ & S^{(0)}(\mathbf{p}+\mathbf{q}; t_0', s_0')_{ff} V_\nu^a(\mathbf{p}+\mathbf{q}, -\mathbf{p}, -\mathbf{q}; s_0', t_0, u_0'),\end{aligned} \tag{5.77}$$

$$\begin{aligned}\Sigma_2^{(1)}(\mathbf{p}; s_0, t_0) = & -\frac{1}{2}\frac{1}{L^3} \sum_{\mathbf{q}} \sum_{\mu,\nu} \sum_{u_0, u_0'} D_{\nu\mu}(\mathbf{q}; u_0', u_0) \\ & V_{\mu\nu}^a(\mathbf{p}, -\mathbf{p}, \mathbf{q}, -\mathbf{q}; s_0, t_0, u_0, u_0'),\end{aligned} \tag{5.78}$$

and

$$\begin{aligned}\Gamma_1^{(1)}(\Gamma_X; \mathbf{p}; s_0, x_0, t_0)_{f_1 f_2} =& \frac{1}{L^3} \sum_{\mathbf{q}} \sum_{\mu,\nu} \sum_{u_0, u_0'} \sum_{s_0', t_0'} D_{\nu\mu}(\mathbf{q}; u_0', u_0) \\ & V_\mu^a(\mathbf{p}, -\mathbf{p}-\mathbf{q}, \mathbf{q}; s_0, t_0', u_0) \mathcal{S}(\Gamma_X; \mathbf{p}+\mathbf{q}; t_0', x_0, s_0')_{f_1 f_2} \\ & V_\nu^a(\mathbf{p}+\mathbf{q}, -\mathbf{p}, -\mathbf{q}; s_0', t_0, u_0').\end{aligned} \tag{5.79}$$

Note that $\Sigma_1^{(1)}$ is a vector in flavour space, $\Sigma_2^{(1)}$ is a scalar in flavour, and $\Gamma_1^{(1)}$ is a flavour tensor. The momenta sums run over all allowed lattice momenta $q_k = 2\pi n_k / L$ with $n_k \in [0, L-1]$ and $k = 1, 2, 3$. The sums over the temporal variables u_0 and u_0' of the gluon fields run for $u_0, u_0' \in [0, T-1]$, and the sums over the the fermionic temporal variables s_0' and t_0' are defined for $s_0', t_0' \in [0, T]$[14]. The contribution to the quark self energy given by the gluon tadpole $\Sigma_2^{(1)}$ is a pure lattice artefact with no

[14]Note again that in the standard SF the sums over temporal variables for the fermions would run only in the interval $[1, T-1]$

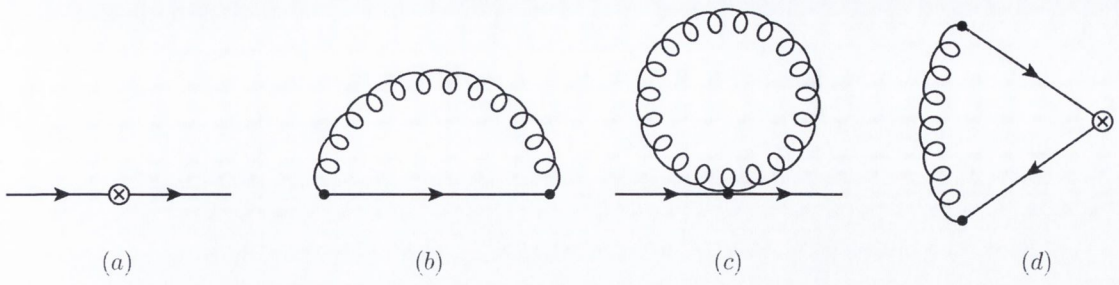

Figure 5.2.3: Diagrammatic representation of the functions $\mathcal{S}$ (diagram a), $\Sigma_1^{(1)}$ (diagram b), $\Sigma_2^{(1)}$ (diagram c) and $\Gamma_1^{(1)}$ (diagram d), needed to construct the 1-loop diagrams.

continuum counterpart[15].

Having defined these functions, we can finally give the expressions for the contributions $\mathrm{g}_X(\mathbf{p}; x_0)_n^{(1)}$ of each diagram in figure (5.2.4). Diagrams 1a and 1b correspond to the second order contributions of the links at the boundaries. They are proportional to the tree-level diagram eq.(5.74) and are given by

$$\mathrm{g}_X^{f_1 f_2}(\mathbf{p}; x_0)_{1\mathrm{a}}^{(1)} = \mathrm{g}_X^{f_1 f_2}(\mathbf{p}; x_0)_{1\mathrm{b}}^{(1)} = -\frac{C_2(\mathcal{R})}{2L^3} \sum_{\mathbf{q}} D_{00}(\mathbf{q}; 0, 0) \mathrm{g}_X^{f_1 f_2}(\mathbf{p}; x_0)^{(0)}, \qquad (5.80)$$

where $C_2(\mathcal{R})$ is the quadratic Casimir operator in the representation $\mathcal{R}$ (we refer again to the appendix A.3 for a list of group theoretical factors).

Diagram 2 comes from the contraction between the $O(g_0)$ terms in both boundary link variables and reads

$$\mathrm{g}_X^{f_1 f_2}(\mathbf{p}; x_0)_2^{(1)} = \frac{C_2(\mathcal{R})}{L^3} \sum_{\mathbf{q}} D_{00}(\mathbf{q}; 0, 0) \mathrm{g}_X^{f_1 f_2}(\mathbf{p} + \mathbf{q}; x_0)^{(0)} \qquad (5.81)$$

The contractions of the $O(g_0)$ terms in the boundary link variables with the quark-quark-gluon vertex inserted on the quark propagators yields diagrams 3a and 3b when contracted to the adjacent quark line, and to diagrams 4a and 4b when contracted

[15]Needed, however, to preserve unitarity of perturbative calculations with a lattice regulator.

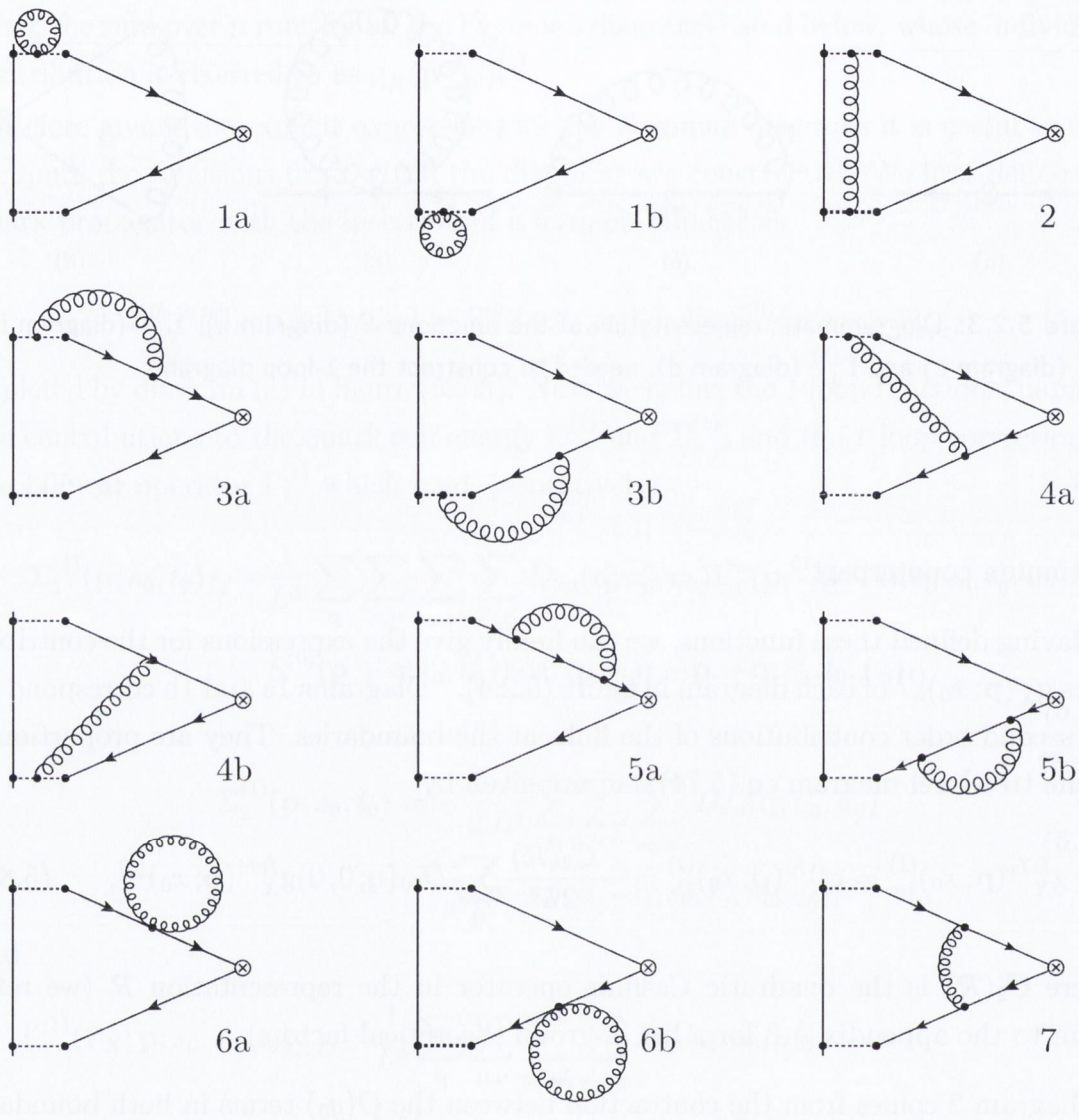

Figure 5.2.4: 1-loop diagrams contributing to the $\mathrm{g}_X^{f_1 f_2 (1)}$.

with the opposite quark line. The expressions for these diagrams read

$$\mathrm{g}_X^{f_1 f_2}(\mathbf{p}; x_0)^{(1)}_{3\mathrm{a}} = \frac{1}{2L^3} \sum_{\mathbf{q}} \sum_{\mu} \sum_{s_0, t_0, u_0} D_{0\mu}(\mathbf{q}; 0, u_0) \mathrm{Tr} \Big\{ T^a \Gamma^{f_2 f_1}_{\mathcal{Q}_5} \mathcal{S}(\Gamma_X; \mathbf{p}; 1, x_0, s_0)_{f_1 f_2} V^a_\mu(\mathbf{p}, -\mathbf{p}-\mathbf{q}, \mathbf{p}; s_0, t_0, u_0) S^{(0)}_{f_2 f_2}(\mathbf{p}+\mathbf{q}; t_0, 1) \Big\}, \tag{5.82}$$

$$\mathrm{g}_X^{f_1f_2}(\mathbf{p};x_0)^{(1)}_{3\mathrm{b}} = -\frac{1}{2L^3}\sum_{\mathbf{q}}\sum_{\mu}\sum_{s_0,t_0,u_0} D_{\mu 0}(\mathbf{q};u_0,0)\mathrm{Tr}\left\{T^a\Gamma^{f_2f_1}_{\mathcal{Q}_5} S^{(0)}_{f_1f_1}(\mathbf{p}+\mathbf{q};1,s_0)V^a_\mu(\mathbf{p}+\mathbf{q},-\mathbf{p},-\mathbf{q};s_0,t_0,u_0)\mathcal{S}(\Gamma_X;\mathbf{p};t_0,x_0,1)_{f_1f_2}\right\}, \tag{5.83}$$

and

$$\mathrm{g}_X^{f_1f_2}(\mathbf{p};x_0)^{(1)}_{4\mathrm{a}} = \frac{1}{2L^3}\sum_{\mathbf{q}}\sum_{\mu}\sum_{s_0,t_0,u_0} D_{0\mu}(\mathbf{q};0,u_0)\mathrm{Tr}\left\{T^a\Gamma^{f_2f_1}_{\mathcal{Q}_5} S^{(0)}_{f_1f_1}(\mathbf{p};1,s_0)V^a_\mu(\mathbf{p},-\mathbf{p}-\mathbf{q},\mathbf{q};s_0,t_0,u_0)\mathcal{S}(\Gamma_X;\mathbf{p}+\mathbf{q};t_0,x_0,1)_{f_1f_2}\right\}, \tag{5.84}$$

$$\mathrm{g}_X^{f_1f_2}(\mathbf{p};x_0)^{(1)}_{4\mathrm{b}} = -\frac{1}{2L^3}\sum_{\mathbf{q}}\sum_{\mu}\sum_{s_0,t_0,u_0} D_{\mu 0}(\mathbf{q};u_0,0)\mathrm{Tr}\left\{T^a\Gamma^{f_2f_1}_{\mathcal{Q}_5} \mathcal{S}(\Gamma_X;\mathbf{p}+\mathbf{q};1,x_0,s_0)_{f_1f_2}V^a_\mu(\mathbf{p}+\mathbf{q},-\mathbf{p},-\mathbf{q};s_0,t_0,u_0)S^{(0)}_{f_2f_2}(\mathbf{p};t_0,1)\right\}. \tag{5.85}$$

Next, the diagrams with the 2 different contributions to the self energy are the pairs 5a and 5b, containing $\Sigma_1^{(1)}$, and 6a and 6b containing $\Sigma_2^{(1)}$. They are given by

$$\mathrm{g}_X^{f_1f_2}(\mathbf{p};x_0)^{(1)}_{5\mathrm{a}} = \frac{1}{2}\sum_{s_0,t_0}\mathrm{Tr}\left\{\Gamma^{f_2f_1}_{\mathcal{Q}_5}\mathcal{S}(\Gamma_X;\mathbf{p};1,x_0,s_0)_{f_1f_2} \Sigma^{(1)}_1(\mathbf{p};s_0,t_0)_{f_2f_2}S^{(0)}_{f_2f_2}(\mathbf{p};t_0,1)\right\}, \tag{5.86}$$

$$\mathrm{g}_X^{f_1f_2}(\mathbf{p};x_0)^{(1)}_{5\mathrm{b}} = \frac{1}{2}\sum_{s_0,t_0}\mathrm{Tr}\left\{\Gamma^{f_2f_1}_{\mathcal{Q}_5}S^{(0)}_{f_1f_1}(\mathbf{p};1,s_0) \Sigma^{(1)}_1(\mathbf{p};s_0,t_0)_{f_1f_1}\mathcal{S}(\Gamma_X;\mathbf{p};t_0,x_0,1)_{f_1f_2}\right\}, \tag{5.87}$$

and

$$\mathrm{g}_X^{f_1f_2}(\mathbf{p};x_0)^{(1)}_{6\mathrm{a}} = \frac{1}{2}\sum_{s_0,t_0}\mathrm{Tr}\left\{\Gamma^{f_2f_1}_{\mathcal{Q}_5}\mathcal{S}(\Gamma_X;\mathbf{p};1,x_0,s_0)_{f_1f_2} \Sigma^{(1)}_2(\mathbf{p};s_0,t_0)S^{(0)}_{f_2f_2}(\mathbf{p};t_0,1)\right\}, \tag{5.88}$$

$$\mathrm{g}_X^{f_1 f_2}(\mathbf{p}; x_0)_{6\mathrm{b}}^{(1)} = \frac{1}{2} \sum_{s_0, t_0} \mathrm{Tr} \left\{ \Gamma_{\mathcal{Q}_5}^{f_2 f_1} S_{f_1 f_1}^{(0)}(\mathbf{p}; 1, s_0) \right. \\ \left. \Sigma_2^{(1)}(\mathbf{p}; s_0, t_0) \mathcal{S}(\Gamma_X; \mathbf{p}; t_0, x_0, 1)_{f_1 f_2} \right\}. \tag{5.89}$$

Finally, the contribution with the correction to the bilinear operator, obtained by contracting a gluon line from the $O(g_0)$ vertices inserted in both fermion lines, reads

$$\mathrm{g}_X^{f_1 f_2}(\mathbf{p}; x_0)_7^{(1)} = \frac{1}{2} \sum_{s_0, t_0} \mathrm{Tr} \left\{ \Gamma_{\mathcal{Q}_5}^{f_2 f_1} S_{f_1 f_1}^{(0)}(\mathbf{p}; 1, s_0) \right. \\ \left. \Gamma_1^{(1)}(\mathbf{p}; \Gamma_X; s_0, x_0, t_0)_{f_1 f_2} S_{f_2 f_2}^{(0)}(\mathbf{p}; t_0, 1) \right\}. \tag{5.90}$$

Note that the color part of the trace in all the previous expressions is simply a trace over products of generators of the group which will yield overall factors proportional to $C_2(\mathcal{R})\mathrm{d}(\mathcal{R})$. This fact will be used in section 5.4 to state our results in a way independent of the gauge group and the color representation. In presence of a background field the situation would be quite different [93]. There would be extra tadpole diagrams due to interactions with the background field, the vertices and propagators would be modified, and the trace over the color structure would not be trivial.

Until this point the discussion has been very similar to that for the standard SF [83, 92]. After deriving the Feynman rules for the χSF, the contractions we have carried out are very close to those for the standard SF except for the extent of the temporal sums for the fermionic temporal variables and except for the presence of a non trivial flavour structure.

Next, we take into account the contribution due to the boundary counterterms in eq.(5.75). For convenience, we recall here the expression for the boundary counterterms in the χSF eq.(4.102) from section 4.3.6, which read

$$\delta\mathcal{D}_{\mathrm{W}}\psi(x) = (\delta_{x_0,0} + \delta_{x_0,T}) \left[(z_f - 1) + (d_s - 1)\mathbf{D}_s \right] \psi(x). \tag{5.91}$$

To order $O(g_0^2)$ eq.(5.91) has an expansion

$$\delta\mathcal{D}_{\mathrm{W}} = \delta\mathcal{D}_{\mathrm{W}}^{(0)} + g_0^2 \delta\mathcal{D}_{\mathrm{W}}^{(2)} + O(g_0^4). \tag{5.92}$$

The tree-level term is given by

$$\delta\mathcal{D}_{\mathrm{W}}^{(0)}\psi(x) = (\delta_{x_0,0} + \delta_{x_0,T}) \left[\left(z_f^{(0)} - 1 \right) + \left(d_s^{(0)} - 1 \right) \mathbf{D}_s \right] \psi(x). \tag{5.93}$$

This contribution has already been taken into account when calculating the quark propagator in eq.(5.54).[16] At order $O(g_0^2)$ there are two contributions proportional to d_s and z_f respectively, given by

$$\begin{aligned} \delta\mathcal{D}_{\mathrm{W}}^{(2)}\psi(x) &= \left(\delta\mathcal{D}_{d_s} + \delta\mathcal{D}_{z_f} \right) \psi(x) \\ &= (\delta_{x_0,0} + \delta_{x_0,T})\, d_s^{(1)} \mathbf{D}_s \psi(x) + (\delta_{x_0,0} + \delta_{x_0,T})\, z_f^{(1)} \psi(x). \end{aligned} \tag{5.94}$$

In the time momentum representation, $\delta\mathcal{D}_{\mathrm{W}}^{(2)}$ acts on th fermion propagator as

$$\begin{aligned} \delta\mathcal{D}_{\mathrm{W}}^{(2)} S(\mathbf{p}; x_0, y_0) =& z_f^{(1)} \left(\delta_{x_0,0} + \delta_{x_0,T}\right) S(\mathbf{p}; x_0, y_0) \\ &+ d_s^{(1)} A(\mathbf{p}) \left(\delta_{x_0,0} + \delta_{x_0,T}\right) S(\mathbf{p}; x_0, y_0), \end{aligned} \tag{5.95}$$

with $A(\mathbf{p})$ being a matrix given by

$$A(\mathbf{p}) = i\widetilde{p}_k^{+}\gamma_k + \frac{1}{2}\sum_{k=1}^{3} \left(\widehat{p}_k^{+}\right)^2, \tag{5.96}$$

and the lattice momenta given by

$$\begin{aligned} p_k^{+} &= p_k + \theta/L, \\ \widetilde{p}_k &= \sin(p_k), \\ \widehat{p}_k &= 2\sin\left(p_k/2\right). \end{aligned} \tag{5.97}$$

Note that if the operator $\mathbf{D}_s$ had been defined without the Wilson term as in eq.(4.103) instead of eq.(4.106), the second term in the right hand side of eq.(5.96) would be absent. The contribution to eq.(5.75) due to the boundary counterterms is depicted by the diagrams in figure (5.2.5).

[16] In fact, this contribution is precisely what forces us to compute numerically the quark propagator when $d_s^{(0)} \neq 1$ as in the present case.

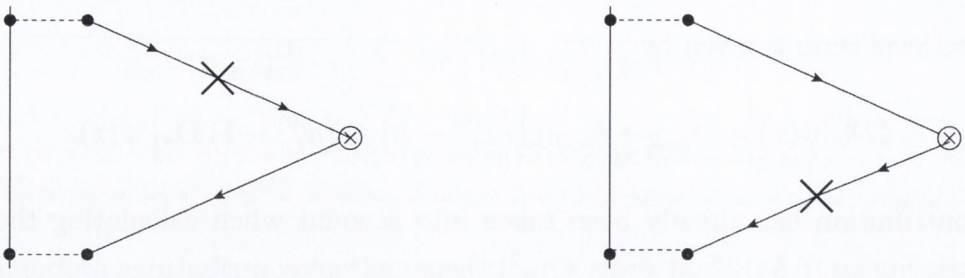

Figure 5.2.5: Diagrams depicting the contribution of boundary and mass counterterms to eq.(5.75).

The counterterm proportional to z_f yields a contribution

$$\begin{aligned} \mathrm{g}_X^{f_1 f_2}(\mathbf{p}; x_0)^{(1)}_{z_f} =& z_f^{(1)} \mathrm{Tr} \left\{ \Gamma^{f_2 f_1}_{\mathcal{Q}_5} S^{(0)}_{f_1 f_1}(\mathbf{p}; 1, x_0) \Gamma_X \right. \\ & \left. \left(S^{(0)}_{f_2 f_2}(\mathbf{p}; x_0, 0) S^{(0)}_{f_2 f_2}(\mathbf{p}; 0, 1) + S^{(0)}_{f_2 f_2}(\mathbf{p}; x_0, T) S^{(0)}_{f_2 f_2}(\mathbf{p}; T, 1) \right) \right\}, \end{aligned} \tag{5.98}$$

whereas the contribution from the term proportional to $d_s^{(1)}$ is

$$\begin{aligned} \mathrm{g}_X^{f_1 f_2}(\mathbf{p}; x_0)^{(1)}_{d_s} = & d_s^{(1)} \mathrm{Tr} \left\{ \Gamma^{f_2 f_1}_{\mathcal{Q}_5} S^{(0)}_{f_1 f_1}(\mathbf{p}; 1, x_0) \Gamma_X \right. \\ & \left. \left(S^{(0)}_{f_2 f_2}(\mathbf{p}; x_0, 0) A(\mathbf{p}) S^{(0)}_{f_2 f_2}(\mathbf{p}; 0, 1) + S^{(0)}_{f_2 f_2}(\mathbf{p}; x_0, T) A(\mathbf{p}) S^{(0)}_{f_2 f_2}(\mathbf{p}; T, 1) \right) \right\}. \end{aligned} \tag{5.99}$$

This last contribution is zero for $\mathbf{p} = 0$ and $\theta = 0$ (since $A(\mathbf{p} = 0, \theta = 0) = 0$). This fact will be very useful for the determination of $z_f^{(1)}$ without the knowledge of $d_s^{(1)}$ in section 5.4.

Finally, the last contribution to eq.(5.75) comes from the mass counterterm. It is depicted by the same diagrams as the boundary counterterms fig.(5.2.5). It can be calculated using the derivative

$$\frac{\partial}{\partial m_0} S^{(0)}(\mathbf{p}; x_0, y_0) = - \sum_{s_0} S^{(0)}(\mathbf{p}; x_0, s_0) S^{(0)}(\mathbf{p}; s_0, y_0) \tag{5.100}$$

which yields

$$\frac{\partial}{\partial m_0} \mathrm{g}_X^{f_1 f_2}(\mathbf{p}; x_0)^{(0)} = - \sum_{s_0} \mathrm{Tr} \left\{ \Gamma^{f_2 f_1}_{\mathcal{O}} S^{(0)}_{f_1 f_1}(\mathbf{p}; 1, x_0) \Gamma_X S^{(0)}_{f_2 f_2}(\mathbf{p}; x_0, s_0) S^{(0)}_{f_2 f_2}(\mathbf{p}; s_0, 1) \right\}. \tag{5.101}$$

The discussion of the expansion of the l_Y follows exactly the same directions we

have taken for the expansion of g_X. The diagrams contributing to $l_Y^{(1)}$ are identical to those shown in figures (5.2.4) and (5.2.5). The only difference with respect to the calculation of $\mathrm{g}_X^{(1)}$ is the gamma structure of both the bulk and boundary bilinear operators. The expressions for the different contributions to $l_Y^{f_1 f_2(1)}$ can be obtained directly from those for $\mathrm{g}_X^{f_1 f_2(1)}$ by replacing

$$\Gamma_X \longrightarrow \Gamma_{Y_k} \qquad \text{and} \qquad \Gamma_{\mathcal{Q}_5}^{f_1 f_2} \longrightarrow \Gamma_{\mathcal{Q}_k}^{f_1 f_2}, \tag{5.102}$$

and by taking the average over the spatial components $\frac{1}{3}\sum_{k=1}^{3}$.

5.2.4 Expansion of g_1 and l_1

In this section we describe the calculation to 1-loop of the boundary to boundary correlation functions defined in eqs.(5.41) and (5.42). The ideas for the calculation are the same as those sketched for the g_X and l_Y correlation functions. First one needs to integrate the fermion functional integral and then insert into the resulting expression the expansions of the boundary link variables and the quark propagators to g_0^2. Finally, the gauge functional integral is performed. At this point, the gluon contractions will yield all the diagrams contributing to the expansion of g_1 and l_1. In the following pages we will present in detail this calculation for the g_1 correlation functions, and comment at the end how to adapt the calculation for the l_1 correlations (which is done analogously as for l_Y).

The form of g_1 after performing the fermion contractions is given by eq.(5.48), with its expansion given by eq.(5.51). The Feynman rules needed for the calculation of the tree-level and 1-loop terms $\mathrm{g}_1^{f_1 f_2(0)}$ and $\mathrm{g}_1^{f_1 f_2(1)}$ are the same as those needed in the expansion of g_X, which have been derived in subsection 5.2.2. However, the amount of contractions involved in the term $\mathrm{g}_1^{f_1 f_2(1)}$ is significatively larger.

For the tree-level term the gauge functional integral is trivial and leads to the expression

$$\mathrm{g}_1^{f_1 f_2(0)} = \frac{1}{2}\mathrm{Tr}\left\{\Gamma_{\mathcal{Q}_5'}^{f_2 f_1} S_{f_1 f_1}^{(0)}(\mathbf{0}; T-1, 1)\Gamma_{\mathcal{Q}_5}^{f_1 f_2} S_{f_2 f_2}^{(0)}(\mathbf{0}; 1, T-1)\right\}, \tag{5.103}$$

depicted by the diagram in fig.(5.2.6).

A little inspection shows that the terms $\mathrm{g}_1^{f_1 f_2(0)}$ can be rewritten as a linear com-

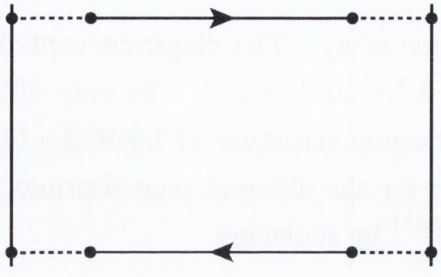

Figure 5.2.6: Diagram depicting the tree level contribution to $\mathrm{g}_1^{f_1 f_2}$.

bination of the terms $\mathrm{g}_X^{f_1 f_2(0)}(x_0)$ of the boundary to bulk correlations evaluated at $x_0 = T - 1$. These combinations will depend on the choice of flavours in $\mathrm{g}_1^{f_1 f_2}$. For instance,

$$\begin{aligned}
\mathrm{g}_1^{uu'(0)} &= -\frac{1}{2}\left\{\mathrm{g}_A^{uu'}(T-1)^{(0)} - i\mathrm{g}_S^{uu'}(T-1)^{(0)}\right\}, \\
\mathrm{g}_1^{dd'(0)} &= -\frac{1}{2}\left\{\mathrm{g}_A^{dd'}(T-1)^{(0)} + i\mathrm{g}_S^{dd'}(T-1)^{(0)}\right\}, \\
\mathrm{g}_1^{ud(0)} &= \frac{1}{2}\left\{\mathrm{g}_P^{du}(T-1)^{(0)} - i\mathrm{g}_V^{du}(T-1)^{(0)}\right\}, \\
\mathrm{g}_1^{du(0)} &= \frac{1}{2}\left\{\mathrm{g}_P^{ud}(T-1)^{(0)} + i\mathrm{g}_V^{ud}(T-1)^{(0)}\right\}.
\end{aligned} \tag{5.104}$$

These equalities can be used as a check of the correct implementation of the diagrams in their numerical evaluation. Similar equalities hold for some of the diagrams that contribute to the 1-loop term as we will see below. The relations in eq.(5.104) can be summarised in the form

$$\mathrm{g}_1^{f_1 f_2(0)} = \frac{\mathcal{N}_{f_1,f_2}}{2}\left\{\mathrm{g}_X^{f_2 f_1}(T-1)^{(0)} + i\mathcal{M}_{f_1}\mathrm{g}_{X'}^{f_2 f_1}(T-1)^{(0)}\right\}, \tag{5.105}$$

where

$$\mathcal{N}_{f_1,f_2} = \begin{cases} -1, & \text{if} \quad f_1 = f_2, \\ 1, & \text{if} \quad f_1 \neq f_2, \end{cases} \qquad \mathcal{M}_{f_1} = \begin{cases} -1, & \text{if} \quad f_1 = u, u', \\ 1, & \text{if} \quad f_1 = d, d', \end{cases} \tag{5.106}$$

and

$$X = \begin{cases} A & \text{if } f_1 = f_2, \\ P & \text{if } f_1 \neq f_2, \end{cases} \qquad X' = \begin{cases} S & \text{if } f_1 = f_2, \\ V & \text{if } f_1 \neq f_2. \end{cases} \tag{5.107}$$

Note that when writing $f_1 = f_2$ we are being a bit sloppy with the notation. We understand $f_1 = f_2$ as an equality only between flavour types ($u = u'$ and $d = d'$)

in the four flavour context described in section 5.1. If we were actually considering equal flavours ($f_1 = f_2 = u$ or d) then disconnected diagrams should also have to be considered.

The 1-loop term $g_1^{f_1 f_2 (1)}$ receives contributions from the diagrams corresponding to all possible gluon contractions, from the boundary counterterms and from the mass counterterm

$$\begin{aligned} g_1^{(1)} = & \sum_n g_{1,n}^{(1)} + d_s^{(1)} g_{1,d_s}^{(1)} + z_f^{(1)} g_{1,z_f}^{(1)} \\ & + m_c^{(1)} \frac{\partial}{\partial m_0} g_1^{(0)}. \end{aligned} \tag{5.108}$$

The 1-loop diagrams $g_{1,n}^{(1)}$ are depicted in figures (5.2.7) and (5.2.8). When performing the gluon contractions it is possible to show that, the diagrams $n =$ 1a, 1b, 3a, 3b, 5a, 5b, 6a and 6b satisfy similar relations as for the tree level diagram, so that

$$g_{1,n}^{f_1 f_2 (1)} = \frac{\mathcal{N}_{f_1,f_2}}{2} \left\{ g_X^{f_2 f_1} (T-1)_n^{(1)} + i \mathcal{M}_{f_1} g_{X'}^{f_2 f_1} (T-1)_n^{(1)} \right\}. \tag{5.109}$$

The contributions of diagrams $n =$ 2, 4a, 4b and 7 are slightly more complicated. After performing the gluon contractions and going to the time-momentum representation, one obtains similar relations to those in eq.(5.109) but where the g_X functions are projected to zero momentum within the loop. That is, only the term with $\mathbf{q} = 0$ contributes to the sum over momenta of eqs.(5.81), (5.84), (5.85) and (5.90). This happens due to the presence of an extra delta function of the momenta appearing inside the loop. We can write these relations as

$$g_{1,n}^{f_1 f_2 (1)} = \frac{\mathcal{N}_{f_1,f_2}}{2} \left\{ g_X^{f_2 f_1} (T-1)_n^{(1)} + i \mathcal{M}_{f_1} g_{X'}^{f_2 f_1} (T-1)_n^{(1)} \right\} \Big|_{\mathbf{q}=0}. \tag{5.110}$$

where $\ldots|_{\mathbf{q}=0}$ means that in equations (5.81) ,(5.84) ,(5.85) and (5.90) we only take into account the term with $\mathbf{q} = 0$ in the sum over momenta.

The remaining diagrams involve the contraction with the gluons coming from the boundary links at $x_0 = T-1$. Diagrams $n =$ 8a and 8b correspond to the contractions of the 2 gluons appearing in the same link at $O(g_0^2)$, and read

$$g_{1,8a}^{f_1 f_2 (1)} = g_{1,8b}^{f_1 f_2 (1)} = -\frac{C_2(\mathcal{R})}{2L^3} g_1^{f_1 f_2 (0)} \sum_{\mathbf{q}} D_{00}(\mathbf{q}; T-1, T-1). \tag{5.111}$$

Diagram 9 comes from contracting the gluons between the 2 boundary links,

$$\mathrm{g}_{1,9}^{f_1 f_2(1)} = \frac{C_2(\mathcal{R})}{L^3} \mathrm{g}_1^{f_1 f_2(0)} D_{00}(\mathbf{0}; T-1, T-1). \tag{5.112}$$

Next, the contraction of the gluons from the links at the top boundaries with the gluon on a vertex inserted in the fermion lines leads to diagrams n = 10a, 10b, 11a and 11b, which read

$$\begin{aligned}\mathrm{g}_{1,10\mathrm{a}}^{f_1 f_2(1)} =& \frac{1}{2L^3} \sum_{\mathbf{q}} \sum_{\mu} \sum_{s_0,t_0,u_0} D_{\mu 0}(\mathbf{q}; u_0, T-1) \mathrm{Tr} \Big\{ T^a \Gamma_{\mathcal{Q}_5'}^{f_2 f_1} S_{f_1 f_1}^{(0)}(\mathbf{q}; T-1, s_0) \\ & V_\mu^a(\mathbf{q}, \mathbf{0}, -\mathbf{q}; s_0, t_0, u_0) S_{f_1 f_1}^{(0)}(\mathbf{0}; t_0, 1) \Gamma_{\mathcal{Q}_5}^{f_1 f_2} S_{f_2 f_2}^{(0)}(\mathbf{0}; 1, T-1) \Big\},\end{aligned} \tag{5.113}$$

$$\begin{aligned}\mathrm{g}_{1,10\mathrm{b}}^{f_1 f_2(1)} =& -\frac{1}{2L^3} \sum_{\mathbf{q}} \sum_{\mu} \sum_{s_0,t_0,u_0} D_{0\mu}(\mathbf{q}; T-1, u_0) \mathrm{Tr} \Big\{ T^a \Gamma_{\mathcal{Q}_5'}^{f_2 f_1} S_{f_1 f_1}^{(0)}(\mathbf{0}; T-1, 1) \\ & \Gamma_{\mathcal{Q}_5}^{f_1 f_2} S_{f_2 f_2}^{(0)}(\mathbf{0}; 1, s_0) V_\mu^a(\mathbf{0}, -\mathbf{q}, \mathbf{q}; s_0, t_0, u_0) S_{f_2 f_2}^{(0)}(\mathbf{q}; t_0, T-1) \Big\},\end{aligned} \tag{5.114}$$

and

$$\begin{aligned}\mathrm{g}_{1,11\mathrm{a}}^{f_1 f_2(1)} =& \frac{1}{2L^3} \sum_{\mu} \sum_{s_0,t_0,u_0} D_{0\mu}(\mathbf{0}; T-1, u_0) \mathrm{Tr} \Big\{ T^a \Gamma_{\mathcal{Q}_5'}^{f_2 f_1} S_{f_1 f_1}^{(0)}(\mathbf{0}; T-1, 1) \\ & \Gamma_{\mathcal{Q}_5}^{f_1 f_2} S_{f_2 f_2}^{(0)}(\mathbf{0}; 1, s_0) V_\mu^a(\mathbf{0}, \mathbf{0}, \mathbf{0}; s_0, t_0, u_0) S_{f_2 f_2}^{(0)}(\mathbf{0}; t_0, T-1) \Big\},\end{aligned} \tag{5.115}$$

$$\begin{aligned}\mathrm{g}_{1,11\mathrm{b}}^{f_1 f_2(1)} =& -\frac{1}{2L^3} \sum_{\mu} \sum_{s_0,t_0,u_0} D_{0\mu}(\mathbf{0}; T-1, u_0) \mathrm{Tr} \Big\{ T^a \Gamma_{\mathcal{Q}_5'}^{f_2 f_1} S_{f_1 f_1}^{(0)}(\mathbf{0}; T-1, s_0) \\ & V_\mu^a(\mathbf{0}, \mathbf{0}, \mathbf{0}; s_0, t_0, u_0) S_{f_1 f_1}^{(0)}(\mathbf{0}; t_0, 1) \Gamma_{\mathcal{Q}_5}^{f_1 f_2} S_{f_2 f_2}^{(0)}(\mathbf{0}; 1, T-1) \Big\}.\end{aligned} \tag{5.116}$$

The last diagrams contributing at this order are n = 12a, 12b, 13a and 13b, which connect the link variables between the two boundaries, given by

$$\begin{aligned}\mathrm{g}_{1,12\mathrm{a}}^{f_1 f_2(1)} =& \frac{C_2(\mathcal{R}) \mathrm{d}(\mathcal{R})}{2L^3} \sum_{\mathbf{q}} D_{00}(\mathbf{q}; 0, T-1) \\ & \mathrm{Tr} \Big\{ \Gamma_{\mathcal{Q}_5'}^{f_2 f_1} S_{f_1 f_1}^{(0)}(\mathbf{q}; T-1, 1) \Gamma_{\mathcal{Q}_5}^{f_1 f_2} S_{f_2 f_2}^{(0)}(\mathbf{0}; 1, T-1) \Big\},\end{aligned} \tag{5.117}$$

$$\begin{aligned} \mathrm{g}_{1,12\mathrm{b}}^{f_1 f_2(1)} = \frac{C_2(\mathcal{R})\mathrm{d}(\mathcal{R})}{2L^3} \sum_{\mathbf{q}} D_{00}(\mathbf{q}; T-1, 0) \\ \mathrm{Tr}\left\{ \Gamma_{\mathcal{Q}_5'}^{f_2 f_1} S_{f_1 f_1}^{(0)}(\mathbf{0}; T-1, 1) \Gamma_{\mathcal{Q}_5}^{f_1 f_2} S_{f_2 f_2}^{(0)}(\mathbf{q}; 1, T-1) \right\}, \end{aligned} \tag{5.118}$$

and finally

$$\begin{aligned} \mathrm{g}_{1,13\mathrm{a}}^{f_1 f_2(1)} = \mathrm{g}_{1,13\mathrm{b}}^{f_1 f_2(1)} = -\frac{C_2(\mathcal{R})\mathrm{d}(\mathcal{R})}{2L^3} D_{00}(\mathbf{0}; T-1, 0) \\ \mathrm{Tr}\left\{ \Gamma_{\mathcal{Q}_5'}^{f_2 f_1} S_{f_1 f_1}^{(0)}(\mathbf{0}; T-1, 1) \Gamma_{\mathcal{Q}_5}^{f_1 f_2} S_{f_2 f_2}^{(0)}(\mathbf{0}; 1, T-1) \right\}. \end{aligned} \tag{5.119}$$

The contributions of the boundary and the mass counterterms to g_1, depicted in fig.(5.2.9), can also be expressed in terms of the contributions to the boundary to bulk correlations g_X. For the boundary counterterms we will have

$$\mathrm{g}_{1,z_f,d_s}^{f_1 f_2(1)} = \frac{\mathcal{N}_{f_1,f_2}}{2} \left\{ \mathrm{g}_X^{f_2 f_1}(T-1)_{z_f,d_s}^{(1)} + i\mathcal{M}_{f_1} g_{X'}^{f_2 f_1}(T-1)_{z_f,d_s}^{(1)} \right\}. \tag{5.120}$$

For the mass counterterm this will be

$$\frac{\partial}{\partial m_0} g_1^{f_1 f_2(0)} = \frac{\mathcal{N}_{f_1,f_2}}{2} \frac{\partial}{\partial m_0} \left\{ g_X^{f_2 f_1}(T-1)^{(0)} + i\mathcal{M}_{f_1} g_{X'}^{f_2 f_1}(T-1)^{(0)} \right\}. \tag{5.121}$$

The expressions for the evaluation of $l_1^{f_1 f_2}$ can be obtained as it was done for $l_Y^{f_1 f_2}$, simply by replacing the gamma matrix structure of the boundary operators

$$\Gamma_{\mathcal{Q}_5}^{f_1 f_2} \longrightarrow \Gamma_{\mathcal{Q}_k}^{f_1 f_2} \qquad \text{and} \qquad \Gamma_{\mathcal{Q}_5'}^{f_1 f_2} \longrightarrow \Gamma_{\mathcal{Q}_k'}^{f_1 f_2} \tag{5.122}$$

and taking an average over the spatial components $k = 1, 2, 3$. The diagrams depicting these expressions are identical as those in figures (5.2.7) and (5.2.8). Again, some of the diagrams contributing to $l_1^{f_1 f_2}$ can be expressed in terms of the diagrams of the $l_Y^{f_1 f_2}$ functions, leading to expressions similar to eq.(5.105). For instance, the tree-level diagram can be rewritten as

$$l_1^{f_1 f_2(0)} = -\frac{\mathcal{N}_{f_1,f_2}}{2} \left\{ l_Y^{f_2 f_1}(T-1)^{(0)} + i\mathcal{M}_{f_1} l_{Y'}^{f_2 f_1}(T-1)^{(0)} \right\} \tag{5.123}$$

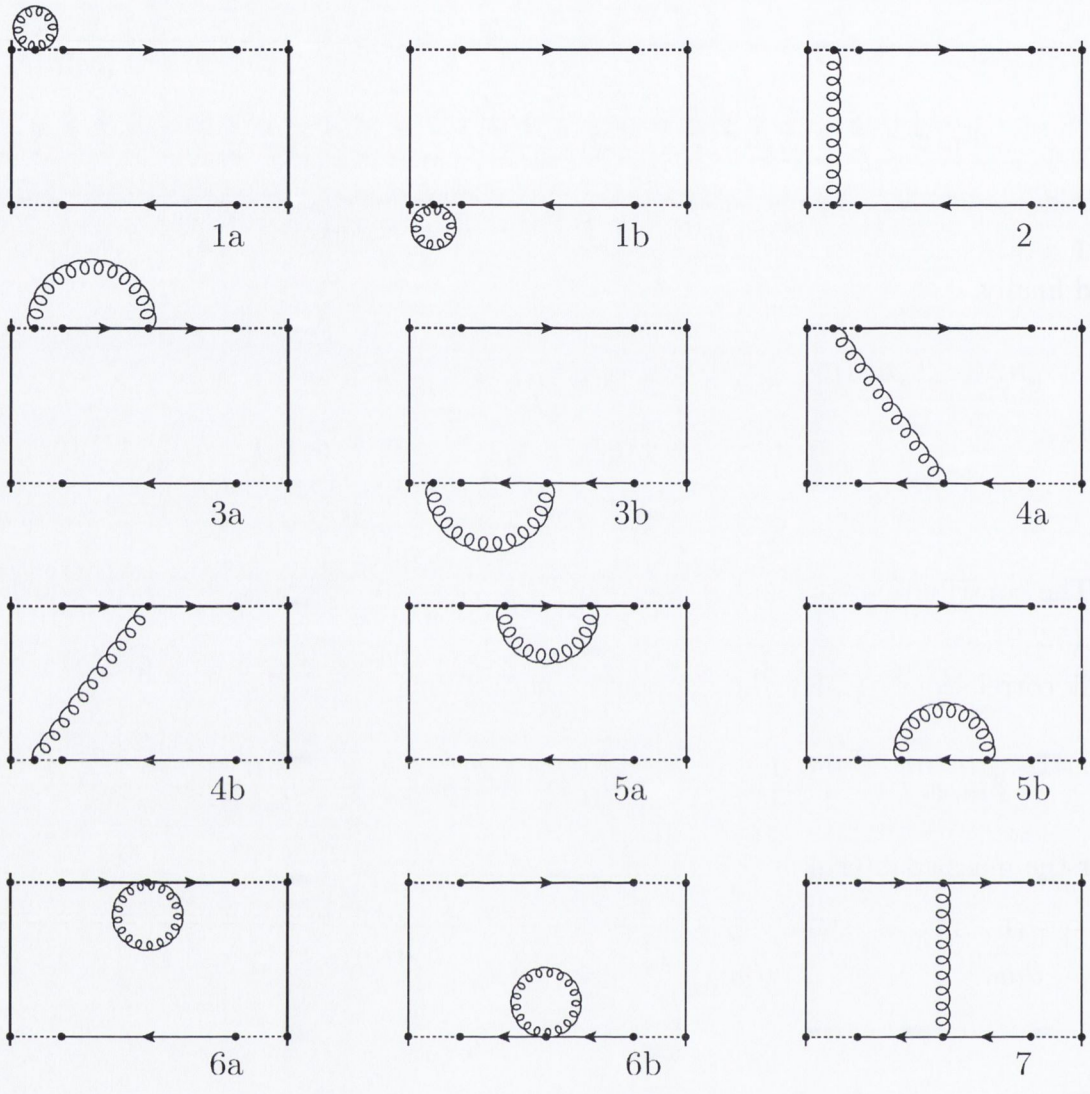

Figure 5.2.7: Diagrams depicting the one loop contribution to the boundary to boundary correlations $g_1^{f_1 f_2}$.

where

$$Y = \begin{cases} V_k & \text{if } f_1 = f_2, \\ T_{k0} & \text{if } f_1 \neq f_2, \end{cases} \qquad Y' = \begin{cases} \widetilde{T}_{k0} & \text{if } f_1 = f_2, \\ A_k & \text{if } f_1 \neq f_2. \end{cases} \tag{5.124}$$

The rest of the l_1 counterparts of the diagrams which for the g_1 functions could be related to g_X will have a similar structure as eq.(5.123).

At this stage, gathering all the expressions together, we are ready for the numerical

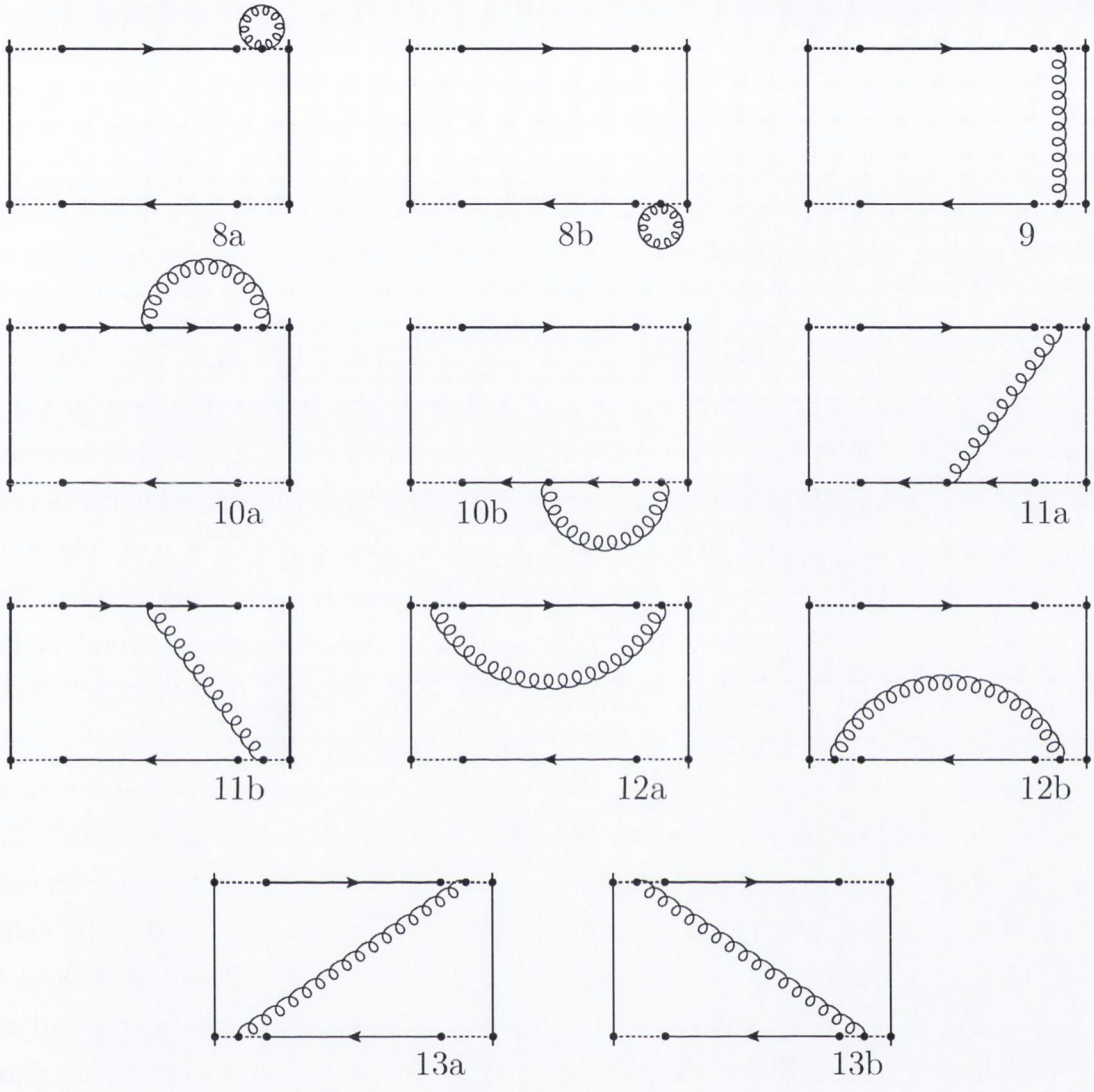

Figure 5.2.8: More diagrams depicting the one loop contribution to the boundary to boundary correlations $g_1^{f_1 f_2}$.

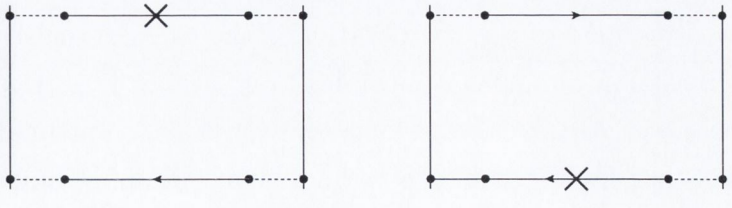

Figure 5.2.9: More diagrams depicting the contribution at one loop of the mass and boundary counterterms to $g_1^{f_1 f_2}$.

evaluation of the expansions to 1-loop of the set of correlation functions defined at the beginning of the chapter.

5.3 Numerical evaluation of the Feynman diagrams

The contributions of all the Feynman diagrams presented in the previous sections to the 1-loop correlation functions have to be evaluated numerically. We have prepared a code in Fortran 90 for evaluating the perturbative expansion of correlation functions in both the standard SF and the χSF setups. The code has been written with the aim of calculating a large number of correlation functions, that is, 10 for the standard SF, and 80 for the χSF[17], each of them with their corresponding sets of diagrams. This gives a total of 4712 expressions to evaluate, each of them involving several matrix multiplications within loops. Some care has to be taken in preparing a code efficiently or, otherwise, the calculation might become quite expensive.

For an efficient computation of the diagrammatic expressions we divide the calculation in 2 steps. First we calculate the function $\mathcal{S}$ and the 1-loop functions $\Sigma_1^{(1)}$, $\Sigma_2^{(1)}$ and $\Gamma_1^{(1)}$ which, as described in section 5.2.3 are the building blocks for constructing the diagrams. These factors are common in all the diagrams and need to be calculated only once. After that, we construct all the diagrams and evaluate the traces. In absence of a BF the color structure of the quark and gluon propagators is trivial and the color trace yields only a multiplicative group theoretical factor in every diagram. By keeping track of these factors in section 5.4 we will be able to extract m_c, z_f and d_s to 1-loop independently of the color group or the color representation chosen for the fermions.

The more expensive part of the computation is the calculation of the 1-loop functions[18], for which a large number of multiplications of 4×4 matrices with complex entries has to be performed inside the loop over momenta. Fortunately, as a consequence of translation invariance, there is permutation symmetry among the momenta summed in the loop which permits to save a factor 6. Every momentum component

[17] $10 \times 4 \times 2$, where the factor 4 comes from all possible flavour combinations, and the factor 2 comes from considering correlation functions constructed with boundary operators with both the correct projectors and with inverted projector structure (see subsection 5.4.3).

[18] In particular $\Gamma_1^{(1)}$.

yields an independent contribution to the sums in eqs.(5.77), (5.78) and (5.79), which makes the problem perfectly suitable for a multithreading approach. Using openMP directives, we distribute the loop into several threads, each thread evaluating the contribution of a momentum component. Since the momentum loop is, by far, the more expensive part of the calculation, we observe a very good scaling with the number of processors. By doubling the number of processors we observe a gain in time of almost a factor 2. This approach could be taken much further using the recently developed CUDA Fortran to export the present program to GPUs, for which hundreds of threads could be calculated at the same time.

Ideally one expects the whole calculation to scale with the size of the lattice as $(L/a)^5$, provided that the diagrams are evaluated only at the middle of the lattice [19] $x_0 = T/2$. A factor $(L/a)^3$ comes from the momentum sum and a factor $(L/a)^2$ from the two sums over time in eqs.(5.77), (5.78) and (5.79).

On the other hand, one would expect the numerical evaluation of the quark propagator to spoil the scaling of the calculation. The evaluation of the propagator consists on the numerical inversion of a $4T \times 4T$ matrix with complex entries for every value of the lattice momenta. The Dirac operator is a sparse matrix where the only components different from zero lie on a 12-diagonal band. We then use the "ZGBTRF" and "ZGBTRS" routines for the numerical inversion, available in the lapack and blas libraries. In practice, on a desktop workstation with 4 intel i5-2500 processors (3.300 GHz each) we observe the timings specified in table 5.3.1 when evaluating only the g_X and g_1 correlations, which is very close to the ideal scaling. Evaluating l_Y and l_1 as well is 4 times more expensive.

L/a	Time(s)	Ideal time(s)
48	48416.24	48416.24
24	1559.46	1513.01
12	54.24	47.28
6	2.81	1.48

Table 5.3.1: Times needed to compute all the diarams contributing to the set of g_X and g_1 correlation functions including all possible flavour combinations. The right column represents the ideal timing provided that the code scaled exactly as $(L/a)^5$.

[19] Or, at most, at $x_0 = T/2 + a$ and $x_0 = T/2 - a$, which is necessary if one aims to evaluate the temporal derivatives of correlation functions

The operations involved in the calculation are essentially sums of products of matrices and hence the general structure of the code is rather simple. However, since the expressions appearing in the calculation can be large and complicated, there is a potential risk of committing errors. For the standard SF a considerable amount of perturbative calculations have been performed in the past so that plenty of data is available for comparison. In particular, we have used the Pastor package [94], designed for the automation of lattice perturbative calculations in the SF, to generate data for a subset of correlation functions for several values of the kinematic parameters, finding agreement with the results generated by our code up to machine precision.

For the χSF no other one loop calculation has been done so far. There are several considerations that can be done to check the correctness of the results. First, we leave the gauge parameter λ_0 as an input parameter to check gauge invariance of the total result, which we confirm for several values of λ_0. After checking gauge invariance on the smaller lattice sizes, we perform the rest of the calculations in the Feynman gauge ($\lambda_0 = 1$), in which the gluon propagator is diagonal, such that all subsequent calculations get considerably simpler.[20] Moreover, due to the symmetries of the vertices and the propagators, the diagrams that come in pairs (labelled as diagrams a and b in the previous section) must contribute the same. This is used to double check the correctness of such expressions. After confirming this, when generating the final data we simply evaluate one expression from each pair. Despite of these checks, it would be very desirable to have a second and independent code to confirm our results, at least for the smallest lattice sizes.

Once we have performed the previous tests, we generate data for all the correlation functions in the SF and the χSF setting $L = T$, for lattice sizes in the range $L/a \in [6, 48]$ for several choices of θ. For the χSF we consider the cases $c_{\rm SW} = 0$ and $c_{\rm SW} = 1$. The data generated this way is analysed in the following section.

The general struture of the code, schematically represented in figure 5.3.1, is divided in three levels. The first level is composed by a set of subroutines to evaluate the objects involved in the Feynman rules in the SF and the χSF i.e. the vertices and the propagators of the different fields. In the second level there are the subroutines to construct the objects $\mathcal{S}$, $\Sigma_1^{(1)}$, $\Sigma_2^{(1)}$ and $\Gamma_1^{(1)}$. This is the core of the program. The 1-loop functions are constructed by calling the Feynmann rules in level 1. Finally,

[20] Practically, a gain in time of a factor of roughly 4 is observed for this choice of gauge.

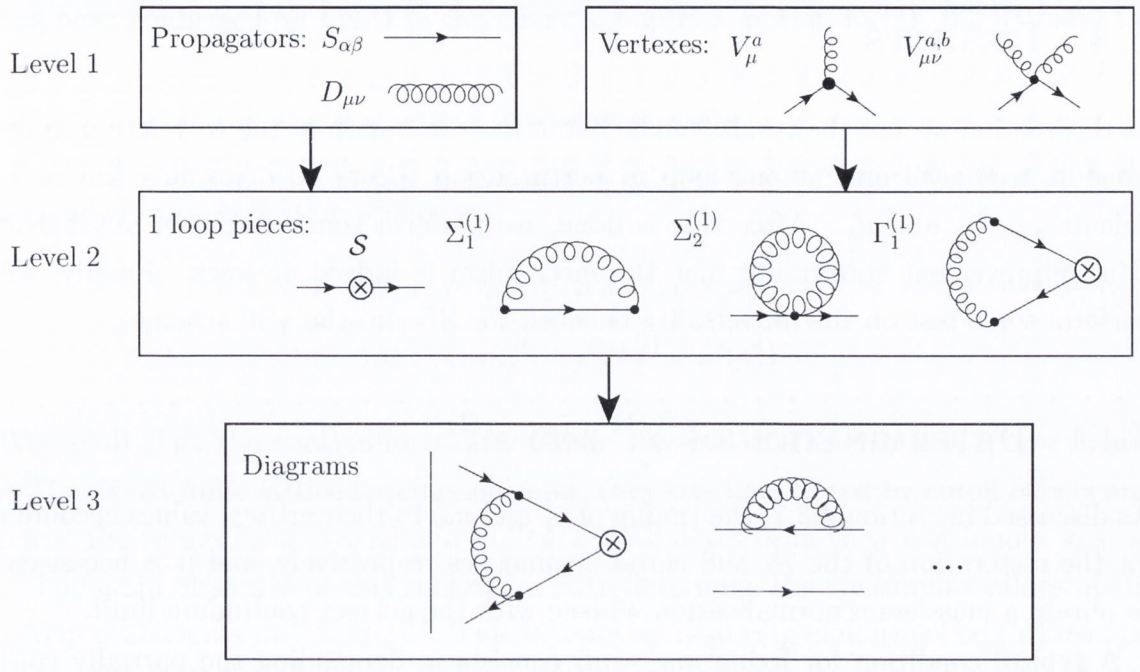

Figure 5.3.1: Schematic representation of the three levels in the code prepared to evaluate numerically the Feynman diagrams.

in the third level, the different diagrams are coded by sticking together the objects constructed in level 2.

The choice between SF and χSF (and also between different gauge actions) is specified in an input file at the beginning of the run. All the Feynmann rules for different actions are kept in level 1, and they are selected for th bulding the objects in level 2 according to the choice in the input parameter.

The code has been prepared in such a way that adding a different action can be done by coding the new Feynman rules in level 1. The diagrammatic expessions for new observables are added in level 3. Level 2 does not need to be modified at all. Detailed documentation of the code exists [95] and is available within the package or on request to the author.[21]

[21]The author would be very happy to share the code.

5.4 Results

In this section we use the results of the numerical evaluation of the correlation functions at tree level and at one loop in perturbation theory to determine the coefficients z_f, m_c and d_s. After this is done, we perform some checks of automatic $O(a)$-improvement confirming that the mechanism is indeed at work. Finally, we perform some test on the universality between the SF and the χSF schemes.

5.4.1 Determination of $z_f^{(1)}$ and $m_c^{(1)}$

As discussed in section 4.3.7, the tuning of z_f and m_0 to their critical values accounts for the restoration of the $\mathcal{P}_5$ and chiral symmetries respectively, and it is necessary to obtain a massless renormalization scheme with the correct continuum limit.

A typical condition for fixing $m_0 = m_c$ consists in demanding the partially conserved axial current (PCAC) mass to vanish at the middle of the lattice. In the χSF setup there are several ways to define the PCAC mass due to the possible flavour combinations in correlation functions.

We take

$$m_{\mathrm{PCAC}} = \frac{\widetilde{\partial}_0 \mathrm{g}_A^{ud}}{2\mathrm{g}_P^{ud}}, \tag{5.125}$$

where $\widetilde{\partial}_0 = (\partial_0 + \partial_0^*)/2$. Demanding the m_{PCAC} to vanish is hence equivalent to imposing the condition

$$\widetilde{\partial}_0 \mathrm{g}_A^{ud}\Big|_{x_0=L/2} = 0. \tag{5.126}$$

The coefficient z_f is fixed to its critical value by demanding a $\mathcal{P}_5$-odd quantity to vanish. Several such conditions can be obtained by requiring the different $\mathcal{P}_5$-odd correlation functions defined in eq.(5.37) to be zero. Different conditions will lead to ambiguities Δz_f of order $O(a)$ (see fig.(5.4.3)), which will induce ambiguities of only $O(a^2)$ on physical observables. Here we will consider four different conditions given by

$$\mathrm{g}_P^{uu'} = 0, \quad \mathrm{g}_A^{ud} = 0, \quad \mathrm{g}_V^{uu'} = 0 \quad \text{and} \quad \mathrm{g}_S^{ud} = 0. \tag{5.127}$$

The tuning of m_0 and z_f is done by solving simultaneously the system consisting of condition eq.(5.126) together with any of the conditions given in eq.(5.127). It turns out that the determination of m_c is quite independent of the value of z_f. This

has been confirmed for QCD in the quenched approximation in [81, 96, 97], and for $SU(2)$ with 2 flavours of adjoint fermions in [98]. In the following we will give further confirmation of this up to 1-loop in perturbation theory.

The two coefficients m_c and z_f are functions of the bare coupling g_0. They are expanded in perturbation theory as

$$\begin{aligned} z_f &= z_f^{(0)} + g_0^2 z_f^{(1)} + O(g_0^4), \\ m_c &= m_c^{(0)} + g_0^2 m_c^{(1)} + O(g_0^4). \end{aligned} \tag{5.128}$$

We recall that the continuum values of the tree-leel coefficients are $z_f^{(0)} = 1$ and $m_c^{(0)} = 0$. At finite lattice spacing, however, they will be affected by cutoff effects and hence the values for $z_f^{(i)}(a/L)$ and $m_c^{(i)}(a/L)$ will differ from their continuum values.

The main objective of this subsection is to determine the continuum values of the 1-loop coefficients $m_c^{(1)}$ and $z_f^{(1)}$. This is done by requiring conditions eq.(5.126) and eq.(5.127) to hold order by order in perturbation theory at each value of a/L. In this way one obtains the series $z_f^{(1)}(a/L)$ and $m_c^{(1)}(a/L)$ from which it is possible to extrapolate the continuum values. We will check the stability of the value $z_f^{(1)}$ by using the different conditions in eq.(5.127) and confirm that at finite lattice spacing, they lead at most to $O(a)$ differences to the value of $z_f^{(1)}(a/L)$.

The continuum value for $m_c^{(1)}$ has been calculated several times in the standard SF scheme in (see [83] and references wherein), and is given by

$$m_c^{(1)} = \begin{cases} -0.2025565(1) \times C_2(\mathcal{R}), & c_{\rm SW} = 1, \\ -0.3257142(4) \times C_2(\mathcal{R}), & c_{\rm SW} = 0. \end{cases} \tag{5.129}$$

This value depends only on the regularization in the bulk. Hence, we expect the series for $m_c^{(1)}(a/L)$ calculated here for the χSF scheme to converge to the same result.[22]

At tree-level we only consider one condition for the tuning of z_f, namely we demand $\mathrm{g}_P^{uu'}$ to vanish. We are then left with the system given by

$$\widetilde{\partial}_0 \mathrm{g}_A^{ud(0)}\Big|_{x_0=L/2} = 0, \qquad \mathrm{g}_P^{uu'(0)}\Big|_{x_0=L/2} = 0, \tag{5.130}$$

At tree-level, the coefficients $z_f^{(0)}$ and $m_0^{(0)}$ enter the definition of the Dirac operator, which is inverted only numerically. In order to find a solution to the system

[22] This is a good test beyond the ones presented in section 5.3 of the correctness of the calculation.

eq.(5.130) one then has to vary the parameters z_f and m_0 until the 2 conditions are simultaneously satisfied. This can be done using Newton's method to find the zero of a function recursively for $z_f^{(0)}$ and $m_0^{(0)}$.

We do this for 3 different choices of the parameters of the system. These are

$$\begin{cases} \text{Choice A}: & \theta = 0,\ \mathbf{p} = \mathbf{0},\ \text{no BF}, \\ \text{Choice B}: & \theta = 0.5,\ \mathbf{p} = \mathbf{0},\ \text{no BF}, \\ \text{Choice C}: & \theta = \pi/2,\ \mathbf{p} = \mathbf{0},\ \text{BF}. \end{cases} \tag{5.131}$$

Although the discussion in the current chapter has been done for a setup without background field, we consider here, only for the tree-level analysis, the tuning in presence of the background field given by eq.(4.30), which has been the standard choice in numerical simulations of QCD. At present order in perturbation theory the only difference in the calculation with respect to the situation without BF is that one has to include the BF explicitly in the Dirac operator before inverting it to obtain the propagator. Including a BF in the 1-loop analysis would require to modify the Feynman rules and include more diagrams [83, 93] which is far beyond the scope of this thesis. The results obtained for Choice C will be used later on when studying the SF coupling in perturbation theory in chapter 6.

For choice A the situation is extremely simple since $g_P^{uu'(0)} = g_A^{ud(0)} = 0$ exactly for all lattice spacings, and hence $z_f^{(0)}(a/L) = 1$ and $m_c^{(0)}(a/L) = 0$ for all a/L.

In figure (5.4.1) the (z_f, m_0) plane is shown for $L/a = 6$ and $L/a = 12$, where every line represents the region of the plane for which the tuning conditions are satisfied for each of the choices in eq.(5.131). The intersection between the lines associated to the two conditions (with the same choice of parameters) correspond to the tuned values of $z_f^{(0)}(a/L)$ and $m_c^{(0)}(a/L)$ for that choice. The horizontality of the lines associated to the vanishing of the PCAC mass confirms that the value of $m_c^{(0)}$ is independent of $z_f^{(0)}$ in the absence of BF. With a BF there is a dependence, but it is, however, very small.

For the determination of the one loop coefficients $z_f^{(1)}$ and $m_c^{(1)}$ we use the one loop expansion of the conditions eq.(5.126) and eq.(5.127), which read

$$\begin{aligned} 0 = \widetilde{\partial}_0 \mathrm{g}_A^{ud(a)} + m_c^{(1)}(L/a)\widetilde{\partial}_0 \mathrm{g}_A^{ud(b)} + z_f^{(1)}(L/a)\widetilde{\partial}_0 \mathrm{g}_A^{ud(c)} \\ + d_s^{(1)}(L/a)\widetilde{\partial}_0 \mathrm{g}_A^{ud(d)} + Z_A^{(1)}(L/a)\widetilde{\partial}_0 \mathrm{g}_A^{ud(0)} \quad , \end{aligned} \tag{5.132}$$

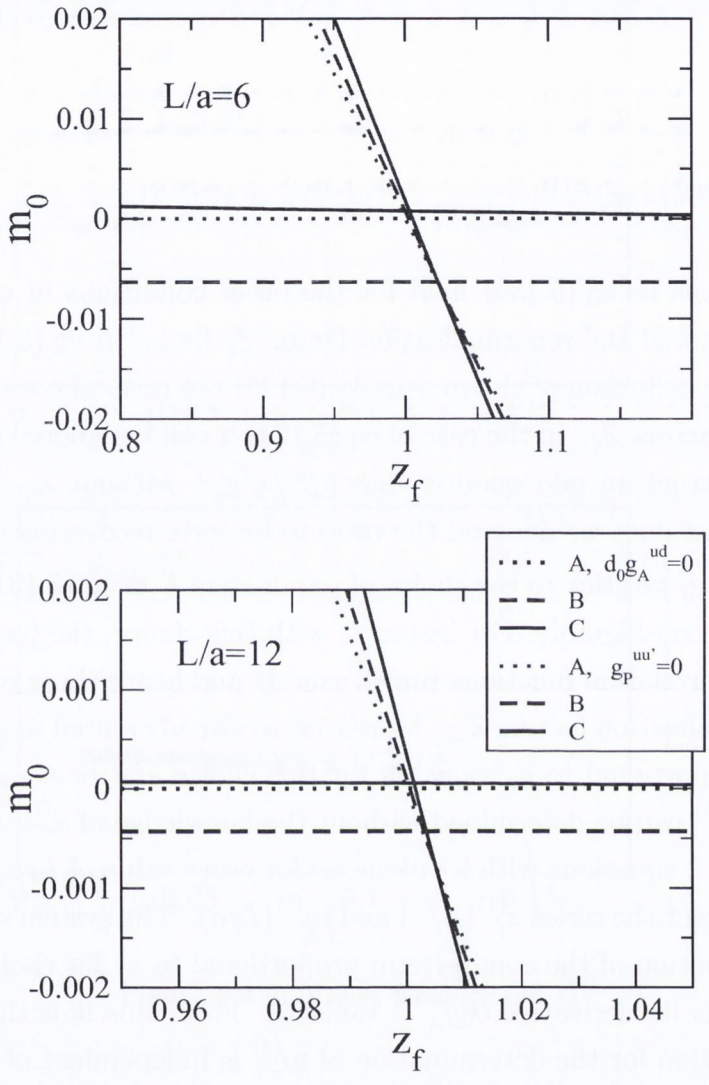

Figure 5.4.1: (m_0, z_f) plane at tree level in perturbation theory for $L/a = 6$ (top panel) and $L/a = 12$ (bottom panel). Red lines correspond to the points where $g_P^{uu'(0)} = 0$, and blue lines to $\widetilde{\partial}_0 g_A^{ud(0)} = 0$, for the different choices of parameters given in eq.(5.131). The intersection of the red lines with the blue lines associated to the same choice of parameters corresponds to the values for $m_c^{(0)}(a/L)$ and $z_f^{(0)}(a/L)$.

and

$$0 = g_P^{uu'(a)} + m_c^{(1)}(L/a) g_P^{uu'(b)} + z_f^{(1)}(L/a) g_P^{uu'(c)} + d_s^{(1)}(L/a) g_P^{uu'(d)} + Z_P^{(1)}(L/a) g_P^{uu'(0)} \quad , \tag{5.133}$$

where we define

$$\begin{aligned} \mathrm{g}_X^{f_1f_2(a)} &= \sum_n \mathrm{g}_{X,n}^{f_1f_2(1)}\Big|_{x_0=L/2}, & \mathrm{g}_X^{f_1f_2(b)} &= \partial_{m_0}\, \mathrm{g}_X^{f_1f_2(0)}\Big|_{x_0=L/2}, \\ \mathrm{g}_X^{f_1f_2(c)} &= \mathrm{g}_{X,z_f}^{f_1f_2(1)}\Big|_{x_0=L/2}, & \mathrm{g}_X^{f_1f_2(d)} &= \mathrm{g}_{X,d_s}^{f_1f_2(1)}\Big|_{x_0=L/2}. \end{aligned} \tag{5.134}$$

Similar expressions as eq.(5.134) hold for the other conditions in eq.(5.127). Note that we have ignored the renormalization factor Z_ζ here. In eq.(5.133) this can be done since in the definition of the m_{PCAC} eq.(5.125) the ratio of correlation functions cancels out the factors Z_ζ. In the case of eq.(5.134) it can be ignored as well since one can always construct an odd quantity like $\mathrm{g}_P^{uu'}/\sqrt{\mathrm{g}_1^{uu'}}$ without Z_ζ. The correlation $\mathrm{g}_1^{uu'}$ will disappear once we demand the ratio to be zero, recovering eq.(5.134).

In the following, we stick to the choice of parameters A in eq.(5.131), which simplifies the problem considerably. For instance, with this choice, the tree-level functions $\mathrm{g}_X^{f_1f_2(0)}$ for odd correlation functions vanish exactly and hence there is no contribution from the renormalization factors Z_X. Moreover, as already stated in section 5.2.3, the counterterm proportional to d_s vanishes for this choice and hence $\mathrm{g}_X^{f_1f_2(d)} = 0$ such that $z_f^{(1)}$ and $m_c^{(1)}$ can be determined without the knowledge of $d_s^{(1)}$. We are left then with a system of 2 equations with 2 unknowns for every value of L/a, from which one can trivially extract the series $z_f^{(1)}(L/a)$ and $m_c^{(1)}(L/a)$. The system simplifies further since the contribution of the counterterm proportional to z_f for choice A is constant in time, and thus its derivative $\widetilde{\partial}_0 g_A^{ud(c)}$ vanishes. From this it is then clear that at 1-loop the condition for the determination of $m_c^{(1)}$ is independent of z_f. We perform the calculation for $c_{\mathrm{SW}} = 1$ and $c_{\mathrm{SW}} = 0$. Although changing c_{SW} will only produce an $O(a^2)$ effect on physical quantities, the odd correlation functions considered here, which are pure cutoff effects, will be affected by this already at $O(a)$.

We generate this way the series for $m_c^{(1)}(a/L)$ and $z_f^{(1)}(a/L)$ for $6 < L/a < 48$, for even and odd values of L/a. These are shown in fig.(5.4.2) for the four conditions to tune z_f given in eq.(5.127). Numerical values for the series can be found in appendix E. From these series, we extrapolate their continuum values following the method described in [52]. We find:

$$\begin{aligned} m_c^{(1)}(c_{\mathrm{SW}} = 1) &= -0.2025565(1) \times C_2(R), & z_f^{(1)}(c_{\mathrm{SW}} = 1) &= 0.167572(2) \times C_2(R), \\ m_c^{(1)}(c_{\mathrm{SW}} = 0) &= -0.325721(7) \times C_2(R), & z_f^{(1)}(c_{\mathrm{SW}} = 0) &= 0.33023(6) \times C_2(R). \end{aligned} \tag{5.135}$$

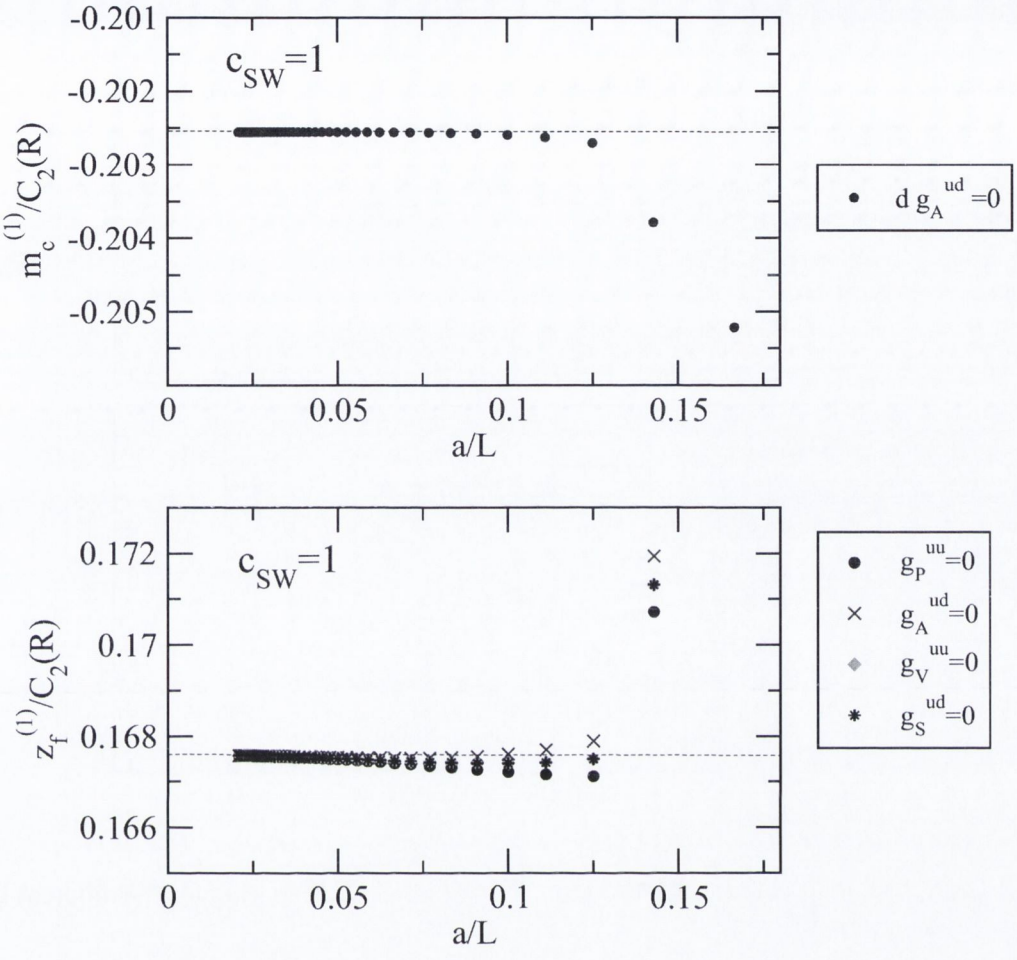

Figure 5.4.2: Values for $m_c^{(1)}$ and $z_f^{(1)}$

The continuum values we obtain for $m_c^{(1)}$ match exactly the values given in eq.(5.129) as expected since it only depends on the regularization in the bulk.[23] This is a further confirmation of the correctness of our perturbative calculation. The continuum values for $z_f^{(1)}$ are presented here for the first time. We extrapolate the same continuum value up to five decimal digits for the four conditions in eq.(5.127). The error in $z_f^{(1)}$ quoted in eq.(5.135) accounts for the discrepancies in the extrapolations (starting in the sixth decimal digit) for the different conditions.

We calculate as well the differences $\Delta z_f^{(1)}(a/L)$ between $z_f^{(1)}(a/L)$ obtained using

[23]Note that the precision of $m_c^{(1)}$ and $z_f^{(1)}$ is a bit lower for $c_{\rm SW} = 0$. These results are preliminary and can still be improved.

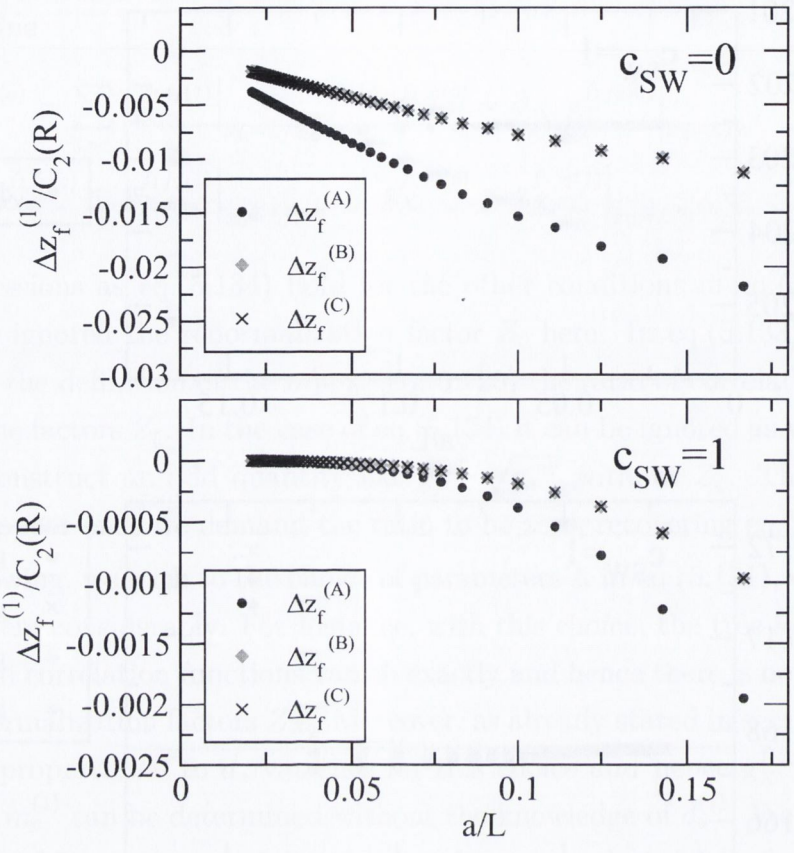

Figure 5.4.3: Differences in the 1-loop value $z_f^{(1)}$ at finite lattice spacing for the different tuning conditions given in eq.(5.127).

the different conditions eq.(5.127). These are given by

$$\begin{cases} \Delta z_f^{(A)} = z_f^{(1)}\Big|_{g_A^{ud}=0} - z_f^{(1)}\Big|_{g_P^{uu'}=0}, \\ \Delta z_f^{(B)} = z_f^{(1)}\Big|_{g_V^{uu'}=0} - z_f^{(1)}\Big|_{g_P^{uu'}=0}, \\ \Delta z_f^{(C)} = z_f^{(1)}\Big|_{g_S^{ud}=0} - z_f^{(1)}\Big|_{g_P^{uu'}=0}. \end{cases} \tag{5.136}$$

The three $\Delta z_f^{(i)}$ are displayed in fig.(5.4.3). The fact that for $c_{SW} = 1$ (bottom panel in fig.(5.4.3)) the differences $\Delta z_f^{(1)}(a/L)$ don't behave linearly as $a/L \to 0$ is an accident of the particular choice of parameters, for which linear lattice artefacts are very suppressed.

5.4.2 Determination of $d_s^{(1)}$

The determination of the 1-loop boundary improvement coefficient $d_s^{(1)}$ can be done by requiring the absence of $O(a)$ terms at 1-loop in some $\mathcal{P}_5$-even quantity. Here we follow the same strategy as was done in [83] to compute the boundary improvement coefficient $\widetilde{c}_t^{(1)}$ for the standard SF (see section 5.5 of [83] for further details). In [83] it was suggested that a good quantity for the extraction of $\widetilde{c}_t^{(1)}$ was the ratio

$$\left.\frac{[f_P(x_0,\theta,a/L)]_R}{[f_P(x_0,0,a/L)]_R}\right|_{x_0=T/2}. \tag{5.137}$$

Their extrapolation yielded

$$\widetilde{c}_t^{(1)} = -0.0135(1)\times C_2(R) \tag{5.138}$$

for different values of θ, and the result was further confirmed by studying the ratio

$$\left.\frac{[f_A(x_0,\theta,a/L)]_R}{[f_A(x_0,0,a/L)]_R}\right|_{x_0=T/2}. \tag{5.139}$$

In analogy to to this, here we consider the quantity

$$\left.\frac{\left[\mathrm{g}_P^{ud}(x_0,\theta,a/L)\right]_R}{\left[\mathrm{g}_P^{ud}(x_0,0,a/L)\right]_R}\right|_{x_0=T/2}. \tag{5.140}$$

A more detailed study considering further quantities is on the way but will not be ready by the time of writing this thesis. Requiring $O(a)$ improvement on eq.(5.140) to one loop implies that

$$\begin{aligned} d_s^{(1)}\left.\frac{\mathrm{g}_P^{ud(c)}}{\mathrm{g}_P^{ud(0)}}\right|_\theta = C &- \left(\left.\frac{\mathrm{g}_P^{ud(a)}}{\mathrm{g}_P^{ud(0)}}\right|_\theta - \left.\frac{\mathrm{g}_P^{ud(a)}}{\mathrm{g}_P^{ud(0)}}\right|_{\theta=0}\right) + am_c^{(1)}\left(\left.\frac{\mathrm{g}_P^{ud(b)}}{\mathrm{g}_P^{ud(0)}}\right|_\theta - \left.\frac{\mathrm{g}_P^{ud(b)}}{\mathrm{g}_P^{ud(0)}}\right|_{\theta=0}\right) \\ &+ z_f^{c(1)}\left(\left.\frac{\mathrm{g}_P^{ud(c)}}{\mathrm{g}_P^{ud(0)}}\right|_\theta - \left.\frac{\mathrm{g}_P^{ud(c)}}{\mathrm{g}_P^{ud(0)}}\right|_{\theta=0}\right) + O(a^2). \end{aligned} \tag{5.141}$$

where C is a constant. In order to remove the constant in eq.(5.141), we take the difference of the elements of the series evaluated at $L+a$ and $L-a$ and multiply them by $-L/2a$, obtaining then a series which extrapolates to $d_s^{(1)}$. For $\theta = 0.1,\ 0.5$

and 1.0 we find

$$d_s^{(1)} = -0.0009(3) \times C_2(R). \tag{5.142}$$

5.4.3 Check of automatic $O(a)$ improvement

As already discussed, once m_0 and z_f are fixed to their critical value bulk automatic $O(a)$ improvement should hold. When z_f is tuned the boundary conditions eq.(4.91) should hold up to cutoff effects.

In order to check this one can consider $\mathcal{P}_5$-even correlation functions as the ones introduced in section 5.1, replacing the projectors in the boundary source fields by their opposite counterparts

$$\widetilde{Q}_{\pm} \longrightarrow \widetilde{Q}_{\mp}. \tag{5.143}$$

We denote these correlation functions as $g_{X-}^{f_1 f_2}(x_0)$ and $l_{Y-}^{f_1 f_2}(x_0)$, where the "$-$" subscript denotes the usage of inverted projectors, in contrast to the standard forms eqs.(5.38) and (5.35). A list with the Γ structures for these correlation functions is collected in appendix B. Provided that the boundary conditions eq.(4.99) are correctly implemented in the lattice, then the $g_{X-}^{f_1 f_2}(x_0)$ and $l_{Y-}^{f_1 f_2}(x_0)$ should vanish in the continuum limit.

Moreover, the $\mathcal{P}_5$-odd correlation functions eqs.(5.37) and (5.40) will be a pure cutoff effect that must vanish as the continuum limit is approached.

We check these considerations in perturbation theory for the choice of parameters A in eq.(5.131). For this choice the tree level functions $g_{X-}^{f_1 f_2(0)}$ and $l_{Y-}^{f_1 f_2(0)}$ vanish exactly.

At 1-loop we evaluate the set of $g_{X-}^{f_1 f_2(1)}$ and $l_{Y-}^{f_1 f_2(1)}$ correlation functions using the values at finite lattice spacing for $z_f^{(1)}(L/a)$ and $m_c^{(1)}(L/a)$ extracted in section 5.4.1.

As can be seen from fig.(5.4.4), the values of the functions $g_{X-}^{f_1 f_2(1)}$ and $l_{Y-}^{f_1 f_2(1)}$ are very small already at the largest lattice spacings we consider and vanish in the continuum limit, confirming that the boundary conditions are correctly implemented [81]. Both choices of $c_{\rm SW} = 0$ and $c_{\rm SW} = 1$ lead to comparable lattice artefacts.

After confirming the correct realization of the boundary conditions, we calculate the set of g_X and l_Y $\mathcal{P}_5-$odd correlations functions. These are displayed in fig.(5.4.5) for the choice $c_{\rm SW} = 0$ and in fig.(5.4.6) for $c_{\rm SW} = 1$. The calculation is done using 2 different conditions for the tuning of z_f, for which all the odd correlation functions

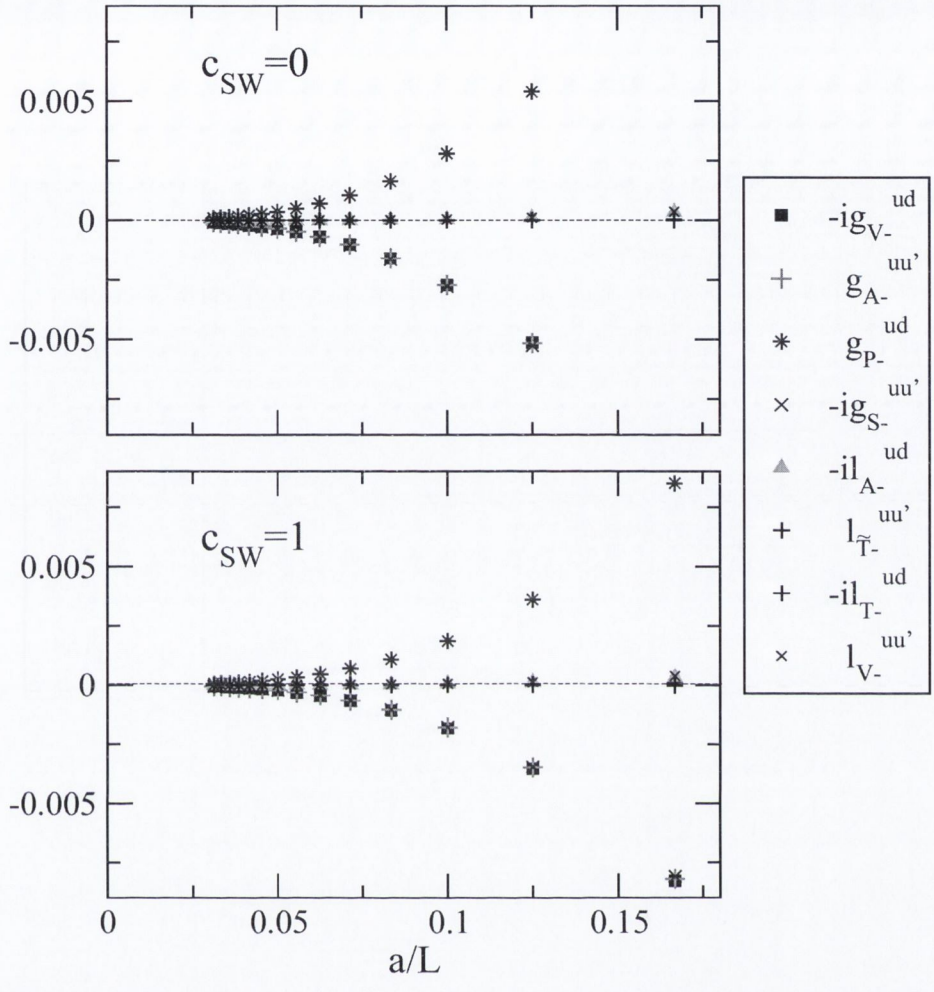

Figure 5.4.4: Vanishing correlation functions with the inverted projectors.

vanish in the continuum limit. For $c_{\rm SW} = 0$ all the correlation functions vanish linearly as $a/L \to 0$ as expected, confirming that the odd-correlations are indeed a pure $O(a)$ effect and hence that the mechanism of automatic $O(a)$ improvement is at work. Odd correlation functions, being a pure cutoff effect, are affected by the clover term already at $O(a)$. Their good convergence for $c_{\rm SW} = 1$ is a particular effect of this choice of parameters for which $O(a)$ effects are strongly suppressed.

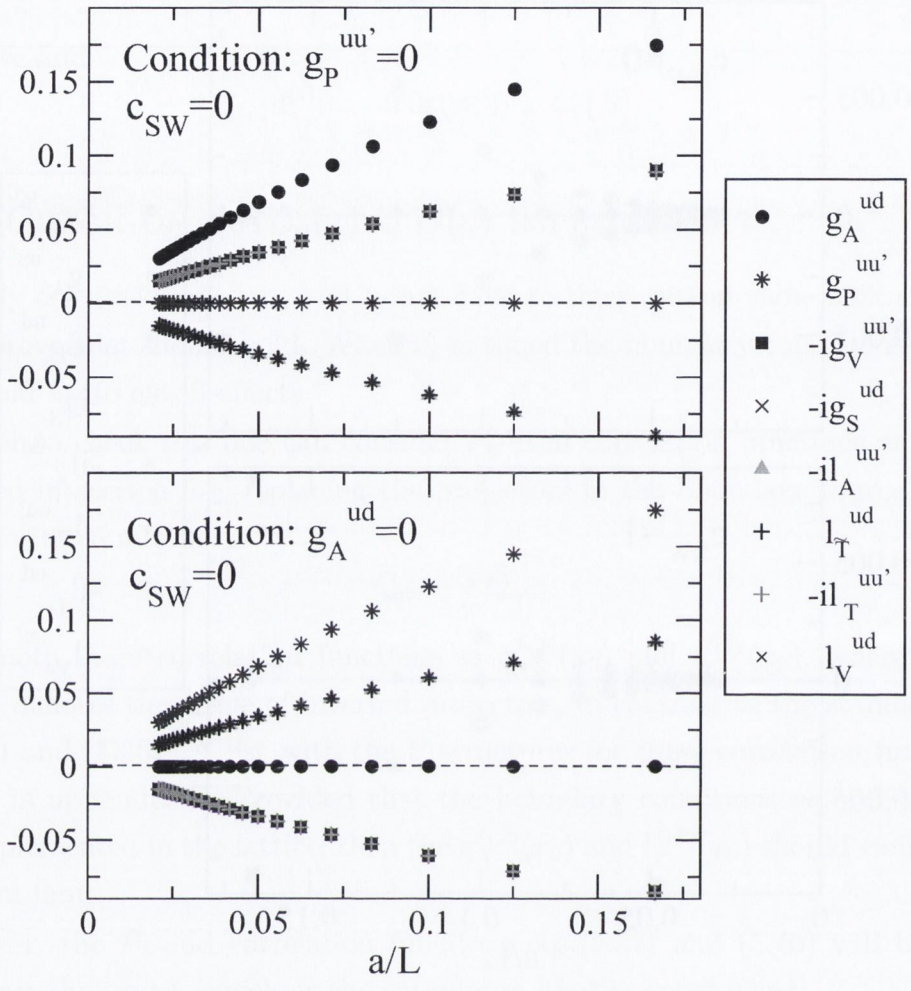

Figure 5.4.5: Vanishing odd correlation functions at 1-loop calculated for $c_{\rm SW} = 0$ with 2 different renormalization conditions for z_f.

5.4.4 Universality

The equalities between SF and χSF correlation functions presented in eqs.(5.36), (5.39), (5.37) and (5.40) are continuum relations which, once we are using a lattice regulator, will only hold up to cutoff effects. As the continuum limit is approached, these relations are expected to hold when considering renormalized correlation functions. For instance, the ratios

$$\left[\frac{\mathrm{g}_A^{uu'}(T/2)}{\sqrt{\mathrm{g}_1^{uu'}}}\right] \times \left[\frac{f_A(T/2)}{\sqrt{f_1}}\right]^{-1} \quad \text{or} \quad \left[\frac{\mathrm{g}_P^{ud}(T/2)}{\sqrt{\mathrm{g}_1^{ud}}}\right] \times \left[\frac{f_P(T/2)}{\sqrt{f_1}}\right]^{-1}, \tag{5.144}$$

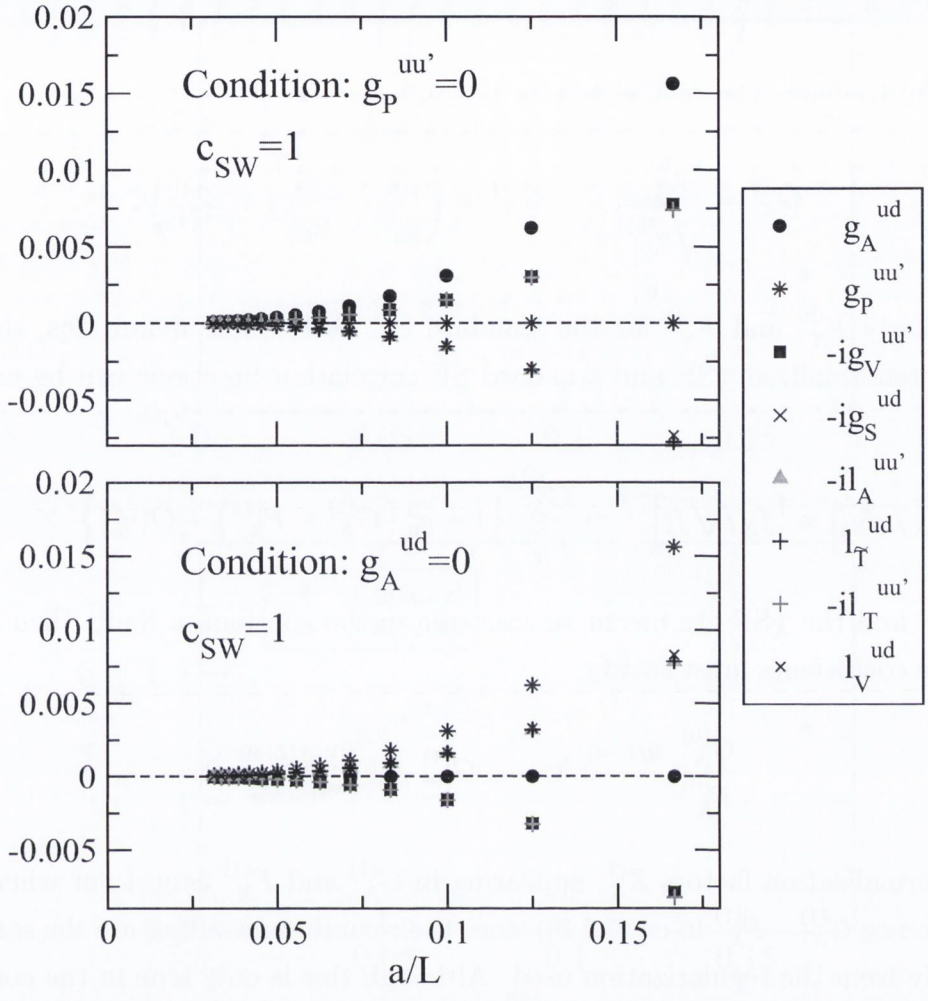

Figure 5.4.6: Vanishing odd correlation functions 1-loop calculated for $c_{\rm SW} = 1$ with 2 different renormalization conditions for z_f.

should approach 1 as $a/L \longrightarrow 0$.[24]

Once the $z_f^{(1)}$ and $m_c^{(1)}$ coefficients are known we can study the universality relations in eq.(5.144) order by order in perturbation theory.

The expansion for a generic ratio between renormalized correlation functions $\left[g_X/\sqrt{g_1}\right]_R$ (and similarly for the f_X and f_1 correlations) is given by

$$\left[\frac{g_X}{\sqrt{g_1}}\right]_R = \frac{g_X^{(0)}}{\sqrt{g_1^{(0)}}}\left\{1 + g_0^2\left(\frac{g_X^{(1)}}{g_X^{(0)}} - \frac{g_1^{(1)}}{2g_1^{(0)}} + Z_X^{(1)}\right) + O(g_0^4)\right\}. \qquad (5.145)$$

[24]Similar ratios between any other correlation function in the equalities listed in eqs.(5.36), (5.37), (5.39) and (5.40) could have been considered here. These will as well be expected to approach 1 as $a/L \longrightarrow 0$.

It is useful to define the coefficients for the χSF

$$G_X^{(0)} = \frac{\mathrm{g}_X^{(0)}}{\sqrt{\mathrm{g}_1^{(0)}}}, \qquad G_X^{(1)} = \left(\frac{\mathrm{g}_X^{(0)}}{\mathrm{g}_1^{(0)}} - \frac{\mathrm{g}_1^{(1)}}{2\mathrm{g}_1^{(0)}} + Z_X^{(1)} \right), \tag{5.146}$$

and similarly $F_X^{(0)}$ and $F_X^{(1)}$ for the standard SF. With these definitions, the ratios between renormalized χSF and standard SF correlation functions can be expanded as

$$[\mathrm{g}_X/\sqrt{\mathrm{g}_1}] \times \left[f_X/\sqrt{f_1} \right]^{-1} = \frac{G_X^{(0)}}{F_X^{(0)}} \left\{ 1 + g_0^2 \left(G_X^{(1)} - F_X^{(1)} \right) + O(g_0^4) \right\} \tag{5.147}$$

If the SF and the χSF are meant to converge in the continuum limit, then the perturbative coefficients must satisfy

$$\frac{G_X^{(0)}}{F_X^{(0)}} \xrightarrow{a/L \to 0} 1; \qquad G_X^{(1)} - F_X^{(1)} \xrightarrow{a/L \to 0} 0. \tag{5.148}$$

The renormalization factors $Z_X^{(1)}$ appearing in $G_X^{(1)}$ and $F_X^{(1)}$ cancel out when taking the difference $G_X^{(1)} - F_X^{(1)}$ in eq.(5.148) since their continuum values are the same independently from the regularization used. Although this is only true in the continuum limit, ignoring the factors $Z_X^{(1)}$ at finite lattice spacingswill only induce cutoff effects without compromising the correct convergence to the continuum limit.

We study the tree-level universality relations for the 3 choices in eq.(5.131). The realisation is trivially satisfied for choice A for all values of a/L. Choices B and C are shown in fig.(5.4.7), from which we confirm the expected convergence of the universality relations. It is however remarkable that the cutoff effects in presence of the background field (choice C) can be much larger than without it (choice B). This is particularly clear for the ratio involving the pseudo-scalar correlation functions.

At 1-loop in perturbation theory we study the universality relations only for choice A, which are displayed in fig.(5.4.8). Again, we confirm the expected convergence of the universality relations as the continuum limit is approached.

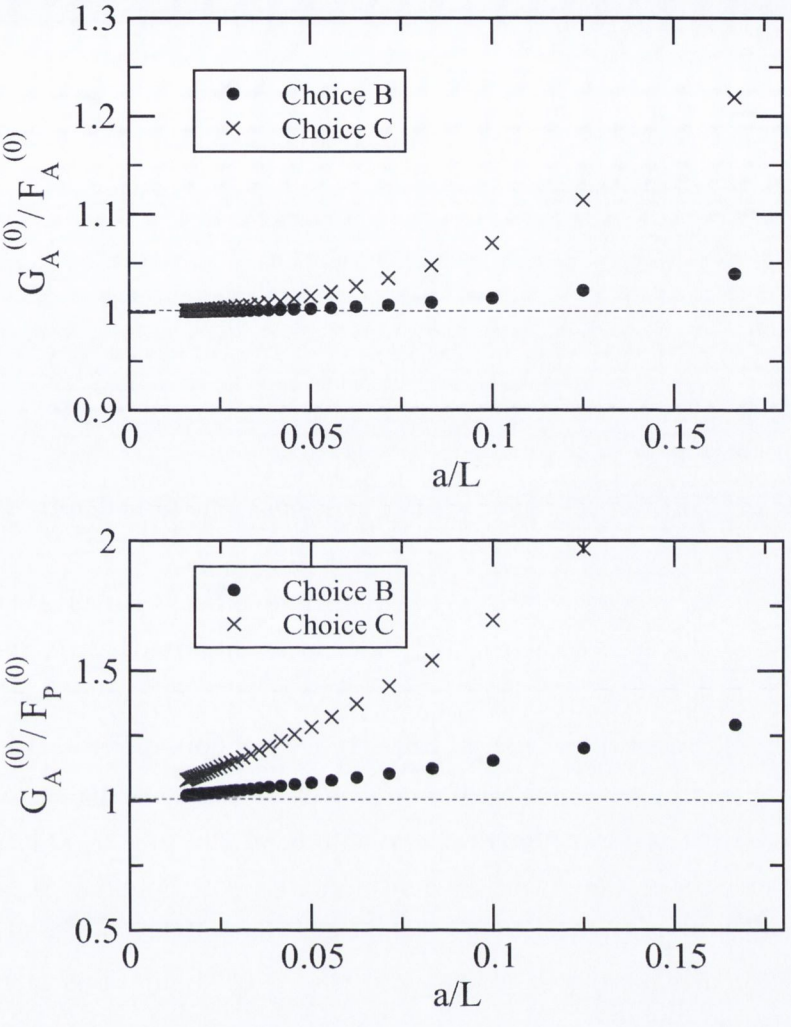

Figure 5.4.7: Check of universality at tree level in perturbation theory.

5.5 Summary of chapter 5

In this chapter we have introduced correlation functions in the SF and χSF schemes in the continuum theory and discussed their lattice implementation. We have shown how to relate correlation functions between the 2 schemes in the continuum. For the lattice regularized theory we have presented strategies for the tuning of the critical mass m_c and the coefficient z_f appearing in the boundary counterterm, and for testing if the mechanism of automatic $O(a)$ improvement is at work. The central part of the chapter has been the perturbative expansion of the correlation functions in the χSF, which has been described in detail in section 5.2. The results of the perturbative

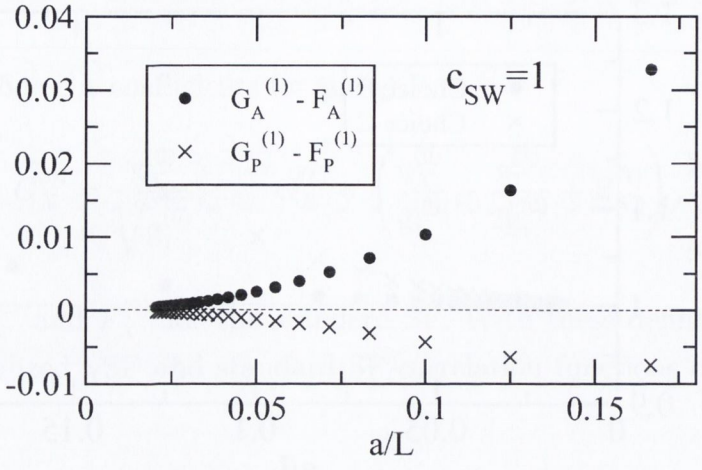

Figure 5.4.8: Check of universality at 1-loop in perturbation theory.

calculations have been used to study the renormalization, universality and correct implementation of the lattice theory to 1-loop order in perturbation theory.

The main result of this work is the extraction of the 1-loop boundary coefficient $z_f^{(1)}$ and $d_s^{(1)}$, which will be of fundamental importance for non-perturbative calculations. The coefficient $z_f^{(1)}$ will be useful for checking the consistency of simulations at weak coupling and guiding the non-perturbative tuning of the full z_f. The knowledge of $d_s^{(1)}$ is needed to remove the cutoff effects in the fermion boundaries to $O(ag_0^4)$. We have also been able to show up to 1-loop the weak dependence of the critical mass on the coefficient z_f, a behaviour which has been seen in simulations at not very large couplings [81, 96, 98]. The correct implementation of the theory has been confirmed by checking that correlation functions with inverted correlators vanish in the continuum limit. The realization of automatic $O(a)$ improvement has been shown to 1-loop by confirming that odd-correlation functions are in fact $O(a)$ effects (for $c_{\rm SW} = 0$). Finally the universality of the continuum limit of both SF and χSF regularizations has been shown by studying the convergence of ratios of correlation functions in both setups.

The code written for the numerical evaluation of the Feynman diagrams is easily extendible for computing more complicated observables.[25] Other gauge actions [44, 45] more frequently used in non-perturbative simulations could be easily added as well since only the gluon propagator is modified with respect to the present calculation[26].

[25] Like the point split vector current $\widetilde{V}_\mu$, four fermion operators,...

[26] This extension has already been implemented.

"The same thing we always do. Fight 'em until we can't. "

Kara "Starbuck" Thrace

6

The QCD running coupling in the χSF

One of the main reasons which lead to the construction of the Schrödinger Functional as a finite volume renormalization scheme was the possibility of defining a renormalized coupling whose evolution could be calculated all the way from the hadronic world at low energies to the perturbative high energy regime.

For this to be feasible, the running coupling must satisfy some criteria. First of all, since it must ultimately be evaluated non-perturbatively, it has to be easy to measure in Monte Carlo simulations. Furthermore, it must be weakly affected by lattice artefacts, such that continuum extrapolations can be safely carried out without large uncertainties. Finally, it has to be relatively easy to handle in perturbation theory, such that the β-function can be computed at high enough order so that the matching to other perturbative regimes can be made.

The original proposal for a coupling in the SF was based on the response of the system to a background field [23]. By now, other definitions satisfying the previous criteria exist, for example, those recently proposed based on the gradient flow [99].

In the present chapter we will study the original proposal in perturbation theory in

the χSF setup. In section 6.1 we will review its definition. In section 6.2 we perform the perturbative expansion of the coupling, the step scaling function and its cutoff effects up to 2-loops in perturbation theory. The contribution of fermions at 1-loop is calculated in section 6.3. By demanding cutoff effects linear in a/L to be absent in the 1-loop coefficient of the coupling, we will be able to extract the contribution to the gauge boundary coefficient $c_t^{(1)}$ due to fermions regulated with the χSF setup. Moreover, we will examine the size of the remaining cutoff effects and compare them to those in the standard SF setup. In section 6.4 we will study a one parameter family of renormalized couplings which leads us to define the SF_ν and $\chi\mathrm{SF}_\nu$ renormalization schemes. Using data from 2-loop calculations available in the literature, we will be able to study the dependence of the cutoff effects on the parameter ν up to 2-loops. Moreover, we will compute tha matching coefficients to the $\overline{\mathrm{MS}}$ scheme to 2-loops and extract the 3-loop β-function on the SF_ν scheme.

6.1 Definitions

A particular definition of a running coupling in Schrödinger functional schemes satisfying the requirements given above was proposed in [23] as a response of the system to the induced chromo-electric field. With the values for the boundary gauge fields C and C' specified as in eq.(4.24) with the phases given by eq.(4.30), a renormalized coupling is defined by

$$\frac{1}{\overline{g}^2} = \frac{1}{k}\left[\frac{\partial\Gamma}{\partial\eta}\right]_{\eta=\nu=0}, \tag{6.1}$$

where Γ is the quantum effective action defined in eq.(4.21), and η and ν are the dimensionless parameters of the background field (their role will be clear in section 6.4, when we introduce the SF_ν and $\chi\mathrm{SF}_\nu$ schemes). The normalisation constant k is given by

$$k = \left[\frac{\partial\Gamma_0}{\partial\eta}\right]_{\eta,\nu=0}, \tag{6.2}$$

and ensures that at tree level the coupling $\overline{g}^2$ is equal to the bare coupling g_0^2 (see eq.(4.22)).

The derivative with respect to the parameter η eliminates divergent contributions to the effective action that do not depend on the background field, such that the resulting coupling is indeed a renormalized coupling. Moreover, $\overline{g}^2$ depends only on

one physical scale, the size of the box L (where we assume the ratio $T/L = \rho$ to be fixed), which is identified with the renormalization scale $L = 1/\mu$ as explained in section 3.3. The running of the coupling with the scale L can then be computed by evaluating $\overline{g}^2$ at different physical box sizes.

With the definition eq.(6.1), once a lattice regularization for the SF is implemented, the observable to evaluate in simulations is given by

$$\Gamma' = \left\langle \left. \frac{\partial S}{\partial \eta} \right|_{\eta=\nu=0} \right\rangle . \tag{6.3}$$

The coupling $\overline{g}^2$ is then simply given by the expectation value of a local operator, which is inexpensive to evaluate in a computer simulation. However, the quantity eq.(6.3), being a pure gauge quantity, is susceptible to large statistical fluctuations. Fortunately, the level of accuracy achievable with a reasonable statistical ensemble is satisfactory after all.

The renormalized coupling eq.(6.1) is hence suitable for being used in the process of finite size scaling described in section 3.3. The main observable to compute is thus its associated step scaling function $\sigma(u)$[1]. As discussed in chapter 3, in practice, the non-perturbative evaluation of the coupling $\overline{g}^2(L)$ is done on a finite size scheme defined on the lattice. One then obtains the lattice counterpart of the step scaling function $\Sigma(u, a/L)$, which will coincide with $\sigma(u)$ in the continuum limit,

$$\sigma(u) = \lim_{a/L \to 0} \Sigma(u, a/L) \tag{6.4}$$

The continuum SSF $\sigma(u)$ is obtained by performing simulations on pairs of lattices to determine $\Sigma(u, a/L)$, and then performing a controlled continuum extrapolation. The quantity $\Sigma(u, a/L)$ is affected by cutoff effects and hence its convergence to the continuum limit will depend on the details of the regularization being used. It is of vital importance to obtain regularizations for which cutoff effects are as small as possible.

Cutoff effects in the SSF can be monitored by comparing the lattice and continuum counterparts

$$\delta(u, a/L) = \frac{\Sigma(u, a/L) - \sigma(u)}{\sigma(u)}. \tag{6.5}$$

[1]For the rest of this chapter we will assume steps of $s = 2$, defining $\sigma(u) \equiv \sigma(s = 2, u)$.

The continuum quantity $\sigma(u)$ is not known a prior.[2] It will be possible, however, to monitor cutoff effects order by order in perturbation theory. In the following subsection we sketch the perturbative expansion of the coupling, the step scaling function and its associated lattice artefacts.

6.2 Perturbative expansion of the coupling

The SF coupling $\overline{g}^2$ can be expanded in powers of the bare coupling g_0^2,

$$\overline{g}^2(L/a) = g_0^2 + p_1(L/a)g_0^4 + p_2(L/a)g_0^6 + O(g_0^8). \tag{6.6}$$

From the perturbative expansion eq.(4.22) of the effective action $\Gamma[B]$, we see that the expansion coefficients $p_1(L/a)$ and $p_2(L/a)$ are given by

$$p_1(L/a) = -\frac{1}{k}\frac{\partial\Gamma_1[B]}{\partial\eta}\bigg|_{\eta=\nu=0}, \tag{6.7}$$

$$p_2(L/a) = -\frac{1}{k}\frac{\partial\Gamma_2[B]}{\partial\eta}\bigg|_{\eta=\nu=0} + \left(\frac{1}{k}\frac{\partial\Gamma_1[B]}{\partial\eta}\bigg|_{\eta=\nu=0}\right)^2. \tag{6.8}$$

As already discussed in section 4.4, for the perturbative computation one has to perform an expansion of the gauge fields around the background field, which requires to go through a gauge fixing procedure. Since the gauge part of the χSF is identical to the standard SF, the gauge fixing procedure in presence of a background field can be directly imported from [23]. We refer the reader to the original literature for details. After this, the one loop contribution to the effective action is given by

$$\Gamma_1[B] = -\ln\det\Delta_0 + \frac{1}{2}\ln\det\Delta_1 - \frac{1}{2}\ln\det\Delta_2. \tag{6.9}$$

Here Δ_0 is the ghost quadratic operator, introduced during the gauge fixing procedure. Δ_1 is the quadratic gluon operator, resulting from the expansion of the fields around the background field V in the gauge part of the action S_{G} eq.(4.51). Finally, Δ_2 is the quadratic fermion operator in the background field V, for the chosen regularization. We refer to [23] for explicit expressions for the operators Δ_0 and Δ_1 The fermionic

[2] In fact, determining $\sigma(u)$ is the target of all the step scaling programme.

operator Δ_2 is given by

$$\Delta_2 = \left(\mathcal{D}_{\mathrm{W}}^{\dagger}\mathcal{D}_{\mathrm{W}}\right) = \left(\gamma_5\tau^1\left(\mathcal{D}_{\mathrm{W}} + \delta\mathcal{D}_{\mathrm{W}} + m_0\right)\right)^2, \tag{6.10}$$

for the χSF. A similar expression holds for the SF, replacing the operator $\mathcal{D}_{\mathrm{W}}$ with the corresponding one and removing the Pauli matrix τ^1 [80].

Inserting eq.(6.9) into the definition of the coupling one obtains the one loop term given by

$$p_1(L/a) = -\frac{1}{k}\left\{-\frac{\partial}{\partial\eta}\ln\det\Delta_0 + \frac{1}{2}\frac{\partial}{\partial\eta}\ln\det\Delta_1 - \frac{\mathbb{1}}{2}\frac{\partial}{\partial\eta}\ln\det\Delta_2\right\} \tag{6.11}$$

At this order in perturbation theory, it is possible to separate the pure gauge contribution $p_{1,0}(L/a)$, containing the ghost and gluonic operators, from the pure fermionic contribution $p_{1,1}(L/a)$, which will be proportional to the number of flavours in the theory. The one loop coupling decomposes into

$$p_1(L/a) = p_{1,0}(L/a) + N_f p_{1,1}(L/a). \tag{6.12}$$

The two contributions read

$$p_{1,0}(L/a) = \frac{1}{k}\left\{\frac{\partial}{\partial\eta}\ln\det\Delta_0 - \frac{1}{2}\frac{\partial}{\partial\eta}\ln\det\Delta_1\right\}_{\eta=\nu=0}, \tag{6.13}$$

$$p_{1,1}(L/a) = \frac{1}{2kN_f}\frac{\partial}{\partial\eta}\ln\det\Delta_2\Big|_{\eta=\nu=0}. \tag{6.14}$$

These coefficients will depend on the specific choice of background field used in the calculation.[3] The coefficient $p_{1,0}$ was computed in [50] for $SU(3)$ and in [23] for $SU(2)$. In both cases the background fields used were those in eqs.(4.29) and (4.30). The gauge coefficient $p_{1,0}$ is independent from the fermion regularization, so we don't need to recalculate it here. The calculation of $p_{1,1}$ was done in [80] in the standard SF setup. In section 6.3 we will adapt the arguments of [80] to the χSF setup and calculate $p_{1,1}$ for this case.

From Symanzik's analysis of cutoff effects (see eq.(4.121)), for $a/L \to 0$ the coeffi-

[3] We remark again that every choice of background field is a different choice of renormalization scheme.

cients $p_{1,x}$ have an asymptotic form

$$p_{1,x}(L/a) \sim \sum_{n=0}^{\infty}(r_{n,x} + s_{n,x}\ln(L/a))(a/L)^n, \qquad x = 0, 1. \tag{6.15}$$

the coefficients $r_{n,0}$ and $s_{n,0}$ denote the order n coefficients of the gauge contribution $p_{1,0}$, while $r_{n,1}$ and $s_{n,1}$ denote the order n coefficients of the fermionic contribution. The coefficient $r_{0,x}$ is the continuum value, which will depend on the details of the renormalization scheme. The term linear in a/L can be cancelled entirely by adjusting the coefficient c_t of the boundary gauge improvement counterterm. This will be done in section 6.3.3. The logarithmic divergences in the series come from the fact that the coefficient p_1 relates a bare coupling to a renormalized coupling in eq.(6.6). These divergencies can be cancelled by the renormalization of the bare coupling [23]. Their coefficients are given by $s_{0,x} = 2b_{0,x}$, where $b_{0,x}$ are the gluonic and fermionic contributions to the 1 loop coefficient of the beta function eq.(3.3). For QCD they read

$$b_0 = b_{0,0} + N_f b_{0,1}, \qquad b_{0,0} = \frac{11}{4\pi^2}, \qquad b_{0,1} = -\frac{2}{12\pi^2}. \tag{6.16}$$

The terms proportional to $(a/L)\ln(L/a)$ are entirely cancelled by the clover term by setting $c_{\rm SW}$ to the tree level value $c_{\rm SW}^{(0)} = 1$.

The computation of the 2 loop coefficient $p_2(L/a)$ is much more cumbersome and it is far beyond the scope of this thesis. The reason we present $p_2(L/a)$ here is because it will be needed for the discussions in section 6.4. The 2 loop coefficient gets contributions up to order N_f^2 [52],

$$p_2(L/a) = p_{2,0}(L/a) + N_f p_{2,1}(L/a) + N_f^2 p_{2,2}(L/a). \tag{6.17}$$

The computation of these coefficients requires the evaluation of 2 loop Feynman diagrams. The pure gauge coefficient $p_{2,0}$ was computed in [90] for $SU(3)$ and in [100] for $SU(2)$. The coefficients $p_{2,1}$ and $p_{2,2}$ where computed in [52].

At small coupling ($u = \overline{g}^2$), the step scaling function can be expanded in terms of the renormalised coupling u as

$$\sigma(u) = u + \sigma_1 u^2 + \sigma_2 u^3 + O(u^3), \tag{6.18}$$

with the 1 and 2 loop terms related to the 1 and 2 loop coefficients of the β-function

through

$$\begin{aligned}\sigma_1 &= 2b_0 \ln 2, \\ \sigma_2 &= (2b_0 \ln 2)^2 + 2b_1 \ln 2.\end{aligned} \tag{6.19}$$

The coefficients σ_0 and σ_1 of the step scaling function are thus scheme independent as well. The expansion of the lattice step scaling function is given by

$$\Sigma(u, a/L) = u + \Sigma_1(a/L)u^2 + \Sigma_2(a/L)u^3 + O(u^4) \tag{6.20}$$

with the first two coefficients given by

$$\begin{aligned}\Sigma_1(L/a) &= p_1(2L/a) - p_1(L/a), \\ \Sigma_2(L/a) &= p_2(2L/a) - p_2(L/a) - 2p_1(L/a)\left[p_1(2L/a) - p_1(L/a)\right].\end{aligned} \tag{6.21}$$

Finally, the cutoff effects eq.(6.5) can be expanded as well leading to

$$\delta(u, a/L) = \delta_1(a/L)u + \delta_2(a/L)u^2 + ..., \tag{6.22}$$

with the terms

$$\begin{aligned}\delta_1(a/L) &= \Sigma_1(a/L) - \sigma_1, \\ \delta_2(a/L) &= \Sigma_2(a/L) - \sigma_2 - \sigma_1\Sigma_1(a/L) + \sigma_1^2.\end{aligned} \tag{6.23}$$

6.2.1 Fixing θ

Recalling the spatial boundary conditions for the fermion fields eq.(4.36), we still have to choose a particular value for the angle θ. A natural option would be to choose $\theta = 0$, recovering periodic boundary conditions. This has been the choice for studying correlation functions in chapter 5.

Beyond esthetical criteria, we will follow here a more technical guideline principle established in [80]. We review this criteria here since it will be necessary again for the determination of θ for other fermionic representations in chapter 7.

In numerical simulations the efficiency of the inversion algorithms depends on the condition number, i.e. the ratio $\lambda_{\max}/\lambda_{\min}$ between the largest and smallest eigenvalues of the squared fermion matrix Δ_2. While $\lambda_{\min}$ strongly depends on θ, $\lambda_{\max}$ is rather insensitive to it. Hence, by choosing the angle θ such that $\lambda_{\min}$ is as large as possible the condition number is then minimised, optimising the performance of the

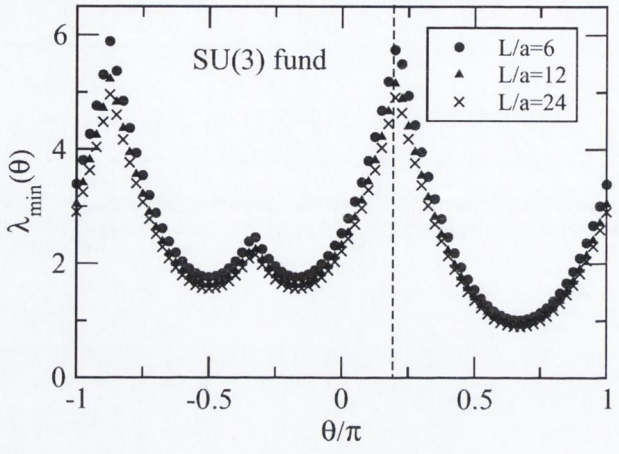

Figure 6.2.1: Lowest eigenvalue $\lambda_{\min}$ (in units of L^{-2}) as a function of θ for the fundamental representation of $SU(3)$. The vertical discontinuous line marks the chosen value $\theta = \pi/5$.

simulations at least close to the perturbative regime. Whenever more than one value of θ leads to a large $\lambda_{\min}$, we choose the value of θ closer to zero, to avoid possible cutoff effects induced by a large value of θ. The profile $\lambda_{\min}(\theta)$ depends on the chosen background field and the fermion representation considered. For QCD $\lambda_{\min}(\theta)$ is shown in fig.(6.2.1), from where we confirm the value $\theta = \pi/5$ given in [80]. We keep this value for the rest of the chapter.

We will come back to this argument when discussing the coupling beyond QCD in chapter 7.

6.3 The contribution from fermions in the χSF

In this section we focus on the fermionic contribution $p_{1,1}(L/a)$ to the one loop coupling in the χSF. This discussion follows very closely that found in Appendix A of [80]. There the coefficient $p_{1,1}(L/a)$ for the standard SF was calculated. We have recalculated it as well to compare with [80] and to have an idea about the quality of our numerical data compared to the known results.

Moreover, we study the sensitivity of the 1 loop SSF $\Sigma_{1,1}(L/a)$ to the parameters m_0 and z_f of the χSF. For this one has to consider the derivatives

$$\frac{\partial}{\partial m_0} p_{1,1}(L/a) \qquad \text{and} \qquad \frac{\partial}{\partial z_f} p_{1,1}(L/a), \tag{6.24}$$

which, as we will describe below, can be computed simultaneously to $p_{1,1}(L/a)$. Technical details concerning the present calculation are left for appendix C.

6.3.1 Determination of $p_{1,1}(L/a)$

The calculation of the contribution to the 1-loop coupling $p_{1,1}(L/a)$ due to fermions starts by inseting the operator Δ_2 given in eq.(6.10) into eq.(6.14), obtaining

$$p_{1,1}(L/a) = \frac{1}{kN_f}\frac{\partial}{\partial\eta}\ln\det\mathcal{D}_{5,1}\Big|_{\eta=\nu=0}, \tag{6.25}$$

where $\mathcal{D}_{5,1} = \gamma_5\tau_1\left(\mathcal{D}_W + \delta\mathcal{D}_W + m_0\right)$. The operator $\mathcal{D}_{5,1}$ is hermitean up to a flavour exchange, with real eigenvalues coming in pairs $\pm\sqrt{\lambda_n}$, where λ_n $(n = 0, 1, ..., n_{\max})$ are the eigenvalues of Δ_2.

For the computation of eq.(6.25) it is useful to consider the symmetry structure of the Hilbert space. This can be factorised in different sectors in terms of the symmetries of the eigenfunctions of $\mathcal{D}_{5,1}$. The Abelian background fields considered imply that $\mathcal{D}_{5,1}$ is diagonal in color space. Moreover, it is also diagonal in spatial momentum due to translation invariance in the spatial directions. The eigenfunctions of $\mathcal{D}_{5,1}$ are hence

$$\psi(x) = e^{ip_k x_k}u_{n_c}f(x_0), \tag{6.26}$$

where p_k are the momentum components in the spatial directions given by

$$p_k = (2\pi n_k + \theta)/L; \qquad k = 1, 2, 3, \tag{6.27}$$

and $\{u_{n_c}, n_c = 1, 2, 3\}$ is the canonical basis in color space.

The functions $f(x_0)$ are flavour doublets with spinor component. They depend on time and live in a subspace of fixed spatial momentum $\mathbf{p}$ and color n_c.

The structure of the eigenfunctions $\psi(x)$ permits to factorize the determinant of $\mathcal{D}_{5,1}$ into the product

$$\det\left(\mathcal{D}_{5,1}\right) = \prod_{n_c=1}^{3}\prod_{\mathbf{p}}\det\widetilde{\mathcal{D}}_{5,1}(n_c, \mathbf{p}), \tag{6.28}$$

where $\widetilde{\mathcal{D}}_{5,1}(n_c, \mathbf{p})$ is the reduced Dirac operator which acts on the functions $f(x_0)$ at

fixed color n_c and momenta $\mathbf{p}$. Thus, eq.(6.25) decomposes into the evaluation of $p_{1,1}$ in the different color and momentum sectors,

$$p_{1,1}(L/a) = \frac{1}{kN_f}\sum_{n_c=1}^{3}\sum_{\mathbf{p}}\frac{\partial}{\partial\eta}\ln\det\widetilde{\mathcal{D}}_{5,1}(n_c,\mathbf{p})\Big|_{\eta=0} = \sum_{n_c=1}^{3}\sum_{\mathbf{p}} p_{1,1}(L/a)|_{n_c,\mathbf{p}}\,. \quad (6.29)$$

The computation of $\det\widetilde{\mathcal{D}}_{5,1}$ can be done following the recursive technique introduced in appendix C of [23] for quadratic operators and extended to linear operators in [80], which we review in appendix C adapting it to the present setup.[4]

We have written a code for the calculation of $p_{1,1}(L/a)$ to 128-bits of precision. For checking that the results are correct, a second independent code has been used for comparison on the smaller lattices. Results agree up to machine precision.[5] In tables E.3.3 and E.3.8 of appendix E, we present the results obtained for $p_{1,1}(L/a)$, calculated on lattices in the range $L \in [6, 64]$, with $\theta = \pi/5$, and for the two choices $c_{\rm SW} = 0, 1$ respectively.

In the approach to the continuum limit ($L/a \to \infty$) we expect $p_{1,1}(L/a)$ to follow the asymptotic form given by eq.(6.15). We can extract the first coefficients of the series following the method described in [49]. For that, we have prepared our own analysis code written in Mathematica. In Table (6.3.1) we show the results for the extracted coefficients in both the SF and χSF setups. We include the results for the standard SF for comparison with the literature [80].

The coefficient $s_{0,1}$ of the logarithmically divergent term is universal and should be exactly given by[6]

$$s_{0,1} = 2b_{0,1} = -\frac{1}{12\pi^2}. \quad (6.30)$$

We find agreement with our numerical data up to 6 decimal digits. The coefficient $s_{1,1}$ must be zero in absence of $O(a)$ effects in the bulk. We confirm this result for the χSF for both $c_{\rm SW} = 0, 1$, up to 5 decimal digits, which shows that bulk $O(a)$ effects are absent independently from the value of $c_{\rm SW}$.[7] This confirms again that automatic $O(a)$ improvement is at work. To extract $r_{0,1}$ and $r_{1,1}$ we assume the exact value for

[4]Note that for the standard SF the computation of $p_{1,1}$ can be done for a single flavour [80]. In the preent case, however, the flavour structure has to be taken into account when evaluating eq.(6.29).

[5]The calculations for the cross check of the results have been done at double precision only.

[6]Note that when considering other fermion representations this coefficient will vary.

[7]The clover term will affect physical obervables with effects starting at $O(a^2)$.

$s_{0,1}$ from eq.(6.30) and $s_{1,1} = 0$. The continuum value $r_{0,1}$ is identical in the SF and χSF, which is a further test of the universality of both setups in the continuum limit. The value $r_{1,1}$ is the coefficient of the $O(a)$ effects coming from the boundaries, which will be removed by tuning $c_t^{(1,1)}$ in the following section.

	$r_{0,1}$	$s_{0,1}$	$r_{1,1}$	$s_{1,1}$
χSF, $c_{\rm SW} = 0$	$-0.00986816(1)$	$-0.0084434(1)$	$-0.0132289(4)$	$0.0000(1)$
χSF, $c_{\rm SW} = 1$	$-0.03466492(1)$	$-0.008443(1)$	$0.013776(3)$	$0.000001(1)$
SF, $c_{\rm SW} = 0$	$-0.00986822(3)$	$-0.0084434(2)$	$0.0328605(3)$	$0.02533(1)$
SF, $c_{\rm SW} = 1$	$-0.034664940(1)$	$-0.0084436(2)$	$0.038282(2)$	$0.00001(1)$

Table 6.3.1: Asymptotic expansion coefficients of $p_{1,1}(L/a)$ for the χSF and SF, calculated at $\theta = \pi/2$, for $c_{\rm SW} = 0, 1$.

The SF and χSF schemes are equivalent in the continuum and chiral limit. It is not a surprise then that the 1-loop coefficient $p_{1,1}(L/a)$ extrapolates to the same continuum value $r_{0,1}$ for both schemes. This will be true also for the higher order coefficients of the renormalized coupling. Hence, the relation between the χSF scheme and the $\overline{\rm MS}$ scheme will be the same as between the SF and the $\overline{\rm MS}$. In particular, when the 2 couplings are related through an expression like eq.(3.11), the coefficients of the relation will be exactly those already known for the standard SF. Hence, the ratio between $\Lambda_{\rm QCD}$ parameters in the χSF and the $\overline{\rm MS}$ is also already known.

6.3.2 Sensitivity of the coupling to z_f and m_0

Ideally, in a non-perturbative calculation of the step scaling function Σ, we want to fix the bare parameters to their critical values. The bare mass m_0 is fixed to the critical mass m_c so that $m_{\rm PCAC} = 0$. The renormalization coefficient z_f is fixed to its critical value such that an odd-correlation function vanishes (for example $g_p^{uu'} = 0$). Finally, the physical scale of the system is fixed by demanding $u =$ constant, which is called a *condition of constant physics*. In practice, however, there will always be uncertainties in the conditions to determine m_c, z_f and u, which will subsequently induce uncertainties to the step scaling function $\Delta\Sigma$ given by

$$\Delta\Sigma = \Delta u \frac{\partial \Sigma}{\partial u} + \Delta z \frac{\partial \Sigma}{\partial z} + \Delta z_f \frac{\partial \Sigma}{\partial z_f}, \tag{6.31}$$

where we define the dimensionless parameter $z = m_0 L$. It is important to know how precisely the bare coefficients have to be tuned in order not to induce intolerable uncertainties in $\Delta\Sigma$. In the following analysis we will consider only the sensitivity to m_0 and z_f. We therefore ignore the term $\Delta u \frac{\partial \Sigma}{\partial u}$. The estimation presented here is done for $c_{\mathrm{SW}} = 1$.

Since the tuning of m_0 and z_f is done by solving simultaneously two conditions which depend on both m_0 and z_f, the uncertainties Δz_f and Δz will be interrelated. We define $\Delta X^{(X)}$ to be the intrinsic uncertainty in the quantity X due to the limited precision achieved for the condition which determines X. Moreover, we define $\Delta X^{(Y)}$ to be the uncertainty in the quantity X induced by an uncertainty in determining the condition which fixes Y. The uncertainties Δz and Δz_f will then be given by

$$\begin{aligned} \Delta z &= \Delta z^{(z)} + \Delta z^{(z_f)} = \Delta z^{(z)} + \Delta z_f^{(z_f)} \frac{dz}{dz_f}; \\ \Delta z_f &= \Delta z_f^{(z_f)} + \Delta z_f^{(z)} = \Delta z_f^{(z_f)} + \Delta z^{(z)} \frac{dz_f}{dz}; \end{aligned} \tag{6.32}$$

We calculate the cross derivatives $\frac{dz}{dz_f}$ and $\frac{dz_f}{dz}$ evaluated at the asymptotic values $m_0 = 0$ and $z_f = 1$ simply by taking finite differences such that

$$\frac{dX}{dY} \approx \frac{X(Y+\epsilon) - X(Y-\epsilon)}{2\epsilon}. \tag{6.33}$$

We do this for a sequence of decreasing ϵ and extrapolate the results for $\epsilon \to 0$. From these, by taking the continuum extrapolation $a/L \to 0$, it can be seen that

$$\frac{dz}{dz_f} = 0.0000001(2), \qquad \text{and} \qquad \frac{dz_f}{dz} = -0.29826(2). \tag{6.34}$$

It is clear here that the dependence on z_f in the determination of m_0 is a pure lattice artefact, while the determination of z_f does in fact depend on m_0. This is in agreement with the results obtained in section 5.4.1 for the tuning of z_f and m_0.

Next, we need to evaluate the sensitivity of the fermionic part of the step scaling function $\Sigma_{1,1}$ to the parameters z and z_f. This is given by

$$\begin{aligned} \frac{\partial}{\partial z_f} \Sigma_{1,1}(L/a) &= \frac{\partial}{\partial z_f} p_{1,1}(2L/a) - \frac{\partial}{\partial z_f} p_{1,1}(L/a); \\ \frac{\partial}{\partial z} \Sigma_{1,1}(L/a) &= \frac{\partial}{\partial z} p_{1,1}(2L/a) - \frac{\partial}{\partial z} p_{1,1}(L/a). \end{aligned} \tag{6.35}$$

The calculation of the derivatives of the one loop coupling $\partial_X p_{1,1}$ with respect to a parameter X can be done in parallel to the evaluation of $p_{1,1}$. Details on how to perform this calculation can be found in appendix C.

We find that both terms are pure cutoff effects with leading coefficients given by

$$\begin{aligned} \frac{\partial}{\partial z_f}\Sigma_{1,1} &= 0.0057993(8)\left(\frac{a}{L}\right) + O(a^2), \\ \frac{\partial}{\partial z}\Sigma_{1,1} &= 0.012003(1)\left(\frac{a}{L}\right) + O(a^2), \end{aligned} \tag{6.36}$$

These quantities are small already for the smallest lattices considered. Thus, since the derivatives are $|dz/dz_f| < 1$ and $|dz_f/dz| < 1$ always, we can safely consider that the dominant contribution to the uncertainties eq.(6.32) will be given directly by the intrinsic uncertainties in the determination of the parameters z and z_f

$$\Delta z \simeq \Delta z^{(z)}, \qquad \Delta z_f \simeq \Delta z_f^{(z_f)}. \tag{6.37}$$

Finally, the typical precision achieved in Monte Carlo simulations is $\Delta(\overline{g}^{-2}) = 0.003$ (see [27]). This means that we can tolerate ambiguities of

$$\Delta z < \frac{0.25}{N_f}, \qquad \text{and} \qquad \Delta z_f < \frac{0.52}{N_f}, \tag{6.38}$$

without compromising the evaluation of Σ. This is a quite tolerant range, comparable to the acceptable range in z observed for the standard SF [27].

6.3.3 Determination of $c_t^{(1,1)}$

With the knowledge of the asymptotic coefficients of $p_{1,1}$ it is now possible to determine the fermionic contribution to the gauge boundary improvement coefficient $c_t^{(1,1)}$.

Following the discussion in section 4.4, one can see that in presence of the boundary counterterm $\delta S_{\mathrm{G,b}}$, the effective action gets an extra contribution. The one loop expansion will then read

$$\Gamma_1[B] = -\ln\det\Delta_0 + \frac{1}{2}\ln\det\Delta_1 - \frac{1}{2}\ln\det\Delta_2 + c_t^{(1)}\frac{\partial\Gamma_0[B]}{\partial c_t}. \tag{6.39}$$

When introducing this into the definition eq.(6.7), one can see that the boundary counterterm contributes to the coupling $\overline{g}^2$ to one loop as

$$\overline{g}^2 = g_0^2 + g_0^4 \left(p_1(L/a) - c_t^{(1)} \frac{[\partial^2 \Gamma_0[B]/\partial\eta\partial c_t]_{\eta=0}}{[\partial\Gamma_0[B]/\partial\eta]_{\eta=0}} \right) + O(g_0^6). \tag{6.40}$$

The second derivative in the contribution of the boundary counterterm is calculated from eq.(4.61). From there, one obtains the simple relation

$$\frac{\partial^2}{\partial\eta\partial c_t}\Gamma_0[B] = \frac{2a}{L}\frac{\partial}{\partial\eta}\Gamma_0[B]. \tag{6.41}$$

The derivative of the tree-level effective action cancels out, leaving only a contribution proportional to a. It is then clear that the boundary counterterm at one loop contributes to the coupling $\overline{g}^2$ as

$$\overline{g}^2 = g_0^2 + g_0^4 \left(p_1(L/a) - c_t^{(1)} \frac{2a}{L} \right) + O(g_0^6), \tag{6.42}$$

The terms of $p_1(L/a)$ linear on a can be removed by adjusting $c_t^{(1)}$. This is achieved by setting

$$c_t^{(1)} = \frac{r_1}{2}. \tag{6.43}$$

The pure gauge and fermionic contributions can be separated into $c_t^{(1)} = c_t^{(1,0)} + N_f c_t^{(1,1)}$, from where we obtain the fermionic term

$$c_t^{(1,1)} = \begin{cases} -0.00661445(5), & \chi\text{SF}\ , c_{\text{SW}} = 0, \\ 0.006888(3), & \chi\text{SF}\ , c_{\text{SW}} = 1, \\ 0.0191405(2), & \text{SF}\ , c_{\text{SW}} = 1. \end{cases} \tag{6.44}$$

The values of $c_t^{(1,1)}$ for the χSF have been calculated here for the first time, and have been presented in [101, 102]. The value for the SF is in agreement with the value $c_t^{(1,1)}$ given in [80]. The value of the gauge part $c_t^{(1,0)} = -0.8900(5)$ is known from ref [23].

6.3.4 Lattice artefacts in the SSF at one loop

We now discuss the size of the lattice artefacts in the fermionic countribution to the step scaling function $\Sigma_{1,1}(L/a)$ before and after setting $c_t^{(1,1)}$ to its correct value. We have seen that by properly tuning c_t, the $O(a)$ lattice artefacts can be removed at one loop in perturbation theory. Nevertheless, cutoff effects of higher order in a are still present and must be quantified. For the discussion of this subsection we define the relative deviations of the SSF from its pure gauge and pure fermionic continuum coefficients as

$$\delta_{1,0}(a/L) = \frac{\Sigma_{1,0}(L/a) - \sigma_{1,0}}{\sigma_{1,0}}, \qquad \delta_{1,1}(a/L) = \frac{\Sigma_{1,1}(L/a) - \sigma_{1,1}}{\sigma_{1,1}}. \tag{6.45}$$

Note that these are normalized to the pure gauge coefficient $\sigma_{1,0}$ and pure fermionic coefficient $\sigma_{1,1}$ respectively, which is not the same normalization given in eq.(6.22) (the latter is more common in the literature). We choose to use the normalization in eq.(6.45) for studying the cutoff effects due to the individual fermion contribution $p_{1,1}$ in both the standard SF and χSF setups. This will be very useful as well in chapter 7, when considering cutoff effects due to fermions transforming under different representations of the gauge group.

In fig.(6.3.1) we show the cutoff effects $\delta_{1,1}(a/L)$ for both the χSF and SF at different levels of improvement. For the χSF (fig.(6.3.1), top panel), the cutoff effects behave asymptotically as $O(a^2)$ once $c_t^{(1,1)}$ is fixed to the value given in eq.(6.44). It is surprising, however, that after implementing the improvement at the boundaries the remaining cutoff effects are so similar for both choices $c_{\rm SW} = 0$ and $c_{\rm SW} = 1$. A variation of $c_{\rm SW}$ induces differences of $O(a^2)$ in physical observables so, a priori, there is no need to expect that the remaining cutoff effects after boundary improvement behave the same way for different $c_{\rm SW}$, as can be seen in fig.(6.3.1). For the standard SF (fig.(6.3.1) bottom panel), cutoff effects are essentially zero after improvement is implemented in the bulk and in the boundaries. The smallness of the remaining cutoff effects is likely to be a kinematic accident for this particular choice of background field and parameters. A remarkable point is the large size of the lattice artefacts cancelled by both $c_{\rm SW}$ and $c_t^{(1,1)}$ for the standard SF and by $c_t^{(1,1)}$ for the χSF.

To conclude this section, we remark that knowing the values of the residual cutoff effects at a specific order in perturbation theory, it is possible to remove from a

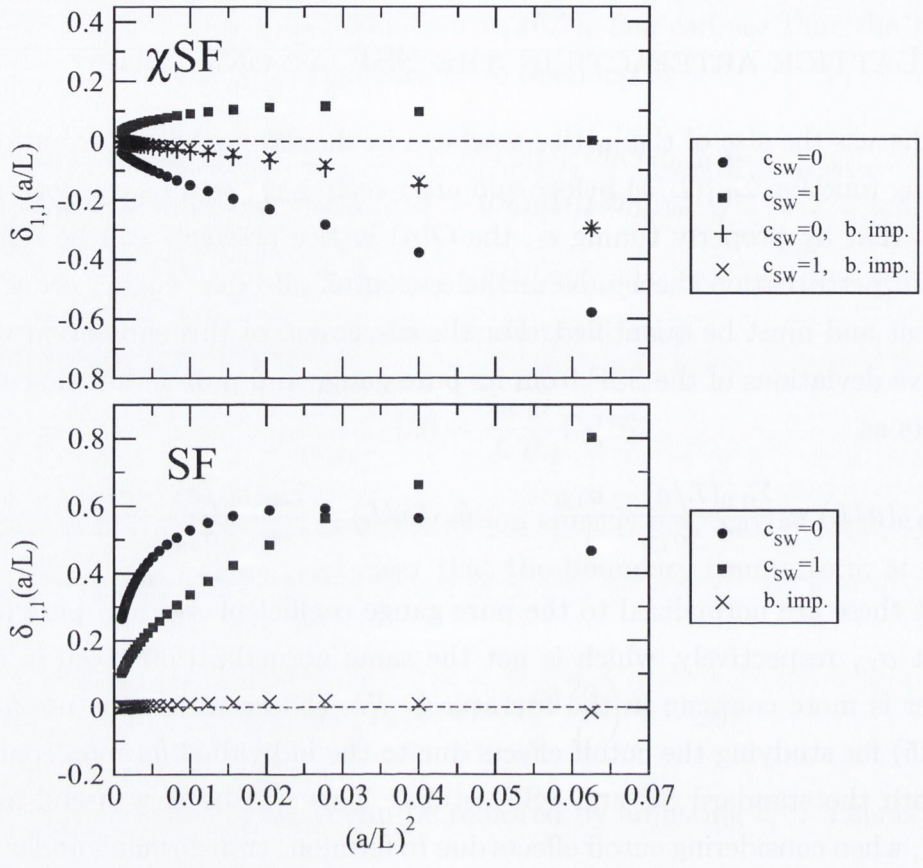

Figure 6.3.1: Cutoff effects $\delta_{1,1}$ of the fermionic part of the one loop SSF for the χSF (top panel) and the standard SF (bottom panel). For the χSF we show the results with and without clover coefficient. The legend "b. imp." denotes the situations where boundary improvement has been implemented, i.e. $c_t^{(1,1)}$ has been set to the values given in eq.(6.44).

non-perturbative quantity all the remaining lattice artefacts at that order in g_0[50].

6.4 The SF$_\nu$ and χSF$_\nu$ schemes

In this section we are going to re-examine the definition of the running coupling given in eq.(6.1) to construct a family of renormalization schemes in the SF and χSF setups. They will be called, respectively, the SF$_\nu$ and χSF$_\nu$ schemes. Part of the discussion in the present section relies on already published data which can be taken from the literature. When published data is used the appropriate references will be given.

In order to define a running coupling in $SU(3)$ one takes derivatives of the effective action Γ respect to the parameter η appearing in the boundary phases ϕ_i and ϕ'_i of

the Abelian BF defined in eq.(4.30).

In $SU(3)$ another renormalized observable $\overline{v}$ can be defined [50] as

$$\overline{v}(L) = \frac{1}{k}\frac{\partial}{\partial\nu}\left\{\left.\frac{\partial\Gamma}{\partial\eta}\right|_{\eta=0}\right\}\Bigg|_{\nu=0}. \tag{6.46}$$

This can be combined with the coupling $\overline{g}^2$ to obtain a family of renormalized couplings given by

$$\frac{1}{\overline{g}^2_\nu(L)} = \frac{1}{\overline{g}^2(L)} - \nu\overline{v}(L). \tag{6.47}$$

parametrised by the real number ν.

The dependence of Γ' on the parameter ν is linear, and hence both $\overline{g}^2$ and $\overline{v}$ are ν-independent. Moreover, the observable $\overline{v}$ vanishes at tree level. The couplings in the family $\overline{g}^2_\nu$ are thus proper definitions of renormalized couplings since at tree level they will be equal to the bare coupling g_0^2.

The family of couplings $\overline{g}^2_\nu$ can be understood from a geometric point of view in the following way. The boundary fields C and C' (see eq.(4.24)) can be written in a more intuitive form by separating all η-dependence in the boundary phases eq.(4.30), obtaining[8]

$$C_k = \frac{i}{L}\mathrm{diag}\,(\phi_1,\phi_2,\phi_3) + \frac{i}{L}\eta\frac{\sqrt{3}}{2}\widetilde{\lambda}_8, \tag{6.48}$$

$$C'_k = \frac{i}{L}\mathrm{diag}\,(\phi'_1,\phi'_2,\phi'_3) - \frac{i}{L}\eta\frac{\sqrt{3}}{2}\widetilde{\lambda}_8, \tag{6.49}$$

where now the boundary phases are given by

$$\phi = (-\pi/3, 0, \pi/3), \qquad \text{and} \qquad \phi' = (-\pi, \pi/3, 2\pi/3), \tag{6.50}$$

which do not depend on η. Writing apart the η dependence permits to understand the term proportional to η as a deformation of the background field in the direction of the algebra $su(3)$ given by the generator $\widetilde{\lambda}_8$.[9] This deformation is used to define the renormalised coupling eq.(6.1) and it is fixed to zero after differentiation. The

[8]The matrices $\widetilde{\lambda}_8$ and $\widetilde{\lambda}_3$ are a permutation of the diagonal components of the standard abelian Gell-Mann matrices. They are defined in appendix A.3 as $\widetilde{\lambda}_8 = 1/\sqrt{3}\mathrm{diag}(2,-1,-1)$ and $\widetilde{\lambda}_3 = \mathrm{diag}(0,1,-1)$.

[9]See appendix A.3 for the explicit form of the generators of SU(3).

coupling $\overline{g}^2$ can then be understood as a response of the system to a deformation of the background field in the Abelian direction given by $\widetilde{\lambda}_8$. In this context one could consider deformations of the background field in any Abelian direction, which for $SU(3)$ will be given by a linear combination of the generators $\widetilde{\lambda}_8$ and $\widetilde{\lambda}_3$. This accounts for replacing in eq.(6.49)

$$\eta \frac{\sqrt{3}}{2}\widetilde{\lambda}_8 \longrightarrow \eta \left(\frac{\sqrt{3}}{2}\widetilde{\lambda}_8 + \nu \widetilde{\lambda}_3 \right). \tag{6.51}$$

By adjusting the parameter ν, different directions in the Abelian subspace of $su(3)$ are considered when taking derivatives respect to η. Since after differentiation η is fixed to 0, the modification eq.(6.51) only plays a role at the level of defining the renormalized coupling, and does not affect the background field at all.

The two observables $\overline{g}^2$ and $\overline{v}$ can hence be regarded as the response of the system to deformations of the background field along the directions given by $\widetilde{\lambda}_8$ and $\widetilde{\lambda}_3$ respectively. These can be combined to form the family $\overline{g}^2_\nu$, which will be the response of the system to a deformation in an arbitrary direction within the abelian part of $su(3)$, parameterised by ν. The advantage of this is that both observables $\overline{g}^2$ and $\overline{v}$, and thus the whole family $\overline{g}^2_\nu$, can be obtained in a single numerical simulation. The parameter ν can be changed at no extra cost when analysing numerical data.

As we will see in section 6.4.2, cutoff effects on the SSF are strongly influenced by the choice of ν. Cutoff effects turn out to be minimised for a particular choice of ν which depends on the regularization being used.

The renormalized observable $\overline{v}$ is a pure quantum effect. In numerical simulations the signal for $\overline{v}$ is poorer than the signal for $1/\overline{g}^2$, but it is not clear a priori how the resulting $1/\overline{g}^2_\nu$ will behave. A systematic study of the quality of the signal as a function of ν is currently on the way [103]. In practice, there will be a balance to strike between the size of the cutoff effects and the size of the statistical fluctuations on $\overline{g}^2_\nu$.

By considering a coupling constant defined through eq.(6.47) instead of the standard coupling eq.(6.1), one obtains a family of renormalization schemes which we denote as SF_ν and $\chi\mathrm{SF}_\nu$ schemes. The SF_ν and $\chi\mathrm{SF}_\nu$ schemes, taken at the same value of ν, are equivalent in the chiral and continuum limits. They will be particularly useful in chapter 7 when considering couplings in theories with fermions in representations others than the fundamental. Note that when considering the gauge group

$SU(2)$, since the only Abelian direction in the algebra is that given by τ^3, schemes like SF_ν and $\chi\mathrm{SF}_\nu$ cannot be defined. Moreover, for gauge groups with $N > 3$, a family of observables $\overline{v}_i$ could be defined, with i being every extra Abelian direction in $su(N)$. Hence, generalized SF_ν and $\chi\mathrm{SF}_\nu$ schemes could be obtained by defining a further family of couplings given by

$$\frac{1}{\overline{G}^2_{\mathrm{N}}(L)} = \frac{1}{\overline{g}^2(L)} - \sum_{i=1}^{R(N)-1} \nu_i \overline{v}_i(L). \tag{6.52}$$

parametrized by the set of parameters ν_i, where $R(N)$ is the rank of $SU(N)$, such that $R(N) - 1$ corresponds to the number of extra abelian directions one can consider.[10]

6.4.1 Expansion of $\overline{g}^2_\nu$

In this subsection we expand the couplings $\overline{g}^2_\nu$ to 2 loops in perturbation theory. We will use the results here to compute the dependence of the cutoff effects on ν in both the $\chi\mathrm{SF}_\nu$ and SF_ν schemes. For the SF_ν, we will use the results in the literature to reconstruct the cutoff effects to 2 loops and obtain the three loop beta function.

The observable $\overline{v}(L/a)$ can be expanded in terms of the bare coupling g_0^2 [104]

$$\overline{v}(L/a) = v_1(L/a) + g_0^2 v_2(L/a) + O(g_0^4). \tag{6.53}$$

The coefficients of the expansion receive pure gauge, pure fermionic and a mixed contribution

$$\begin{aligned} v_1(L/a) &= v_{10}(L/a) + N_f v_{11}(L/a), \\ v_2(L/a) &= v_{20}(L/a) + N_f v_{21}(L/a) + N_f^2 v_{22}(L/a), \end{aligned} \tag{6.54}$$

with the continuum values for these coefficients (for $c_{\mathrm{SW}} = 1$) given by [27, 50, 80]

$$\begin{aligned} &\lim_{a/L\to 0} v_1(a/L) = v_1 = 0.0694603(1) + 0.0245370(1) N_f, \\ &\lim_{a/L\to 0} v_2(a/L) = v_2 = -0.001364(14) - 0.000101(17) N_f - 0.0003362(30) N_f^2. \end{aligned} \tag{6.55}$$

Note that the continuum values in eq.(6.55) are the same for the SF and the χSF.

[10] For $SU(N)$ the rank is $R(N) = N - 1$, corresponding to the total nuber of abelian directions. Hence, appart from the standard abelian direction in the definition of $\overline{g}^2$, there will be $R(N) - 1$ extra directions to consider in eq.(6.52).

The couplings $\overline{g}^2_\nu$ are expanded in terms of the bare coupling g_0^2 as

$$\overline{g}^2_\nu(L) = g_0^2 + p_1^\nu(L/a)g_0^4 + p_2^\nu(L/a)g_0^6 + O(g_0^8) \tag{6.56}$$

with the 1 and 2 loop coefficients given by

$$\begin{aligned} p_1^\nu(L/a) &= p_1(L/a) + \nu v_1(L/a), \\ p_2^\nu(L/a) &= p_2(L/a) + \nu v_2(L/a) + 2\nu p_1(L/a)v_1(L/a) + \nu^2 v_1^2(L/a). \end{aligned} \tag{6.57}$$

In this subsection we are interested in determining the approach towards the continuum limit of $p_1^\nu(L/a)$ as a function of ν in both the SF and χSF setups. For this, since we already know $p_1(L/a)$ from section 6.3, we only need to determine $v_1(L/a)$. Rather than using the explicit definition eq.(6.46), we can take advantage of the fact that eq.(6.47) is linear in ν and extract $\overline{v}$ from the finite difference

$$\overline{v}(L) = \frac{1}{k(\nu_2 - \nu_1)} \left[\left. \frac{\partial \Gamma[B]}{\partial \eta} \right|_{\eta=0,\nu_1} - \left. \frac{\partial \Gamma[B]}{\partial \eta} \right|_{\eta=0,\nu_2} \right]. \tag{6.58}$$

A comfortable choice of values for ν is to set $\nu_1 = 0$ and $\nu_2 = 1$ for which the 1-loop coefficient v_1 reads

$$v_1(L/a) = p_1^{\nu=1}(L/a) - p_1(L/a). \tag{6.59}$$

The coefficient $v_1(a/L)$ is automatically finite in the limit $a/L \to 0$, since the (universal) logarithmic divergences cancel when taking the difference in eq.(6.59). Moreover, since the contribution of the boundary counterterm proportional to c_t is independent of ν, it will not contribute to $v_1(L/a)$.

From the series $v_1(a/L)$ calculated using both χSF and SF we extract the continuum value

$$v_{1,1} = 0.0245370(1), \tag{6.60}$$

in complete agreement with the result in eq.(6.55) known from [80]. The continuum 1-loop coefficient p_1^ν of the coupling $\overline{g}^2_\nu$ in the SF$_\nu$ scheme (with $c_{\rm SW} = 1$ and $\theta = \pi/5$) is obtained simply by considering in eq.(6.57) the pure fermionic and pure gluonic contributions to p_1 and v_1, such that

$$\begin{aligned} p_{1,1}^\nu &= -0.034664940(1) + \nu \times 0.0245370(1), \\ p_{1,0}^\nu &= 0.0368283(1) + \nu \times 0.00694603(1). \end{aligned} \tag{6.61}$$

The data for the pure gauge part $p^\nu_{1,0}$ is taken from [104].

6.4.2 Cutoff effects in the SF_ν and χSF_ν schemes

In this subsection we calculate the residual cutoff effects on the SSF at 1-loop as a function of ν.

The step scaling function associated to the coupling $\overline{g}^2_\nu$ is defined as in eq.(3.25) through

$$\Sigma^\nu(u, a/L) \equiv \overline{g}^2_\nu(2L)\big|_{u=\overline{g}^2_\nu(L)} . \tag{6.62}$$

This SSF is expanded as a series of the renormalized coupling $u = \overline{g}^2_\nu(L)$ (not $\overline{g}^2(L)$), which reads

$$\Sigma^\nu(u, a/L) = u + \Sigma^\nu_1(a/L)u^2 + \Sigma^\nu_2(a/L)u^3 + O(u^4), \tag{6.63}$$

with the first 2 coefficients given by

$$\begin{aligned} \Sigma^\nu_1(L/a) &= p^\nu_1(2L/a) - p^\nu_1(L/a), \\ \Sigma^\nu_2(L/a) &= p^\nu_2(2L/a) - p^\nu_2(L/a) - 2p^\nu_1(L/a)\left\{p^\nu_1(2L/a) - p^\nu_1(L/a)\right\}. \end{aligned} \tag{6.64}$$

The continuum limit of Σ^ν defines the step scaling function σ^ν as

$$\sigma^\nu(u) \equiv \lim_{a/L\to 0} \Sigma^\nu(u, a/L). \tag{6.65}$$

Note that the 1 and 2 loop coefficients of $\sigma(u)$ only depend on the 1 and 2 loop coefficients of the β function, which are universal quantities. This means that for different values of ν, the quantities Σ^ν_1 and Σ^ν_2 will approach the same continuum value given by σ_0 and σ_1. The approach to σ_0 and σ_1 will however depend on ν. One can hence scan a range in ν seeking for a window in which the continuum values are reached as fast as possible.

The convergence to a universal value will not be true beyond 2-loops, where for every value of ν one would approach a continuum value which is as well a function of ν. In fact, in subsection 6.4.5 we will calculate the values for the 3-loop beta function with its explicit dependence on ν. However, one can still use the minimisation of the 1 and 2-loop cutoff effects as a criterion for choosing a preferred ν.

We define the relative cutoff effects as a function of ν of the pure fermionic and

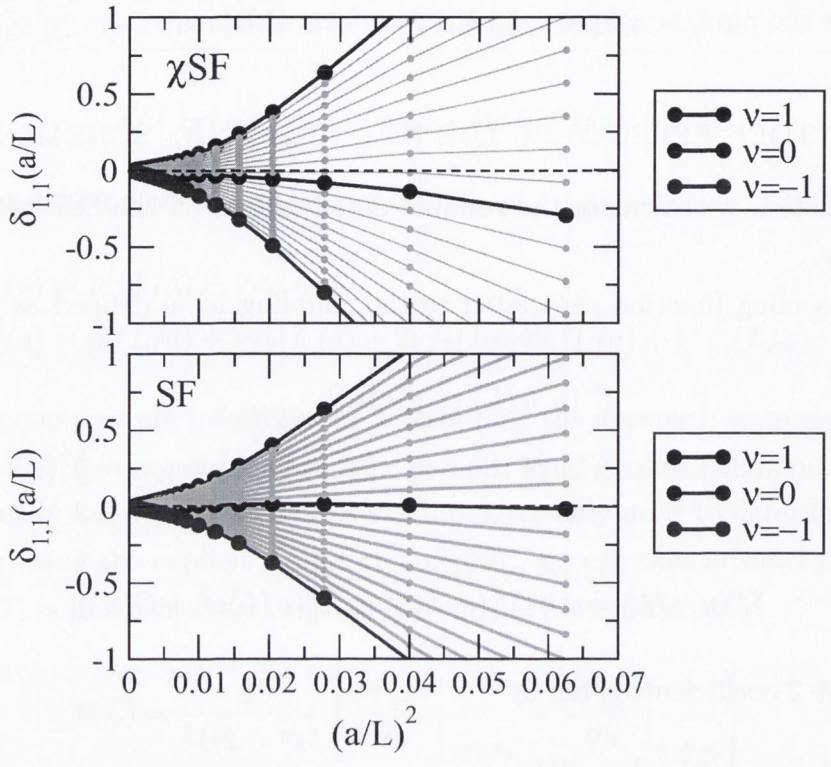

Figure 6.4.1: Cutoff effects $\delta^{\nu}_{1,1}$ of the fermionic part of the one loop SSF for the χSF (top panel) and the standard SF (bottom panel) setups, in the window $\nu \in [-1, 1]$. Orange lines are separated by steps of equal size $\Delta\nu = 0.1$. In both cases, boundary $O(a)$ improvement has been implemented and $c_{\rm SW} = 1$. Black lines ($\nu = 0$) correspond to the values shown in fig.(6.3.1).

pure gauge parts of the 1-loop SSF as in eq.(6.45) such that they are respectively normalized to the pure gauge and pure fermionic continuum SSF,

$$\delta^{\nu}_{1,0}(a/L) = \frac{\Sigma^{\nu}_{1,0}(a/L) - \sigma_{1,0}}{\sigma_{1,0}}, \qquad \delta^{\nu}_{1,1}(a/L) = \frac{\Sigma^{\nu}_{1,1}(a/L) - \sigma_{1,1}}{\sigma_{1,1}}. \tag{6.66}$$

The effects $\delta^{\nu}_{1,1}$ due to fermions are shown in figure (6.4.1) for the χSF_{ν} (top panel) and for the SF_{ν} (bottom panel). In both cases we see a very strong dependence of the cutoff effects on the parameter ν. There is always an optimal value of ν for which the cutoff effects are minimal even for the smallest lattices. The optimal value of ν is however not universal and depends on the regularization considered. For the χSF a value of $\nu \sim 0.1$ seems to be the optimal one, although cutoff effects are reasonably small already for $\nu = 0$. For the standard SF the choice $\nu = 0$ is clearly the optimal from the very beginning.

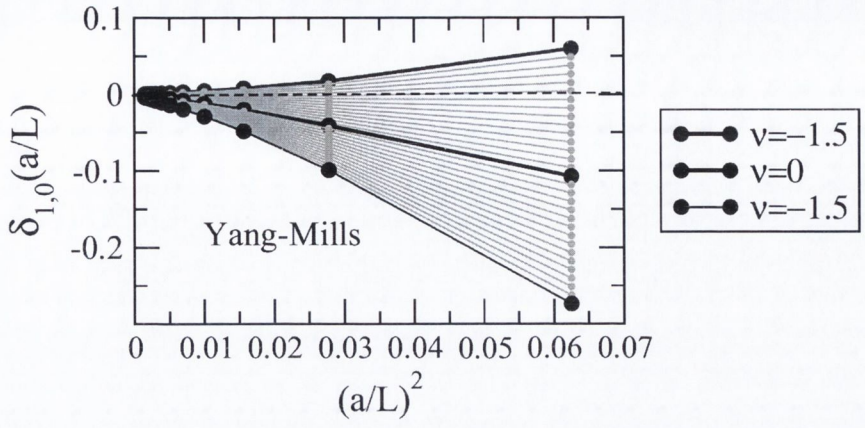

Figure 6.4.2: Cutoff effects $\delta^\nu_{1,0}$ of the pure Yang-Mills part of the one loop SSF in the window $\nu \in [-1, 5, 1.5]$. Orange lines are separated by steps of equal size $\Delta\nu = 0.1$. Boundary $O(a)$ improvement has been implemented.

At this stage one might wonder whether it is useful or not to consider these alternative schemes with different values of ν, since the cutoff effects in both regularizations are small for the standard coupling $\overline{g}^2$ at $\nu = 0$. The case of $SU(3)$ with fundamental fermions is particularly well behaved in the χSF and SF regularizations. A similar study with staggered fermions [103], however, shows the presence of much larger cutoff effects which can be dramatically reduced by going to larger values of ν. In chapter 7 we will see that when considering fermions in representations other than the fundamental, the residual cutoff effects in the SSF after implementing $O(a)$ improvement are in fact huge until an intolerable level. It is within these situations where the χSF_ν and SF_ν schemes are very promising tools since they allow a reduction of cutoff effects .

Another example are the cutoff effects of the pure Yang-Mills theory $\delta^\nu_{1,0}$ shown in figure (6.4.2). In this situation it is clear that the choice $\nu = 0$ is by far not the optimal choice concerning the reduction of lattice artefacts. However, these are very small from the starting point,[11] such that using different values of ν might be contraproductive. We remark again that one has to find a balance between the suppression of cutoff effects and the preservation of a good signal when computing observables numerically in simulations.

[11] At the 10% level for lattices $L/a = 4$, and already below the 5% level for lattices $L/a = 6$.

6.4.3 2 LOOP CUTOFF EFFECTS

A natural question to address is whether the picture presented in the previous section remains valid beyond 1 loop or is simply a consequence of a fortunate interplay between the cutoff effects in the 1 loop functions $p_1(L/a)$ and $v_1(L/a)$.

Without engaging into the involved details of a 2-loop calculation, we can use the data already available in the literature to reconstruct the 2-loop cutoff effects on the SSF and their dependence on the parameter ν.

The 2 loop coefficients in the expansions for $\overline{g}^2_\nu$ and Σ^ν are given in eq.(6.56) and eq.(6.63) respectively.

In the following we will extract the cutoff effects on Σ^ν at 2-loop order. At this order, Σ^ν_2 receives mixed contributions due to fermionic and gluonic loops. A separation of cutoff effects with the normalisations of eq.(6.45) is then not useful. Thus, we will consider directly the cutoff effects normalized to the full continuum SSF eq.(6.5), such that

$$\delta_\nu(u, a/L) = \frac{\Sigma^\nu(u, a/L) - \sigma(u)}{\sigma(u)} = \delta^\nu_1(a/L)u + \delta^\nu_2(a/L)u^2 + ... \tag{6.67}$$

with the first two terms given by

$$\begin{aligned} \delta^\nu_1 &= \Sigma^\nu_1 - \sigma_1, \\ \delta^\nu_2 &= \Sigma^\nu_1 - \sigma_2 - \sigma_1\Sigma^\nu_1 + (\sigma_1)^2. \end{aligned} \tag{6.68}$$

The series $p_2(L/a)$ can be reconstructed from reference [52]. There, p_2 is decomposed in the three different contributions given in eq.(6.17), with the coefficients

$$\begin{aligned} p_{20} =& p^a_2 + c_t^{(1,0)}p^b_2 + \left[c_t^{(1,0)}\right]^2 p^c_2 + c_t^{(2,0)}p^d_2 - p^2_{10}, \\ p_{21} =& p^e_2 + c_t^{(1,1)}p^b_2 + 2c_t^{(1,0)}c_t^{(1,1)}p^c_2 + c_t^{(2,1)}p^d_2 \\ &+ c_t^{(1,0)}p^f_2 + \widetilde{c}_t^{(1)}p^g_2 + c^{(1)}_{\mathrm{SW}}p^h_2 + m_c^{(1)}p^i_2 + 2p_{10}p_{11}, \\ p_{22} =& p^j_2 + \left[c_t^{(1,1)}\right]^2 p^c_2 + c_t^{(1,1)}p^d_2 + c_t^{(1,1)}p^f_2 - p^2_{11}. \end{aligned} \tag{6.69}$$

The explicit values for all the series p^k_2 can be found in the appendices in [52]. The improvement coefficients appearing in the previous expression are collected in table 4.4.1 at the end of chapter 4, where we give the references where they have been taken

from.

Moreover, the series $v_2(L/a)$ can be found in [27]. From there, one obtains the function

$$\Omega(u, a/L) = (v_1 + v_2 u)(1 + \epsilon_1(a/L) + \epsilon_2(a/L)u) + O(u^2), \tag{6.70}$$

where v_1 and v_2 are the continuum values in eq.(6.55) and $\epsilon_1(a/L)$ and $\epsilon_2(a/L)$ are the cutoff effects in $\overline{v}$ which can be found in the appendix of [27]. In this way we can reconstruct the series

$$v_2(a/L) = v_2(1 + \epsilon_1(a/L)) + v_1\epsilon_2(a/L). \tag{6.71}$$

Unfortunately, $\epsilon_1(a/L)$ and $\epsilon_2(a/L)$ are only given in [27] for the specific choices of $N_f = 0, 2$, so that one cannot disentangle the cutoff effects due to a single fermion.[12]

In fig.(6.4.3) we show the ν dependance of δ_1^ν (top panel) and δ_2^ν (bottom panel) for the 2 flavour theory ($N_f = 2$). It is interesting to see that when considering the full theory $\nu = 0$ does not seem to be the optimal choice for the reduction of cutoff effects at 1-loop any more. $\nu = 0$ is a good choice for the purely fermionic cutoff effects, but when merged together with the pure gauge contribution, the latter seems to push ν away from zero. At two loops, we see that again the residual cutoff effects δ_2^ν are very sensitive to ν. In the top panel of fig.(6.4.3) we have superimposed the 2-loop effects δ_2^ν (green band) for comparing its magnitude with δ_1^ν as the continuum limit is approached.

For the pure Yang-Mills theory (see fig.(6.4.4)) the scenario is similar, but there are some points to remark. The 2 loop effects δ_2^ν still show a dependence on ν, although much weaker than for the $N_f = 2$ case. While for the $N_f = 2$ theory, a window of $\nu \in [-1, 1]$ covers a range of $\Delta\delta_1^\nu \sim 0.06$ and $\Delta\delta_2^\nu \sim 0.01$ for the smallest latices, for the pure gauge theory the ranges are $\Delta\delta_1^\nu \sim 0.04$ and $\Delta\delta_2^\nu \sim 0.001$. Moreover, for the pure Yang-Mills theory, δ_2^ν seems to push the value of ν in the opposite direction than δ_1^ν. For δ_1^ν the preferred value is $\nu \sim -1$, while for δ_2^ν the optimal value is $\nu > 1$.

Since the dominant effects are those coming from $\delta^{(1)}$ one would chose its preferred value of ν ignoring $\delta^{(2)}$. However, far from the weak coupling regime, the interplay between cutoff effects at higher orders in PT could lead ν away from its ideal value at 1 loop.

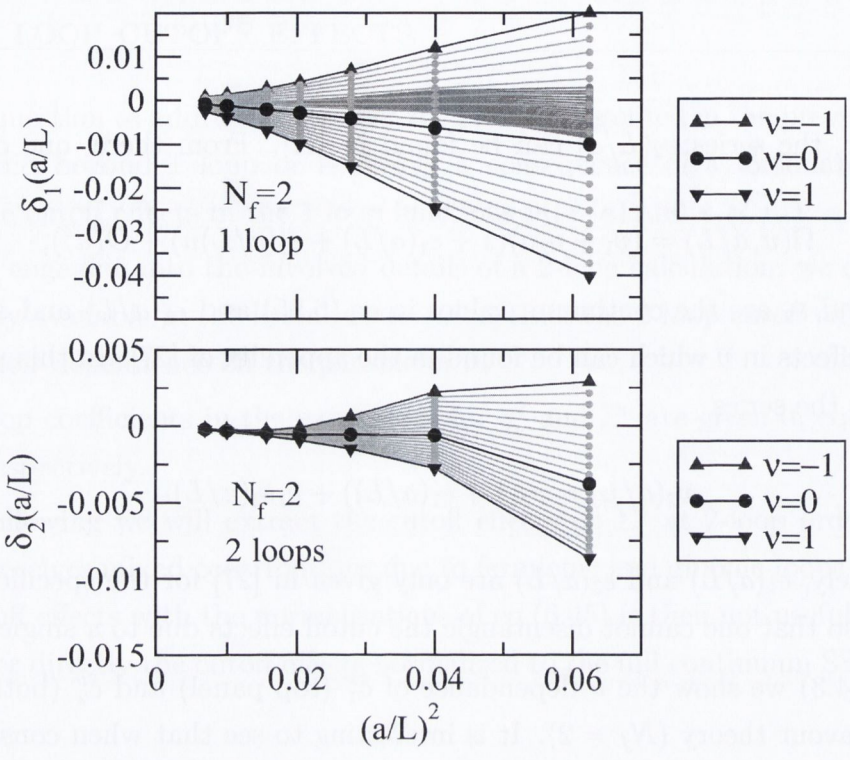

Figure 6.4.3: Cutoff effects δ_1^ν (top panel) and δ_2^ν (bottom panel) of the SSF for the 2 flavour theory. Orange lines are separated by steps of equal size $\Delta\nu = 0.1$. Boundary $O(a)$ improvement has been implemented. The green band in the top panel corresponds to the two loop δ_2^ν superimposed for comparison.

We stress again that the cutoff effects in both QCD and the pure Yang-Mills theory have been well understood both perturbatively and non-perturbatively in the past, and many studies have been done by now with continuum extrapolations well under control. The objective of this section is not to contradict those studies but to gain some systematic understanding on the family of couplings $\overline{g}_\nu^2$ and their perturbative cutoff effects. Understanding the lattice artefacts at different orders in PT for these schemes will become useful later on when considering theories beyond QCD for which, as we will see, the standard improvement strategies are not enough.

[12]In fact, this is the reason for which we are not using the same normalisation convention for the cutoff effects as in sections 6.3.4 and 6.4.2.

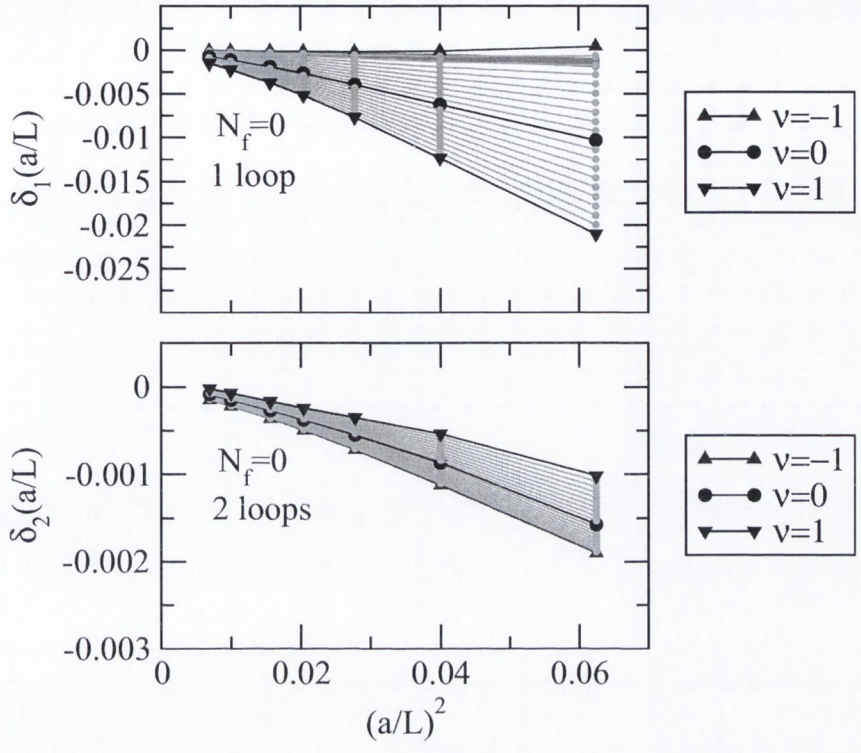

Figure 6.4.4: Cutoff effects δ_1^ν (top panel) and δ_2^ν (bottom panel) of the SSF for the pure Yang-Mills theory. Orange lines are separated by steps of equal size $\Delta\nu = 0.1$. Boundary $O(a)$ improvement has been implemented. The green band in the top panel corresponds to the two loop δ_2^ν superimposed for comparison.

6.4.4 Matching with the $\overline{\text{MS}}$ scheme

In this subsection we calculate the relation between the running cupling in the SF_ν scheme and the $\overline{\text{MS}}$ to two loops. We remark again that since in the continuum both the SF_ν and χSF_ν are completely equivalent, the relation to the $\overline{\text{MS}}$ will be the same. Moreover, we can relate Λ_{SF_ν} parameter to $\Lambda_{\overline{\text{MS}}}$ in the $\overline{\text{MS}}$ scheme through the 1-loop relation between the couplings in both schemes, as we discussed in section 3.2. This is done in two steps. We first relate the SF_ν scheme to the standard SF. After this is done, we can use the relation between the SF and the $\overline{\text{MS}}$ known up to 2-loops [52] to bridge the SF_ν with the $\overline{\text{MS}}$.

The renormalized couplings in the SF_ν and SF schemes are related at 2-loop order via ($\alpha = \overline{g}^2/4\pi$)

$$\alpha_{SF_\nu} = \alpha_{SF} + c_1^\nu \alpha_{SF}^2 + c_2^\nu \alpha_{SF}^3 + ... \tag{6.72}$$

The coefficients c_1^ν and c_2^ν, which are of course functions of ν, can be obtained using

the expansions of $\overline{g}^2$ eq.(6.6) and $\overline{g}^2_\nu$ eq.(6.56) in terms of the bare coupling g_0^2. One finds,

$$\begin{aligned} c_1^\nu &= 4\pi\nu v_1, \\ c_2^\nu &= 16\pi^2\left(\nu v_2 + \nu^2 v_1^2\right), \end{aligned} \tag{6.73}$$

where the values of v_1 and v_2 can be read from eq.(6.55). From here, we obtain the relation between $\Lambda_{\rm QCD}$ in both schemes using eq.(3.12)

$$\frac{\Lambda_{\rm SF}}{\Lambda_{{\rm SF}_\nu}} = \exp\left\{-\frac{c_1^\nu}{8\pi b_0}\right\}, \tag{6.74}$$

which clearly depends on ν. Some numerical examples of the ratio $\Lambda_{{\rm SF}_\nu}/\Lambda_{\rm SF}$ for different number of flavours N_f and different values of ν is given in table (6.4.1).

	$N_f = 0$	2	3	4
$\nu = 0.5$	1.28311(1)	1.62270(2)	1.87307(2)	2.21229(3)
0.1	1.05112(1)	1.10166(1)	1.13373(1)	1.17211(1)
−0.1	0.951365(1)	0.907721(1)	0.882041(1)	0.853163(1)
−0.5	0.779354(1)	0.602(1)	0.566(1)	0.45202(1)

Table 6.4.1: Numerical values of the ratio $\Lambda_{{\rm SF}_\nu}/\Lambda_{\rm SF}$ for some choices of Nf and ν.

The relation between the $\overline{\rm MS}$ and the SF couplings is known up to two loops [52], and reads

$$\alpha_{\overline{\rm MS}}(sq) = \alpha_{\rm SF}(q) + c_1(s)\alpha^2_{\rm SF}(q) + c_2(s)\alpha^3_{\rm SF}(q) + \ldots \tag{6.75}$$

where s is an arbitrary scale factor and the coefficients c_1 and c_2 are obtained from [52] and read

$$\begin{aligned} c_1(s) =& 1.255621(2) + 0.0398629(2)N_f - 8\pi b_0 \ln(s), \\ c_2(s) =& c_1(s)^2 + 1.197(10) + 0.140(6)N_f - 0.0330(2)N_f^2 \\ & - 32\pi^2 b_1 \ln(s). \end{aligned} \tag{6.76}$$

Inverting eq.(6.72) and inserting it into eq.(6.75) yields the desired relation

$$\alpha_{\overline{\rm MS}}(sq) = \alpha_{{\rm SF}_\nu}(q) + \tilde{c}_1^\nu(s)\alpha^2_{{\rm SF}_\nu}(q) + \tilde{c}_2^\nu(s)\alpha^3_{{\rm SF}_\nu}(q) + \ldots \tag{6.77}$$

with the matching coefficients $\widetilde{c}_1^\nu(s)$ and $\widetilde{c}_2^\nu(s)$ (which are functions of ν) given by

$$\begin{aligned}\widetilde{c}_1^\nu(s) &= c_1(s) - 4\pi\nu v_1, \\ \widetilde{c}_2^\nu(s) &= c_2(s) - 8\pi\nu\left(c_1(s)v_1 + 2\pi v_2\right) + 16\pi^2\nu^2 v_1^2.\end{aligned} \tag{6.78}$$

Finally, the relation between the lambda parameters in the 2 schemes is given by

$$\frac{\Lambda_{\mathrm{SF}_\nu}}{\Lambda_{\overline{\mathrm{MS}}}} = \exp\left\{-\frac{\widetilde{c}_1(\nu)}{8\pi b_0}\right\}. \tag{6.79}$$

6.4.5 The 3 loop β-function

Starting from the relation between the coupling in two different schemes eq.(3.11), by acting on both sides of the equation with $\mu\frac{d}{d\mu}$ one can prove the scheme independence of the first two coefficient of the β-function b_0 and b_1. Moreover, one obtains the difference between the 3-loop coefficient b_2 of the β-function in the two schemes, given by

$$b_2^X - b_2^Y = \frac{b_1 c_{YX}^{(1)}(1)}{4\pi} - \frac{b_0\left[c_{YX}^{(2)}(1) - \left(c_{YX}^{(1)}(1)\right)^2\right]}{16\pi^2} \tag{6.80}$$

This means that, provided that the 3-loop coefficient b_2 is known in 1 scheme, it can be extracted in any other scheme via a 2-loop calculation.

Since the 3-loop coefficient $b_2^{\overline{\mathrm{MS}}}$ in the $\overline{\mathrm{MS}}$ is known [105], we can extract the 3-loop coefficient $b_2^{\mathrm{SF}_\nu}$ in the SF_ν via eq.(6.80) and the relation coefficients $\overline{c}_1^\nu$ and $\overline{c}_2^\nu$ extracted in the previous subsection.

The 3-loop coefficient in the $\overline{\mathrm{MS}}$ scheme is given by [105]

$$b_2^{\overline{\mathrm{MS}}} = b_{20}^{\overline{\mathrm{MS}}} + b_{21}^{\overline{\mathrm{MS}}} N_f + b_{22}^{\overline{\mathrm{MS}}} N_f^2 \tag{6.81}$$

with

$$\begin{aligned}b_{20}^{\overline{\mathrm{MS}}} &= \frac{1}{(4\pi)^6}\frac{2857N^3}{54}, \\ b_{21}^{\overline{\mathrm{MS}}} &= -\frac{1}{(4\pi)^6}\left(\frac{1709N^2}{54} - \frac{187}{36} - \frac{1}{4N^2}\right), \\ b_{22}^{\overline{\mathrm{MS}}} &= \frac{1}{(4\pi)^6}\left(\frac{56N}{27} - \frac{11}{18N}\right).\end{aligned} \tag{6.82}$$

With these values at hand, the coefficient $b_2^{\mathrm{SF}_\nu}$ finally reads

$$b_2^{\mathrm{SF}_\nu} = b_2^{\overline{\mathrm{MS}}} + \frac{b_1 \widetilde{c}_1^{\nu}(1)}{4\pi} - \frac{b_0 \left[\widetilde{c}_2^{\nu}(1) - (\widetilde{c}_1^{\nu}(1))^2\right]}{16\pi^2}. \tag{6.83}$$

We give the value of the 3-loop coefficient $b_2^{\mathrm{SF}_\nu}$ as a function of ν for the choices of flavours $N_f = 0$ and $N_f = 2$,

$$\begin{aligned} b_2^{\mathrm{SF}_\nu}(N_f = 0) &= 0.482(7) \times (4\pi)^{-3} - \nu \times 0.752(7) \times (4\pi)^{-3}, \\ b_2^{\mathrm{SF}_\nu}(N_f = 2) &= 0.064(10) \times (4\pi)^{-3} - \nu \times 1.076(10) \times (4\pi)^{-3}. \end{aligned} \tag{6.84}$$

For $\nu = 0$, of course, we recover the values for b_2^{SF} quoted in the literature [27]. It is interesting that even if the matching parameter $\widetilde{c}_2^{\nu}$ depends quadratically on ν, this dependence cancels out in the 3-loop beta function, leaving only a linear dependence on ν. A few numerical examples for $b_2^{\mathrm{SF}_\nu}$ for different flavour numbers N_f are given in table 6.4.2.

	$N_f = 0$	2	3	4
$\nu = 0.5$	−0.107(14)	−0.474(24)	−0.693(38)	−0.867(59)
0.1	0.407(10)	−0.043(17)	−0.190(28)	0.294(43)
0.0	0.483(9)	0.063(16)	−0.063(25)	−0.150(39)
−0.1	0.558(8)	0.172(14)	0.062(22)	−0.007(36)
−0.5	0.859(5)	0.602(8)	0.566(17)	0.566(20)

Table 6.4.2: Numerical values of $b_2^{\mathrm{SF}_\nu} \times (4\pi)^3$ for some choices of N_f and ν.

With this we end the discussion of the SF_ν scheme. We will come back to it in the following chapter when discussing theories beyond QCD.

6.5 Summary of chapter 6

In this chapter we have discussed the running coupling in the Schrödinger functional which was originally introduced in [23]. It can be understood as a response of the system to the induced chromo-electrcic field.

We have calculated the fermionic contribution $p_{1,1}(L/a)$ to the 1-loop coefficient of the coupling in both the SF and χSF schemes. In the standard SF, the calculation was

originally done in [80]. The contribution of fermions in the χSF has been calculated here for the first time. Some results have already been presented in [101, 102]. With the knowledge of $p_{1,1}(L/a)$ we have been able to extract the fermionic $c_t^{(1,1)}$ part of the gauge boundary improvement coefficient. After that, we have studied the cutoff effects in the step scaling function at different levels of improvement. In the χSF, after implementing boundary improvement, the remaining cutoff effects are small and automatic $O(a)$-improvement is at work. For the standard SF, boundary and bulk improvement cancels large cutoff effects and the remaining lattice artefacts are essentially zero. We have also studied the sensitivity of $p_{1,1}(L/a)$ to the coefficients m_0 and z_f of the action to estimate the uncertainties in the step scaling function induced by an uncertainty in m_0 and z_f. The dependence seems to be rather small which leaves a quite generous margin of tolerance for the uncertainties in the determination of m_0 and z_f. Since both the SF and the χSF setups are equivalent in the continuum limit, they yield the same continuum extrapolation of $p_{1,1}(L/a)$. This means that the coefficients to match the coupling to the $\overline{\text{MS}}$ scheme will be identical in both setups.

In section 6.4 we have re-examined the definition of the Schrödinger Functional coupling. By combining $\overline{g}^2$ with another renormalised observable $\overline{v}$, a whole new family of couplings $\overline{g}^2_\nu$ can be constructed, which depends on a single parameter ν. This way we define the SF$_\nu$ and χSF$_\nu$ renormalization schemes. Since both $\overline{g}^2$ and $\overline{v}$ can be calculated simultaneously from a single numerical simulation, the whole family $\overline{g}^2_\nu$ can be evaluated at no extra cost when analysing the data. We have calculated the 1-loop coefficient $p^\nu_{1,1}(L/a)$ of this family of couplings and the 1-loop step scaling function. The cutoff effects in the SSF show a very strong dependence on the parameter ν. For the χSF, even if cutoff effects are already small at $\nu = 0$, we observe that they can be minimised by chosing values $\nu \sim 0.1$. In fact, for every lattice regularization minimal cutoff effects are obtained for a different value of ν. This has been observed also for the two different regularizations of staggered fermions [103]. By deviating from the choice $\nu = 0$, very large cutoff effects can be introduced in the SSF. This might seem contra-productive, given the good behaviour of the cutoff effects after implementing $O(a)$ improvement. However, the strong dependence on ν will be particularly useful when considering fermions transforming under 2-index representations of the gauge group in chapter 7. For these, cutoff effects in the SSF turn out to be very large even after $O(a)$ improvement. By using the couplings $\overline{g}^2_\nu$, one can always find a value of ν inducing large cancellations of lattice artefacts and

end up in a situation where cutoff effects are minimal.

Using data extracted from the literature, we have been able to reconstruct the 2-loop coefficient $p_2^\nu(L/a)$ for the SF$_\nu$ scheme and its 2-loop step scaling function. At this order, we also observe the dependence of the cutoff effects on ν such that the scenario just described is preserved beyond 1-loop. We have obtained the matching coefficients in the coupling between the SF$_\nu$ and the $\overline{\text{MS}}$ schemes up to 2-loops. With the 1-loop matching coefficient, the Λ_{SF_ν} and the $\Lambda_{\overline{\text{MS}}}$ parameters have been related. Finally, with the knowledge of the 3-loop coefficient of the β-function in the $\overline{\text{MS}}$ scheme, we have been able to extract the 3-loop coefficient in the SF$_\nu$ scheme. The matching coefficients and the 3-loop term of the β-function are the same for the SF$_\nu$ and the χSF$_\nu$ since both schemes are equivalent in the continuum limit.

"Sometimes the only sane answer to an insane world is insanity. "

Fox Mulder

7

The coupling beyond QCD

THE TECHNIQUES OF QCD can be exported to study the more general class of theories consisting on Yang-Mills fields coupled to fermionic matter transforming under arbitrary representations of the gauge group. These have been introduced in section 3.4, and are generically described by the lagrangian eq.(3.27). A particular theory is chosen by specifying the three parameters $(N, N_f, \mathcal{R})$, i.e. the gauge group $SU(N)$, the number of fermionic flavours, and the representation under which the fermions transform, respectively.

In this section we will focus on theories where the fermions transform under the 2-index representations, namely the *adjoint*, the 2-*index symmetric* and the 2-*index anti-symmetric* representations of the gauge groups $SU(2)$ and $SU(3)$.[1] These theories are commonly studied in non-perturbative simulations following the finite size scaling strategy described in section 3.3. For this reason, we study them here in perturbation theory using the same techniques as for QCD in chapter 6. It is worth noting that

[1]For $SU(2)$ the anti-symmetric representation is trivial, and for $SU(3)$ it is equivalent to the anti-fundamental representation

since all results in chapter 5 were given with explicit group theoretical factors which depend on the choices of $(N, N_f, \mathcal{R})$, they are hence valid for the theories beyond QCD considered here.

In this chapter we calculate the Schrödinger functional coupling defined in eq.(6.1) to one loop in perturbation theory for the previous groups and representations. We perform the calculation in both the standard SF and the χSF setups. This will permit us to compare the size of the cutoff effects before and after improvement in both setups. The calculation follows very similar steps as for QCD, so the techniques explained in chapter 6 can be directly imported for the present computation. In section 7 we explain the necessary adaptations for the evaluation of the coupling and present the results of the perturbative calculation. In section 7.2 we perform the improvement of the coupling to $O(a)$, and study the size of the remaining cutoff effects. As we will see, these can be very large. In section 7.2 we will study different strategies for a further reduction of remaining cutoff effects.

7.1 The coupling at 1-loop

In this section we calculate the fermionic 1 loop contribution $p_{1,1}(L/a)$ to the running coupling in the SF and the χSF, for a set of gauge groups and fermionic representations of the color group. The calculation follows very closely the discussion in section 6.3, so we refer to that section for all the details on the expansion of the effective action and the coupling. We first describe the adaptation of the Wilson-Dirac operator to act over arbitrary representations, and then we present the results for $p_{1,1}(L/a)$.

7.1.1 The Dirac operator in a generic representation

The massless Dirac operator in an infinite volume lattice is given by eq.(2.29). For QCD, the link variables $U_\mu(x)$ in eq.(2.29) are $SU(3)$ matrices acting on fundamental fermions, i.e. 3×3 matrices multiplying color vectors of dimension 3.[2] Eq.(2.29) can be easily generalised to an arbitrary representation $\mathcal{R}$ of the color group. For this, one simply needs to replace

$$U_\mu(x) \longrightarrow U_\mu^{\mathcal{R}}(x), \tag{7.1}$$

[2]For $SU(2)$ $U_\mu(x)$ are obviously 2×2 matrices multiplying color vectors of dimension 2.

where $U_\mu^{\mathcal{R}}(x)$ denotes the link variables in the representation $\mathcal{R}$. Let T_F^a and $T_{\mathcal{R}}^a$ be the generators of the color group in the fundamental representation and in a generic representation $\mathcal{R}$ respectively. The conventions and notation used in this work are given in appendix A.3. If the link variables in the fundamental representation are written as

$$U_\mu(x) = \exp\left[iag_0 A_\mu^a(x) T_F^a\right], \tag{7.2}$$

then the link variables in the representation $\mathcal{R}$ read

$$U_\mu^{\mathcal{R}}(x) = \exp\left[iag_0 A_\mu^a(x) T_{\mathcal{R}}^a\right], \tag{7.3}$$

where the real functions A_μ^a are the *same* in both representations. It is possible to work out case by case an explicit relation between the link variables in different representations (see appendix A.3). For example, for the adjoint representation of $SU(N)$ the relation is given by

$$U_{a,b}^{\mathrm{Adj}} = \frac{1}{2}\mathrm{tr}\left[T_F^a U T_F^b U^\dagger\right]. \tag{7.4}$$

The (massive) Wilson-Dirac $D_{\mathrm{W}}^{\mathcal{R}}$ operator acts on a fermion field on an arbitrary representation as

$$\begin{aligned} D_{\mathrm{W}}^{\mathcal{R}}\psi(x) &= (4/a + m_0)\psi(x) - \frac{1}{2a}\sum_\mu \left\{(1-\gamma_\mu)U_\mu^{\mathcal{R}}(x)\psi(x+\hat{\mu}) + \right. \\ &\quad \left. + (1+\gamma_\mu)U_\mu^{\mathcal{R}}(x-\hat{\mu})^\dagger\psi(x-\hat{\mu})\right\}. \end{aligned} \tag{7.5}$$

The fermion field $\psi(x)$ is a vector of the dimension of the representation $\dim(\mathcal{R})$ and, hence, the link variables will be $\dim(\mathcal{R}) \times \dim(\mathcal{R})$ matrices.

When upgrading the background field $V_\mu(x)$ to an arbitrary representation the resulting $V_\mu^{\mathcal{R}}(x)$ might not be diagonal any more. For example, for an $SU(2)$ abelian boundary link variable W_k with the phases eq.(4.29), the mapping eq.(7.4) yields the adjoint link variable

$$W_k^{\mathrm{F}} = \begin{pmatrix} e^{i\frac{a}{L}\phi} & 0 \\ 0 & e^{-i\frac{a}{L}\phi} \end{pmatrix} \quad \longrightarrow \quad W_k^{\mathrm{A}} = \begin{pmatrix} \cos(\frac{a}{L}\phi) & -\sin(\frac{a}{L}\phi) & 0 \\ \sin(\frac{a}{L}\phi) & \cos(\frac{a}{L}\phi) & 0 \\ 0 & 0 & 1 \end{pmatrix}. \tag{7.6}$$

It is always possible to find a unitary transformation which brings back the boundary field to a diagonal form (see appendix C). For the case of $SU(2)$ in the adjoint representation, the resulting diagonal boundary field will be given by

$$W_k^{\mathrm{A}} = \begin{pmatrix} e^{i\frac{2a}{L}\phi} & 0 & 0 \\ 0 & e^{-i\frac{2a}{L}\phi} & 0 \\ 0 & 0 & 1 \end{pmatrix}. \tag{7.7}$$

Thus, an abelian boundary field can always be written in an arbitrary representation as a diagonal matrix

$$W_k^{\mathcal{R}} = \exp(aC_k^{\mathcal{R}}), \qquad C_k^{\mathcal{R}} = \frac{i}{L}\mathrm{diag}\left(\phi_1^{\mathcal{R}}, ..., \phi_{d_{\mathcal{R}}}^{\mathcal{R}}\right), \tag{7.8}$$

where the phases $\phi_i^{\mathcal{R}}$ are linear combinations of the fundamental phases. The same statement is true for the boundary field W_k' and thus the induced background field $V_k(x)^{\mathcal{R}}$ will still have a diagonal form.[3]

Note that changing the representation of the fermions does not affect the pure gauge part of the action. Even if the link variables in the Dirac operator are upgraded to an arbitrary representation $\mathcal{R}$, the link variables in the Wilson gauge action eq.(2.24) are left in the fundamental representation. In principle any other representation could be used for the gauge part of the action, but all choices lead to the same continuum limit.[4]

7.1.2 The θ phase (revisited)

Before calculating the coefficient $p_{1,1}(L/a)$ we recall the criterion in section 6.2.1 for fixing the value of the angle θ of the spatial boundary conditions for the fermion fields. In section 6.2.1 θ is chosen such that the minimum eigenvalue $\lambda_{\min}$ of the classical quadratic fermion operator Δ_2 is as large as possible.

Once the Dirac operator is promoted to an arbitrary representation $\mathcal{R}$, the resulting

[3] It is interesting to see from eq.(7.7) that the third component of an adjoint $SU(2)$ fermion is not affected by the background field.

[4] However, it has been shown [106] that using a gauge action with a mixture between fundamental and adjoint link variables can avoid problems with a bulk phase transition.

quadratic operator is simply given by

$$\Delta_2^{\mathcal{R}} = \left(\mathcal{D}_{\rm W}^{\mathcal{R}} \mathcal{D}_{\rm W}^{\mathcal{R}\dagger}\right). \tag{7.9}$$

Since the color structure of $\mathcal{D}_{\rm W}^{\mathcal{R}}$ is different from the one for the fundamental representation, the profile $\lambda_{\rm min}(\theta)$ will change and will have to be recomputed for each case considered. We calculate the profile of $\lambda_{\rm min}(\theta)$ for the standard choices of BF eq.(4.29) and eq.(4.30). The preferred choices of θ, leading to a maximal value for $\lambda_{\rm min}$ are collected in table (7.1.1). In fig.(7.1.1) we show the profile $\lambda_{\rm min}(\theta)$ for the adjoint representation of $SU(2)$ and for the symmetric and adjoint representation of $SU(3)$.

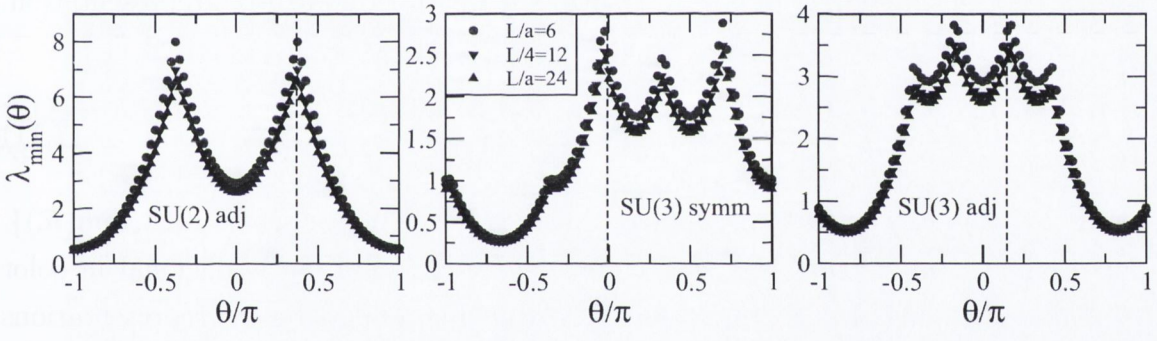

Figure 7.1.1: Lowest eigenvalue $\lambda_{\rm min}$ (in units of L^{-2}) as a function of θ for the adjoint representation of $SU(2)$ and the symmetric and adjoint representations of $SU(3)$. The BF are the standard choices eq.(4.29) and eq.(4.30) for $SU(2)$ and $SU(3)$ respectively. Their vertical discontinuous line denotes the selected value of θ.

	$SU(2)_F$	$SU(2)_A$	$SU(3)_F$	$SU(3)_A$	$SU(3)_S$
θ	0	$2\pi/5$	$\pi/5$	$\pi/6$	0

Table 7.1.1: Angle θ in the fermionic boundary conditions in the spatial directions which leads to a highest $\lambda_{\rm min}$.

7.1.3 Contribution to the coupling from fermions in arbitrary representations

Finally, we are ready to compute the one loop coefficient $p_1(L/a)$. Since the gauge part of the action is not modified when considering other representations, the contributions coming from the ghost operator Δ_0 and the gluon operator Δ_1 will not change and hence neither does $p_{1,0}(L/a)$.

We only need to calculate the fermionic contribution $p_{1,1}(L/a)$, which will be given by

$$p_{1,1}(L/a) = \frac{1}{2kN_f} \frac{\partial}{\partial \eta} \ln \det \Delta_2^{\mathcal{R}} \Big|_{\eta=\nu=0} . \tag{7.10}$$

The normalisation k is the same as for the fundamental representation, given in in eq.(6.2). The calculation follows the steps sketched in 6.3, with the following adaptation. Once the operator $\mathcal{D}_{\mathrm{W}}^{\mathcal{R}}$ is written in the time momentum representation, the eigeinfunctions factorise as

$$\psi(x) = e^{ip_k x_k} u_{n_c} f(x_0), \tag{7.11}$$

where now the canonical basis in color space is given by $\{u_{n_c}, n_c = 1, ..., \dim(\mathcal{R})\}$. The original Dirac operator in the fundamental representation is diagonal in color space (for the abelian background fields). After upgrading to some representations it might be necessary to diagonalise the operator in color space, as shown in section 7.1.1, before performing a factorisation of the form eq.(6.28). It is very simple to show that this diagonalisation can always be done (see appendix C), such that the determinant of the Dirac operator factorizes to

$$\det \left(\mathcal{D}_{5,1}^{\mathcal{R}} \right) = \prod_{n_c=1}^{\dim(\mathcal{R})} \prod_{\mathbf{p}} \det \widetilde{\mathcal{D}}_{5,1}^{\mathcal{R}}(n_c, \mathbf{p}), \tag{7.12}$$

where $\widetilde{\mathcal{D}}_{5,1}^{\mathcal{R}}(n_c, \mathbf{p})$ is the reduced Dirac operator on an arbitrary representation $\mathcal{R}$, which acts on functions $f(x_0)$ on fixed color n_c and momenta $\mathbf{p}$. The 1 loop coefficient $p_{1,1}(L/a)$ for a representation $\mathcal{R}$ is then given by

$$p_{1,1}(L/a) = \frac{1}{k} \sum_{n_c=1}^{\dim(\mathcal{R})} \sum_{\mathbf{p}} \frac{\partial}{\partial \eta} \ln \det \widetilde{\mathcal{D}}_{5,1}^{\mathcal{R}}(n_c, \mathbf{p}) \Big|_{\eta=0} . \tag{7.13}$$

For evaluating this we use the same code prepared for the computation of $p_{1,1}(L/a)$ in QCD (see section 6.3 for further details). We perform the calculation for the χSF setup for $c_{\rm SW} = 1$ and $c_{\rm SW} = 0$, and for the standard SF setup with $c_{\rm SW} = 1$. The value of θ is fixed to the values in table (7.1.1). Tables with numerical values of the series $p_{1,1}(L/a)$ for the different groups and representations considered in this chapter can be found in appendix E.

The first terms of the expansion of $p_{1,1}(L/a)$ are shown in table (7.1.2) for the χSF and in table (7.1.3) for the standard SF.

	$r_{0,1}$	$s_{0,1}$	$r_{1,1}$	$s_{1,1}$
$SU(2)_f$	$-0.034266552(1)$	$-0.0084433(2)$	$0.0137838(3)$	$0.000001(2)$
$SU(2)_a$	$-0.1302285(3)$	$-0.03376(1)$	$0.05506(4)$	$0.001(2)$
$SU(3)_f$	$-0.03466492(1)$	$-0.008443(1)$	$0.013776(3)$	$0.000001(1)$
$SU(3)_a$	$-0.180341(2)$	$-0.05061(5)$	$0.0825(2)$	$0.002(3)$
$SU(3)_s$	$-0.1627196(5)$	$-0.04219(4)$	$0.068785(5)$	$0.002(3)$

Table 7.1.2: Asymptotic expansion coefficients of $p_{1,1}(L/a)$ for several gauge groups and representations for the χSF calculated at $c_{\rm SW} = 1$ and θ fixed to the values of table (7.1.1).

	$r_{0,1}$	$s_{0,1}$	$r_{1,1}$	$s_{1,1}$
$SU(2)_f$	$-0.034266653(1)$	$-0.0084434(1)$	$0.0382815(3)$	$0.000005(8)$
$SU(2)_a$	$-0.1302287(1)$	$-0.03376(2)$	$0.15306(2)$	$0.0006(8)$
$SU(3)_f$	$-0.034664940(1)$	$-0.0084436(2)$	$0.038281(2)$	$0.00001(1)$
$SU(3)_a$	$-0.180342(1)$	$-0.05063(5)$	$0.2295(1)$	$0.002(2)$
$SU(3)_s$	$-0.16271966(5)$	$-0.04220(1)$	$0.1914(1)$	$0.001(2)$

Table 7.1.3: Asymptotic expansion coefficients of $p_{1,1}(L/a)$ for several gauge groups and representations for the SF calculated at $c_{\rm SW} = 1$ and θ fixed to the values of table (7.1.1).

In all the studied cases we can confirm the expected value of the universal term

$$s_{0,1} = 2b_{0,1} = -\frac{T_{\mathcal{R}}}{6\pi^2}, \tag{7.14}$$

in the achieved numerical precision. The coefficient $s_{1,1}$ is compatible with zero, indicating the absence of $O(a)$ effects coming from the bulk.

The precision obtained in the extraction of the coefficients for the adjoint or symmetric representations is always lower than for the fundamental representation. This is an indication that the $O(a^2)$ coefficients might not be small after all, as we will see in the following section.

7.1.4 $O(a)$ IMPROVEMENT AND THE REMAINING CUTOFF EFFECTS

The coefficient $c_t^{(1,1)}$ for the improvement at the boundaries can be obtained for a representation $\mathcal{R}$ in the same way as in section 6.3.3 for QCD, by requiring the cancellation of cutoff effects linear in (a/L) in the 1-loop coefficient $p_{1,1}(L/a)$. On the other hand, it is possible to see[5] one can obtain $c_t^{(1,1)}$ for a representation $\mathcal{R}$ by scaling the value for the fundamental representation through

$$c_t^{(1,1)}(\mathcal{R}) = \frac{T_{\mathcal{R}}}{T_F} c_t^{(1,1)}(F). \tag{7.15}$$

This relation has been used to check the consistency of the $r_{1,1}$ coefficients extracted in our calculation (see tables (7.1.2) and (7.1.3)). However, since the quality of the extrapolations seems to be better for the fundamental representation than for the two-index ones, for quoting a final value for $c_t^{(1,1)}(\mathcal{R})$ we use the value of $c_t^{(1,1)}(F)$ scaled via eq.(7.15). For convenience, the values for $c_t^{(1,1)}(\mathcal{R})$ in the different setups are collected in table (7.1.4).

	SF	χSF, $c_{\rm SW} = 1$	χSF, $c_{\rm SW} = 0$
$SU(3)_{\rm F}$	0.019141(1)	0.006888(1)	−0.00661445(5)
$SU(3)_{\rm A}$	0.114846(6)	0.041328(6)	−0.0396867(3)
$SU(3)_{\rm S}$	0.095705(5)	0.034440(5)	−0.0330723(3)
$SU(2)_{\rm F}$	0.019141(1)	0.006888(1)	−0.00661445(5)
$SU(2)_{\rm A}$	0.076564(4)	0.027552(4)	−0.0264578(2)

Table 7.1.4: Boundary coefficient $c_t^{(1,1)}$ for the groups and representations considered in this work. The values for the SF setup correspond to $c_{\rm SW} = 1$.

Once the improvement coefficients are known we can proceed to examine the cutoff effects in the SSF at the different stages of the improvement procedure, as it is done in section 6.3.4.

[5]The Feynman diagrams which contribute to the coupling at 1-loop are tadpole diagrams. The fermionic tadpoles are proportional to $T_{\mathcal{R}}$ for a given representation $\mathcal{R}$.

The fermionic contribution to the 1-loop cutoff effects $\delta_{1,1}$, defined in eq.(6.45) are shown for the representations of $SU(2)$ in fig.(7.1.2), and for the fundamental and symmetric representations of $SU(3)$ in figure (7.1.3). The adjoint representation of $SU(3)$ has also been considered but, since it shows the same trends as the symmetric representation, we have decided not to display it in the present discussion.

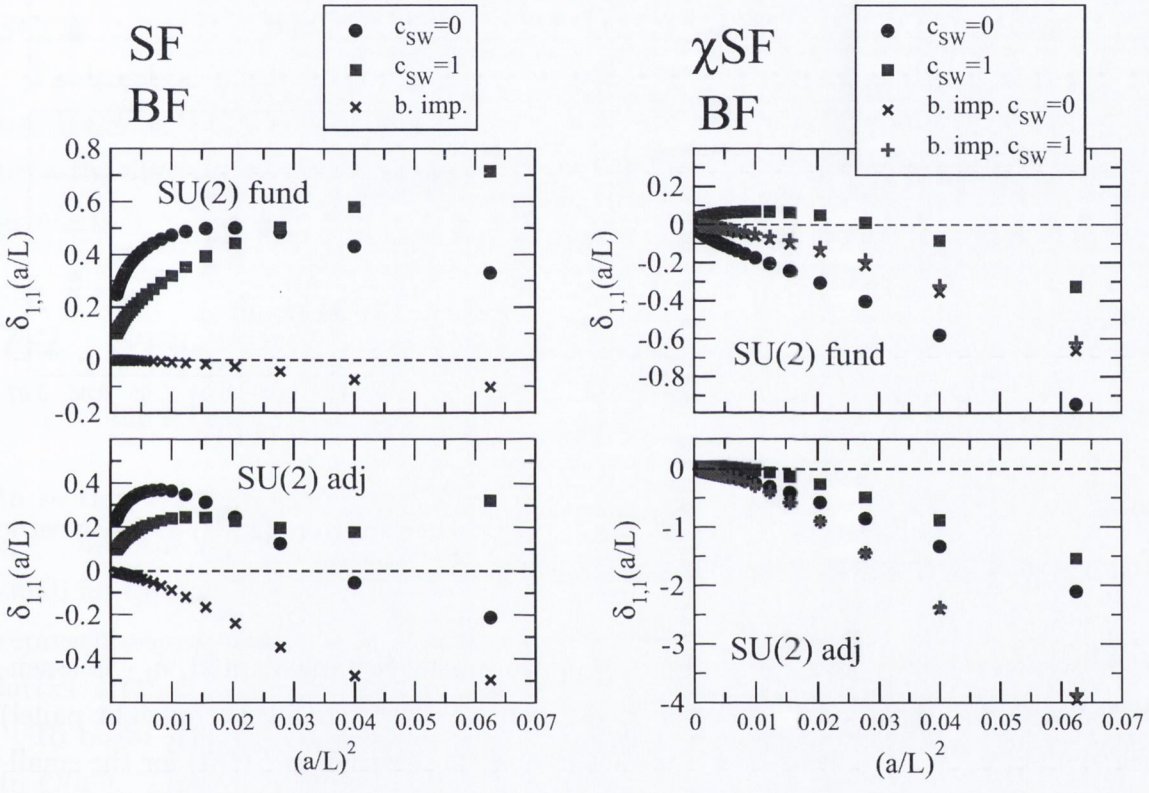

Figure 7.1.2: Cutoff effects $\delta_{1,1}$ for $SU(2)$ in the fundamental (top panels) and adjoint (bottom panels) representations of the gauge group.

We calculate $\delta_{1,1}$ in all the cases for both the standard SF (left panels of figures (7.1.2) and (7.1.3)) and the χSF (right panels of figures (7.1.2) and (7.1.3)).

The cutoff effects for the fundamental representation of $SU(3)$ have already been discussed in section 6.3.4 when studying the coupling for QCD.[6] For $SU(2)$ in the fundamental representation (fig.(7.1.2)), cutoff effects behave in a very similar way as for $SU(3)$. For the standard SF (fig.(7.1.2) top-left panel) $\delta_{1,1}$ is quite large before

[6]We include them here again just for comparison to the other reprsentations

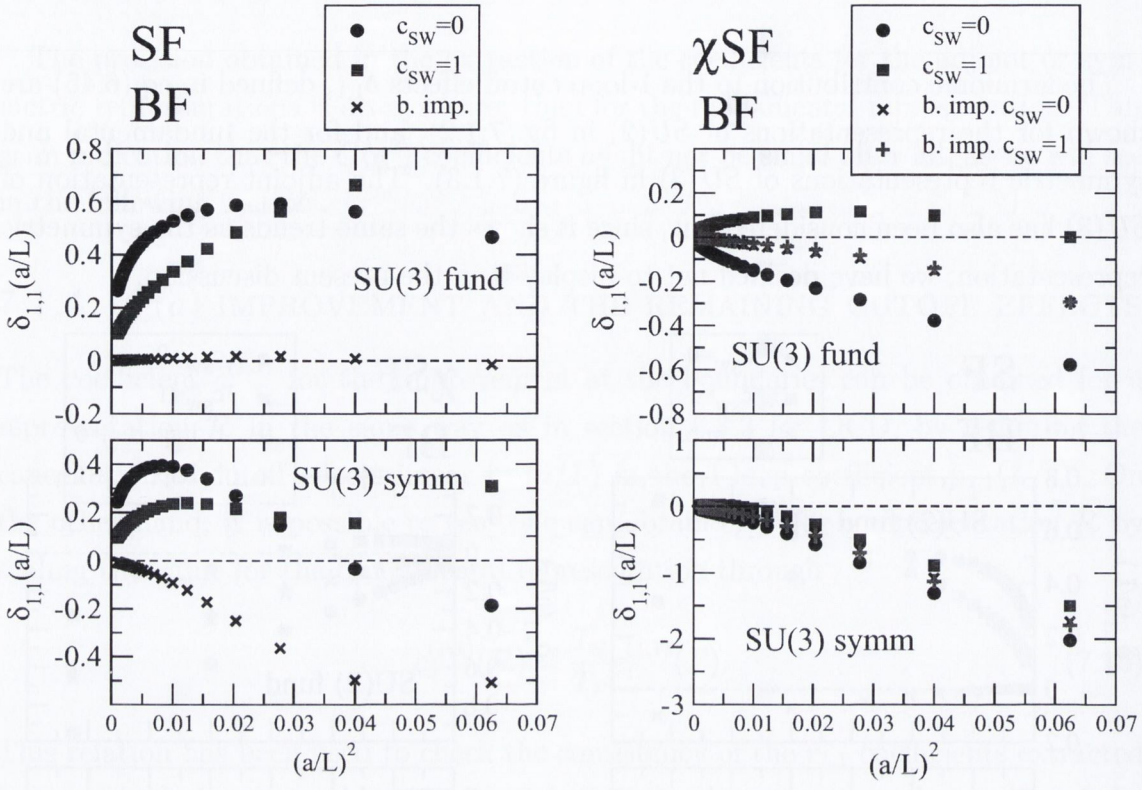

Figure 7.1.3: Cutoff effects $\delta_{1,1}$ for $SU(3)$ in the fundamental (top panels) and symmetric (bottom panels) representations of the gauge group.

improvement. After bulk and boundary improvement is implemented, $\delta_{1,1}$ is essentially zero except for the smallest lattices. For the χSF (fig.(7.1.2) top-right panel) the remaining cutoff effects after improvement are larger than in $SU(3)$ for the smallest lattices. However, they are already below the 20% level at $L/a = 6$. We recall here the observation made in section 5.4.1, where no simultaneous tuning of m_0 and z_f could be performed for $L/a = 4, 5$. Since, after all, for the χSF it might make no sense to consider these small lattices, one shouldn't worry about the size of the cutoff effects in them.

The situation is drastically different when considering other fermion representations. In the adjoint representation of $SU(2)$ cutoff effects remain large even after $O(a)$ improvement is implemented. For the standard SF (fig.(7.1.2) bottom-left panel) one does not observe the dramatic cancellations present for the fundamental representation. Relatively large higher order cutoff effects are still present, and a regime linear in $(a/L)^2$ is not reached until lattices of order $L/a \sim 12$. This issue might

compromise continuum extrapolations in non-perturbative calculations.

This situation seems to be much worse for the χSF (fig.(7.1.2) bottom-right panel). After implementing boundary improvement, the residual cutoff effects are still very large, reaching levels of about 150% for $L/a = 6$ lattices. The linear behaviour in $(a/L)^2$ is again reached quite late.

For $SU(3)$, the symmetric (fig.(7.1.2) bottom panel) and the adjoint (not shown) representations show a very similar bad behaviour as the adjoint representation in $SU(2)$.

The presence of large higher order cutoff effects for the non-fundamental representations is, of course, intolerable if one wants to extract meaningful information from the SSF. Thus, further strategies have to be examined to deal with these lattice artefacts.[7]

7.2 Strategies to reduce higher order cutoff effects

In section 7.1 we have shown that while after adjusting the boundary counterterm $c_t^{(1,1)}$, and the $c_{\rm SW}$ for the standard SF setup, the cutoff effects in the SSF are very small for fundamental representation, the situation seems to be much worse for other representations, and further work must be done to reduce the size of the remaining lattice artefacts. In this section we will discuss different strategies to do so.

To begin with, one could think of carrying out the improvement programme up to $O(a^2)$. This would involve obtaining all possible operators of dimension 6 in the bulk and dimension 5 in the boundaries allowed by the symmetries of the theory, and the further determination of all the improvement coefficients that will come with each operator. Moreover, the numerical simulation of an action with these operators would become expensive and the remaining setup would not be useful in practice.[8]

Instead, we will explore some simpler possibilities by re-examining the definition of the coupling in QCD and re-adapting it to deal with other gauge groups and generic

[7] Even if the presence of large lattice arteffacts in representations other than the fundamental has been pointed out on several occasions [101, 102, 107], many non-perturbative studies have been done up to date completely ignoring the issue.

[8] Note that $O(a^2)$ improvement of the fermion action would involve the inclusion of counterterms with four fermion operators. The resulting ation would not be bilinear in the fermion fields and standard simulation algorithms would not be useful anymore.

fermion representations. In particular we will reconsider the usual choices of BF which have been used in the past and, for the representations of $SU(3)$, we will use the SF_ν and $\chi\mathrm{SF}_\nu$ schemes introduced in chapter 6.

7.2.1 A "WEAKER" BACKGROUND FIELD

The calculations of the running coupling in theories with higher dimensional representations are usually done [31–34] by importing directly the same setups that have proven to be very successful in QCD. Their success in QCD, however, does not mean that the same setups should be equally useful when considering other theories. As we have shown in section 7.1, the options chosen for QCD lead to very large lattice artefacts in the step scaling function. Here we will reconsider the choice of background field from section 4.1.2.

One of the sources of cutoff effects in Schrödinger functional setups is the presence of the background field. We have already noticed this in chapter 5 even at tree-level, when looking at the universality relations between the SF and the χSF correlation functions, where the convergence to the expected continuum limit seems to be much slower in presence of the BF.

Considering the $SU(2)$ theory, by looking at the relation eq.(7.7), one can observe that adjoint fermions are coupled to an abelian background field with phases twice as large as those for the fundamental fermions, given in eq.(4.30) (a similar statement can be made for the symmetric and adjoint fermions in $SU(3)$).

Following this observation we choose to modify the background field for the non-fundamental representations by scaling the original BF with a factor $1/2$, expecting that a weaker version of the BF would induce smaller cutoff effects on the fermions. This is done simply by replacing the phases in eq.(4.29) by

$$\phi_i \longrightarrow \frac{\phi_i}{2}. \tag{7.16}$$

Note that the modification of the phases ϕ_i affects as well the normalisation k in eq.(6.2).

With the new BF, which we will denote as halved BF (HBF), we proceed to calculate again the 1 loop fermionic contribution to the coupling $p_{1,1}(L/a)$ to determine the size of the cutoff effects in the SSF. Note, however, that a modification of the background field affects the spectrum of the Dirac operator, and hence the profile of

minimum eigenvalues $\lambda_{\min}(\theta)$ as a function of the phase θ must be scanned again to fix a value which minimizes the condition number. A list of values for the HBF is shown in table (7.2.1).

	$SU(2)_f$	$SU(2)_a$	$SU(3)_f$	$SU(3)_a$	$SU(3)_s$
θ	0	$\pi/6$	$\pi/10$	$\pi/8$	0

Table 7.2.1: Angle θ in the fermionic boundary conditions in the spatial directions which leads to a highest $\lambda_{\min}$ for the weaker background field HBF.

After fixing θ again, we are ready to compute the 1 loop cutoff effects as we have done many times by now in this thesis.

The results for the fundamental and adjoint representations of $SU(2)$ are shown in fig.(7.2.1). The large cutoff effects seen for the adjoint representation with the original BF have disappeared. Their behaviour for the HBF (fig.(7.2.1) bottom panels) resembles the behaviour in the fundamental representation with the original BF. For the standard SF, $\delta_{1,1}$ due to adjoint fermions is practically zero after improvement. For the χSF, some lattice artefacts are left in the smallest lattices but are already at the 15% level for $L/a = 6$, which is an order of magnitude below the case for the original BF. We can conclude that for the HBF, the cutoff effects due to adjoint fermions are completely understood.

However, when switching from the BF to the HBF, the good behaviour of the fundamental representation is spoiled. For the HBF the cutoff effects $\delta_{1,1}$ due to fundamental fermions are large in the SF (fig.(7.2.1) top-left panel) and very large for the χSF (fig.(7.2.1) top-right panel). Also, the regime linear in $(a/L)^2$ is reached quite late. This is analogous to the cutoff effects due to adjoint fermions with the original BF.

The situation is very similar for $SU(3)$. In figure (7.2.2) we show the fundamental and symmetric representations of $SU(3)$ after switching to the HBF. As in the case for $SU(2)$, the large cutoff effects for the symmetric representation have disappeared, but the good behaviour of the fundamental representation has been lost.

Once embarking on non-perturbative simulations, it is necessary to have cutoff effects as small as possible. In particular, if one trusts the 1 loop cutoff effects, the situation for the non-fundamental representations with the original choice of BF seems

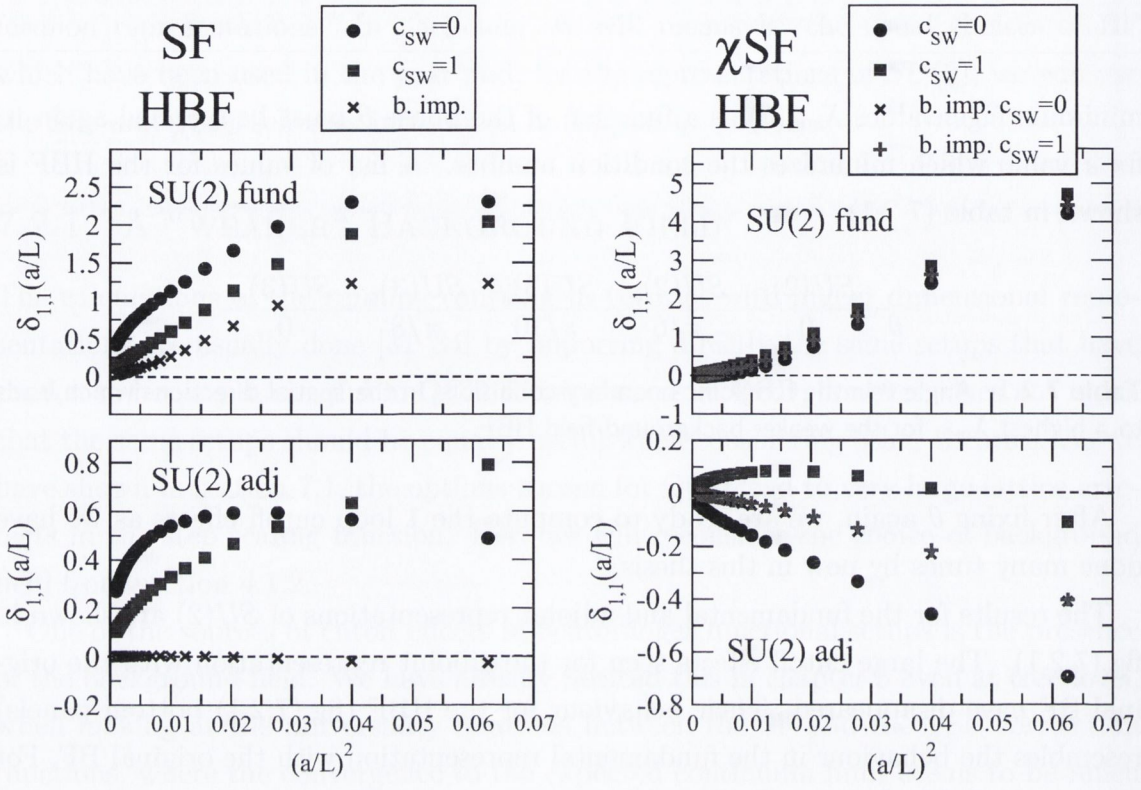

Figure 7.2.1: Cutoff effects $\delta_{1,1}$ for $SU(2)$ in the fundamental (top panels) and adjoint (bottom panels) representations of the gauge group, using the weak version of the background field HBF.

intolerable. The lattice artefacts for the lattice sizes currently used in simulations are too large, and the regime linear in $(a/L)^2$ is reached too late. This can compromise the continuum extrapolation. Considering the weakened version of the background field HBF seems a natural choice to avoid this problem. A more systematic study on these lines has appeared in [107], where they vary the parameters of the boundary fields within a specific window, seeking for values for which cutoff effects are minimal. Their conclusion matches the results presented here. A non-perturbative study of $SU(2)$ with two flavours of adjoint fermions following the strategy presented here is currently being done [98].

A drawback of altering the background field along the way described, is that the HBF does not satisfy the criteria presented in section 4.1.2, which lead to a particularly well behaved family of BF. Some numerical tests calculating the coupling constant seem to indicate that the HBF leads to a reduction of the signal to noise ratio, such that in order to obtain the same variance in the coupling as it is typically

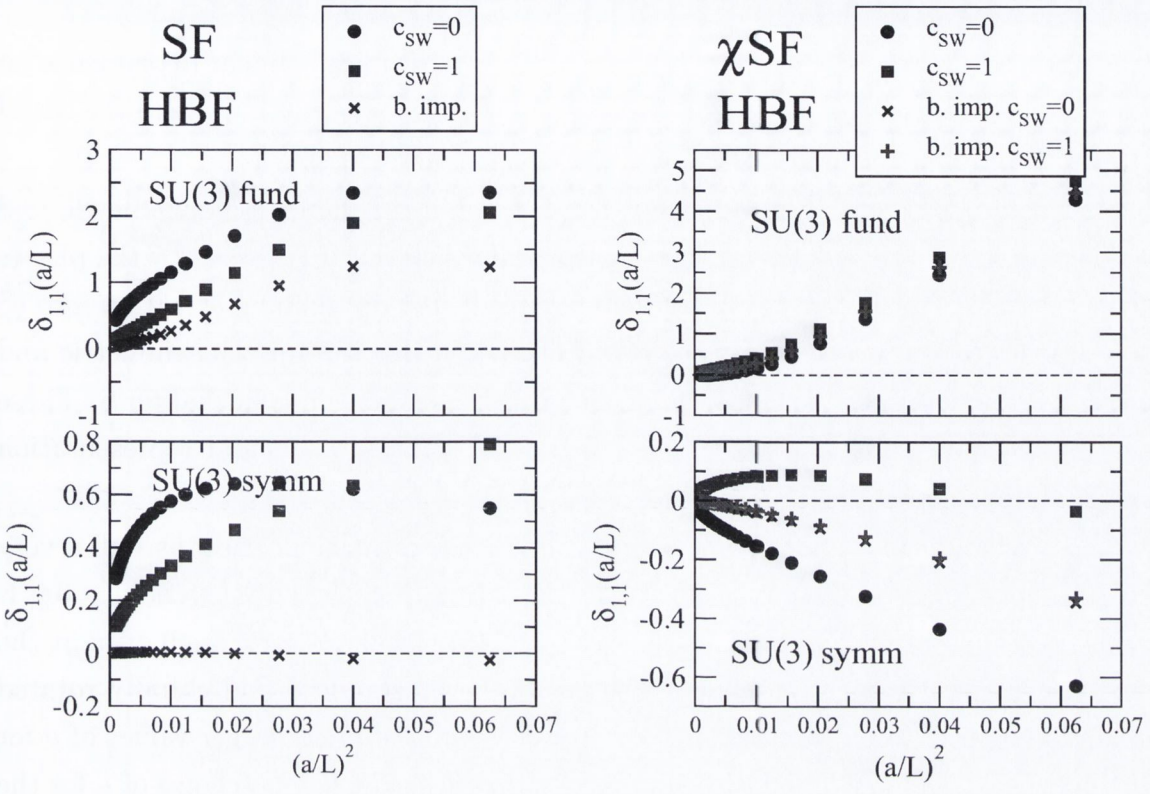

Figure 7.2.2: Cutoff effects $\delta_{1,1}$ for $SU(3)$ in the fundamental (top panels) and symmetric (bottom panels) representations of the gauge group, using the weak version of the background field HBF.

obtained for the original BF, with the HBF one would need roughly four times more statistics. Moreover, modifying the BF requires to recompute again the pure gauge contributions to the 1-loop coupling to know the total cutoff effects.

7.2.2 Using the SF_ν scheme

For $SU(3)$ we can consider another strategy to reduce the large cutoff effects in the step scaling function. In section 6.4.2, after defining the SF_ν and χSF_ν schemes, we have observed a very strong dependence of the cutoff effects on the parameter ν. In fact, by considering large deviations from $\nu = 0$, we have shown that very large cutoff effects can be induced for fundamental fermions, reaching a situation which resembles that of the non-fundamental representations seen in section 7.1.4.

A natural question to ask is then whether the cutoff effects in the SSF for fermions

transforming under non-fundamental representations display a similar dependence on the parameter ν. If so, adjusting ν correctly could lead to a situation where the cutoff effects are minimal without modifying the background field at all.

We explore this idea by computing the observable $\overline{v}(L/a)$ for the symmetric and adjoint representations of $SU(3)$, using the standard choice of BF given by the phases eq.(4.30). Then the SF_ν and χSF_ν schemes are set up by combining $\overline{g}^2$ with $\overline{v}$ into $\overline{g}^2_\nu$ through eq.(6.47). We calculate the cutoff effects on the SSF for the symmetric and adjoint representations in the SF_ν and χSF_ν schemes as was done in chapter 6. These are displayed in fig.(7.2.3) together with those for the fundamental representation calculated in section 6.4.2.

The cutoff effects $\delta_{1,1}$ for the non-fundamental representations show as well a very strong dependence on the parameter ν. By departing from the initial value $\nu = 0$ it is always possible to find a situation where the cutoff effects are very small even at the smallest lattices considered. This is true in both the standard and chirally rotated setups. As can be seen from fig.(7.2.3), the χSF seems to prefer larger values of ν for the minimization of $\delta^\nu_{1,1}$. For the symmetric representation, a good choice of ν for the SF is $\nu \sim 0.3$, while for the χSF is $\nu \sim 0.7$. In the case of the adjoint representation, one would consider $\nu \sim -0.6$ for the SF and $\nu \sim -0.9$ for the χSF.

After considering the cutoff effects due to a single fermion, we study the ν dependence of the cutoff effects for some examples of real theories. For doing this, we need the pure gauge contribution to the cutoff effects. These were calculated in section 6.4.2. When combining the relative fermionic cutoff effects with the pure gauge relative cutoff effects one has to take into account the different normalizations used in the definition eq.(6.45). If we want the full 1-loop cutoff effects normalised to the 1-loop continuum value of the full SSF

$$\delta_1(a/L) = \frac{\Sigma_1(a/L) - \sigma_1}{\sigma_1}, \tag{7.17}$$

then we must combine $\delta_{1,0}$ and $\delta_{1,1}$ following

$$\delta_1(a/L) = A\left(\delta_{1,0}(a/L) + B\delta_{1,1}(a/L)\right), \tag{7.18}$$

where $B = N_f b_{0,1}/b_{1,1}$ and $A = (1+B)^{-1}$.

We consider three particular cases, i.e. $SU(3)$ with $N_f = 4$ fundamental fermions

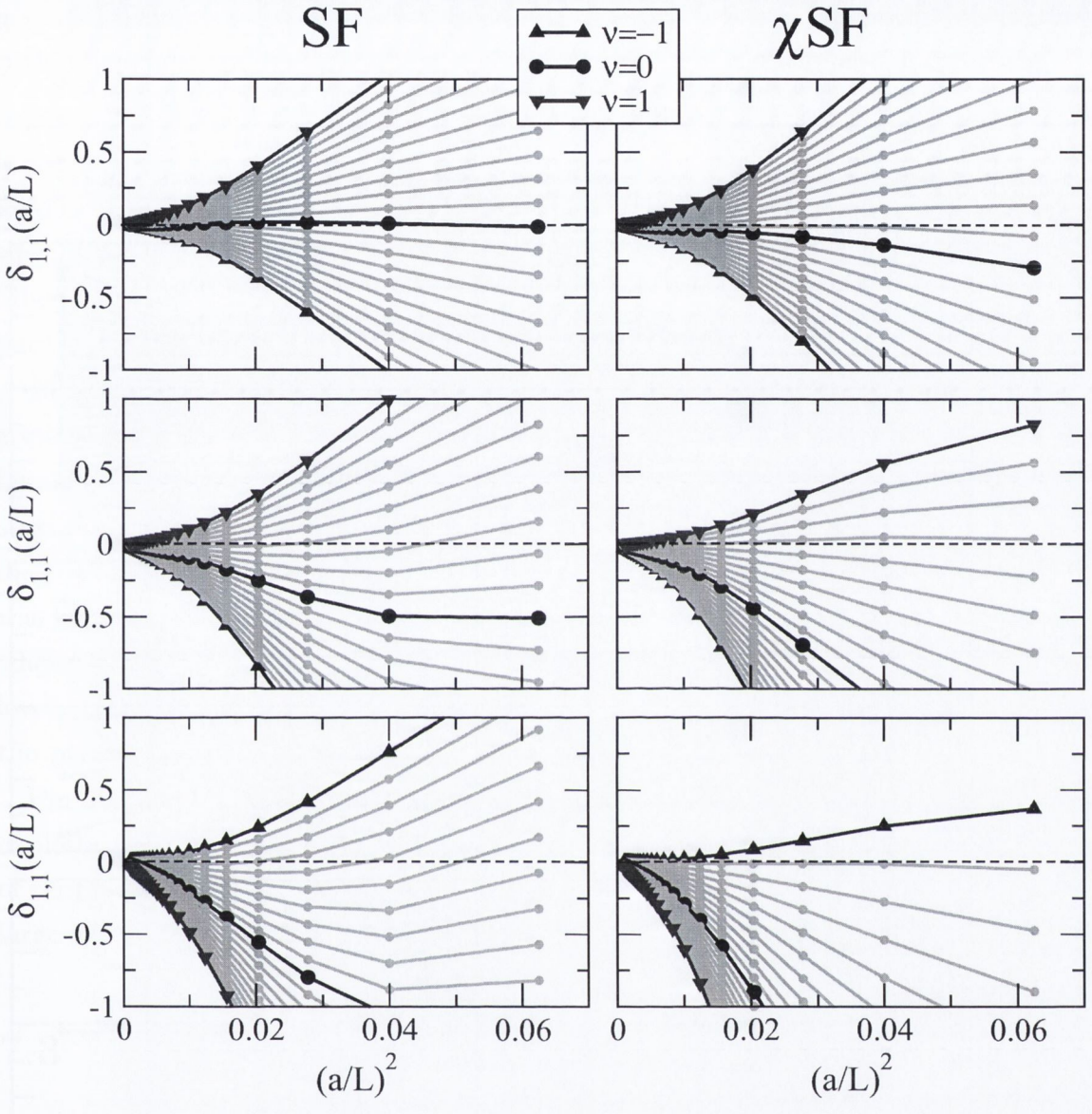

Figure 7.2.3: Cutoff effects $\delta_{1,1}$ as a function of ν for the 1-loop fermionic contribution to the SSF for the fundamental, symmetric and adjoint representations of $SU(3)$. Both the standard SF and χSF setups are considered.

(4 flavour QCD), with $N_f = 2$ symmetric fermions and with $N_f = 2$ adjoint fermions. The cutoff effects in these cases as a function of ν are shown in figure(7.2.4). The general picture is the same as already discussed for the pure fermionic part. However, when considering the full theories, the dependence of the cutoff effect in ν seems to be weaker in 4 flavour QCD than what is seen for the pure fermionic part alone. On

the contrary, the dependence on ν seems stronger for the full adjoint and symmetric theories than what is observed from the contribution of a single flavour.

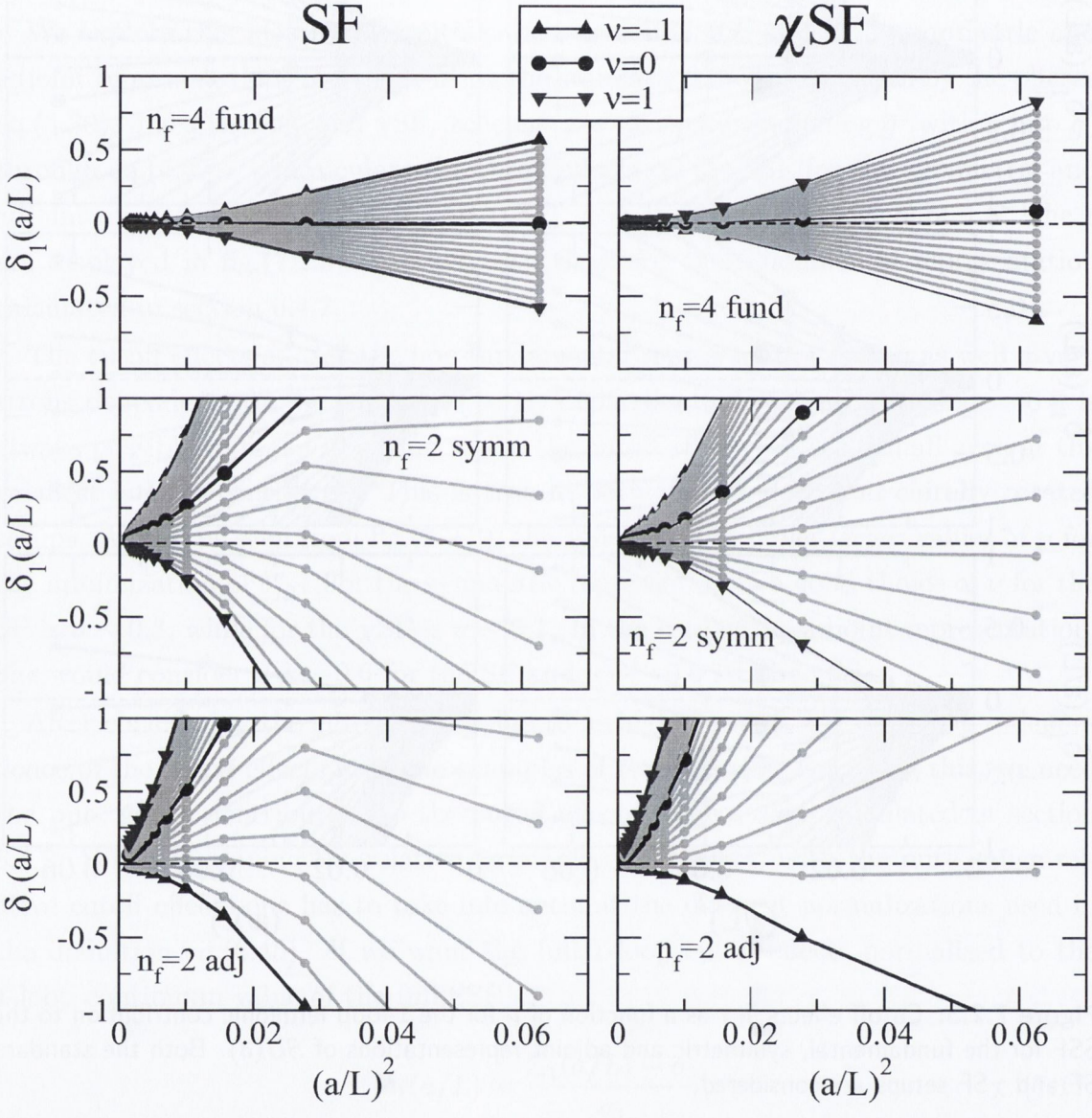

Figure 7.2.4: Cutoff effects δ_1 as a function of ν in the 1-loop SSF. Three theories are considered: $SU(3)$ with four fundamental flavours (top panels), that is, 4 flavour QCD; $SU(3)$ with 2 symmetric flavours (middle panels); and $SU(3)$ wirh 2 adjoint flavours (bottom panels).

Using this strategy has some advantages with respect to the modification of the background field proposed in section 7.2.1. To begin with, as we discussed in section

6.4, considering different values of ν in the boundary phases does not alter the BF since, after taking the derivative in eq.(6.1), the parameter η is set to zero and any reference to ν disappears from the BF. Hence, the good statistical properties seen for the standard choice of BF are not spoiled. Moreover, $\overline{g}^2$ and $\overline{v}$ can be measured independently and then combined into $\overline{g}^2_\nu$ at the data analysis stage. Thus no extra simulations are required for the measurement of the whole family of couplings $\overline{g}^2_\nu$. Since the BF is not modified, all the perturbative calculations for the pure gauge part remain the same and can be recycled from previous calculations.

This strategy, however, has 2 obvious drawbacks. The first is that it cannot be applied to $SU(2)$, since there is only one abelian direction in the algebra $su(2)$ and hence an observable like $\overline{v}$ cannot be constructed. The second drawback is that the statistial fluctuations in $\overline{v}$ tend to be quite larger than those for $\overline{g}^2$. These larger fluctuations will be transmitted into the coupling $\overline{g}^2_\nu$. Fortunately, if the value of ν was kept different from zero but not too large ($|\nu| < 1$), it is possible to find situations where the cutoff effects are reduced and the quality of the signal is kept at a tolerable level. One thus has to find a balance between the elimination of lattice artefacts and the preservation of a good statistical behaviour.

Finally, this strategy is easily extended to gauge groups with $N > 3$ where, as explained in section 6.4, there are more abelian directions in the algebra and a set of renormalized observables $\overline{v}_i$ can be constructed. This could be of use in studies of large N gauge theories such as [77].

7.3 Summary of chapter 7

In this chapter we have examined some of the most common theories studied in search of an infrared fixed point. Among these, the minimal candidate to display either conformal or walking behaviour is $SU(2)$ with two adjoint fermions (popularly known as Minimal Walking Technicolor), which by today has received much attention from several groups. The techniques used to study these models are a direct heritage from QCD.

Here we have calculated the coupling $\overline{g}^2$ in both the SF and the χSF schemes for the fundamental and adjoint representations of $SU(2)$, and for the fundamental, adjoint and symmetric representations of $SU(3)$, to one loop in perturbation theory. We have derived the value of the improvement coefficient $c_t^{(1,1)}$, and computed the

remaining cutoff effects in the SSF. These turn out to be intolerably large for the non-fundamental representations.

In order to reduce the large lattice artefacts we have devised two different strategies. In the first, a modification of the boundary fields is done resulting in a weaker version of the BF. In the second, the SF_ν and $\chi\mathrm{SF}_\nu$ schemes introduced in section 6.4 are used to define the family of couplings $\overline{g}^2_\nu$. The cutoff effects for the step scaling function in these schemes can be minimised by a proper choice of ν.

Although both strategies seem to work a priori, an immedeiate outcome of using them is a worsening of the statistical behaviour of the coupling. In the first case this happens because the weaker HBF does not satisfy the criteria established in section 4.1.2. In the second case, larger statistical fluctuations are induced by using the observable $\overline{v}$ to construct the family of couplings $\overline{g}^2_v$.

In real numerical simulations one desires to have small statistical fluctuations. However, cutoff effects are systematic errors that must be well understood in order to extract reliable physical information. Hence, a balance between a good statistical signal and a reduction of otherwise very large lattice artefacts must be obtained.

The strategy where the BF is weakened is currently under investigation for $SU(2)$ with two adjoint fermions, and its real benefits in numerical simulations still remain inconclusive.

It is important to understand the difficulties associated to the realization of infrared conformality in the lattice. Many studies performed so far represent the first attempts of classification of theories in the (N, N_f) phase diagram. Being exploratory studies, their standards are usually below those expected for traditional QCD.[9] In order to obtain conclusive evidence on the nature of such theories, it is important to revise the methods originally designed for QCD and adapt them carefully.

[9] An alarming fact is the following: in the last few years more studies of beyond QCD theories using SF schemes have appeared than studies for QCD in twenty years.

"I know now why you cry, but it is something I will never do."

Cyberdine Systems 101, model T-800.

8

Concluding Remarks

In this thesis we have studied several aspects of Schrödinger Functional schemes in perturbation theory. In the first chapters we have reviewed some basic ideas of lattice QCD and the use of the Schrödinger Functional as a finite volume scheme for non-perturbative renormalization problems. The chirally rotated (χSF) formulation of the SF was proposed in [1] as a way to restore the mechanism of automatic $O(a)$ improvement in presence of SF boundary conditions for fermions. If automatic $O(a)$ improvement is at work, any bulk $O(a)$ effect in physical observables vanishes. Any remaining $O(a)$ lattice artefacts arise from boundary effects and must be eliminated by adding boundary counterterms in a similar way as for the standard SF. In order to achieve automatic $O(a)$ improvement two parameters must be tuned to their critical values. The first one is the bare quark mass m_0, which must be tuned to m_c. The need for this additive renormalization is common to any lattice regularization using Wilson fermions, since these break explicitly chiral symmetry. The second parameter z_f is the coefficient of a dimension 3 counterterm at the boundaries. It must be tuned to restore the $\gamma_5\tau^1$ symmetry broken by the lattice regulator. The parameter z_f is

exclusive to the χSF formulation. After automatic $O(a)$ improvement is implemented, the standard improvement terms proportional to the coefficient $c_{\rm SW}$ and to any $O(a)$ improvement coefficient for composite fields[1] are not needed any more.[2] In practice, the removal of boundary $O(a)$ effects from physical quantities can be performed by adding only 2 boundary counterterms. The first one, proportional to a coefficient c_t, is added to the gauge part of the action. The second one, proportional to d_s, is needed for improving the fermion action, and is analogous to the $\widetilde{c}_t$ counterterm in the standard SF. A perturbative determination of the boundary coefficients will be enough for a reasonable cancellation of the $O(a)$ boundary effects.

In chapter 5 we have presented the definition of a set of correlation functions in both the SF and the χSF setups. We have expanded them to one loop in perturbation theory and used the results of their numerical evaluation for discussing several aspects of the χSF. In particular, the following points have been addressed:

- For the standard SF we have considered the family of correlation functions given by f_X, k_Y, f_1 and k_1, where X and Y denote different combinations of gamma matrices in the fermion bilinears. For the χSF, we have considered the family given by the correlations $g_X^{f_1,f_2}$, $l_Y^{f_1,f_2}$, $g_1^{f_1,f_2}$ and $l_1^{f_1,f_2}$, where f_1 and f_2 are flavour indices.

- The previous correlation functions have been expanded to 1-loop in perturbation theory for a setup with a vanishing background field. A program has been written in Fortran for the numerical evaluation of all the correlation functions in both the SF and χSF setup. The simultaneous evaluation of all the correlation functions in a given setup can be done up to lattice sizes of $L/a = 48$ within reasonable time. For the SF, direct comparison could be done with data calculated in previous studies. In particular, we have used the Pastor package to generate data for small lattices with several choices of kinematic parameters and confirmed our results to machine precision. For the χSF, this is the first perturbative study to appear and no comparison has been done yet with an independent calculation. We have performed, however, a set of consistency checks on our data. For instance, we have checked that the final results are independent from the choice of gauge, that paired diagrams contribute in exactly

[1] Like for example $c_{\rm A}$ and $c_{\rm V}$ for the flavour currents [24].
[2] When considering physical observables.

the same way, and (as we will later explain) that some results as the critical mass calculated in the χSF setup converge in the continuum limit to the value obtained in the standard SF setup.

- With the results of the perturbative calculation, we have been able to extract the 1-loop coefficients $m_c^{(1)}(L/a)$, $z_f^{(1)}(L/a)$ and $d_s^{(1)}(L/a)$, from which we extrapolate their continuum values. The coefficients $m_c^{(1)}$ and $z_f^{(1)}$ have been obtained for the choices $c_{\rm SW} = 0$ and $c_{\rm SW} = 1$. As expected, the values for $m_c^{(1)}$ match exactly the known results from the literature, which is a confirmation of the correctness of our calculation. $z_f^{(1)}$ is evaluated using several renormalization conditions, all leading to the same continuum result. At finite lattices, the differences Δz_f in the determination of $z_f^{(1)}(L/a)$ from different conditions behave linearly in a/L for $c_{\rm SW} = 0$, and at a higher rate in a for $c_{\rm SW} = 1$. $d_s^{(1)}$ has only been calculated for $c_{\rm SW} = 1$. The coefficients $z_f^{(1)}$ and $d_s^{(1)}$ are presented here for the first time. These are given as explicit functions of group theoretical factors. Hence, they can be used for any group and representation.

- After determining $m_c^{(1)}(L/a)$ and $z_f^{(1)}(L/a)$ we perform a set of tests to confirm that automatic $O(a)$ improvement is at work. First, the correct realisation of the boundary conditions are tested by studying correlation functions constructed with opposite projectors in the boundary operators. These vanish as $a \to 0$, confirming then that the correct boundary conditions are recovered in the continuum. Then, a set of odd correlation functions are studied. For $c_{\rm SW} = 0$ they vanish linearly as the continuum limit is approached, which confirms that they are indeed an $O(a)$ effect. For the choice $c_{\rm SW} = 1$, they vanish at a rate higher in a. The particular choice of parameters $c_{\rm SW} = 1$ and $\theta = 0$ yields a situation where cutoff effects are highly suppressed.

- Finally, we consider some universality relations of correlation functions between the SF and the χSF. In particular we study the convergence of the ratios $\left[g_X/\sqrt{g_1}\right] \times \left[f_X/\sqrt{f_1}\right]^{-1} \xrightarrow{a/L\to 0} 1$, with $X = A, P$. At tree level we confirm the expected behaviour with and without the presence of a background field. It is remarkable that cutoff effects are much larger in the case where the BF is present. At 1-loop, we study only the case without background field, for which universality is again confirmed.

In chapter 6 we move to a setup with an abelian background field in order define the running coupling in the Schrödinger Functional in the usual way. We first discuss the definition of the step scaling function and its cutoff effects and we write their expansion to 2-loops. The chapter is then divided into two different parts. The first part is composed of sections 6.2 and 6.3. The main results achieved in this part are:

- In section 6.2, after reviewing the perturbative expansion of the coupling, the step scaling function and its cutoff effects, we re-consider the criterion to fix the boundary phase θ of the spatial boundary conditions for the fermion fields. θ is chosen as in ref [80] to minimise the condition number of the squared fermion operator Δ_2. We review this criterion here for its later use in chapter 7.

- We have calculated the 1-loop contribution to the coupling due to fermions regularised with the χSF setup. The calculation of the coefficient $p_{1,1}(L/a)$ in the χSF has been done here for the first time. We have extracted the first coefficients of the asymptotic expansion of $p_{1,1}$ in a/L. The continuum coefficient is equal to the one obtained for the standard SF, which is a further confirmation of the universality of the two setups.

- The fermionic contribution $c_t^{(1,1)}$ to the boundary improvement coefficient of the gauge action has been calculated by demanding cutoff effects linear in a/L to be absent from $p_{1,1}(L/a)$. The value of $c_t^{(1,1)}$ has been obtained directly from the coefficient of the term linear in a/L in the asymptotic expansion of $p_{1,1}$. The value of $c_t^{(1,1)}$ has been calculated in this thesis for the first time, although it has already been presented in conference proceedings [101, 102].

- An important question to address for non-perturbative calculations is how precisely the tuning of the coefficients m_0 and z_f should be done. Uncertainties in satisfying the tuning conditions will induce uncertainties in physical observables. For that, we study the sensitivity of $p_{1,1}$ and of the step scaling function $\Sigma_{1,1}$ to the parameters m_0 and z_f. The derivatives $dp_{1,1}/dz$ and $dp_{1,1}/dz_f$, where $z = Lm_0$, are calculated simultaneously to $p_{1,1}$. We find that the uncertainties induced on $\Sigma_{1,1}$ are in fact small for a quite tolerant range of uncertainties for z_f and m_0.

- Finally, we study the cutoff effects $\delta_{1,1}(a/L)$ on the fermionic part of the step scaling function $\Sigma_{1,1}$ for both the χSF and the SF setup. For the χSF, cutoff

effects are small after implementing boundary improvement. The form of the cutoff effects is very similar for the choices $c_{\rm SW} = 0$ and 1. For the standard SF, after implementing boundary improvement and fixing $c_{\rm SW} = 1$, the remaining cutoff effects are essentially zero. It is remarkable that before improvement the size of the cutoff effects is quite large.

In the second part of chapter 6 we have combined the renormalized coupling $\overline{g}^2$ with the renormalized observable $\overline{v}$ to construct a family of couplings $\overline{g}^2_\nu$ which depends on a parameter ν. The two observables $\overline{g}^2$ and $\overline{v}$ can be computed in the same simulation, and hence all the family $\overline{g}^2_\nu$ can be calculated at no extra cost. This permits to define the renormalization schemes denoted by SF_ν and $\chi\mathrm{SF}_\nu$. For the value $\nu = 0$ the standard SF and χSF schemes are recovered. Also, in the chiral and continuum limit, the SF_ν and the $\chi\mathrm{SF}_\nu$ are equivalent. For these schemes, we have performed the following studies:

- We have expanded the coupling $\overline{g}^2_\nu$ to 2-loops in perturbation theory. The 1-loop coefficient $p^\nu_{1,1}(L/a)$ has been computed explicitely for the χSF.

- For both SF_ν and $\chi\mathrm{SF}_\nu$, we have studied the ν dependence of the cutoff effects in the step scaling function. We find a very strong dependence on the parameter ν. In fact, when going to large values of ν, very large lattice artefacts are induced even if $O(a)$ improvement is implemented. Different fermion regularizations seem to display minimal cutoff effects for different choices of ν. The choice $\nu = 0$ leads to minimal cutoff effects in the standard SF. For the χSF, the optimal value is $\nu \sim 0.1$. A similar observation has been made for staggered regularizations [103]. Using data available in the literature, we have been able to reconstruct the ν dependence of the cutoff effects up to two loop order. This has been done for the pure Yang-Mills and the two flavor theory. The scenario dependence on ν seen in the one loop cutoff effects is preserved at two loops.

- Finally, we have computed the coefficients to match the coupling $\overline{g}^2_\nu$ with the coupling in the $\overline{\mathrm{MS}}$ scheme to two loops. This will be the same for both SF_ν and $\chi\mathrm{SF}_\nu$, since both are equivalent in the continuum limit. Making use of the 1-loop matching coefficient, the relation between lambda parameters $\Lambda_{\mathrm{SF}_\nu}/\Lambda_{\overline{\mathrm{MS}}}$ in both schemes has been established. Morover, since the 3 loop coefficient of the β-function for the $\overline{\mathrm{MS}}$ scheme is known, we have been able to obtain the 3 loop coefficient in the SF_ν as well.

The application of SF_ν and $\chi\mathrm{SF}_\nu$ will be particularly useful when considering theories with fermions which transform under other representations of the gauge group, for which cuttoff effects can be extremely large.

In chapter 7 we study the application of the techniques discussed previously to other strongly interacting theories. In particular, we consider theories with the gauge groups $SU(2)$ and $SU(3)$, with fermions transforming under the fundamental, adjoint and symmetric representations (for $SU(2)$ the adjoint and symmetric representations are equivalent). In the present chapter we have performed the following studies:

- We have adapted the Dirac operator to an arbitrary representation $\mathcal{R}$ by mapping the fundamental link variables to the desired representation. A modification in the color structure implies a change in the eigenvalues of the Dirac operator. Hence, we recalculate the optimal value of θ for all the cases considered.

- The 1-loop fermionic contribution to the coupling $p_{1,1}(L/a)$ has been calculated for the previous groups and representations in both SF and χSF setups. The fermion contribution to the boundary improvement coefficient is obtained by scaling the values calculated for the fundamental representation in chapter 6. We have calculated the remaining cutoff effects on the step scalimg function which, for non-fundamental representations, turn out to be very large even after $O(a)$ improvement.

- In order to reduce the large higher order cutoff effects we consider two different strategies. Firstly, we consider a weaker version of the background field by dividing the boundary phases. This seems to cure the large cutoff effects for the non-fundamental representations, but spoils the good behaviour of the fundamental (In both $SU(2)$ and $SU(3)$). Moreover, the quality of the signal in numerical simulations seems to be worse in this case. The second strategy consists in using the SF_ν and $\chi\mathrm{SF}_\nu$ schemes defined in chapter 6. We can take advantage of the large dependence of the cutoff effects on the parameter ν to find choices for which the remaining lattice artefacts are dramatically reduced. This strategy seems to work very well but, unfortunately, can only be applied with groups of rank ≥ 2.

A non-perturbative study of the $SU(2)$ theory with $N_f = 2$ adjoint fermions using the weakened version of the BF is currently under way [98].

Summarising, in this thesis we have tested the chirally rotated Schrödinger functional scheme to 1-loop order in perturbation theory. With the results presented here the renormalization and $O(a)$ improvement of the action in the χSF scheme to 1-loop order is completed. The universality of both SF and χSF has been confirmed. We have presented some strategies to deal with strongly interacting theories other than QCD. Our results are a starting point for the use of the χSF in non-perturbative simulations of either QCD or other strongly coupled theories. The codes developed are easily extendible to include highly improved gauge actions like the Lüscher-Weisz action. Moreover, the perturbative calculations presented here are the basis for further perturbative computations, for instance, of the renormalization coefficients Z_X of composite operators.

A

Notation and conventions

In the present appendix we specify the notational conventions used in the thesis, together with some useful group theoretical factors and relations.

A.1 Index conventions

Here we collect some notation involving the different indices used in the thesis. Any difference to these conventions would be explicitly indicated in the text.

- Lorentz indices are denoted $\mu, \nu, ...$ and run from 0 to 3.
- Spatial indices are denoted $k, l, ...$ and run from 1 to 3. The temporal component is denoted by 0.
- Dirac indices are denoted $\alpha, \beta, ...$ and run from 1 to 4.
- Flavour indices are denoted $f_1, f_2, ...$ and are used to denote specific flavour components rather than to index the generators of the flavour group. They adopt values u, u', d and d'.

- Color components are denoted $a, b, ...$ and run from 1 to $d_{\mathcal{R}}$, where $d_{\mathcal{R}}$ is the dimension of the representation of the color group.
- 4-vectors are denoted by variables in italic $x, p, ...$
- 3-vectors are denoted by variables in bold $\mathbf{x}, \mathbf{p}, ...$
- Sums over indices are in general written explicitly. If they are omitted for notational clarity, repeated indices are always assumed to be summed over. The contrary will be explicitly indicated.
- Scalar products of the form $px = p_\mu x_\mu$ are always taken with Euclidean metric. In case the Minkowski metric is needed in a specific expression it will be stated explicitly.

A.2 Dirac Matrices in Euclidean space and relation to Minkowski space

The Euclidean metric is given by $g_{\mu\nu} = \delta_{\mu\nu}$, such that there is no difference between covariant and contravariant vectors. We use the Dirac matrices in the chiral basis, which in Euclidean space is given by

$$\gamma_\mu = \begin{pmatrix} 0 & e_\mu \\ e_\mu^\dagger & 0 \end{pmatrix}. \tag{A.1}$$

The 2×2 matrices e_μ are given by

$$e_0 = -\mathbb{I}_{2\times 2}, \qquad e_k = -i\sigma_k, \tag{A.2}$$

where σ_k are the Pauli matrices defined below. The Dirac algebra is given by

$$\{\gamma_\mu, \gamma_\nu\} = 2\delta_{\mu\nu}, \qquad \gamma_\mu = \gamma_\mu^\dagger. \tag{A.3}$$

The fifth gamma matrix is defined as $\gamma_5 \equiv \gamma_0\gamma_1\gamma_2\gamma_3$. In the chiral basis it reads

$$\gamma_\mu = \begin{pmatrix} \mathbb{I}_{2\times 2} & 0 \\ 0 & -\mathbb{I}_{2\times 2} \end{pmatrix}, \tag{A.4}$$

and satisfies

$$\gamma_5 = \gamma_5^\dagger, \qquad \gamma_5^2 = \mathbb{I}, \qquad \{\gamma_\mu, \gamma_5\} = 0. \tag{A.5}$$

The hermitean tensor $\sigma_{\mu\nu}$ is defined as

$$\sigma_{\mu\nu} = \frac{i}{2}\left[\gamma_\mu, \gamma_\nu\right], \qquad \sigma_{\mu\nu}^\dagger = \sigma_{\mu\nu}. \tag{A.6}$$

The components of $\sigma_{\mu\nu}$ are explicitly given by

$$\sigma_{0k} = \begin{pmatrix} \tau^k & 0 \\ 0 & -\tau^k \end{pmatrix}, \qquad \sigma_{ij} = -\epsilon_{ijk} \begin{pmatrix} \tau^k & 0 \\ 0 & \tau^k \end{pmatrix}. \tag{A.7}$$

The Wick rotation from Euclidean to Minkowski space amounts to a rotation of the temporal coordinate of $\alpha = \pi/2$ in the complex plane, such that the Euclidean and Minkowski temporal coordinates are related by

$$x_0^E = -ix_0^M. \tag{A.8}$$

The Minkowski metric is given by $g_{\mu\nu} = \mathrm{diag}(-1, 1, 1, 1)$. With this metric, the scalar product of two 4-vectors $x = (ct, \mathbf{x})$ and $p = (E/c, \mathbf{p})$ is given by

$$px = p^\mu x_\mu = g_{\mu\nu} p^\mu x^\nu = -Et + \mathbf{px}. \tag{A.9}$$

The Dirac matrices in Euclidean space are related to their Minkowski versions via

$$\gamma_0^E = -i\gamma_0^M \qquad \gamma_k^E = \gamma_k^M. \tag{A.10}$$

They satisfy the relations

$$(\gamma_M^\mu)^\dagger = \gamma_M^0 \gamma_M^\mu \gamma_M^0, \qquad \{\gamma_M^\mu, \gamma_M^\nu\} = 2g^{\mu\nu}, \tag{A.11}$$

and their squares are

$$\left(\gamma_M^0\right)^2 = -\mathbb{I}, \qquad \left(\gamma_M^k\right)^2 = \mathbb{I}. \tag{A.12}$$

Finally, the relation between the covariant and contravariant versions of the Dirac

matrices in Minkowski space is given by

$$\gamma_M^0 = -\gamma_0^M, \qquad \gamma_M^k = \gamma_k^M. \tag{A.13}$$

A.3 Group Theory

Here we collect all the concepts and notation of group theory appearing through the thesis. We denote by $SU(N)$ the special unitary Lie groups and by $su(N)$ their corresponding Lie algebras. An element of $SU(N)$ is a complex, unitary matrix of determinant 1.

A group element $U \in SU(N)$ is represented as the exponential of a complex, anti-hermitean and traceless matrix $A \in su(N)$ as

$$U = e^A, \tag{A.14}$$

which guarantees unitarity

$$U^\dagger U = \mathbb{I} \quad \Rightarrow \quad U^\dagger = U^{-1}. \tag{A.15}$$

The most general matrix $A \in su(N)$ can be written as

$$A = i \sum_{a=1}^{N^2-1} \omega^a T^a, \tag{A.16}$$

where ω^a are $N^2 - 1$ real parameters and T^a are the $N^2 - 1$ generators of the algebra $su(N)$. The generators satisfy

$$\left[T^a, T^b\right] = i f^{abc} T^c, \qquad \mathrm{tr}\left[T^a T^b\right] = \frac{1}{2}\delta_{ab}, \tag{A.17}$$

where f^{abc} are the totally anti-symmetric structure constants.

For the case of $SU(2)$, the generators are usually constructed as

$$T^a = \frac{1}{2}\tau^a, \tag{A.18}$$

where τ^a are the Pauli matrices defined as

$$\tau^1 = \begin{pmatrix} 0 & 1 \\ 1 & 0 \end{pmatrix}, \qquad \tau^2 = \begin{pmatrix} 0 & -i \\ i & 0 \end{pmatrix}, \qquad \tau^3 = \begin{pmatrix} 1 & 0 \\ 0 & -1 \end{pmatrix}. \tag{A.19}$$

The generators of $SU(3)$ are the constructed as

$$T^a = \frac{1}{2}\lambda_a. \tag{A.20}$$

where λ_a are the Gell-Mann matrices given by

$$\begin{aligned}
\lambda_1 &= \begin{pmatrix} 0 & 1 & 0 \\ 1 & 0 & 0 \\ 0 & 0 & 0 \end{pmatrix} & \lambda_2 &= \begin{pmatrix} 0 & -i & 0 \\ i & 0 & 0 \\ 0 & 0 & 0 \end{pmatrix}, \\
\lambda_4 &= \begin{pmatrix} 0 & 0 & 1 \\ 0 & 0 & 0 \\ 1 & 0 & 0 \end{pmatrix} & \lambda_5 &= \begin{pmatrix} 0 & 0 & -i \\ 0 & 0 & 0 \\ i & 0 & 0 \end{pmatrix}, \\
\lambda_6 &= \begin{pmatrix} 0 & 0 & 0 \\ 0 & 0 & 1 \\ 0 & 1 & 0 \end{pmatrix} & \lambda_7 &= \begin{pmatrix} 0 & 0 & 0 \\ 0 & 0 & -i \\ 0 & i & 0 \end{pmatrix}, \\
\lambda_3 &= \begin{pmatrix} 1 & 0 & 0 \\ 0 & -1 & 0 \\ 0 & 0 & 0 \end{pmatrix} & \lambda_8 &= \tfrac{1}{\sqrt{3}} \begin{pmatrix} 1 & 0 & 0 \\ 0 & 1 & 0 \\ 0 & 0 & -2 \end{pmatrix}.
\end{aligned} \tag{A.21}$$

An alternative basis to the $su(3)$ algebra commonly used is the set of matrices $\widetilde{\lambda}_a$, which coincide with the Gell-Mann matrices λ_a in all cases except for the two diagonal matrices, which read

$$\widetilde{\lambda}_3 = -\frac{1}{2}\lambda_3 + \frac{\sqrt{3}}{2}\lambda_8, \tag{A.22}$$

$$\widetilde{\lambda}_8 = \frac{\sqrt{3}}{2}\lambda_3 + \frac{1}{2}\lambda_8. \tag{A.23}$$

Another set of generators $\widetilde{T}^a$ can be defined normalising the $\widetilde{\lambda}_a$ matrices as,

$$\widetilde{T}^a = \frac{1}{2}\widetilde{\lambda}_a. \tag{A.24}$$

A.3.1 Group theory factors

In a generic representation of the group $SU(N)$, the normalisation of the generators is fixed by demanding that

$$\left[T^a_{\mathcal{R}}, T^b_{\mathcal{R}}\right] = if^{abc}T^c_{\mathcal{R}}, \tag{A.25}$$

where the structure constants f^{abc} have the same values in all representations. The normalisation of the trace in a generic representation $T_{\mathcal{R}}$ and the quadratic Casimir operator $C_2(\mathcal{R})$ are defined through

$$\mathrm{tr}_{\mathcal{R}}\left(T^aT^b\right) = \mathrm{tr}\left(T^a_{\mathcal{R}}T^b_{\mathcal{R}}\right) = T_{\mathcal{R}}\delta^{ab}, \tag{A.26}$$

and

$$\sum_a \left(T^a_{\mathcal{R}}T^a_{\mathcal{R}}\right)_{AB} = C_2(\mathcal{R})\delta_{AB}, \tag{A.27}$$

such that

$$T_{\mathcal{R}} = \frac{1}{N^2-1}C_2(\mathcal{R})d(\mathcal{R}), \tag{A.28}$$

where $d(\mathcal{R})$ is the dimension of the representation $\mathcal{R}$. The quadratic Casmir operator in the representation $\mathcal{R}$ can be computed from the Young tableau of the representation of $SU(N)$ through the formula

$$C_2(\mathcal{R}) = \frac{1}{2}\left(nN + \sum_{i=1}^{m} n_i(n_i + 1 - 2i) - \frac{n^2}{N}\right), \tag{A.29}$$

where n is the number of boxes in the diagram, the range of i goes over the rows of the Young tableau, m is the number of rows and n_i is the number of boxes in the i-th row.

In table tab.(A.3.1) we collect the quantities $d(\mathcal{R})$, $T_{\mathcal{R}}$ and $C_2(\mathcal{R})$ for the 2-index representations.

A.3.2 Mapping to 2-index representations

Starting from the fundamental representation of $SU(N)$, other irreducible representations can be obtained through the tensor product of vector spaces. The 2-index

$\mathcal{R}$	$d(\mathcal{R})$	$T_{\mathcal{R}}$	$C_2(\mathcal{R})$
Fundamental	N	$1/2$	$(N-1)/2N$
Adjoint	N^2-1	N	N
Symmetric	$N(N+1)/2$	$(N+2)/2$	$C_2(F)2(N+2)/(N+1)$
Antisymmetric	$N(N-1)/2$	$(N-2)/2$	$C_2(F)2(N-2)/(N+1)$

Table A.3.1: Group theoretical factors for the 2-index representations of $SU(N)$.

representations are constructed through

$$N \otimes N = \overline{\frac{N(N-1)}{2}} \oplus \frac{N(N+1)}{2}, \tag{A.30}$$

corresponding to the 2-index antisymmetric and 2-index symmetric representations, and

$$N \otimes \overline{N} = 1 \oplus N^2 - 1, \tag{A.31}$$

corresponding to the trivial and adjoint representations. For $SU(2)$ this will read

$$\begin{aligned} 2 \otimes 2 &= \overline{1} \oplus 3, \\ 2 \otimes \overline{2} &= 1 \oplus 3, \end{aligned} \tag{A.32}$$

where, since in $SU(2)$ the fundamental 2 and antifundamental $\overline{2}$ representations are equivalent, the adjoint and 2-index symmetric are the same representation with dimension $d(\mathrm{A}) = d(\mathrm{S}) = 3$, and the 2-index antisymmetric is simply the singlet representation. For $SU(3)$, the tensor product yields

$$\begin{aligned} 3 \otimes 3 &= \overline{3} \oplus 6, \\ 3 \otimes \overline{3} &= 1 \oplus 8, \end{aligned} \tag{A.33}$$

The antisymmetric corresponds to the antifundamental with $d(\mathrm{As}) = 3$, the symmetric has dimension $d(\mathrm{S}) = 6$ and the adjoint representation has dimension $d(\mathrm{A}) = 8$.

To write elements $U \in SU(N)$ in arbitrary representations we need the representation function $\widehat{\mathcal{R}}$ which maps from the fundamental to a given representation $\mathcal{R}$ as

$$\widehat{\mathcal{R}} : U \longrightarrow U^{\mathcal{R}}, \tag{A.34}$$

For this purpose, we first have to define for each representation an orthonormal basis

$e_{\mathcal{R}}$ for the appropriate vector space of matrices.

In the fundamental representation, the basis is taken to be formed by the anti-hermithean generators T_F^a constructed as follows. For each pair of integers $1 \leq k < l \leq N$, we define two generators as:

$$\begin{aligned} \left(T_F^{lk,+}\right)_{mn} &= \frac{1}{2}\left(\delta_{mk}\delta_{nl} + \delta_{ml}\delta_{nk}\right), \\ \left(T_F^{lk,-}\right)_{mn} &= \frac{i}{2}\left(\delta_{mk}\delta_{nl} - \delta_{ml}\delta_{nk}\right), \end{aligned} \tag{A.35}$$

and for each $1 \leq k < N$ we define another generator as:

$$\left(T_F^k\right) = \frac{1}{\sqrt{2k(k+1)}}\mathrm{diag}\left(\underbrace{1, 1, ..., -k}_{k+1 \text{ terms}}, 0, ..., 0\right), \tag{A.36}$$

The generators T_F^a are normalized so that $T_F = 1/2$. For $SU(2)$, the generators are $T_F^a = \tau^a/2$, where τ^a are Pauli matrices. For $SU(3)$, they correspond to $T_F^a = \lambda^a/2$, where λ^a are Gell-Mann matrices.

For the adjoint representation we define the basis e_A for the $N \times N$ traceless hermitean matrices to be

$$e_A^a = \frac{T_F^a}{\sqrt{T_F}}; \qquad a = 1, ..., N^2 - 1, \tag{A.37}$$

For the 2-index symmetric representation the basis $e_S^{(ij)}$, with $i \leq j$, for the $N \times N$ symmetric matrices is:

$$\begin{aligned} \left(e_S^{(ij)}\right)_{kl} &= \frac{1}{\sqrt{2}}\left(\delta_{ik}\delta_{jl} + \delta_{jk}\delta_{il}\right), && \text{for } i \neq j, \\ \left(e_S^{(ij)}\right)_{kl} &= \delta_{ki}\delta_{li}, && \text{for } i = j, \end{aligned} \tag{A.38}$$

For the 2-index antisymmetric representation the base $e_{As}^{(ij)}$, with $i < j$, for the $N \times N$ antisymmetric matrices is:

$$\left(e_{As}^{(ij)}\right)_{kl} = \frac{1}{\sqrt{2}}\left(\delta_{ik}\delta_{jl} - \delta_{jk}\delta_{il}\right); \qquad \text{where } i < j. \tag{A.39}$$

Finally, the maps $\widehat{\mathcal{R}}$ are given explicitly by

$$\left(\widehat{\mathcal{R}}(A)U\right)_{ab} = U^{\mathrm{A}}_{ab} = 2\mathrm{Tr}[e^a_A U e^b_A U^\dagger]; \qquad a,b = 1,...,N^2-1, \tag{A.40}$$

for the adjoint representation,

$$\left(\widehat{\mathcal{R}}(S)U\right)_{(ij)(lk)} = U^{\mathrm{S}}_{(ij)(lk)} = \mathrm{Tr}\left[\left(e^{(ij)}_S\right)^\dagger U e^{(lk)}_S U^T\right]; \qquad i \le j, l \le k, \tag{A.41}$$

for the 2-index symmetric representation, and

$$\left(\widehat{\mathcal{R}}(As)U\right)_{(ij)(lk)} = U^{\mathrm{As}}_{(ij)(lk)} = \mathrm{Tr}\left[\left(e^{(ij)}_{As}\right)^\dagger U e^{(lk)}_{As} U^T\right]; \qquad i < j, l < k, \tag{A.42}$$

for the 2-index antisymmetric representation. The group generators on a given representation $T^a_{\mathcal{R}}$ are obtained by acting with the map $\widehat{\mathcal{R}}$ on the generators in the fundamental representation.

A.4 Momenta on the Lattice

It is useful to define some expressions of the momenta which occur frequently in lattice calculations. Given a momentum variable p, we define

$$\widehat{p}_\mu = \left(\frac{2}{a}\right)\sin\left(\frac{ap_\mu}{2}\right), \qquad \widetilde{p}_\mu = \left(\frac{1}{a}\right)\sin\left(ap_\mu\right). \tag{A.43}$$

If boundary conditions are periodic up to a phase θ, the phase usually enters expressions involving the momenta. Hence, we define

$$p^\pm_\mu = p_\mu \pm \frac{\theta_\mu}{L}. \tag{A.44}$$

Spatial momentum 3-vectors are denoted as

$$\mathbf{p} = (p_1, p_2, p_3) \tag{A.45}$$

for which similar expressions as eq.(A.43) can be defined

$$\widehat{p}_k = \left(\frac{2}{a}\right)\sin\left(\frac{ap_k}{2}\right), \qquad \widetilde{p}_k = \left(\frac{1}{a}\right)\sin\left(ap_k\right). \tag{A.46}$$

It is also useful to consider the squares

$$\begin{aligned} \widehat{p}^2 &= \sum_\mu \widehat{p}_\mu \widehat{p}_\mu, \qquad & \widetilde{p}^2 &= \sum_\mu \widetilde{p}_\mu \widetilde{p}_\mu, \\ \widehat{\mathbf{p}}^2 &= \sum_k \widehat{p}_k \widehat{p}_k, \qquad & \widetilde{\mathbf{p}}^2 &= \sum_k \widetilde{p}_k \widetilde{p}_k. \end{aligned} \tag{A.47}$$

A.5 Lattice Derivatives

We define the lattice covariant derivatives acting on a field $\psi(x)$ transforming under the color group. The covariant derivatives involve the link variables $U_\mu(x)$. For clarity, we write the definition of the covariant derivatives acting on fundamental vectors. If other representations of the color group are considered, one should only replace the link variable $U_\mu(x)$ with its associated link variable $U_\mu^{\mathcal{R}}(x)$ in the representation $\mathcal{R}$.

The action on the right of forward and backwards derivatives is given by

$$\begin{aligned} \nabla_\mu \psi(x) &= \frac{1}{a}\left[U_\mu(x)\psi(x+a\hat{\mu}) - \psi(x)\right], \\ \nabla_\mu^* \psi(x) &= \frac{1}{a}\left[\psi(x) - U_\mu(x-a\hat{\mu})^\dagger \psi(x-a\hat{\mu})\right]. \end{aligned} \tag{A.48}$$

The action on the left is similarly given by

$$\begin{aligned} \overline{\psi}(x)\overleftarrow{\nabla}_\mu &= \frac{1}{a}\left[\overline{\psi}(x+a\hat{\mu})U_\mu(x)^\dagger - \overline{\psi}(x)\right], \\ \overline{\psi}(x)\overleftarrow{\nabla}_\mu^* &= \frac{1}{a}\left[\overline{\psi}(x) - \overline{\psi}(x-a\mu)U_\mu(x-a\hat{\mu})\right]. \end{aligned} \tag{A.49}$$

We can further define the symmetric lattice derivatives acting on the right and on the left as

$$\begin{aligned} \frac{1}{2}\left(\nabla_\mu + \nabla_\mu^*\right)\psi(x) &= \frac{1}{2a}\left[U_\mu(x)\psi(x+a\hat{\mu}) - U_\mu(x-a\hat{\mu})^\dagger \psi(x-a\hat{\mu})\right], \\ \overline{\psi}(x)\frac{1}{2}\left(\overleftarrow{\nabla}_\mu + \overleftarrow{\nabla}_\mu^*\right) &= \frac{1}{2a}\left[\overline{\psi}(x+a\hat{\mu})U_\mu(x)^\dagger - \overline{\psi}(x-a\hat{\mu})U_\mu(x-a\hat{\mu})\right], \end{aligned} \tag{A.50}$$

Finally, the covariant lattice version of the d'Alembertian operator is given by

$$\begin{aligned} \nabla_\mu^* \nabla_\mu \psi(x) &= \frac{1}{a^2}\left[U_\mu(x)\psi(x+a\hat{\mu}) + U_\mu(x-a\hat{\mu})^\dagger \psi(x-a\hat{\mu}) - 2\psi(x)\right], \\ \overline{\psi}(x)\overleftarrow{\nabla}_\mu^*\overleftarrow{\nabla}_\mu &= \frac{1}{a^2}\left[\overline{\psi}(x+a\hat{\mu})U_\mu(x)^\dagger + \overline{\psi}(x-a\hat{\mu})U_\mu(x-a\hat{\mu}) - 2\overline{\psi}(x)\right]. \end{aligned} \tag{A.51}$$

A.6 Measures

Here we collect definitions and properties for the Haar and the Grassmann measures used, respectively, in the gauge and the fermionic path integrals.

$$\int_G f(U)dU = \int_G f(U^\dagger)dU$$

A.6.1 Haar measure

The *Haar measure* dU is the measure for integration over a continuous compact group G. It is invariant under left and right multiplication with a group element $V \in G$, i.e.,

$$dU = d(UV) = d(VU). \tag{A.52}$$

When considering a gauge group $SU(N)$, the property eq.(A.52) ensures gauge invariance of the measure in a path integral. The measure dU can be normalised as

$$\int_G dU = 1, \tag{A.53}$$

where the subscript G denotes integration over all the group G. Let $f(U)$ be a function on an element $U \in G$. Integration over G satisfies

$$\int_G f(U)dU = \int_G f(VU)dU = \int_G f(UV)dU \qquad \forall\, V \in G, \tag{A.54}$$

and

$$\int_G f(U)dU = \int_G f(U^\dagger)dU \tag{A.55}$$

An explicit form for dU can be given for the special unitary group $SU(N)$ as follows. Let $U = U(\omega)$ be a group element parametrised through the set of real numbers ω^a as in eq.(A.16). The measure is then given by

$$dU = c\sqrt{\det\left[g(\omega)\right]} \prod_a d\omega^a, \tag{A.56}$$

where c is a normalisation constant to ensure that eq.(A.53) is satisfied, and $g(\omega)$ is a metric tensor in the group defined as

$$g(\omega)_{nm} = \mathrm{tr}\left\{ \frac{\partial U(\omega)}{\partial \omega^n} \frac{\partial U(\omega)^\dagger}{\partial \omega^m} \right\}. \tag{A.57}$$

Since $SU(N)$ are compact groups, the parameters ω^a only need to be integrated over a finite interval for $U(\omega)$ to cover all group elements.

A.6.2 Grassmann measure

In the path integral formulation fermion fields are represented as anti-commuting numbers, called *Grassmann numbers*. A set of Grassmann numbers η_i, $i = 1, ..., N$ obey

$$\eta_i \eta_j = -\eta_j \eta_i, \qquad \forall i, j. \tag{A.58}$$

This implies they are nilpotent, i.e., $\eta_i^2 = 0$. Only polynomials can be functions of Grassmann variables, since the power series terminates after a finite number of terms,

$$A = a + \sum_i a_i \eta_i + \sum_{i<j} a_{ij} \eta_i \eta_j + ... + a_{12...N} \eta_1 \eta_2 ... \eta_N, \tag{A.59}$$

with complex coefficients a, a_i, a_{ij}, ..., $a_{12...N}$. The polynomials A form the *Grassmann algebra*. Grassmann numbers are the *generators* of the Grassmann algebra.

The rules of differentiation with respect to Grassmann variables are given by

$$\frac{\partial}{\partial \eta_i} 1 = 0, \qquad \frac{\partial}{\partial \eta_i} \eta_i = 1, \tag{A.60}$$

and

$$\frac{\partial}{\partial \eta_i} \frac{\partial}{\partial \eta_j} = -\frac{\partial}{\partial \eta_j} \frac{\partial}{\partial \eta_i}, \qquad \frac{\partial}{\partial \eta_i} \eta_j = -\eta_j \frac{\partial}{\partial \eta_i}, \quad \forall i \neq j. \tag{A.61}$$

A Grassmann integral is a functional that takes polynomials A in the Grassmann algebra to $\mathbb{C}$

$$\int d^N \eta A \in \mathbb{C}, \tag{A.62}$$

where the measure $d^N \eta$ is the product of the individual measures

$$d^N \eta = d\eta_N d\eta_{N-1} ... d\eta_1. \tag{A.63}$$

It is linear

$$\int d^N \eta \, (\lambda_1 A_1 + \lambda_2 A_2) = \lambda_1 \int d^N \eta A_1 + \lambda_2 \int d^N \eta A_2, \tag{A.64}$$

It satisfies

$$\int d^N\eta \frac{\partial}{\partial \eta_i} A = 0. \tag{A.65}$$

The individual measures $d\eta_i$ obey

$$\int d\eta_i 1 = 0, \qquad \int d\eta_i \eta_i = 1, \qquad d\eta_i d\eta_j = -d\eta_j d\eta_i. \tag{A.66}$$

These properties imply

$$\int d^N\eta \eta_1 \eta_2 ... \eta_N = 1, \qquad and \qquad \int d^N\eta A = a_{12...N}. \tag{A.67}$$

The measure $d\eta_i$ and the derivatives $\partial/\partial\eta_i$ obey the same algebraic properties.

B

On the correlation functions in the SF and the χSF

Fermion fields in the standard SF satisfy Dirichlet boundary conditions

$$\begin{aligned} P_+\psi(x)|_{x_0=0} &= 0, \qquad P_-\psi(x)|_{x_0=T} = 0, \\ \overline{\psi}(x)P_-|_{x_0=0} &= 0, \qquad \overline{\psi}(x)P_+|_{x_T=0} = 0, \end{aligned} \tag{B.1}$$

where $P_\pm = \frac{1}{2}(1 \pm \gamma_0)$.

Assuming ψ' and $\overline{\psi}'$ to be an isospin doublet satisfying the conditions eq.(B.1), the chirally rotated fields can be obtained in the χSF through a chiral non-singlet rotation

$$\psi(x) = R(\alpha)\psi(x), \qquad \overline{\psi}'(x) = \overline{\psi}(x)R(\alpha), \qquad R(\alpha) = \exp(i\alpha\gamma_5\tau^3/2). \tag{B.2}$$

For $\alpha = \pi/2$ the rotated fields satisfy boundary conditions

$$\begin{aligned} \widetilde{Q}_+\psi(x)|_{x_0=0} &= 0, \qquad & \widetilde{Q}_-\psi(x)|_{x_0=T} &= 0, \\ \overline{\psi}(x)\widetilde{Q}_+|_{x_0=0} &= 0, \qquad & \overline{\psi}(x)\widetilde{Q}_-|_{x_T=0} &= 0, \end{aligned} \tag{B.3}$$

with the projectors $\widetilde{Q}_\pm = \frac{1}{2}(1 \pm i\gamma_0\gamma_5\tau^3)$.

The boundary fermion fields (non-Dirichlet components) in both setups are given by the identification

$$\begin{aligned} \zeta(\mathbf{x}) &= \psi(0_+, \mathbf{x}), \qquad & \overline{\zeta}(\mathbf{x}) &= \overline{\psi}(0_+, \mathbf{x}), \\ \zeta'(\mathbf{x}) &= \psi'(T_-, \mathbf{x}), \qquad & \overline{\zeta}'(\mathbf{x}) &= \overline{\psi}'(T_-, \mathbf{x}). \end{aligned} \tag{B.4}$$

The projectors $P_\pm$ and $\widetilde{Q}_\pm$ are not included here. They will be added explicitly to the definition of the boundary bilinears for the correlation functions.

Correlation functions in the SF and the χSF are related by transforming the fields through $R(\alpha)$

$$\begin{aligned} \langle O[\psi, \overline{\psi}]\rangle_{\mathrm{SF}} &= \langle \mathcal{O}[R(\pi/2)\psi, \overline{\psi}R(\pi/2)]\rangle_{\chi\mathrm{SF}}, \\ \langle O[\psi, \overline{\psi}]\rangle_{\chi\mathrm{SF}} &= \langle \mathcal{O}[R(-\pi/2)\psi, \overline{\psi}R(-\pi/2)]\rangle_{\mathrm{SF}}, \end{aligned} \tag{B.5}$$

All the correlation functions considered through this thesis involve fermion bilinears. The list of all possible fermion bilinears is given by

$$\begin{aligned} V_\mu^{f_1f_2}(x) &= \overline{\psi}^{f_1}(x)\gamma_\mu\psi^{f_2}(x), \qquad & A_\mu^{f_1f_2}(x) &= \overline{\psi}^{f_1}(x)\gamma_\mu\gamma_5\psi^{f_2}(x), \\ S^{f_1f_2}(x) &= \overline{\psi}^{f_1}(x)\psi^{f_2}(x), \qquad & P^{f_1f_2}(x) &= \overline{\psi}^{f_1}(x)\gamma_5\psi^{f_2}(x), \\ T_{\mu\nu}^{f_1f_2}(x) &= \overline{\psi}^{f_1}(x)\mathrm{i}\sigma_{\mu\nu}\psi^{f_2}(x), \qquad & \widetilde{T}_{\mu\nu}^{f_1f_2}(x) &= \overline{\psi}^{f_1}(x)\gamma_5\mathrm{i}\sigma_{\mu\nu}\psi^{f_2}(x), \end{aligned} \tag{B.6}$$

where explicit flavor indices are used instead of the usual labelling through the generators of the flavor group.

The rotation eq.(B.2) is sensitive to the flavour content of the fermion bilinears used to build the SF correlation functions, so for every SF correlation function one obtains a family of χSF correlation functions with different flavour specifications. The

fermion bilinears in eq.(B.6) transform under the rotation eq.(B.2) as

$$
\begin{aligned}
A &\xrightarrow{R(\alpha)} A^{uu'}, A^{dd'}, -iV^{ud}, iV^{du} \\
V &\longrightarrow V^{uu'}, V^{dd'}, -iA^{ud}, iA^{du} \\
P &\longrightarrow iS^{uu'}, -iS^{dd'}, P^{ud}, P^{du} \\
S &\longrightarrow iP^{uu'}, -iP^{dd'}, S^{ud}, S^{du} \\
T &\longrightarrow i\widetilde{T}^{uu'}, -i\widetilde{T}^{dd'}, T^{ud}, T^{du} \\
\widetilde{T} &\longrightarrow iT^{uu'}, -iT^{dd'}, \widetilde{T}^{ud}, \widetilde{T}^{du}.
\end{aligned}
$$

List of boundary bilinears

Here we give a list of the boundary bilinears appearing in the SF and the χSF formulations. Note the explicit subindex "$\pm$". The subindex "+" denotes the boundary operators which have been constructed with the standard choice of projector. The subindex "$-$" denotes the boundary operators constructed with the opposite projectors. Correlation functions built with the "$-$" operators must vanish if homogeneous boundary conditions for the fermion fields are satisfied in the lattice construction.

Boundary bilinears for the standard SF

Boundary at $x_0 = 0$:

$$
\begin{aligned}
\mathcal{O}_{5,\pm}^{f_1 f_2} &= \int d^3y d^3z \overline{\zeta}_{f_1}(\mathbf{y})\gamma_5 P_{\mp}\zeta_{f_2}(\mathbf{z}), \\
\mathcal{O}_{5,}^{f}\mathcal{O}_{k,\pm}^{f_1 f_2} &= \int d^3y d^3z \overline{\zeta}_{f_1}(\mathbf{y})\gamma_k P_{\mp}\zeta_{f_2}(\mathbf{z}). \\
\mathcal{O}_{k,\pm}^{f_1 f_2} &= \int d^3y d^3z \overline{\zeta}_{f_1}(\mathbf{y})\gamma_k P_{\mp}\zeta_{f_2}(\mathbf{z}).
\end{aligned}
\tag{B.7}
$$

Boundary at $x_0 = T$:

$$
\begin{aligned}
\mathcal{O}'^{f_1 f_2}_{5,\pm} &= \int d^3y d^3z \overline{\zeta}'_{f_1}(\mathbf{y})\gamma_5 P_{\mp}\zeta'_{f_2}(\mathbf{z}), \\
\mathcal{O}'^{f_1 f_2}_{k,\pm} &= \int d^3y d^3z \overline{\zeta}'_{f_1}(\mathbf{y})\gamma_k P_{\mp}\zeta'_{f_2}(\mathbf{z}).
\end{aligned}
\tag{B.8}
$$

Boundary bilinears for the χSF

The transformation that takes to the chirally rotated basis is sensitive to the flavour content of the bilinears. Hence, we must account for the different flavour combinations that one can have.

Boundary at $x_0 = 0$.

Operators rotated from $\mathcal{O}_5$:

$$\begin{aligned}
\mathcal{Q}^{uu}_{5,\pm} &= \pm \int d^3y d^3z \overline{\zeta}_u(\mathbf{y})\gamma_0\gamma_5 Q_{\mp}\zeta_u(\mathbf{z}),\\
\mathcal{Q}^{dd}_{5,\pm} &= \pm \int d^3y d^3z \overline{\zeta}_d(\mathbf{y})\gamma_0\gamma_5 Q_{\pm}\zeta_d(\mathbf{z}),\\
\mathcal{Q}^{ud}_{5,\pm} &= \int d^3y d^3z \overline{\zeta}_u(\mathbf{y})\gamma_5 Q_{\pm}\zeta_d(\mathbf{z}),\\
\mathcal{Q}^{du}_{5,\pm} &= \int d^3y d^3z \overline{\zeta}_d(\mathbf{y})\gamma_5 Q_{\mp}\zeta_u(\mathbf{z}).
\end{aligned} \tag{B.9}$$

Operators rotated from $\mathcal{O}_k$:

$$\begin{aligned}
\mathcal{Q}^{uu}_{k,\pm} &= \int d^3y d^3z \overline{\zeta}_u(\mathbf{y})\gamma_k Q_{\mp}\zeta_u(\mathbf{z}),\\
\mathcal{Q}^{dd}_{k,\pm} &= \int d^3y d^3z \overline{\zeta}_d(\mathbf{y})\gamma_k Q_{\pm}\zeta_d(\mathbf{z}),\\
\mathcal{Q}^{ud}_{k,\pm} &= \pm \int d^3y d^3z \overline{\zeta}_u(\mathbf{y})\gamma_0\gamma_k Q_{\pm}\zeta_d(\mathbf{z}),\\
\mathcal{Q}^{du}_{k,\pm} &= \pm \int d^3y d^3z \overline{\zeta}_d(\mathbf{y})\gamma_0\gamma_k Q_{\mp}\zeta_u(\mathbf{z}).
\end{aligned} \tag{B.10}$$

BOUNDARY AT $x_0 = T$.

Operators rotated from $\mathcal{O}'_5$:

$$\begin{aligned}
\mathcal{Q}'^{uu}_{5,\pm} &= \mp \int d^3y d^3z \overline{\zeta}'_u(\mathbf{y})\gamma_0\gamma_5 Q_\pm \eta'_u(\mathbf{z}), \\
\mathcal{Q}'^{dd}_{5,\pm} &= \mp \int d^3y d^3z \overline{\zeta}'_d(\mathbf{y})\gamma_0\gamma_5 Q_\mp \eta'_d(\mathbf{z}), \\
\mathcal{Q}'^{ud}_{5,\pm} &= \int d^3y d^3z \overline{\zeta}'_u(\mathbf{y})\gamma_5 Q_\mp \eta'_d(\mathbf{z}), \\
\mathcal{Q}'^{du}_{5,\pm} &= \int d^3y d^3z \overline{\zeta}'_d(\mathbf{y})\gamma_5 Q_\pm \eta'_u(\mathbf{z}).
\end{aligned} \tag{B.11}$$

Operators rotated from $\mathcal{O}'_k$:

$$\begin{aligned}
\mathcal{Q}'^{uu}_{k,\pm} &= \int d^3y d^3z \overline{\zeta}'_u(\mathbf{y})\gamma_k Q_\pm \zeta'_u(\mathbf{z}), \\
\mathcal{Q}'^{dd}_{k,\pm} &= \int d^3y d^3z \overline{\zeta}'_d(\mathbf{y})\gamma_k Q_\mp \zeta'_d(\mathbf{z}), \\
\mathcal{Q}'^{ud}_{k,\pm} &= \mp \int d^3y d^3z \overline{\zeta}'_u(\mathbf{y})\gamma_0\gamma_k Q_\mp \zeta'_d(\mathbf{z}), \\
\mathcal{Q}'^{du}_{k,\pm} &= \mp \int d^3y d^3z \overline{\zeta}'_d(\mathbf{y})\gamma_0\gamma_k Q_\pm \zeta'_u(\mathbf{z}).
\end{aligned} \tag{B.12}$$

LIST OF CORRELATION FUNCTIONS IN THE SF AND THE χSF

The following is a list of the different correlation functions we will consider in this work. The Wick contractions are done leading to an explicit expression ready to be evaluated. For the sake of clarity in the discussion of chapter 5, we have avoided the $\pm$ subindex there. Whenever the subindex are absent in a correlation function we understand that this has been constructed with the standard choice of projector, i.e. we define $f_{X,+} \equiv f_X$, and similarly for the other correlations. We only write the $\pm$ index explicitly here in the appendix.

Correlation functions in the SF

The boundary to bulk correlations are

$$\begin{aligned} f_{X,\pm}(x_0,\mathbf{p}) =& \frac{1}{2}\sum_{\mathbf{y},\mathbf{z}} e^{i\mathbf{p}(\mathbf{y}-\mathbf{z})} \\ & \langle \mathrm{Tr}\left\{ S(x;a,\mathbf{y})U_0(0,\mathbf{y})^\dagger \Gamma_{\mathcal{O}_{5,\pm}} U_0(0,\mathbf{z}) S(a,\mathbf{z};x)\Gamma_X \right\}\rangle, \end{aligned} \tag{B.13}$$

and

$$\begin{aligned} k_{Y,\pm}(x_0,\mathbf{p}) =& \frac{1}{6}\sum_{k=1}^{3}\sum_{\mathbf{y},\mathbf{z}} e^{i\mathbf{p}(\mathbf{y}-\mathbf{z})} \\ & \langle \mathrm{Tr}\left\{ S(x;a,\mathbf{y})U_0(0,\mathbf{y})^\dagger \Gamma_{\mathcal{O}_{k,\pm}} U_0(0,\mathbf{z}) S(a,\mathbf{z};x)\Gamma_{Y_k} \right\}\rangle. \end{aligned} \tag{B.14}$$

The boundary to boundary correlation functions are

$$\begin{aligned} f_1 =& \frac{1}{2}\sum_{\mathbf{u},\mathbf{v},\mathbf{y},\mathbf{z}} e^{i\mathbf{p}(\mathbf{u}-\mathbf{v})} e^{i\mathbf{q}(\mathbf{y}-\mathbf{z})} \langle \mathrm{Tr}\left\{ U_0(0,\mathbf{z}) S(a,\mathbf{z};T-a,\mathbf{u}) U_0(T-a,\mathbf{u}) \right. \\ & \left. \Gamma_{\mathcal{O}'_{5,+}} U_0^\dagger(T-a,\mathbf{v}) S(T-a,\mathbf{v};a,\mathbf{y}) U_0(0,\mathbf{y}) \Gamma_{\mathcal{O}_{5,+}} \right\}\rangle, \end{aligned} \tag{B.15}$$

and

$$\begin{aligned} k_1 =& \frac{1}{6}\sum_{k}^{3}\sum_{\mathbf{u},\mathbf{v},\mathbf{y},\mathbf{z}} e^{i\mathbf{p}(\mathbf{u}-\mathbf{v})} e^{i\mathbf{q}(\mathbf{y}-\mathbf{z})} \langle \mathrm{Tr}\left\{ U_0(0,\mathbf{z}) S(a,\mathbf{z};T-a,\mathbf{u}) U_0(T-a,\mathbf{u}) \right. \\ & \left. \Gamma_{\mathcal{O}'_{k,+}} U_0^\dagger(T-a,\mathbf{v}) S(T-a,\mathbf{v};a,\mathbf{y}) U_0(0,\mathbf{y}) \Gamma_{\mathcal{O}_{k,+}} \right\}\rangle, \end{aligned} \tag{B.16}$$

Correlation functions in the χSF

In the χSF, in practice, one can avoid the calculation of disconnected diagrams by considering a partially quenched setup with four flavours by replacing the quark doublet via

$$\psi = \begin{pmatrix} \psi_u \\ \psi_d \end{pmatrix} \quad \longrightarrow \quad \psi = \begin{pmatrix} \psi_u \\ \psi_d \\ \psi_{u'} \\ \psi_{d'} \end{pmatrix}. \tag{B.17}$$

This way, it is possible to consider correlation funtions of the same flavour type without having flavour singlets. In this situation, the Pauli matrix τ^3 must be upgraded to

$$\tau^3 \longrightarrow \mathbb{I}_2 \otimes \tau^3 = \mathrm{diag}(1,-1,1,-1). \tag{B.18}$$

The projectors will read

$$\widetilde{Q}_\pm\Big|_{N_f=2} = \mathrm{diag}(Q_\pm, Q_\mp), \qquad \widetilde{Q}_\pm\Big|_{N_f=4} = \mathrm{diag}(Q_\pm, Q_\mp, Q_\pm, Q_\mp), \tag{B.19}$$

with

$$Q_\pm = \frac{1}{2}(1 \pm i\gamma_0\gamma_5). \tag{B.20}$$

The boundary to bulk correlation functions are given by

$$\begin{aligned} \mathrm{g}^{f_1 f_2}_{X,\pm}(x_0,\mathbf{p}) =& \frac{1}{2}\sum_{\mathbf{y},\mathbf{z}} e^{i\mathbf{p}(\mathbf{y}-\mathbf{z})} \\ & \langle \mathrm{Tr}\left\{ S(x;a,\mathbf{y})_{f_2 f_2} U_0(0,\mathbf{y})^\dagger \Gamma^{f_2 f_1}_{\mathcal{Q}_{5,\pm}} U_0(0,\mathbf{z}) S(a,\mathbf{z};x)_{f_1 f_1} \Gamma_X \right\}\rangle, \end{aligned} \tag{B.21}$$

and

$$\begin{aligned} l^{f_1 f_2}_{Y,\pm}(x_0,\mathbf{p}) =& \frac{1}{6}\sum_{k=1}^{3}\sum_{\mathbf{y},\mathbf{z}} e^{i\mathbf{p}(\mathbf{y}-\mathbf{z})} \\ & \langle \mathrm{Tr}\left\{ S(x;a,\mathbf{y})_{f_2 f_2} U_0(0,\mathbf{y})^\dagger \Gamma^{f_2 f_1}_{\mathcal{Q}_k,\pm} U_0(0,\mathbf{z}) S(a,\mathbf{z};x)_{f_1 f_1} \Gamma_{Y_k} \right\}\rangle. \end{aligned} \tag{B.22}$$

The boundary to boundary correlation functions are given by

$$\begin{aligned} \mathrm{g}^{f_1 f_2}_1 =& \frac{1}{2}\sum_{\mathbf{u},\mathbf{v},\mathbf{y},\mathbf{z}} e^{i\mathbf{p}(\mathbf{u}-\mathbf{v})} e^{i\mathbf{q}(\mathbf{y}-\mathbf{z})} \langle \mathrm{Tr}\left\{ U_0(0,\mathbf{z}) S(a,\mathbf{z};T-a,\mathbf{u})_{f_2 f_2} U_0(T-a,\mathbf{u}) \right. \\ & \left. \Gamma^{f_2 f_1}_{\mathcal{Q}'_{5,+}} U_0^\dagger(T-a,\mathbf{v}) S(T-a,\mathbf{v};a,\mathbf{y})_{f_1 f_1} U_0(0,\mathbf{y}) \Gamma^{f_1 f_2}_{\mathcal{Q}_{5,+}} \right\}\rangle, \end{aligned} \tag{B.23}$$

and

$$\begin{aligned} l^{f_1 f_2}_1 =& \frac{1}{6}\sum_{k=1}^{3}\sum_{\mathbf{u},\mathbf{v},\mathbf{y},\mathbf{z}} e^{i\mathbf{p}(\mathbf{u}-\mathbf{v})} e^{i\mathbf{q}(\mathbf{y}-\mathbf{z})} \langle \mathrm{Tr}\left\{ U_0(0,\mathbf{z}) S(a,\mathbf{z};T-a,\mathbf{u})_{f_2 f_2} U_0(T-a,\mathbf{u}) \right. \\ & \left. \Gamma^{f_2 f_1}_{\mathcal{Q}'_{\parallel},+} U_0^\dagger(T-a,\mathbf{v}) S(T-a,\mathbf{v};a,\mathbf{y})_{f_1 f_1} U_0(0,\mathbf{y}) \Gamma^{f_1 f_2}_{\mathcal{Q}_{k,+}} \right\}\rangle, \end{aligned} \tag{B.24}$$

List of combinations of gamma matrices

The spin matrices that can be inserted in the bilinear operators for the bulk are the following.

For Γ_X:

$$\begin{aligned} \Gamma_{A_0} &= \gamma_0\gamma_5, & \Gamma_{V_0} &= \gamma_0, \\ \Gamma_P &= \gamma_5, & \Gamma_S &= \mathbb{I}. \end{aligned} \tag{B.25}$$

For Γ_{Y_k}

$$\begin{aligned} \Gamma_{A_k} &= \gamma_k\gamma_5, & \Gamma_{V_k} &= \gamma_k, \\ \Gamma_{T_{k0}} &= \mathrm{i}\sigma_{k0}, & \Gamma_{\widetilde{T}_{k0}} &= \mathrm{i}\gamma_5\sigma_{k0}. \end{aligned} \tag{B.26}$$

The spin matrices for the standard SF boundary operators are

$$\begin{aligned} \Gamma_{\mathcal{O}_{5,\pm}} &= \Gamma_{\mathcal{O}'_{5,\pm}} = P_{\mp}\gamma_5, \\ \Gamma_{\mathcal{O}_{k,\pm}} &= \Gamma_{\mathcal{O}'_{k,\pm}} = P_{\mp}\gamma_k, \end{aligned} \tag{B.27}$$

The spin matrices that can be inserted in the boundary operators for the χSF are

$$\begin{aligned} \Gamma^{uu}_{\mathcal{Q}_{5,\pm}} &= \pm\gamma_0\gamma_5 Q_{\mp}, & \Gamma^{dd}_{\mathcal{O}_{5\pm}} &= \pm\gamma_0\gamma_5 Q_{\pm}, \\ \Gamma^{ud}_{\mathcal{Q}_{5,\pm}} &= \gamma_5 Q_{\pm}, & \Gamma^{du}_{\mathcal{O}_{5\pm}} &= \gamma_5 Q_{\mp}, \end{aligned} \tag{B.28}$$

and

$$\begin{aligned} \Gamma'^{uu}_{\mathcal{Q}_{5\pm}} &= \mp\gamma_0\gamma_5 Q_{\pm}, & \Gamma'^{dd}_{\mathcal{O}_{5\pm}} &= \mp\gamma_0\gamma_5 Q_{\mp}, \\ \Gamma'^{ud}_{\mathcal{Q}_{5\pm}} &= \gamma_5 Q_{\mp}, & \Gamma'^{du}_{\mathcal{O}_{5\pm}} &= \gamma_5 Q_{\pm}. \end{aligned} \tag{B.29}$$

Finally, the spin matrices to be inserted in χSF boundary operators with an open spatial index are

$$\begin{aligned} \Gamma^{uu}_{\mathcal{Q}_{k\pm}} &= \gamma_k Q_{\mp}, & \Gamma^{dd}_{\mathcal{O}_{k\pm}} &= \pm\gamma_k Q_{\pm}, \\ \Gamma^{ud}_{\mathcal{Q}_{k\pm}} &= \pm\gamma_0\gamma_k Q_{\pm}, & \Gamma^{du}_{\mathcal{O}_{k\pm}} &= \pm\gamma_0\gamma_k Q_{\mp}, \end{aligned} \tag{B.30}$$

and

$$\begin{aligned} \Gamma'^{uu}_{\mathcal{Q}_{k\pm}} &= \gamma_k Q_{\pm}, & \Gamma'^{dd}_{\mathcal{O}_{k\pm}} &= \gamma_k Q_{\mp}, \\ \Gamma'^{ud}_{\mathcal{Q}_{k\pm}} &= \mp\gamma_0\gamma_k Q_{\mp}, & \Gamma'^{du}_{\mathcal{O}_{k\pm}} &= \mp\gamma_0\gamma_k Q_{\pm}. \end{aligned} \tag{B.31}$$

List of 2-point functions

Here we provide with a list of the 2-point functions necessary to calculate the correlation functions considered in this thesis.

$$
\begin{aligned}
&[\psi(x)\overline{\psi}(y)]_F = S(x;y), \\
&[\psi(x)\overline{\zeta}(\mathbf{y})]_F = S(x;a,\mathbf{y})U_0(0,\mathbf{y})^\dagger, \\
&[\psi(x)\overline{\zeta}'(\mathbf{y})]_F = S(x;T-a,\mathbf{y})U_0(T-a,\mathbf{y}), \\
&[\zeta(\mathbf{x})\overline{\psi}(y)]_F = U_0(0,\mathbf{x})S(a,\mathbf{x};y), \\
&[\zeta'(\mathbf{x})\overline{\psi}(y)]_F = U_0(T-a,\mathbf{x})^\dagger S(T-a,\mathbf{x};y), \\
&[\zeta(\mathbf{x})\overline{\zeta}(\mathbf{y})]_F = U_0(0,\mathbf{x})S(a,\mathbf{x};a,\mathbf{y})U_0(0,\mathbf{y})^\dagger, \qquad \mathbf{x}\neq\mathbf{y}, \\
&[\zeta(\mathbf{x})\overline{\zeta}'(\mathbf{y})]_F = U_0(0,\mathbf{x})S(a,\mathbf{x};T-a,\mathbf{y})U_0(T-a,\mathbf{y}), \\
&[\zeta'(\mathbf{x})\overline{\zeta}(\mathbf{y})]_F = U_0(T-a,\mathbf{x})^\dagger S(T-a,\mathbf{x};a,\mathbf{y})U_0(0,\mathbf{y})^\dagger, \\
&[\zeta(\mathbf{x})\overline{\zeta}(\mathbf{y})]_F = U_0(T-a,\mathbf{x})^\dagger S(T-a,\mathbf{x};T-a,\mathbf{y})U_0(0,\mathbf{y}), \qquad \mathbf{x}\neq\mathbf{y}.
\end{aligned}
\tag{B.32}
$$

C

Contribution to $\overline{g}^2$ from fermions in the χSF

In this appendix we give details on the calculation of the fermionic contribution $p_{1,1}(L/a)$ to the one loop SF coupling in the χSF. This discussion follows very closely that found in Appendix A of [80]. There the coefficient $p_{1,1}(L/a)$ for the standard SF was calculated. We have recalculated it as well as a check of our calculations and to have an idea about the quality of our numerical data compared to the known results in [80].

Moreover, we consider the derivatives

$$\frac{\partial}{\partial m_0} p_{1,1}(L/a) \qquad \text{and} \qquad \frac{\partial}{\partial z_f} p_{1,1}(L/a), \tag{C.1}$$

which are needed to study the sensitivity of the 1 loop SSF $\Sigma_{1,1}(L/a)$ to the parameters m_0 and z_f of the χSF. As we will show below, the derivatives eq.(C.1) can be computed simultaneously to $p_{1,1}(L/a)$.

Finally, we comment on the modifications needed to compute $p_{1,1}(L/a)$ for fermions

transforming under representations of the gauge group other than the fundamental.

C.1 Determination of $p_{1,1}(L/a)$

The contribution of the fermions to the 1-loop coupling $p_{1,1}(L/a)$ is given in terms of Δ_2 in eq.(6.10).

Here we start our calculation from eq.(6.29), where the coefficient $p_{1,1}(L/a)$ is expressed as a sum of contributions from the different subspace at fixed color and spatial momentum. For clarity, we recall here eq.(6.29),

$$p_{1,1}(L/a) = \frac{1}{kN_f} \sum_{n_c=1}^{3} \sum_{\mathbf{p}} \frac{\partial}{\partial \eta} \ln \det \widetilde{\mathcal{D}}_{5,1}(n_c, \mathbf{p}) \Big|_{\eta=0} . \tag{C.2}$$

The computation of $\det \widetilde{\mathcal{D}}_{5,1}$ can be performed following the recursive technique introduced in appendix C of [23] for quadratic operators and extended to linear operators in [80]. We review this argument here and to adapt it for the χSF setup. Note that while for the standard SF the flavour structure is trivial [80], we have to take full care of it in the present calculation.

The reduced operator $\widetilde{\mathcal{D}}_{5,1}$ acts on functions $f(x_0)$ as a finite difference operator in time for the interval $[0, T]$ (see eq.(4.97)), where $f(x_0)$ have spinor and flavour components. One can write the action of $\widetilde{\mathcal{D}}_{5,1}$ as an infinite volume operator acting on functions for all times as explained in section 4.3.6. For this, the functions $f(x_0)$ must be extended outside the interval $[0, T]$ requiring them to be zero always except within $[0, T]$. Moreover, one has to supplement them with the syntactic extension eq.(4.98) which in terms of $f(x_0)$ will read

$$f(-a) = -i\gamma_0\gamma_5\tau^3 f(0); \qquad f(T+a) = i\gamma_0\gamma_5\tau^3 f(T). \tag{C.3}$$

This extension encodes the action of the operator $\widetilde{\mathcal{D}}_{5,1}$ on the functions $f(x_0)$ close to the boundaries in a lattice with an offset $-a/2$. For now until the end of the section we set $x_0 = t$ and consider lattice units $a = 1$

After doing the extension to all times, the infinite volume operator acts on $f(t)$ as

$$\left(\widetilde{\mathcal{D}}_{5,1} f\right)(t) = -\gamma_5\tau^1 P_- f(t+1) + \gamma_5\tau^1 h(t) f(t) - \gamma_5\tau^1 P_+ f(t-1). \tag{C.4}$$

The function $h(t)$ is given by

$$\begin{aligned} h(t) = 1 + m_0 + \frac{1}{2}\sum_{k=1}^{3} \hat{q}_k(t)^2 + i\widetilde{q}_k(t)\gamma_k \\ - (1 - \delta_{t,0} - \delta_{t,T})\frac{1}{2} c_{\rm SW}\gamma_0\gamma_k p_{0k} \\ + (\delta_{t,0} + \delta_{t,T})\,(z_f - 1) + i\,(\delta_{t,0} + \delta_{t,T})\,(d_s - 1)\widetilde{q}_k(t) \end{aligned} \tag{C.5}$$

where we make use of the lattice notation

$$\begin{aligned} q_k(t) &= \omega t + r_k, \\ \widetilde{q}_k(t) &= \sin q_k(t), \\ \hat{q}_k(t) &= 2\sin\left(\frac{1}{2} q_k(t)\right), \qquad \text{for } k = 1, 2, 3, \end{aligned} \tag{C.6}$$

and

$$\omega = \left(\phi'_{n_c} - \phi_{n_c}\right)/L^2, \qquad r_k = p_k + \phi_{n_c}/L. \tag{C.7}$$

Moreover, $p_{0k} = i\sin\omega$ independently of the spatial direction k. Note that at the boundaries $t = 0$ and $t = T$, the function $h(t)$ contains the contribution coming from the boundary improvement countererms and that the term proportional to $c_{\rm SW}$ is absent there. For a one loop calculation the fermionic bounary coefficients $z_{\rm f}$ and $d_{\rm s}$ ae only required to lowest order, and thus we set,

$$z_{\rm f} = z_{\rm f}^{(0)} = 1, \quad d_{\rm s} = d_{\rm s}^{(0)} = 1/2. \tag{C.8}$$

The $c_{\rm SW}$ coefficient is set to either 0 (to exclude the clover term from the action) or to the tree-level value $c_{\rm SW} = c_{\rm SW}^{(0)} = 1$.

Following [23, 80], for calculating $\det\left(\widetilde{\mathcal{D}}_{5,1}\right)$ the starting point is to consider the eigenvalue equation

$$\left(\widetilde{\mathcal{D}}_{5,1} - \mu\right) f(t) = 0. \tag{C.9}$$

The functions $f(t)$ satisfy the flavour diagonal conditions eq.(C.3). If we multiply the eigenvalue equation by $\gamma_5\tau^1$ from the left we obtain,

$$\left(\widetilde{\mathcal{D}}_{\rm W} + \delta\widetilde{\mathcal{D}}_{\rm W} + m_0 - \mu\gamma_5\tau^1\right) f(t) = 0, \tag{C.10}$$

where $\widetilde{\mathcal{D}}_{\mathrm{W}}$ and $\delta\widetilde{\mathcal{D}}_{\mathrm{W}}$ are the Dirac operator and counterterms acting at fixed color and momentum. We observe that the flavour components decouple for $\mu = 0$, which is the case of interest. In fact, μ is only kept non-zero in order to obtain the correct normalization of the characteristic polynomial and thus the determinant. Before setting $\mu = 0$, we must keep track of the non-trivial flavour structure all the way through the following discussion.

At this point it is possible to write eq.(C.4) as a first order relation. Although $\widetilde{\mathcal{D}}_{5,1}$ seems to act as a second order time difference operator, the first order structure of eq.(C.4) can be recovered by introducing a new function $F(t)$,[1]

$$F(t) = P_- f(t) + P_+ f(t-1), \qquad 0 \leq t \leq T+1; \tag{C.11}$$

which, as a consequence of eq.(C.3), satisfies the boundary conditions

$$\widetilde{Q}_+ F(0) = 0, \tag{C.12}$$

$$\widetilde{Q}_- F(T+1) = 0. \tag{C.13}$$

In terms of $F(t)$, the eigenvalue equation eq.(C.9) can be written as a first order recursion relation on $F(t)$, which reads

$$F(t+1) = A(t)F(t), \tag{C.14}$$

with

$$\begin{aligned} A(t) = -a(t)^{-1} \{ P_- \left[\mu^2 - a(t)^2 + \mu\gamma_5\tau^1 \left(c_k(t)\gamma_k - b_k(t)\gamma_k + 1 \right) \right. \\ \left. c_k(t)\gamma_k \left(b_j(t)\gamma_j - 1 \right) \right] \\ P_+ \left[b_k(t)\gamma_k - \mu\gamma_5 - 1 \right] \} \end{aligned} \tag{C.15}$$

[1] The functions $F(t)$ have spin an flavour components, just as $f(t)$.

where $a(t)$, $b_k(t)$ and $c_k(t)$ are scalar functions of t given by

$$\begin{aligned} a(t) &= 1 + m_0 + \frac{1}{2}\sum_{k=1}^{3} \hat{q}_k(t)^2 + (\delta_{t,0} + \delta_{t,T})\,(z_f - 1) \\ b_k(t) &= i\left[1 + (\delta_{t,0} + \delta_{t,T})\,(d_s - 1)\right]\widetilde{q}_k(t) - \frac{1}{2}\,(1 - \delta_{t,0} - \delta_{t,T})\,c_{SW} p_{0k} \\ c_k(t) &= i\left[1 + (\delta_{t,0} + \delta_{t,T})\,(d_s - 1)\right]\widetilde{q}_k(t) + \frac{1}{2}\,(1 - \delta_{t,0} - \delta_{t,T})\,c_{SW} p_{0k} \end{aligned} \tag{C.16}$$

The function $F(T+1)$ after $T+1$ iterations starting from an arbitrary prescribed value for $F(0)$ is unique and depends linearly on $F(0)$ through

$$F(T+1) = A(T)A(T-1)...A(0)F(0) \tag{C.17}$$

The boundary condition eq.(C.12) implies that

$$F(0) = \widetilde{Q}_- S; \tag{C.18}$$

S being an arbitrary spinor and flavour doublet. The other boundary condition eq.(C.13) implies that

$$\widetilde{Q}_- A(T)A(T-1)...A(0)\widetilde{Q}_- S = M(\mu)^{\widetilde{Q}}_{--} S = 0; \tag{C.19}$$

where $M(\mu)^{\widetilde{Q}}_{--}$ is a $(2\times 4)\times(2\times 4)$ matrix in the subspace defined by the projector $\widetilde{Q}_-$.

In order to have a solution for eq.(C.19) for an arbitrary S, the determinant of $M^{\widetilde{Q}}(\mu)_{--}$ must vanish. Following the reasoning in [23], we can relate the determinant of $\widetilde{\mathcal{D}}_{5,1}$ to the determinant of $M^{\widetilde{Q}}(\mu)_{--}$ through

$$\det\left(\widetilde{\mathcal{D}}_{5,1} - \mu\right) = \det M^{\widetilde{Q}}(\mu)_{--} \prod_{t=0}^{t=T} (a(t)) \tag{C.20}$$

In practice, the terms $a(t)$ multiplying the determinant of $M^{\widetilde{Q}}(\mu)_{--}$ can be avoided by defining the matrix

$$B(t) = a(t)A(t) \tag{C.21}$$

and solving the recursion

$$F(T+1) = B(T)B(T-1)...B(0)F(0) = \mathcal{M}(\mu)F(0) \tag{C.22}$$

Again, the boundary conditions eq.(C.12) and (C.13) imply that

$$\widetilde{Q}_{-}\mathcal{M}(\mu)\widetilde{Q}_{-}F(0) = \mathcal{M}(\mu)^{\widetilde{Q}}_{--}F(0) = 0. \tag{C.23}$$

For simplicity in the following calculation it is convenient to write the matrix $\mathcal{M}(\mu)^{\widetilde{Q}}_{--}$ in terms of the P_{-} projectors. The two projectors $\widetilde{Q}_{-}$ and P_{-} are related through a unitary transformation

$$U^{\dagger}\widetilde{Q}_{-}U = P_{-}, \qquad \text{where } U = (1 - i\tau^3\gamma_5)/\sqrt{2}. \tag{C.24}$$

Hence, eq.(C.23) will read in the P_{-} basis

$$P_{-}(1 + i\tau^3\gamma_5)\mathcal{M}(\mu)(1 - i\tau^3\gamma_5)P_{-}F(0) = \mathcal{M}^{P}_{--}(\mu)F(0) = 0. \tag{C.25}$$

Finally, for $\mu = 0$ one finally obtains

$$\det\left(\widetilde{\mathcal{D}}_{5,1}\right) = \det \mathcal{M}^{(P)}_{--}(0). \tag{C.26}$$

However, as we have observed before, for $\mu = 0$ the two flavours decouple in eq.(C.9), such that the evaluation of eq.(C.26) accounts to consider the two flavours separately. Moreover, the hermiticity of $\gamma_5\tau^1\mathcal{D}_{\mathrm{W}}$ implies that the Dirac operator is composed by two blocks

$$\mathcal{D}_{\mathrm{W}} = \mathrm{diag}\left(\mathcal{D}^{(u)}_{\mathrm{W}}, \mathcal{D}^{(d)}_{\mathrm{W}}\right), \tag{C.27}$$

with the operators for each flavor related through

$$\gamma_5\mathcal{D}^{(u)}_{\mathrm{W}}\gamma_5 = \left(\mathcal{D}^{(d)}_{\mathrm{W}}\right)^{\dagger}. \tag{C.28}$$

Hence, the determinant can be written in terms of a single flavour by

$$\begin{aligned}\det\left(\mathcal{D}_{\rm W}+m_0\right) &= \det\left(\mathcal{D}_{\rm W}^{(u)}+m_0\right)\det\left(\mathcal{D}_{\rm W}^{(d)}+m_0\right)\\ &= \det\left[\left(\mathcal{D}_{\rm W}^{(u)}+m_0\right)^{\dagger}\left(\mathcal{D}_{\rm W}^{(u)}+m_0\right)\right]\\ &= \det\left(\mathcal{D}_{\rm W}^{(u)}+m_0\right)^{2},\end{aligned} \tag{C.29}$$

It is thus possible to express eq.(C.26) in terms of a single flavour through

$$\det\left(\widetilde{\mathcal{D}}_{5,1}\right)=2\det\left(\widetilde{\mathcal{D}}_{5}\right)=2\det\overline{\mathcal{M}}, \tag{C.30}$$

where $\widetilde{\mathcal{D}}_5=\gamma_5\left(\widetilde{\mathcal{D}}_{\rm W}^{(u)}+\delta\widetilde{\mathcal{D}}_{\rm W}^{(u)}+m_0^{(u)}\right)$. The matrix $\overline{\mathcal{M}}\equiv\overline{\mathcal{M}}^{P}_{--}(0)$, which is defined for a single flavour, is constructed as in eq.(C.22) and (C.23) but with $B(t)$ being trivial in flavour and with the projectors Q_- for a single flavour. The bar in $\overline{\mathcal{M}}$ denotes reduction in flavour space.[2]

Taking $N_f=2$ in eq.(C.2), the ontribution to $p_{1,1}$ at fixed color and momentum is given by

$$p_{1,1}(L/a)|_{n_c,\mathbf{p}}=\frac{1}{k}\partial_\eta\ln\det\widetilde{\mathcal{D}}_5=\frac{1}{k}\mathrm{Tr}\left\{\overline{\mathcal{M}}^{-1}\partial_\eta\overline{\mathcal{M}}\right\}. \tag{C.31}$$

At this stage the problem is reduced to calulate the trace in the right hand side of eq.(C.31). The trace involves the evaluation of the inverse and the derivative of a 2×2 matrix. Calculating the inverse is a trivial task. For calculating $\partial_\eta\overline{\mathcal{M}}$ we consider the derivative of eq.(C.22) (for a single flavour). Since $\partial_\eta F(0)=0$ then $\partial_\eta F(T+1)$ is linear in $F(0)$

$$\partial_\eta F(T+1)=\partial_\eta\left(B(T)B(T-1)...B(0)\right)F(0)=\left(\partial_\eta\overline{\mathcal{M}}\right)F(0). \tag{C.32}$$

One can then extract $\overline{\mathcal{M}}$ and $\partial_\eta\overline{\mathcal{M}}$ by simultaneously solving the 2 coupled recursions

$$\begin{aligned}F(t+1)&=B(t)F(t),\\ \partial_\eta F(t+1)&=\left(\partial_\eta B(t)\right)F(t)+B(t)\partial_\eta F(t),\end{aligned} \tag{C.33}$$

using 2 linearly independent starting choices of $F(0)$.

[2]Due to the projectors P_-, $\overline{\mathcal{M}}^{P}_{--}(\mu)$ is simply a 2×2 matri the components of which are the lower right components of the 4×4 matrix $\overline{\mathcal{M}}(\mu)$.

C.2 Determination of $\partial_{z_f} p_{1,1}$ and $\partial_z p_{1,1}$

In order to determine the sensitivity of Σ to the z_f and $z = Lm_0$ parameters one needs to evaluate the derivatives

$$\partial_x p_{1,1}, \qquad x = z_f, z. \tag{C.34}$$

This can be done by extending the calculation of $p_{1,1}$. The contribution of a particular momentum and color sector to the derivative of $p_{1,1}$ with respect to a parameter x can by evaluated by differentiating eq.(C.31)

$$\frac{\partial}{\partial x}\frac{\partial}{\partial \eta} \ln \det \mathcal{D}_5 = \mathrm{Tr}\left\{-\overline{\mathcal{M}}^{-1}\partial_x \overline{\mathcal{M}}\overline{\mathcal{M}}^{-1}\partial_\eta \overline{\mathcal{M}} + \overline{\mathcal{M}}^{-1}\partial_{x\eta}\overline{\mathcal{M}}\right\}. \tag{C.35}$$

The derivatives and second derivatives of $\overline{\mathcal{M}}$ can be obtained by applying Leibnitz's rule for the product of matrices in the recursion eq.(C.32). Since $\partial_x F(0) = 0$ then $\partial_x F(T+1)$ and $\partial_{x,\eta} F(T+1)$ are linear in $F(0)$ such that

$$\begin{aligned} \partial_x F(T+1) &= \left(\partial_x \overline{\mathcal{M}}\right) F(0), \\ \partial_{x,\eta} F(T+1) &= \left(\partial_{x,\eta} \overline{\mathcal{M}}\right) F(0), \end{aligned} \tag{C.36}$$

For determining the derivatives and second derivatives of $\overline{\mathcal{M}}$ with respect to x and μ, it will be necessary to solve simultaneously the 4 coupled recursions

$$\begin{aligned} F(t+1) =& B(t)F(t), \\ \partial_\eta F(t+1) =& \partial_\eta(B(t))F(t) + B(t)\partial_\eta(F(t)), \\ \partial_x F(t+1) =& \partial_x(B(t))F(t) + B(t)\partial_x(F(t)), \\ \partial_{x,\eta} F(t+1) =& \partial_{x,\eta}(B(t))F(t) + \partial_x(B(t))\partial_\eta(F(t)) \\ & + \partial_\eta(B(t))\partial_x(F(t)) + B(t)\partial_{x,\eta}(B(t)), \end{aligned} \tag{C.37}$$

starting from 2 independent conditions for $F(0)$. The problem is hence very similar to the standard calculation of $p_{1,1}(L/a)$

Since we are interested in the derivatives with respect to the 2 parameters z_f and m_0, a total of 6 coupled recursions have to be simultaneously solved following eq.(C.37).

C.3 Contribution to $p_{1,1}$ from non-fundamental fermions

The generalisation of the calculation of $p_{1,1}(L/a)$ to fermions transforming under arbitrary representations is straight forward. When considering non-fundamental fermions, the Dirac operator is upgraded to the desired representation simply by replacing the link variables $U_\mu(x)$ by their counterparts $U_\mu^{\mathcal{R}}(x)$ in the representation $\mathcal{R}$. Explicit mappings to construct the 2-index representations are given in appendix A.3.2. The upgrade only affects the color structure of the Dirac operator, and the factorisation in momentum space is left intact.

We desire to decompose the eigenfunctions of the Dirac operator such that

$$\psi(x) = e^{ip_k x_k} u_{\widetilde{n}_c} f(x_0), \tag{C.38}$$

where now $u_{\widetilde{n}_c}$ is the canonical basis in color space with components running from $\widetilde{n}_c = 1, ..., d(\mathcal{R})$. In this way, the computation of $p_{1,1}$ factorises as in appendix C.1 down to the evaluation of $p_{1,1}|_{\mathbf{p},\widetilde{n}_c}$ at fixed color and momenta. If the Dirac operator in an arbitrary representation $\mathcal{R}$ is not diagonal in the upgraded color structure, it can always be diagonalised by means of a gauge transformation. One can then compute the fermionic contribution to the coupling through

$$p_{1,1}(L/a) = \frac{1}{k} \sum_{n_c=1}^{d(\mathcal{R})} \sum_{\mathbf{p}} \frac{\partial}{\partial \eta} \ln \det \widetilde{\mathcal{D}}_5(n_c, \mathbf{p}) \Big|_{\eta=0}, \tag{C.39}$$

which is an identical calculation to the discussion of appendix C.1, with the difference that the color sum will run through more color components.

D

Argument for automatic $O(a)$-improvement

In this appendix we review the argument for which massless Wilson fermions in a finite volume without boundaries are automatically $O(a)$-improvemed [21], and the reason for why it fails in the presence of SF boundary conditions.

Consider Wilson quarks in the massless limit, which is obtained by tuning the bare quark mass to the critical value $m_0 = m_c$. Cutoff effects can be described through Symanzik's effective continuum action is

$$S_{\text{eff}} = S_0 + a\mathcal{S}_1 + a^2\mathcal{S}_2 + O(a^3), \tag{D.1}$$

with S_0 being the massless QCD continuum action

$$S_0 = -\frac{1}{2g_0^2}\int d^4x \text{Tr}\left\{F_{\mu\nu}(x)F_{\mu\nu}(x)\right\} + \int d^4x \overline{\psi}(x)\gamma_\mu D_\mu \psi(x), \tag{D.2}$$

In the chiral limit, and restricting only to on-shell quantities, the only term appearing

in $\mathcal{S}_1$ is

$$\mathcal{S}_1 = ic_1 \int d^4x \overline{\psi}(x)\sigma_{\mu\nu}\hat{F}_{\mu\nu}(x)\psi(x). \tag{D.3}$$

The effective description for a composite field reads

$$O_{\text{eff}} = O_0 + a\mathcal{O}_1 + O(a^2). \tag{D.4}$$

Given an operator $\mathbf{O}_{\text{eff}}$ constructed as a product of effective fields O_{eff}, a renormalized correlation function is expressed as

$$\langle \mathbf{O}_{\text{eff}} \rangle = \langle \mathbf{O}_0 \rangle_0 - a\langle S_1 \mathbf{O}_0 \rangle_0 + a\langle \mathbf{O}_1 \rangle_0 + O(a^2), \tag{D.5}$$

where $\langle \cdot \rangle_0$ denotes the expectation value taken with the action S_0, and

$$\begin{aligned} \mathbf{O}_0 &= O_0(x_1)...O_0(x_n), \\ \mathbf{O}_1 &= \sum_{k=1}^{n} O_0(x_1)...\mathcal{O}_1(x_k)...O_0(x_n). \end{aligned} \tag{D.6}$$

Consider the γ_5 transformation

$$\psi \longrightarrow \gamma_5\psi, \quad \overline{\psi} \longrightarrow -\overline{\psi}\gamma_5. \tag{D.7}$$

The continuum action S_0 is chirally invariant and hence the γ_5-transformation is a symmetry of the continuum action. The $\mathcal{S}_1$ term, however, picks up a $-$ sign

$$\begin{aligned} \gamma_5 &: S_0 \longrightarrow S_0, \\ \gamma_5 &: \mathcal{S}_1 \longrightarrow -\mathcal{S}_1, \end{aligned} \tag{D.8}$$

Since $(\gamma_5)^2 = \mathbb{I}$, any composite field $\mathbf{O}_{\text{eff}}$ will be the combination of 2 parts $\mathbf{O}_{\text{eff}}^{\text{even}}$ and $\mathbf{O}_{\text{eff}}^{\text{odd}}$, even and odd respectively under the γ_5-transformation,

$$\begin{aligned} \gamma_5 &: \mathbf{O}_{\text{eff}}^{\text{even}} \longrightarrow \mathbf{O}_{\text{eff}}^{\text{even}}, \\ \gamma_5 &: \mathbf{O}_{\text{eff}}^{\text{odd}} \longrightarrow -\mathbf{O}_{\text{eff}}^{\text{odd}}. \end{aligned} \tag{D.9}$$

Assuming that the measure is invariant under γ_5 transformations, a correlation func-

tion of an even composite field $\mathbf{O}_{\text{eff}}^{\text{even}}$ must be even

$$\gamma_5 : \langle \mathbf{O}_{\text{eff}}^{\text{even}} \rangle \longrightarrow \langle \mathbf{O}_{\text{eff}}^{\text{even}} \rangle. \tag{D.10}$$

The leading term in eq.(D.5) is obviously γ_5-even. The second term, however, as S_1 is γ_5-odd and $\mathbf{O}_0$ is γ_5-even, must be γ_5-odd. Moreover, the $O(a)$ counterterm $\mathbf{O}_1$ of a γ_5-even field $\mathbf{O}_{\text{eff}}^{\text{even}}$ is γ_5-odd, and vice versa. Hence, the first terms in eq.(D.5) for a γ_5-even field transform as

$$\begin{aligned} &\gamma_5 : \langle \mathbf{O}_0 \rangle_0 \longrightarrow \langle \mathbf{O}_0 \rangle_0, \\ &\gamma_5 : \langle S_1 \mathbf{O}_0 \rangle_0 \longrightarrow -\langle S_1 \mathbf{O}_0 \rangle_0, \\ &\gamma_5 : \langle \mathbf{O}_1 \rangle_0 \longrightarrow -\langle \mathbf{O}_1 \rangle_0. \end{aligned} \tag{D.11}$$

Since the full correlation function is even (see eq.(D.10) then

$$\begin{aligned} \langle S_1 \mathbf{O}_0 \rangle_0 = -\langle S_1 \mathbf{O}_0 \rangle_0, \qquad &\Rightarrow \qquad \langle S_1 \mathbf{O}_0 \rangle_0 = 0 \\ \langle \mathbf{O}_1 \rangle_0 = -\langle \mathbf{O}_1 \rangle_0, \qquad &\Rightarrow \qquad \langle \mathbf{O}_1 \rangle_0 = 0. \end{aligned} \tag{D.12}$$

so that correlation functions of γ_5-even fields are simply

$$\langle \mathbf{O}_{\text{eff}}^{\text{even}} \rangle = \langle \mathbf{O}_0 \rangle_0 + O(a^2). \tag{D.13}$$

Hence, correlation functions of γ_5-even composite fields have a finite continuum limit and have corrections of order $O(a^2)$. On the other hand, for a γ_5-odd composite field $\mathbf{O}_{\text{eff}}^{\text{odd}}$ one finds the transformation properties

$$\begin{aligned} &\gamma_5 : \langle \mathbf{O}_0 \rangle_0 \longrightarrow -\langle \mathbf{O}_0 \rangle_0, \\ &\gamma_5 : \langle S_1 \mathbf{O}_0 \rangle_0 \longrightarrow +\langle S_1 \mathbf{O}_0 \rangle_0, \\ &\gamma_5 : \langle \mathbf{O}_1 \rangle_0 \longrightarrow +\langle \mathbf{O}_1 \rangle_0. \end{aligned} \tag{D.14}$$

Thus, correlation functions of γ_5-odd fields will be given by

$$\langle \mathbf{O}_{\text{eff}}^{\text{odd}} \rangle = -a\langle S_1 \mathbf{O}_0 \rangle_0 + a\langle \mathbf{O}_1 \rangle_0. \tag{D.15}$$

Correlation functions of γ_5-odd fields are pure cutoff effects which vanish in the continuum limit.

Automatic $O(a)$ improvement does not mean that $O(a)$ effects are absent, but rather that they are contained within γ_5-odd observables. In fact, γ_5-even observables receive only even powers of a, while γ_5-odd observables receive only odd powers of a.

The situation is different in presence of SF boundary conditions. The boundary conditions for the fermions involve the projectors

$$\begin{aligned} P_+\psi(x)|_{x_0=0} &= 0; \qquad P_-\psi(x)|_{x_0=T} = 0 \\ \overline{\psi}(x)P_-|_{x_0=0} &= 0; \qquad \overline{\psi}(x)P_+|_{x_0=T} = 0 \end{aligned} \tag{D.16}$$

The projectors $P_\pm$, however, do not commute with γ_5. Instead,

$$P_\pm\gamma_5 = \gamma_5 P_\mp. \tag{D.17}$$

The non-Dirichlet components of the fields at the boundaries appear in the action as explicit chiral symmetry breaking terms

$$\begin{aligned} S_f\left[A,\psi,\overline{\psi}\right] = &\int d^4x\overline{\psi}(x)\gamma_\mu D_\mu\psi(x) \\ &- \int_0^L d^3x\left[\overline{\psi}(x)P_-\psi(x)\right]_{x_0=0} - \int_0^L d^3x\left[\overline{\psi}(x)P_-\psi(x)\right]_{x_0=T}, \end{aligned} \tag{D.18}$$

which break down the argument for automatic $O(a)$-improvement, since the γ_5 transformation is not a symmetry of the continuum action any more.

In order to render automatic $O(a)$-improvement in the SF, one should modify both SF boundary conditions and the basic γ_5 symmetry transformation so that

$$\left[\widetilde{\gamma_5}, \widetilde{P_\pm}\right] = 0, \tag{D.19}$$

where $\widetilde{\gamma_5}$ and $\widetilde{P_\pm}$ are the modified transformation and the modified projectors. In this situation, one can separate composite operators into a $\widetilde{\gamma_5}$-even and a $\widetilde{\gamma_5}$-odd part and repeat the previous arguments. This is the starting point for the χSF formulation.

E

Tables

In this appendix we collect a set of tables with the raw data used in different continuum extrapolations in chapters 5, 6 and 7. We first collect the values at finite lattice spacing for the one loop coefficients $m_c^{(1)}$ and $z_f^{(1)}$ evaluated both at $c_{\rm SW} = 1$ and $c_{\rm SW} = 0$. We then provide a set of tables with the values of the fermionic contribution to the one loop coupling $p_{1,1}$ in the χSF, for the different representations of the gauge group studied in this thesis.

E.1 Tables for the 1 loop critical mass $m_c^{(1)}(L/a)$

L/a	$m_c^{(1)}(L/a)\big\vert_{c_{\rm SW}=1}/C_2(\mathcal{R})$	$m_c^{(1)}(L/a)\big\vert_{c_{\rm SW}=0}/C_2(\mathcal{R})$
6	−0.20521519082593309	−0.31994335561538961
8	−0.20270516513645237	−0.32379382110998484
10	−0.20259569955818224	−0.32489257113907277
12	−0.20257077916164515	−0.32532297045662734
14	−0.20256297140220850	−0.32551942548036195
16	−0.20255985813386523	−0.32561787134839931
18	−0.20255840316415641	−0.32567037659027154
20	−0.20255764737506918	−0.32569955591464544
22	−0.20255722430466488	−0.32571616304772005
24	−0.20255697387151095	−0.32572567959937992
26	−0.20255681904544462	−0.32573105735317515
28	−0.20255671994510277	−0.32573395737954791
30	−0.20255665469613898	−0.32573534837026952
32	−0.20255661072519415	−0.32573581183233336
34	−0.20255658051804537	−0.32573570507691868
36	−0.20255655943374232	−0.32573525172413320
38	−0.20255654452389421	−0.32573459366516988
40	−0.20255653386911210	−0.32573382176812232
42	−0.20255652619289868	−0.32573299448192627
44	−0.20255652063020635	−0.32573214935582295
46	−0.20255651658498855	−0.32573131030833152
48	−0.20255651364051444	−0.32573049228999673

Table E.1.1: Values at finite lattice spacing for $m_c^{(1)}(L/a)/C_2(\mathcal{R})$, evaluated at $\theta = 0$, for $c_{\rm SW} = 1$ and $c_{\rm SW} = 0$.

E.2 Tables for the 1 loop coefficient $z_f^{(1)}(L/a)$

L/a	$z_f^{(1)}(L/a)\big\vert_{g_P^{uu'}=0}/C_2(\mathcal{R})$	$z_f^{(1)}(L/a)\big\vert_{g_A^{ud}=0}/C_2(\mathcal{R})$	$z_f^{(1)}(L/a)\big\vert_{g_V^{uu'}=0}/C_2(\mathcal{R})$
6	0.17383528686449767	0.17578831085117252	0.17480304566487481
8	0.16711129494238922	0.16788782949699255	0.16749073659019922
10	0.16720607933556930	0.16759454217930891	0.16739501278456559
12	0.16730476302801600	0.16752719333158739	0.16741284918744692
14	0.16737492923099165	0.16751418599667048	0.16744260500341213
16	0.16742327912725366	0.16751620889931695	0.16746844616782533
18	0.16745734834134662	0.16752242082838009	0.16748897219031522
20	0.16748208549710752	0.16752940255482751	0.16750507198420775
22	0.16750055992510673	0.16753602791780423	0.16751777968591999
24	0.16751470170384677	0.16754196179276271	0.16752792582415665
26	0.16752575958092564	0.16754715556690106	0.16753612885326463
28	0.16753456606929931	0.16755166191294404	0.16754284209964387
30	0.16754169193404025	0.16755556350289735	0.16754839882429096
32	0.16754753847881657	0.16755894547414263	0.16755304639105129
34	0.16755239427039514	0.16756188544695674	0.16755697060754482
36	0.16755647100252213	0.16756445070047210	0.16756031279202466
38	0.16755992676922873	0.16756669819938219	0.16756318174342510
40	0.16756288153785226	0.16756867565897027	0.16756566220400337
42	0.16756542765995966	0.16757042287834700	0.16756782090211431
44	0.16756763715608081	0.16757197303502028	0.16756971091916206
46	0.16756956685606553	0.16757335382927788	0.16757137488270327
48	0.16757126208792528	0.16757458845442486	0.16757284733004066

Table E.2.1: Values at finite lattice spacing for $z_c^{(1)}(L/a)/C_2(\mathcal{R})$, evaluated using different improvement conditions and with the parameters $c_{\rm SW} = 1$ and $\theta = 0$.

L/a	$z_f^{(1)}(L/a)\big\vert_{g_P^{uu'}=0}/C_2(\mathcal{R})$	$z_f^{(1)}(L/a)\big\vert_{g_A^{ud}=0}/C_2(\mathcal{R})$	$z_f^{(1)}(L/a)\big\vert_{g_V^{uu'}=0}/C_2(\mathcal{R})$
6	0.30165487691008419	0.32348266126791775	0.31288312280674513
8	0.31437001130402686	0.33247202171417173	0.32357589883649657
10	0.31925979932613152	0.33460006417710941	0.32702238532427802
12	0.32182478494078276	0.33509447957445887	0.32852231920179920
14	0.32338534259669860	0.33506045244917410	0.32926910156449868
16	0.32442427980271260	0.33483912917255104	0.32966775122107306
18	0.32516051522381639	0.33455660870498694	0.32988784604033050
20	0.32570690633225974	0.33426350683692441	0.33000972078934293
22	0.32612709151754787	0.33398054215152939	0.33007481425053747
24	0.32645947181709767	0.33371570792931937	0.33010590215639146
26	0.32672849045237395	0.33347136628893104	0.33011613193781386
28	0.32695039385455882	0.33324737203960014	0.33011339174146587
30	0.32713637367848231	0.33304250845898059	0.33010256126152271
32	0.32729437503689152	0.33285516307424867	0.33008673281373735
34	0.32743018493256587	0.33268364644610676	0.33006790284509352
36	0.32754811288120500	0.33252633825395167	0.33004737799369810
38	0.32765143070795766	0.33238174845161339	0.33002602100413458
40	0.32774266495689380	0.33224853661894027	0.33000440366451583
42	0.32782379623475943	0.33212551115623873	0.32998290412234527
44	0.32789639815835958	0.33201161933117795	0.32996177005330729
46	0.32796173613825363	0.33190593377723321	0.32994116037896865
48	0.32802083886419897	0.33180763824784787	0.32992117323206926

Table E.2.2: Values at finite lattice spacing for $z_c^{(1)}(L/a)/C_2(\mathcal{R})$, evaluated using different improvement conditions and with the parameters $c_{\mathrm{SW}} = 0$ and $\theta = 0$.

E.3 Tables for the 1 loop coupling $p_{1,1}(L/a)$

L/a	$p_{1,1}(L/a)$ $SU(2)_F$
6	$-2.8383052670804406032008703293169 70E-0002$
8	$-2.9465009905402341992751193442462 90E-0002$
10	$-3.0713851498017767684849153849402 30E-0002$
12	$-3.1880639509201564120307482576686 10E-0002$
14	$-3.2936242399201242890163425348697 70E-0002$
16	$-3.3889156845008593197508175724352 40E-0002$
18	$-3.4753431483054838957576478375396 70E-0002$
20	$-3.5542232226290211968786859715350 30E-0002$
22	$-3.6266681969107761410177351837173 30E-0002$
24	$-3.6935921783030655029839498138163 40E-0002$
26	$-3.7557428716806021805109102088276 40E-0002$
28	$-3.8137341275385068215462376321615 70E-0002$
30	$-3.8680734034544667893617650454432 70E-0002$
32	$-3.9191835924538693711864499429886 80E-0002$
34	$-3.9674200314715835636734888758248 90E-0002$
36	$-4.0130836970685646688386200033249 90E-0002$
38	$-4.0564314700197900265296631198894 70E-0002$
40	$-4.0976841668113561951956724300428 90E-0002$
42	$-4.1370328701405762921400734661676 90E-0002$
44	$-4.1746439583349660539831407197803 40E-0002$
46	$-4.2106631332963388250325673547047 80E-0002$
48	$-4.2452186719257432812171976621337 80E-0002$
50	$-4.2784240707887990475335495655620 80E-0002$
52	$-4.3103802129641622945914143773969 70E-0002$
54	$-4.3411771557241535234740861487467 70E-0002$
56	$-4.3708956150877209655485918376703 60E-0002$
58	$-4.3996082063011405982895903395281 70E-0002$
60	$-4.4273804864516068224229468555182 80E-0002$
62	$-4.4542718356258845371362611189100 00E-0002$
64	$-4.4803362055087554687619697321072 00E-0002$

Table E.3.1: Values at finite lattice spacing of the one loop contribution the the coupling $p_{1,1}(L/a)$ for the fundamental representation of $SU(2)$, with the parameters $c_{\rm SW} = 0$ and $\theta = 0$.

L/a	$p_{1,1}(L/a) \quad SU(2)_A$
6	−0.11845620390471632722606171751113 9
8	−0.11548130513268808003434332357801 7
10	−0.11805890697300358313966070513490 5
12	−0.12182373307937589164029247370625 1
14	−0.12564002317171325033795578903946 6
16	−0.12923508554035866636844815213990 7
18	−0.13256161842410595947341748136345 9
20	−0.13563128589421431796386644659606 8
22	−0.13846968483545795384022824718796 2
24	−0.14110357548739284675368576873539 1
26	−0.14355731408777570218227479335148 7
28	−0.14585209852850778736427241780960 6
30	−0.14800609308808308374501744946819 7
32	−0.15003480030412473297947256440100 4
34	−0.15195146592761395193079580617385 8
36	−0.15376744736364535682536777210555 5
38	−0.15549252795082874217050208646658 6
40	−0.15713517788414947704965770814132 3
42	−0.15870276843767502991980060481381 1
44	−0.16020174724541995570357323141487 5
46	−0.16163778180959280393596156647741 7
48	−0.16301587732799111958451870670515 9
50	−0.16434047382598282961869281552437 6
52	−0.16561552660125210217110206121677 4
54	−0.16684457317843057597836204276551 3
56	−0.16803078931736900207036420294838 3
58	−0.16917703610011331621639599164281 0
60	−0.17028589971259644698174803265323 1
62	−0.17135972521514215207745569766115 7
64	−0.17240064534238208101283390724291 8

Table E.3.2: Values at finite lattice spacing of the one loop contribution the the coupling $p_{1,1}(L/a)$ for the adjoint representation of $SU(2)$, with the parameters $c_{\rm SW} = 0$ and $\theta = 2\pi/5$.

L/a	$p_{1,1}(L/a) \quad SU(3)_F$
6	$-2.797107487649481885064608606616750E-0002$
8	$-2.952121609570845070718321331228820E-0002$
10	$-3.092923483490478470282098318474680E-0002$
12	$-3.216344709881011192385949935663960E-0002$
14	$-3.325378310672684914088174668194490E-0002$
16	$-3.422728450148409467878283265039780E-0002$
18	$-3.510494827936089305070465521795930E-0002$
20	$-3.590302190822934867316549367079010E-0002$
22	$-3.663419069498683296885852276562150E-0002$
24	$-3.730846922659537213214975568052960E-0002$
26	$-3.793385901018072352608344483918570E-0002$
28	$-3.851683089118999583289585194248090E-0002$
30	$-3.906267919011201663249407493961250E-0002$
32	$-3.957578324882152586403056038898060E-0002$
34	$-4.005980240507101491487880514051250E-0002$
36	$-4.051782293414677651947783485205940E-0002$
38	$-4.095247006348617579094055028966920E-0002$
40	$-4.136599433650809345985052331749910E-0002$
42	$-4.176033893280016960711004462880580E-0002$
44	$-4.213719269288184875455898761292700E-0002$
46	$-4.249803229469812152464276795458610E-0002$
48	$-4.284415611112723253149478963557670E-0002$
50	$-4.317671162410475512774369314379410E-0002$
52	$-4.349671780071035506088549915910940E-0002$
54	$-4.380508349477336674834960869880160E-0002$
56	$-4.410262268660115360501576697757040E-0002$
58	$-4.439006718735032204230484307661460E-0002$
60	$-4.466807729525925660142248689557060E-0002$
62	$-4.493725078572615534904389617056430E-0002$
64	$-4.519813053702496415209486904604770E-0002$

Table E.3.3: Values at finite lattice spacing of the one loop contribution the the coupling $p_{1,1}(L/a)$ for the fundamental representation of $SU(3)$, with the parameters $c_{\rm SW} = 0$ and $\theta = \pi/5$.

L/a	$p_{1,1}(L/a) \quad SU(3)_A$
6	−0.19419891807378159791636965164542 1
8	−0.17107279756137034412913882633928 6
10	−0.16854734530330501021608837846281 3
12	−0.17163108903419597280175568887196 8
14	−0.17610862954193809119539690444757 3
16	−0.18079177345054358653826221907116 9
18	−0.18533233371329729249462806781120 3
20	−0.18963129373194988501333351773131 9
22	−0.19367038587109709238581433132330 8
24	−0.19745899729947048310749981917083 6
26	−0.20101558941632603721614667042969 0
28	−0.20436069035800709158899127553936 9
30	−0.20751419016039226109309881341301 8
32	−0.21049435946095376536786544007922 4
34	−0.21331758653484239214346422555122 0
36	−0.21599841318693692487859735233581 3
38	−0.21854968678851144282189657946157 0
40	−0.22098274747099340774628799696129 3
42	−0.22330761506445494561478948223346 8
44	−0.22553316129641903469935052811219 7
46	−0.22766726243615726130961588688593 5
48	−0.22971693195487888552639524691767 9
50	−0.23168843464019174619344411279776 9
52	−0.23358738427186449806726835573762 1
54	−0.23541882707481032105973392896540 6
56	−0.23718731302752601525017795196729 3
58	−0.23889695687282133904050400546001 0
60	−0.24055149042561391171771585716767
62	−0.24215430753295288426090526196702 8
64	−0.24370850282749064842726218982485 1

Table E.3.4: Values at finite lattice spacing of the one loop contribution the the coupling $p_{1,1}(L/a)$ for the adjoint representation of $SU(3)$, with the parameters $c_{\mathrm{SW}} = 0$ and $\theta = \pi/6$.

L/a	$p_{1,1}(L/a) \quad SU(3)_S$
6	−0.14756538355936356230807255776413 8
8	−0.14399680750228259489692858221489 5
10	−0.14726964138947308446737659042774 1
12	−0.15202638628238996261022896232104 3
14	−0.15683746169493407457240483054986 8
16	−0.16136137208591143067776837602459 2
18	−0.16554160909416487583334008228961 6
20	−0.16939515199646494571794530371575 3
22	−0.17295568711781411290462079257516 8
24	−0.17625779772616912540249530793217 9
26	−0.17933269120386802864300403053530 9
28	−0.18220738709152323804087437356464 5
30	−0.18490495640605395578942587853612 5
32	−0.18744503891178901981216974290537 4
34	−0.18984438267321553345948933140672 4
36	−0.19211732625054007637535789091459 1
38	−0.19427620589202978770448724465901 6
40	−0.19633169139004222549794702474094 5
42	−0.19829306055102589935229563393370 5
44	−0.20016842299521480698600316406978 8
46	−0.20196490289606405984716551294835 1
48	−0.20368878869546886181560976176625 9
50	−0.20534565630540237659706115794209 3
52	−0.20694047099394941177682497421433 2
54	−0.20847767208061615457520709541766 9
56	−0.20996124370985614276150804547963 4
58	−0.21139477429700734613019917515792 4
60	−0.21278150671151496166653493793353 4
62	−0.21412438084746241049235457859045 2
64	−0.21542606990583133724201621246885 4

Table E.3.5: Values at finite lattice spacing of the one loop contribution the the coupling $p_{1,1}(L/a)$ for the symmetric representation of $SU(3)$, with the parameters $c_{\rm SW} = 0$ and $\theta = 0$.

L/a	$p_{1,1}(L/a) \quad SU(2)_F$
6	$-4.84202518020578801961111312295162 30E-0002$
8	$-5.07163079973103720544350607951691 0E-0002$
10	$-5.26914831669512292750191553501960 0E-0002$
12	$-5.43398743460217630258027125324343 0E-0002$
14	$-5.57375532045666902607759341775562 0E-0002$
16	$-5.69457071423615393776623660326385 0E-0002$
18	$-5.80076008913946794911445529189366 0E-0002$
20	$-5.89538704142451381225198141989688 0E-0002$
22	$-5.98067126007193577152455946202425 0E-0002$
24	$-6.05826220301678549592524623197608 0E-0002$
26	$-6.12941472673429830802445234072740 0E-0002$
28	$-6.19510363595219463949339340824638 0E-0002$
30	$-6.25610020706083862029029005714004 0E-0002$
32	$-6.31302458852963495626981983470520 0E-0002$
34	$-6.36638253181712540606201271684763 0E-0002$
36	$-6.41659169669730219921813975363106 1E-0002$
38	$-6.46400086014538579786115576514377 0E-0002$
40	$-6.50890419189312994391878111925932 0E-0002$
42	$-6.55155203350741076876683965119841 9E-0002$
44	$-6.59215915527109303593447625016507 0E-0002$
46	$-6.63091116416351184091961989917208 0E-0002$
48	$-6.66796953644420883724993585868610 0E-0002$
50	$-6.70347561323140739283450650691300 0E-0002$
52	$-6.73755380450979852051027767097826 0E-0002$
54	$-6.77031418202156274691141304927583 0E-0002$
56	$-6.80185459539616455035204794935128 0E-0002$
58	$-6.83226241272197399899206959128326 0E-0002$
60	$-6.86161596261666104732860259635440 0E-0002$
62	$-6.88998573705858857047128873826178 0E-0002$
64	$-6.91743540098287138368138460746379 0E-0002$

Table E.3.6: Values at finite lattice spacing of the one loop contribution the the coupling $p_{1,1}(L/a)$ for the fundamental representation of $SU(2)$, with the parameters $c_{\mathrm{SW}} = 1$ and $\theta = 0$.

L/a	$p_{1,1}(L/a) \quad SU(2)_A$
6	−0.20024959042256009568323194916268 3
8	−0.20159916351821636190318604718064 4
10	−0.20674987684629740336934353981190 9
12	−0.21223225154257439601434943946536 0
14	−0.21728006244130794422945682810925 2
16	−0.22180245324684479980788331848687 3
18	−0.22585282265033087020037752480054 4
20	−0.22950335234965384712601741131230 6
22	−0.23281826824873708666538807348555 0
24	−0.23585016940662431472565330139271 0
26	−0.23864135849921786199706624471224 1
28	−0.24122589102243417227087432102372 2
30	−0.24363138627314813467630615051185 7
32	−0.24588045594728092519846068152918 6
34	−0.24799179469337032269004781485014 0
36	−0.24998100680681689854041955996424 8
38	−0.25186123482529783180586990296848 6
40	−0.25364364098445194780507983197106 1
42	−0.25533777930732559386090497813424 8
44	−0.25695188593135019649882260493373 5
46	−0.25849310781251141242001096882391 6
48	−0.25996768456326947052503615965597 7
50	−0.26138109431334849078859245342525 6
52	−0.26273817169641228446236944667076 4
54	−0.26404320404644356411561343209514 9
56	−0.26530001041299873711194032344862 9
58	−0.26651200691845048051047937632649 1
60	−0.26768226117347006505814525253657 5
62	−0.26881353786233118699036784509979 7
64	−0.26990833715258962159926361648436 5

Table E.3.7: Values at finite lattice spacing of the one loop contribution the the coupling $p_{1,1}(L/a)$ for the adjoint representation of $SU(2)$, with the parameters $c_{\rm SW} = 1$ and $\theta = 2\pi/5$.

L/a	$p_{1,1}(L/a) \quad SU(3)_F$
6	$-4.8128173116308782755676526919196 50E-0002$
8	$-5.0839134085198616049596613327764 20E-0002$
10	$-5.2950287753914292422067361201112 90E-0002$
12	$-5.4653476659836494413911070615538 10E-0002$
14	$-5.6078133175487548732648102056326 40E-0002$
16	$-5.7301737950043933815436983124835 50E-0002$
18	$-5.8373435240738313390185641083617 10E-0002$
20	$-5.9326372885767025980621794729265 20E-0002$
22	$-6.0183981446231119516232028540843 10E-0002$
24	$-6.0963427789622055244399926939696 50E-0002$
26	$-6.1677655930364320399370779378677 60E-0002$
28	$-6.2336660371128928035321892142527 80E-0002$
30	$-6.2948314616220022044567674250934 60E-0002$
32	$-6.3518928925438851019042774816792 60E-0002$
34	$-6.4053636714482266847514317148709 30E-0002$
36	$-6.4556668935990835285298279952134 50E-0002$
38	$-6.5031553162382880069318784505020 40E-0002$
40	$-6.5481260807870322844888654505220 00E-0002$
42	$-6.5908317855791450740995822409769 40E-0002$
44	$-6.6314889407706954329603640802748 30E-0002$
46	$-6.6702845128806137683865452194128 10E-0002$
48	$-6.7073810534336577959127613041100 80E-0002$
50	$-6.7429207633194459705794995387239 90E-0002$
52	$-6.7770287468423388287748099526642 49E-0002$
54	$-6.8098156415520574853049452919311 40E-0002$
56	$-6.8413797620027990375441456800150 20E-0002$
58	$-6.8718088612408653203230635494816 10E-0002$
60	$-6.9011815888849637928519341251062 60E-0002$
62	$-6.9295687063376659062482893201053 61E-0002$
64	$-6.9570341060452565228394103528024 70E-0002$

Table E.3.8: Values at finite lattice spacing of the one loop contribution the the coupling $p_{1,1}(L/a)$ for the fundamental representation of $SU(3)$, with the parameters $c_{\rm SW} = 1$ and $\theta = \pi/5$.

L/a	$p_{1,1}(L/a) \quad SU(3)_A$
6	−0.31586900685786789151817405698207 9
8	−0.29989812145309218064700814600882 7
10	−0.30141357041658436813231767569880 8
12	−0.30714187565136157560312162485927 5
14	−0.31349960109202012661563424941112 2
16	−0.31959237908441301398355105665717 3
18	−0.32523041884542316725021240223269 4
20	−0.33040859389024622605027102512834 9
22	−0.33516809897072716521410200940874 9
24	−0.33955789929940656172322162882516 9
26	−0.34362385325249038764888118223493 2
28	−0.34740607013814914087907521452954 1
30	−0.35093881333943552001669056965890 9
32	−0.35425114562338008472199713709961 6
34	−0.35736771782530220517679979312714 0
36	−0.36030950578722061956727336345081 3
38	−0.36309444223752391605600158475311 3
40	−0.36573794009184094685494459851057 8
42	−0.36825331966168255415610566083138 0
44	−0.37065215575182307066569240771998 0
46	−0.37294455969906414296655211121896 2
48	−0.37513940917097657064707589903778 0
50	−0.37724453617583275141458420835094 4
52	−0.37926688163409176252272118847665 9
54	−0.38121262312380570296978661460920 5
56	−0.38308728102082116441952470957667 0
58	−0.38489580715807276704538765969258 9
60	−0.38664265927019993103200612889218 8
62	−0.38833186381974543420811418949570 1
64	−0.38996706927770996134566796710604 9

Table E.3.9: Values at finite lattice spacing of the one loop contribution the the coupling $p_{1,1}(L/a)$ for the adjoint representation of $SU(3)$, with the parameters $c_{\rm SW} = 1$ and $\theta = \pi/6$.

L/a	$p_{1,1}(L/a) \quad SU(3)_S$
6	−0.25063809781841266670555154510864 3
8	−0.25214474202642079262226968845309 7
10	−0.25846823181157223057309040364375 6
12	−0.26527699895287603498617780373976 8
14	−0.27156791040911926905600512231315 2
16	−0.27721111373256515237689752620524 1
18	−0.28226815235070538067217880634212 3
20	−0.28682736757923778020057204224282 0
22	−0.29096822008763347060558424792803 7
24	−0.29475603901497853257847934154393 0
26	−0.29824346303000455191408010709855 9
28	−0.30147291390653214946346651847614 4
30	−0.30447881991667018398450668381038 5
32	−0.30728938091082420437589282867794 5
34	−0.30992792003656239670330808909689 4
36	−0.31241391034981220748279064654704 8
38	−0.31476375639508922896119508281339 6
40	−0.31699139336377871467935096333841 5
42	−0.31910875045312324604564894067051 2
44	−0.32112611259070411708437170526544 3
46	−0.32305240549675131285677389207362 5
48	−0.32489542240564367683659300131320 6
50	−0.32666200597938039553425844271287 7
52	−0.32835819549086390812631245191290 2
54	−0.32998934684805440638933791143209 4
56	−0.33156023119771848071930478730220 1
58	−0.33307511649705365501695561176601 7
60	−0.33453783543762366618291323073449 8
62	−0.33595184235338923585558236405522 9
64	−0.33732026117551726292177171749645 3

Table E.3.10: Values at finite lattice spacing of the one loop contribution the the coupling $p_{1,1}(L/a)$ for the symmetric representation of $SU(3)$, with the parameters $c_{\mathrm{SW}} = 1$ and $\theta = 0$.

References

[1] S. Sint, "The Chirally rotated Schrödinger functional with Wilson fermions and automatic O(a) improvement," *Nucl.Phys.*, vol. B847, pp. 491–531, 2011.

[2] S. Glashow, "Partial Symmetries of Weak Interactions," *Nucl.Phys.*, vol. 22, pp. 579–588, 1961.

[3] J. Goldstone, A. Salam, and S. Weinberg, "Broken Symmetries," *Phys.Rev.*, vol. 127, pp. 965–970, 1962.

[4] S. Weinberg, "A Model of Leptons," *Phys.Rev.Lett.*, vol. 19, pp. 1264–1266, 1967.

[5] G. Aad *et al.*, "Observation of a new particle in the search for the Standard Model Higgs boson with the ATLAS detector at the LHC," *Phys.Lett.*, vol. B716, pp. 1–29, 2012.

[6] S. Chatrchyan *et al.*, "Observation of a new boson at a mass of 125 GeV with the CMS experiment at the LHC," *Phys.Lett.*, vol. B716, pp. 30–61, 2012.

[7] F. Englert and R. Brout, "Broken Symmetry and the Mass of Gauge Vector Mesons," *Phys.Rev.Lett.*, vol. 13, pp. 321–323, 1964.

[8] G. Guralnik, C. Hagen, and T. Kibble, "Global Conservation Laws and Massless Particles," *Phys.Rev.Lett.*, vol. 13, pp. 585–587, 1964.

[9] T. Kibble, "Symmetry breaking in nonAbelian gauge theories," *Phys.Rev.*, vol. 155, pp. 1554–1561, 1967.

[10] P. W. Higgs, "Broken Symmetries and the Masses of Gauge Bosons," *Phys.Rev.Lett.*, vol. 13, pp. 508–509, 1964.

[11] P. W. Higgs, "Broken symmetries, massless particles and gauge fields," *Phys.Lett.*, vol. 12, pp. 132–133, 1964.

[12] H. Fritzsch, M. Gell-Mann, and H. Leutwyler, "Advantages of the Color Octet Gluon Picture," *Phys.Lett.*, vol. B47, pp. 365–368, 1973.

[13] D. Gross and F. Wilczek, "Asymptotically Free Gauge Theories. 1," *Phys.Rev.*, vol. D8, pp. 3633–3652, 1973.

[14] D. Gross and F. Wilczek, "ASYMPTOTICALLY FREE GAUGE THEORIES. 2.," *Phys.Rev.*, vol. D9, pp. 980–993, 1974.

[15] H. D. Politzer, "Reliable Perturbative Results for Strong Interactions?," *Phys.Rev.Lett.*, vol. 30, pp. 1346–1349, 1973.

[16] G. 't Hooft, "The renormalization procedure for Yang-Mills fields," *Unpublished*, 1972.

[17] K. G. Wilson, "Confinement of Quarks," *Phys.Rev.*, vol. D10, pp. 2445–2459, 1974.

[18] M. Creutz, "Monte Carlo Study of Quantized SU(2) Gauge Theory," *Phys.Rev.*, vol. D21, pp. 2308–2315, 1980.

[19] K. Symanzik, "Continuum Limit and Improved Action in Lattice Theories. 1. Principles and phi**4 Theory," *Nucl.Phys.*, vol. B226, p. 187, 1983.

[20] K. Symanzik, "Continuum Limit and Improved Action in Lattice Theories. 2. O(N) Nonlinear Sigma Model in Perturbation Theory," *Nucl.Phys.*, vol. B226, p. 205, 1983.

[21] R. Frezzotti and G. Rossi, "Chirally improving Wilson fermions. 1. O(a) improvement," *JHEP*, vol. 0408, p. 007, 2004.

[22] M. Luscher, P. Weisz, and U. Wolff, "A Numerical method to compute the running coupling in asymptotically free theories," *Nucl.Phys.*, vol. B359, pp. 221–243, 1991.

[23] M. Luscher, R. Narayanan, P. Weisz, and U. Wolff, "The Schrodinger functional: A Renormalizable probe for nonAbelian gauge theories," *Nucl.Phys.*, vol. B384, pp. 168–228, 1992.

[24] K. Jansen, C. Liu, M. Luscher, H. Simma, S. Sint, *et al.*, "Nonperturbative renormalization of lattice QCD at all scales," *Phys.Lett.*, vol. B372, pp. 275–282, 1996.

[25] M. Della Morte *et al.*, "Non-perturbative quark mass renormalization in two-flavor QCD," *Nucl.Phys.*, vol. B729, pp. 117–134, 2005.

[26] S. Aoki *et al.*, "Non-perturbative renormalization of quark mass in $N\_f = 2+1$ QCD with the Schroedinger functional scheme," *JHEP*, vol. 1008, p. 101, 2010.

[27] M. Della Morte *et al.*, "Computation of the strong coupling in QCD with two dynamical flavors," *Nucl.Phys.*, vol. B713, pp. 378–406, 2005.

[28] S. Aoki *et al.*, "Precise determination of the strong coupling constant in N(f) = 2+1 lattice QCD with the Schrodinger functional scheme," *JHEP*, vol. 0910, p. 053, 2009.

[29] F. Tekin, R. Sommer, and U. Wolff, "The Running coupling of QCD with four flavors," *Nucl.Phys.*, vol. B840, pp. 114–128, 2010.

[30] M. Guagnelli, J. Heitger, C. Pena, S. Sint, and A. Vladikas, "Non-perturbative renormalization of left-left four-fermion operators in quenched lattice QCD," *JHEP*, vol. 0603, p. 088, 2006.

[31] A. J. Hietanen, K. Rummukainen, and K. Tuominen, "Evolution of the coupling constant in SU(2) lattice gauge theory with two adjoint fermions," *Phys.Rev.*, vol. D80, p. 094504, 2009.

[32] F. Bursa, L. Del Debbio, L. Keegan, C. Pica, and T. Pickup, "Mass anomalous dimension in SU(2) with two adjoint fermions," *Phys.Rev.*, vol. D81, p. 014505, 2010.

[33] T. DeGrand, Y. Shamir, and B. Svetitsky, "Running coupling and mass anomalous dimension of SU(3) gauge theory with two flavors of symmetric-representation fermions," *Phys.Rev.*, vol. D82, p. 054503, 2010.

[34] N. Yamada, M. Hayakawa, K.-I. Ishikawa, Y. Osaki, S. Takeda, *et al.*, "Study of the running coupling constant in 10-flavor QCD with the Schródinger functional method," 2010.

[35] E. T. Neil, "Exploring Models for New Physics on the Lattice," *PoS*, vol. LATTICE2011, p. 009, 2011.

[36] S. Sint, "On the Schrodinger functional in QCD," *Nucl.Phys.*, vol. B421, pp. 135–158, 1994.

[37] W. Bietenholz, U. Gerber, M. Pepe, and U.-J. Wiese, "Topological Lattice Actions," *JHEP*, vol. 1012, p. 020, 2010.

[38] H. B. Nielsen and M. Ninomiya, "Absence of neutrinos on a lattice (I). Proof by homotopy theory," *Nuclear Physics B*, vol. 185, pp. 20–40, jul 1981.

[39] D. Friedan, "A PROOF OF THE NIELSEN-NINOMIYA THEOREM," *Commun.Math.Phys.*, vol. 85, pp. 481–490, 1982.

[40] P. H. Ginsparg and K. G. Wilson, "A Remnant of Chiral Symmetry on the Lattice," *Phys.Rev.*, vol. D25, p. 2649, 1982.

[41] M. Luscher, "Exact chiral symmetry on the lattice and the Ginsparg-Wilson relation," *Phys.Lett.*, vol. B428, pp. 342–345, 1998.

[42] F. Niedermayer, "Exact chiral symmetry, topological charge and related topics," *Nucl.Phys.Proc.Suppl.*, vol. 73, pp. 105–119, 1999.

[43] M. Luscher, S. Sint, R. Sommer, and P. Weisz, "Chiral symmetry and O(a) improvement in lattice QCD," *Nucl.Phys.*, vol. B478, pp. 365–400, 1996.

[44] P. Weisz, "Continuum Limit Improved Lattice Action for Pure Yang-Mills Theory. 1.," *Nucl.Phys.*, vol. B212, p. 1, 1983.

[45] M. Luscher and P. Weisz, "On-Shell Improved Lattice Gauge Theories," *Commun.Math.Phys.*, vol. 97, p. 59, 1985.

[46] B. Sheikholeslami and R. Wohlert, "Improved Continuum Limit Lattice Action for QCD with Wilson Fermions," *Nucl.Phys.*, vol. B259, p. 572, 1985.

[47] G. P. Lepage and P. B. Mackenzie, "On the viability of lattice perturbation theory," *Phys.Rev.*, vol. D48, pp. 2250–2264, 1993.

[48] S. Sint, "Nonperturbative renormalization in lattice field theory," *Nucl.Phys.Proc.Suppl.*, vol. 94, pp. 79–94, 2001.

[49] M. Luscher, R. Sommer, U. Wolff, and P. Weisz, "Computation of the running coupling in the SU(2) Yang-Mills theory," *Nucl.Phys.*, vol. B389, pp. 247–264, 1993.

[50] M. Luscher, R. Sommer, P. Weisz, and U. Wolff, "A Precise determination of the running coupling in the SU(3) Yang-Mills theory," *Nucl.Phys.*, vol. B413, pp. 481–502, 1994.

[51] R. Sommer, "A New way to set the energy scale in lattice gauge theories and its applications to the static force and alpha-s in SU(2) Yang-Mills theory," *Nucl.Phys.*, vol. B411, pp. 839–854, 1994.

[52] A. Bode, P. Weisz, and U. Wolff, "Two loop computation of the Schrodinger functional in lattice QCD," *Nucl.Phys.*, vol. B576, pp. 517–539, 2000.

[53] S. Matsuzaki and K. Yamawaki, "Techni-dilaton at 125 GeV," *Phys.Rev.*, vol. D85, p. 095020, 2012.

[54] V. Riva and J. L. Cardy, "Scale and conformal invariance in field theory: A Physical counterexample," *Phys.Lett.*, vol. B622, pp. 339–342, 2005.

[55] L. Del Debbio, M. T. Frandsen, H. Panagopoulos, and F. Sannino, "Higher representations on the lattice: Perturbative studies," *JHEP*, vol. 0806, p. 007, 2008.

[56] W. E. Caswell, "Asymptotic Behavior of Nonabelian Gauge Theories to Two Loop Order," *Phys.Rev.Lett.*, vol. 33, p. 244, 1974.

[57] T. Banks and A. Zaks, "On the Phase Structure of Vector-Like Gauge Theories with Massless Fermions," *Nucl.Phys.*, vol. B196, p. 189, 1982.

[58] T. Appelquist, J. Terning, and L. Wijewardhana, "The Zero temperature chiral phase transition in SU(N) gauge theories," *Phys.Rev.Lett.*, vol. 77, pp. 1214–1217, 1996.

[59] T. DeGrand, Y. Shamir, and B. Svetitsky, "Infrared fixed point in SU(2) gauge theory with adjoint fermions," *Phys.Rev.*, vol. D83, p. 074507, 2011.

[60] T. DeGrand, Y. Shamir, and B. Svetitsky, "Gauge theories with fermions in the two-index symmetric representation," *PoS*, vol. LATTICE2011, p. 060, 2011.

[61] J. Giedt and E. Weinberg, "Backward running or absence of running from Creutz ratios," *Phys.Rev.*, vol. D84, p. 074501, 2011.

[62] J. Giedt and E. Weinberg, "Finite size scaling in minimal walking technicolor," *Phys.Rev.*, vol. D85, p. 097503, 2012.

[63] T. Karavirta, J. Rantaharju, K. Rummukainen, and K. Tuominen, "Determining the conformal window: SU(2) gauge theory with N_f = 4, 6 and 10 fermion flavours," *JHEP*, vol. 1205, p. 003, 2012.

[64] F. Bursa, L. Del Debbio, L. Keegan, C. Pica, and T. Pickup, "Mass anomalous dimension in SU(2) with six fundamental fermions," *Phys.Lett.*, vol. B696, pp. 374–379, 2011.

[65] T. Karavirta, J. Rantaharju, K. Rummukainen, and K. Tuominen, "Exploring the conformal window: SU(2) gauge theory on the lattice," *PoS*, vol. LATTICE2011, p. 067, 2011.

[66] Y. Shamir, B. Svetitsky, and T. DeGrand, "Zero of the discrete beta function in SU(3) lattice gauge theory with color sextet fermions," *Phys.Rev.*, vol. D78, p. 031502, 2008.

[67] B. Svetitsky, Y. Shamir, and T. DeGrand, "Nonperturbative infrared fixed point in sextet QCD," *PoS*, vol. LATTICE2008, p. 062, 2008.

[68] B. Svetitsky, Y. Shamir, and T. DeGrand, "Sextet QCD: slow running and the mass anomalous dimension," *PoS*, vol. LATTICE2010, p. 072, 2010.

[69] U. M. Heller, "The Schrodinger functional running coupling with staggered fermions and its application to many flavor QCD," *Nucl.Phys.Proc.Suppl.*, vol. 63, pp. 248–250, 1998.

[70] T. Appelquist, G. T. Fleming, and E. T. Neil, "Lattice study of the conformal window in QCD-like theories," *Phys.Rev.Lett.*, vol. 100, p. 171607, 2008.

[71] A. Deuzeman, M. P. Lombardo, and E. Pallante, "The Physics of eight flavours," *Phys.Lett.*, vol. B670, pp. 41–48, 2008.

[72] M. Hayakawa, K.-I. Ishikawa, Y. Osaki, S. Takeda, S. Uno, *et al.*, "Running coupling constant of ten-flavor QCD with the Schródinger functional method," *Phys.Rev.*, vol. D83, p. 074509, 2011.

[73] A. Hasenfratz, "Conformal or Walking? Monte Carlo renormalization group studies of SU(3) gauge models with fundamental fermions," *Phys.Rev.*, vol. D82, p. 014506, 2010.

[74] A. Hasenfratz, "Investigating the critical properties of beyond-QCD theories using Monte Carlo Renormalization Group matching," *Phys.Rev.*, vol. D80, p. 034505, 2009.

[75] A. Patella, "A precise determination of the psibar-psi anomalous dimension in conformal gauge theories," *Phys.Rev.*, vol. D86, p. 025006, 2012.

[76] K. Symanzik, "Schrodinger Representation and Casimir Effect in Renormalizable Quantum Field Theory," *Nucl.Phys.*, vol. B190, p. 1, 1981.

[77] B. Lucini and G. Moraitis, "The Running of the coupling in SU(N) pure gauge theories," *Phys.Lett.*, vol. B668, pp. 226–232, 2008.

[78] M. Luscher, "SCHRODINGER REPRESENTATION IN QUANTUM FIELD THEORY," *Nucl.Phys.*, vol. B254, pp. 52–57, 1985.

[79] S. Sint, "One loop renormalization of the QCD Schrodinger functional," *Nucl.Phys.*, vol. B451, pp. 416–444, 1995.

[80] S. Sint and R. Sommer, "The Running coupling from the QCD Schrodinger functional: A One loop analysis," *Nucl.Phys.*, vol. B465, pp. 71–98, 1996.

[81] S. Sint and B. Leder, "Testing universality and automatic O(a) improvement in massless lattice QCD with Wilson quarks," *PoS*, vol. LATTICE2010, p. 265, 2010.

[82] M. Luscher, "The Schrodinger functional in lattice QCD with exact chiral symmetry," *JHEP*, vol. 0605, p. 042, 2006.

[83] M. Luscher and P. Weisz, "O(a) improvement of the axial current in lattice QCD to one loop order of perturbation theory," *Nucl.Phys.*, vol. B479, pp. 429–458, 1996.

[84] K. Symanzik, "CUTOFF DEPENDENCE IN LATTICE phi**4 in four-dimensions THEORY," 1979.

[85] K. Symanzik, "CONCERNING THE CONTINUUM LIMIT IN SOME LATTICE THEORIES. (TALK)," 1982.

[86] J. Stehr and P. H. Weisz *Lett.Nuovo Cim.*, vol. 37, p. 173, 1983.

[87] A. Gonzalez Arroyo, G. Indurain, and G. Martinelli *Phys. Lett. B*, vol. 117, p. 437, 1982.

[88] R. Groot, J. Hoek, and J. Smit *Nucl. Phys. B*, vol. 237, p. 111, 1984.

[89] R. Wholert, "Improved continuum limit lattice action for quarks," *DESY preprint 87-069*, vol. Unpublished, 1087.

[90] A. Bode, U. Wolff, and P. Weisz, "Two loop computation of the Schrodinger functional in pure SU(3) lattice gauge theory," *Nucl.Phys.*, vol. B540, pp. 491–499, 1999.

[91] S. Sint and P. Weisz, "Further results on O(a) improved lattice QCD to one loop order of perturbation theory," *Nucl.Phys.*, vol. B502, pp. 251–268, 1997.

[92] P. Weisz, "Computation of the improvement coefficient cA to 1-loop (Unpublished notes)," 19995.

[93] S. Kurth, "The Renormalized quark mass in the Schrodinger functional of lattice QCD: A One loop calculation with a nonvanishing background field," 2002.

[94] D. Hesse and R. Sommer, "A one-loop study of matching conditions for static-light flavor currents," *JHEP*, vol. 1302, p. 115, 2013.

[95] P. Vilaseca, "A Perturbative Toolkit in the SF: Documentation," *Private Notes*, 2013.

[96] J. G. Lopez, K. Jansen, D. Renner, and A. Shindler, "A quenched study of the Schroedinger functional with chirally rotated boundary conditions: non-perturbative tuning," *Nucl.Phys.*, vol. B867, pp. 567–608, 2013.

[97] J. G. Lopez, K. Jansen, D. Renner, and A. Shindler, "A quenched study of the Schroedinger functional with chirally rotated boundary conditions: applications," *Nucl.Phys.*, vol. B867, pp. 609–635, 2013.

[98] C. et al. Pica, "In preparation," 2013.

[99] P. Fritzsch and A. Ramos, "The gradient flow coupling in the Schródinger Functional," 2013.

[100] R. Narayanan and U. Wolff, "Two loop computation of a running coupling lattice Yang-Mills theory," *Nucl.Phys.*, vol. B444, pp. 425–446, 1995.

[101] S. Sint and P. Vilaseca, "Perturbative lattice artefacts in the SF coupling for technicolor-inspired models," *PoS*, vol. LATTICE2011, p. 091, 2011.

[102] S. Sint and P. Vilaseca, "Lattice artefacts in the Schródinger Functional coupling for strongly interacting theories," *PoS*, vol. LATTICE2012, p. 031, 2012.

[103] P. Perez-Rubio, M. Dalla Brida, S. Sint, and P. Vilaseca, "In preparation," 2013.

[104] P. Perez-Rubio, S. Sint, and S. Takeda, "An O(a) modified lattice set-up of the Schródinger functional in SU(3) gauge theory," *JHEP*, vol. 1107, p. 116, 2011.

[105] O. Tarsov, A. A. Vladimirov, and A. Y. Zharkov *Phys. Lett. B*, vol. 39, p. 429, 1980.

[106] A. Hasenfratz, "MCRG study of 12 fundamental flavors with mixed fundamental-adjoint gauge action," *PoS*, vol. LATTICE2011, p. 065, 2011.

[107] T. Karavirta, K. Tuominen, and K. Rummukainen, "Perturbative Improvement of the Schrodinger Functional for Lattice Strong Dynamics," *Phys.Rev.*, vol. D85, p. 054506, 2012.